Brunel
UNIVERSITY
L O N D O N

Holoscopic 3D Imaging and Display Technology:

Camera / Processing / Display

By

Mohammad Rafiq Swash

A thesis submitted for the degree of

Doctor of Philosophy

in

Electronic & Computer Engineering

School of Engineering and Design

Brunel University

November 2013

STATEMENT OF ORIGINALITY

The work contained within this thesis is purely that of the author unless otherwise stated. Except what is acknowledged, none of the work presented here has been published or distributed by anyone other than the author.

Mohammad Rafiq Swash

November, 2013, London

ABSTRACT

Holoscopic 3D imaging "Integral imaging" was first proposed by Lippmann in 1908. It has become an attractive technique for creating full colour 3D scene that exists in space. It promotes a single camera aperture for recording spatial information of a real scene and it uses a regularly spaced microlens arrays to simulate the principle of Fly's eye technique, which creates physical duplicates of light field "true 3D-imaging technique".

While stereoscopic and multiview 3D imaging systems which simulate human eye technique are widely available in the commercial market, holoscopic 3D imaging technology is still in the research phase. The aim of this research is to investigate spatial resolution of holoscopic 3D imaging and display technology, which includes holoscopic 3D camera, processing and display.

Smart microlens array architecture is proposed that doubles spatial resolution of holoscopic 3D camera horizontally by trading horizontal and vertical resolutions. In particular, it overcomes unbalanced pixel aspect ratio of unidirectional holoscopic 3D images. In addition, omnidirectional holoscopic 3D computer graphics rendering techniques are proposed that simplify the rendering complexity and facilitate holoscopic 3D content generation.

Holoscopic 3D image stitching algorithm is proposed that widens overall viewing angle of holoscopic 3D camera aperture and pre-processing of holoscopic 3D image filters are proposed for spatial data alignment and 3D image data processing. In addition, Dynamic hyperlinker tool is developed that offers interactive holoscopic 3D video content search-ability and browse-ability.

Novel pixel mapping techniques are proposed that improves spatial resolution and visual definition in space. For instance, 4D-DSPM enhances 3D pixels per inch from 44 3D-PPIs to 176 3D-PPIs horizontally and achieves spatial resolution of 1365×384 3D-Pixels whereas the traditional spatial resolution is 341×1536 3D-Pixels. In addition distributed pixel mapping is proposed that improves quality of holoscopic 3D scene in space by creating RGB-colour channel elemental images.

ACKNOWLEDGEMENTS

TABLE OF CONTENT

LIST OF FIGURES

LIST OF TABLES

LIST OF ALGORITHMS

LIST OF EQUATIONS

LIST OF ACRONYMS

Acronym	Stands for
2D	Two-Dimensional
3D	Three-Dimensional
3D-PPI	3D pixels per inch in space
AR	Augmented Reality
BLU	Back Light Unit
CAD	Computer-Aided Drawing
CCD	Charge-Couple Device
CSG	Constructive Solid Geometry
DPM	Distributed Pixel Mapping
DSPM	Distributed Smart Pixel Mapping
FL	Focal Length
H3D	Holoscopic 3D
HD	High Definition
IOR	Index of refraction
LCD	Liquid Crystal Display
LCPM	Liquid Crystal Pinhole Map
LED	Light Emitting Diode
LP	Lens Pitch
MLA	Microlens Array
PP	Pixel Pitch
PPI	Pixels Per Inch
PPL	Pixels Per Lens
S3D	Stereoscopic 3D
SPM	Smart Pixel Mapping
TPM	Triangular Pixel Mapping

1 Chapter One - Introduction

This chapter presents the overview of the thesis. It briefly discusses the background of the research including its aim and objectives. It presents the research contributions with a list of journal and conference papers including the thesis layout. The layout of this chapter is as follows: 1.1 Preface, 1.2 The Research Aim and Objectives, 1.3 The Research Contributions, 1.4 The Author's Publications, 1.5 The Thesis Outlines and 1.6 Conclusion.

1.1 Preface

Three-dimensional (3D) imaging technology is very appealing as it offers effects, which humans perceive naturally in the real world such as 3D depth and motion parallax (transition between views creates motion parallax) [1]. In addition, it offers more low-level features and cues compared to Two-dimensional (2D) imaging technology [2]. 3D imaging technology has been attracting great interests due to its ability to deliver immersive user experience. Its application areas are enormous such as entertainment, medical, military, and design.

Early 3D systems utilise two perspective images that are for the left and right eye respectively to achieve the 3D depth effect. Viewing this kind of images requires special apparatus to channel the images to the corresponding eye or a parallax barrier technology on the liquid crystal display (LCD) to create and project left image-window and right image-window. Such systems are known as stereoscopic systems [3], which simulates human eye technique.

Wheatstone type [4] 3D stereoscope required bulky optical components for each viewer to perceive 3D depth effect therefore it was not convenient for a group of people due to its cost and bulkiness. Later it was further developed to replace bulky optical components with a pair of glasses. Today's stereoscopic systems [3] employ the form of glasses to solve the issue. The left and right images are projected by projectors/LCDs in either alternatively or overlaid form. Special head-gear glasses such as green-red (or blue-red) filtering glasses, polarizing glasses or LCD shutters glasses [5] enables users to see the left eye image with the left eye and to see the right eye image with the right eye. Stereoscopic systems have their own disadvantages. Besides that they need apparatus for viewing, they cause eye stress after prolong time of viewing. They fail to achieve full natural colour images as the glasses introduce effects to cause the image lighting. In addition, they cannot offer parallax which means users see a scene from a single fixed perspective.

Due to high demand for natural viewing of 3D scene to pursue real-world 3D viewing, autostereoscopic 3D technology has been developed that enables

observers to perceive 3D effects of 3D depth and motion parallax without wearing any special head-gear devices. There are numerous 3D technologies such as multiview [6], holographic [7] and holoscopic [8] "also known as Integral imaging" which pursue autostereoscopic 3D imaging technology.

Multiview 3D technology [6] is based on stereoscopic technology that utilizes parallax barrier or lenticular technology to create multiple view-windows and the observers see two neighbouring view-windows e.g. 1 and 2 or 2 and 3 view-windows to perceive 3D effects without use of any head-gear device. As the observer moves, the view-windows are changed which creates motion parallax. It still simulates human eye technique which has its own limitations e.g. motion sickness, eye fatigue, minimum and maximum viewing limitation and unnatural 3D effect as the viewer focuses on the images.

Holography was initially proposed by D. Gabor in 1948 as an improvement of electron microscopes [10][11], however, it showed great progress as an optical imaging method instead after the improvement of Leith and Upatnieks [12][13][14]. It records the image of a scene by recording the interference fringe pattern formed by the interference of the coherent light source. Although being a significant 3D imaging technology, it has many practical disadvantages. As it utilises coherent light sources to construct a true 3D object in space which makes it impossible to deploy unsupervised environment and due to high end optical requirement, it is rather an expensive approach.

Holoscopic 3D imaging [8] also known as Integral imaging is another major type of autostereoscopic 3D technology that can achieve full natural colour images. It was proposed first by G. Lippmann as integral photography (IP) in 1908 [15]. It mimics fly's eye technique which uses coherent replication of light to construct a true 3D scene in space. Therefore, it offers side effect free 3D depth and motion parallax effect in either continuous unidirectional or omnidirectional parallax depending on the MLA type.

Ives' two-staged recording is the first great improvement on IP that tried to tackle the pseudoscopic image or reversed image problem [16]. The successful development of the one-step integral imaging system solved the pseudoscopic

"inverted depth" problem of the optical image capturing, and makes a step forward towards the future commercial applications[17][18]. IP has been improved and developed gradually into holoscopic 3D imaging, a more comprehensive technology, which includes areas from depth inversing, optical capturing, computer graphics, electronic display, compression and object depth extraction and post-production such as digital refocusing.

1.2   The Research Aim and Objectives

The aim of this research to enhance spatial resolution of holoscopic 3D imaging and display technology as the technology is one of the most promising methods for visualising 3D images, since it provides autostereoscopic viewing without eye fatigue, along with full colour and continues parallax both horizontally and vertically.

Good developments have been made on holoscopic 3D imaging and display technology [19][20][21] including computer graphics 3D rendering.   However, the main challenge remains unresolved such as HD equivalent holoscopic 3D resolutions, immersive motion and depth parallax, holoscopic 3D image conversions, efficient holoscopic 3D computer graphics rendering, immersive 3D data visualisation, and more importantly lack of spatial resolution with high definition of reconstructed H3D scene.

The research will investigate spatial resolution of holoscopic 3D imaging and display technology, which includes design aspect of holoscopic 3D cameras (this includes both real and virtual holoscopic 3D cameras) technology, holoscopic 3D image processing and holoscopic 3D display technology.

Architecture of holoscopic 3D camera will be investigated to improve spatial information such as 3D depth and 3D resolution and also H3D computer graphics rendering techniques will be explored.

H3D image conversion, H3D image stitching, and pre-processing of H3D image will be investigated for advancing the processing of the technology.   Medical image data visualisation will be explored as medical is one of the potential application areas for the technology. In addition, development of H3D content

management system will be explored including 3D content descriptive protocols for enabling interactive 3D multimedia search & retrieval.

In particular, spatial resolution of omnidirectional 3D display will be investigated, therefore it will explore holoscopic 3D pixel mapping techniques to enrich 3D resolutions as well as to achieve better 3D parallax. Currently, the omnidirectional H3D display has equal number of pixels in both horizontal and vertical directions, whereas the horizontal 3D effects e.g. motion parallax is more demanding compared to the vertical direction. Omnidirectional pixel mapping will be investigated to achieve more 3D pixels in horizontal direction.

Objectives of the research involve explorations, development and experimentation of appropriate and practical algorithms / methods for H3D imaging and display technology. The following list highlights the main objectives:

- Prototype omnidirectional and unidirectional holoscopic 3D displays using parallax barrier, lenticular sheet and spherical/square MLA technology.
- Study multiview 3D pixel mapping techniques and apply them to holoscopic 3D display.
- Explore pixel mapping techniques to enhance spatial resolution of unidirectional / omnidirectional holoscopic 3D display as well as quality of reconstructed holoscopic 3D scene in space.
- Develop virtual holoscopic 3D camera plugins for facilitating holoscopic 3D creation in efficient ways.
- Explore holoscopic 3D image reformatting to enhance 3D image compatibility.
- Investigates pre-processing of holoscopic 3D image to filter out noises, which will enhance final image on the playback.
- Investigate holoscopic 3D content visualisation to facilitate holoscopic 3D content search and retrieval.

1.3 The Research Contributions

Figure 1.1 shows summary of contributions in the area of holoscopic 3D camera, processing and display technology.
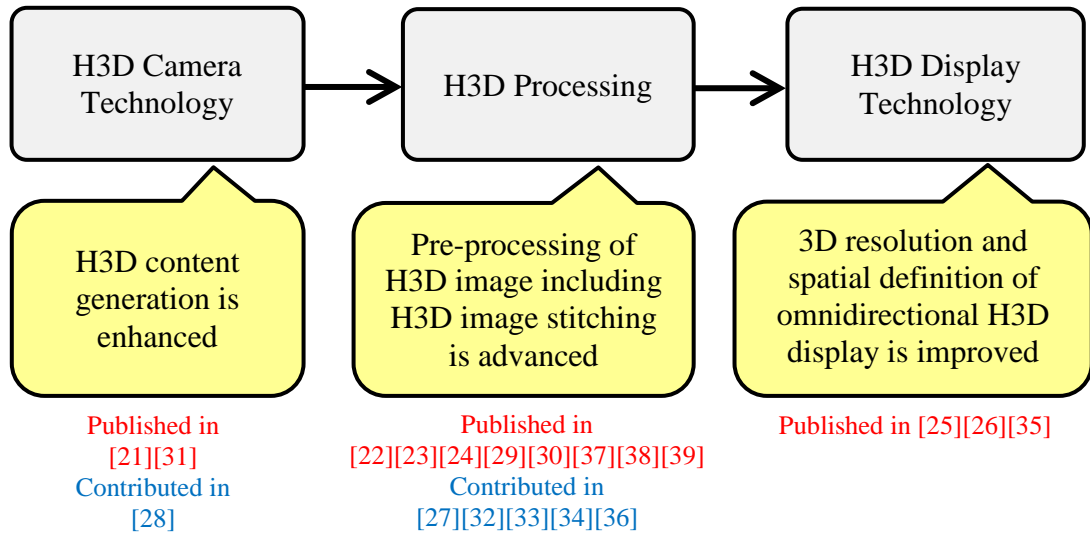
Figure 1.1 - Summary of the research contributions

1.3.1 Holoscopic 3D Camera Technology

Figure 1.2 shows the contributions made in the area of H3D camera technology.
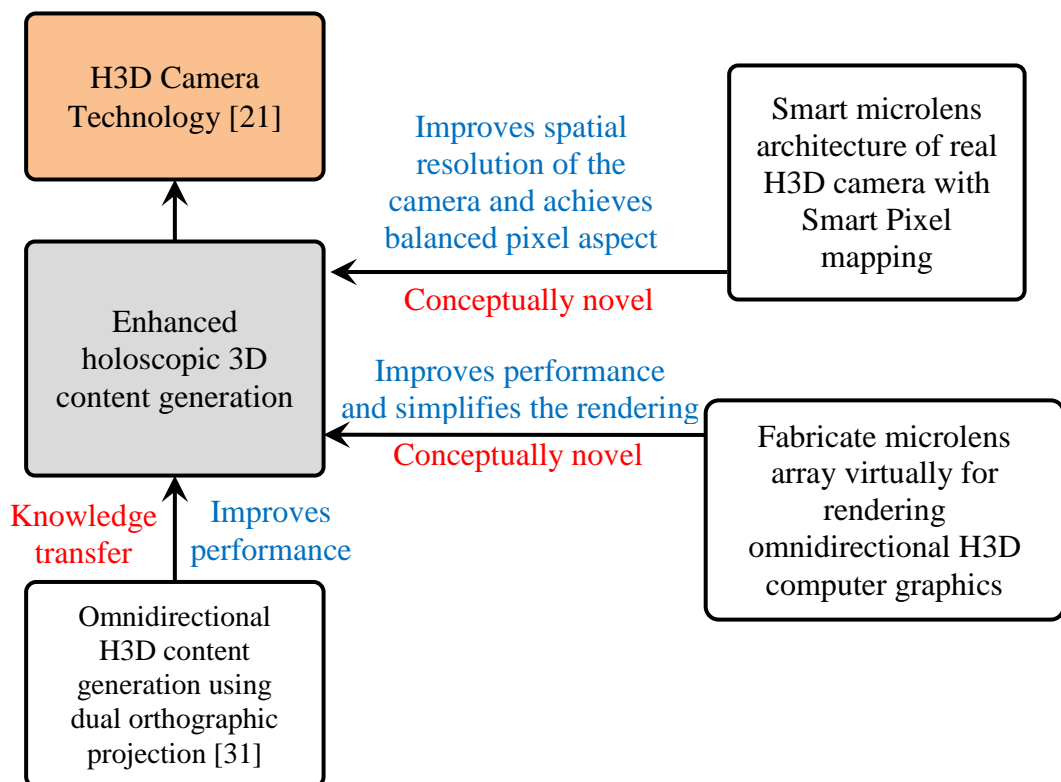
Figure 1.2 - Summary of contributions made in the area of H3D camera technology

- Efficient H3D computer graphics rendering techniques are proposed and implemented that simplify the rendering process to a single step.
- Smart microlens array architecture of H3D camera is proposed that enhances (doubles and triple) spatial resolution of the camera as its smart pixel mapping method pursues scalable approach to achieve the best 3D resolution in the camera level.

1.3.2 Holoscopic 3D Image Processing

Figure 1.3 shows the contributions made in the area of H3D image processing.
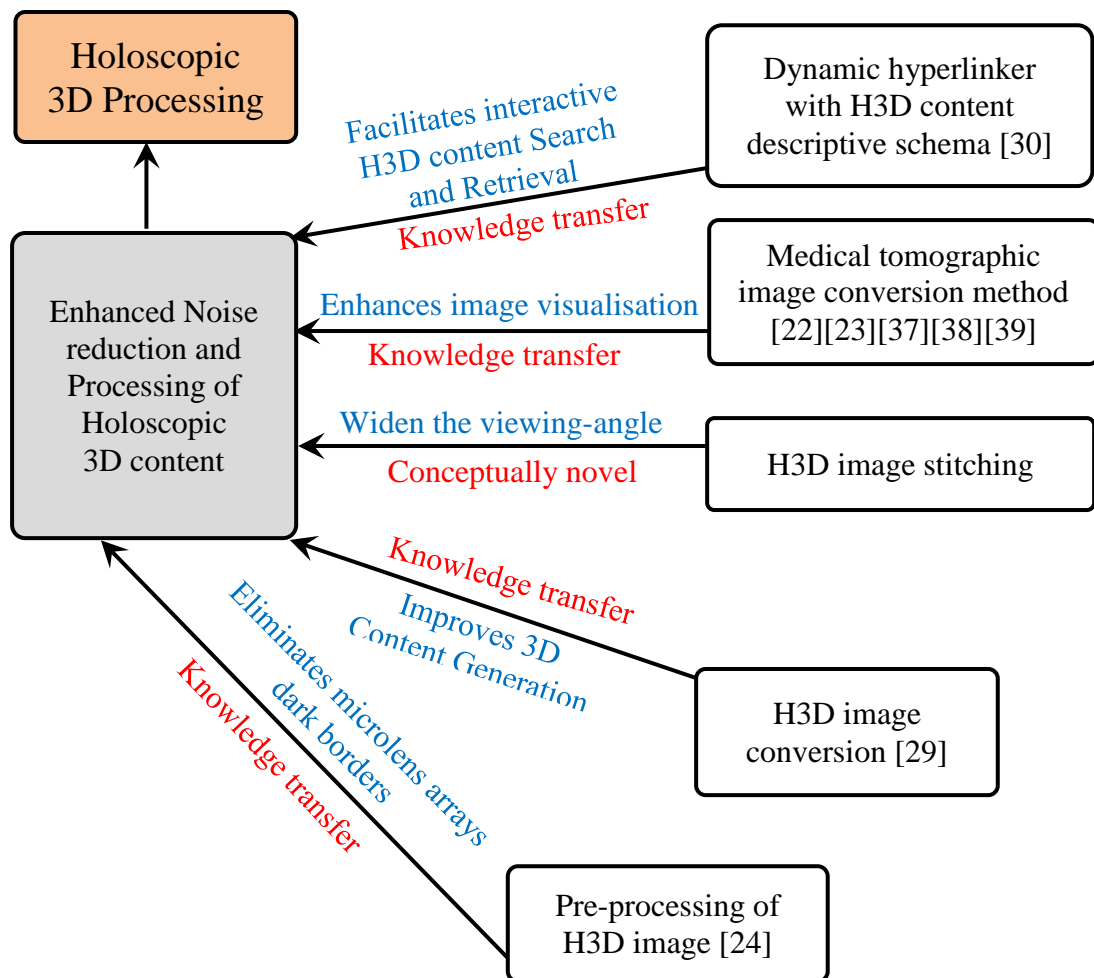
Figure 1.3 - Summary of contributions made in the area of H3D Processing

- Processing of H3D image is improved by automatic calibration grid generation method, self-adaptive reference based dark borders noise reduction technique and H3D image conversion algorithms

- Reference based H3D image stitching algorithm is proposed and implemented that stitches H3D images to widen overall viewing-angle of H3D camera
- Dynamic hyperlinker with 3D content descriptive schema is proposed that facilitates interactive H3D video content search and retrieval

1.3.3 Holoscopic 3D Display Technology

Figure 1.4 shows the contributions made in holoscopic 3D display technology.
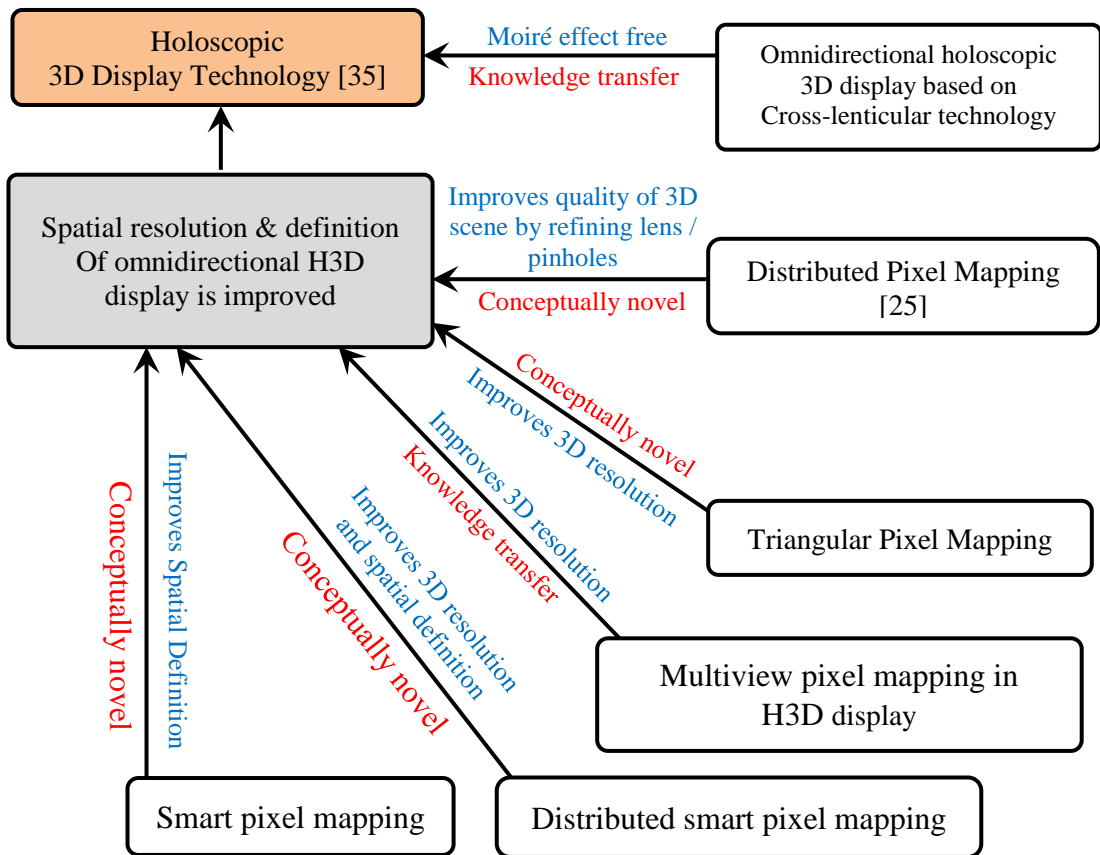
Figure 1.4 - Summary of contributions made in the area of H3D display technology

- Novel pixel mapping methods are proposed that achieves HD equivalent spatial resolution of H3D display. These enable one to achieve scalable 3D pixel aspect ratio of omnidirectional H3D display.
- A novel technique is proposed that eliminates moiré effect of cross-lenticular technology of omnidirectional H3D display. It puts the technology in a good position for mass production.

1.4   The Author's Publications

This section presents the list of journal and conference papers published in international journals and conferences.

i.   **M.R. Swash,** A. Aggoun, O. Abdulfatah, B. Li, J. C. Jacome, E. Alazawi, E. Tsekleves "Pre-Processing of Holoscopic 3D Image For Autostereoscopic 3D Display", 5th International Conference on 3D Imaging (IC3D), Belgium, 3rd – 6th December 2013

ii.   **M.R. Swash,** A. Aggoun, O. Abdulfatah, E. Alazawi, E. Tsekleves, "Distributed Pixel Mapping for Refining Dark Areas in Parallax Barriers Based Holoscopic 3D Displays", 5th International Conference on 3D Imaging (IC3D), Belgium, 3 – 6th December 2013

iii.   **M.R. Swash,** A. Aggoun, O. Abdulfatah, B. Li, J. C. Jacome, E. Alazawi, E. Tsekleves, "Moiré-Free Full Parallax Holoscopic 3D Display based on Cross-Lenticular", 3DTV Conference: Vision beyond Depth AECC, Aberdeen, Scotland, 7-9th October 2013

iv.   O. Abdulfatah, A. Aggoun, **M.R. Swash** , B. Li, J. C. Jacome, E. Tsekleves, "Holoscopic 3D Image Re-formatting for stereoscopic 3D Displays", 3DTV Conference: Vision beyond Depth AECC, Aberdeen, Scotland, 7-9th October 2013 [20%]

v.   E. Alazawi, A. Aggoun, **M. R. Swash**, O. Abdulfatah, M. Abbod and J. Fernandez "Scene Depth Extraction From Holoscopic Imaging Technology", 3DTV-Conference: Vision beyond Depth AECC, UK, 2013 [20%]

vi.   **M.R. Swash**, A. Aggoun, O. Abdulfatah, B. Li, J. C. Jacome, E. Tsekleves, "Holoscopic 3D Image Rendering for Autostereoscopic Multiview 3D Display", IEEE International Symposium on Broadband Multimedia Systems and Broadcasting, London, UK, June 2013.

vii.   **M.R. Swash**, A. Aggoun, O. Abdulfatah, B. Li, J. C. Jacome, E. Tsekleves, "Dynamic Hyperlinker for 3D Search and Retrieval", IEEE International Symposium on Broadband Multimedia Systems and Broadcasting, London, UK, June 2013.

viii. **M.R. Swash**, A. Aggoun, O. Abdulfatah, B. Li, J. C. Jacome, E. Tsekleves, "Omnidirectional Holoscopic 3D Content Generation using Dual Orthographic Projection", IEEE International Symposium on Broadband Multimedia Systems and Broadcasting, London, UK, June 2013.

ix. A. Mehanna, A. Aggoun, O. Abdulfatah, **M. R. Swash**, E. Tsekleves, "Adaptive 3D-DCT based compression algorithms for Integral Images", IEEE International Symposium on Broadband Multimedia Systems and Broadcasting, London, UK, June 2013 [15%]

x. E. Alazawi, A. Aggoun, O. Abdulfatah , **M.R. Swash**, "Adaptive Depth Map Estimation from 3D Integral Images", IEEE International Symposium on Broadband Multimedia Systems and Broadcasting, London, UK, June 2013. [15%] *"Awarded – Best student paper"*

xi. O. Abdulfatah , P. Lanigan, A. Aggoun , **M.R. Swash**, E. Alazawi, B. Li, J. C. Jacome, D. Chen, E. Tsekleves, "Three-Dimensional Integral Image reconstruction based on viewpoint interpolation", IEEE International Symposium on Broadband Multimedia Systems and Broadcasting, London, UK, June 2013 [10%]

xii. J. Makanjuola, A. Aggoun , **M.R. Swash** , P. Grange , B. Challacombe, P. Dasgupta "3D-Holoscopic Imaging: A New Dimension to Enhance Imaging in Minimally Invasive Therapy in Urologic Oncology", Journal of Endourology, Vol. 27 Issue 5, p535, May 2013 [40%]

xiii. A. Aggoun, E. Tsekleves, **M.R. Swash**, D. Zarpalas, A. Dimou, P.Daras, P. Nunes, L.D. Soares "Immersive 3D Holoscopic Video System," MultiMedia, IEEE , vol.20, no.1, pp.28-37, January-March 2013 [20%]

xiv. P. Lanigan, **M.R. Swash**, J. J. Fernandez, A. Aggoun, "Integral Imaging system for capture and display of 3D content", Advances in imaging and displays symposia, Photon12, Durham University, Durham, UK, 3th Sep 2012 [30%]

xv. O. Abdul Fatah, A. Aggoun, M. Nawaz, J.Cosmas, E.Tsekleves, **M. R. Swash**, E. Alazawi, "Depth mapping of Integral images using a hybrid disparity analysis algorithm", IEEE International Symposium On Broadband Multimedia Systems and Broadcasting 2012, Seoul, Korea, 27th Jun 2012 [10%]

xvi. J. Makanjuola , A. Aggoun **, M.R. Swash** , P. Grange , B. Challacombe, P. Dasgupta "3D-Holoscopic Imaging: A New dimension to Enhance Imaging in Minimally Invasive Therapy in Urological oncology", 27th EUS annual meeting, engineering and Urology society, 19th May 2012 [40%] *"Awarded - Top 10 abstracts"*

xvii. J. Makanjuol, P. Grange, A. Aggoun, P. Rouse, P. Lanigan, **M.R. Swash**, H. Yamamoto. "Compound Bionic Eye: A revolutionary dimension in imaging and minimal access therapy", The Cheselden Club: St Thomas' Hospital, London UK. 6th December 2011 [30%]

xviii. J. Makanjuola, P. Grange, A. Aggoun, P. Rouse, P. Lanigan, **M.R. Swash**, H. Yamamoto Compound Bionic Eye: A revolutionary dimension in imaging and minimal access therapy. Journal of Endourology, 25(S1): P1-A373. doi:10.1089/end.2011.2001.supp, November 2011 [30%]

xix. J. Makanjuola, P. Grange, A. Aggoun, P. Rouse, P. Lanigan, **M.R. Swash**, H. Yamamoto. "A Revolutionary Dimension in Imaging and minimal access therapy", 29th World Congress of Endourology and SWL, Kyoto, Japan, 30th Nov. 2011 [30%] *"Selected abstract by the WCE 2011 secretariat on the "take-home-message" 2011 for New Technology and Imaging by Prof. Osamu Ukimura. USC Institute of Urology, Keck School of Medicine of the University of Southern California/Norris Cancer Centre"*

1.5   The Thesis Outlines

This thesis is made of three core chapters, which are holoscopic 3D camera technology, holoscopic 3D image processing, holoscopic 3D display technology with other 3 supplementary chapters "Introduction, exploitation of existing 3D imaging & display technology and conclusions & future work"

1.5.1   Chapter One - Introduction

Chapter one is an introductory chapter, which briefly introduces background of the research, the aim & objectives, the research contributions and the thesis outlines.

1.5.2   Chapter Two - Exploitation of Existing 3D Imaging Technology

Chapter two presents the research literature review. It discusses in details three-dimensional imaging technologies. In particular, it elaborates on state of the art works on H3D imaging and display technology.

1.5.3   Chapter Three - Holoscopic 3D Camera Technology

Chapter three presents a novel method for rendering omnidirectional H3D computer graphics and it also proposes a smart microlens array architecture of H3D camera, which improves visual definition by doubling the spatial resolutions

1.5.4   Chapter four - Holoscopic 3D Image Processing

Chapter four investigates H3D image processing, which includes pre-processing of H3D images, automatic calibration grid generation for barrel distortion correction algorithm and H3D image stitching method. It discusses a 3D image conversion method for reformatting H3D images. In addition, it presents the development of "Dynamic Hyperlinker" with 3D content descriptive protocol to facilitate interactive H3D video content search and retrieval.

1.5.5   Chapter five - Holoscopic 3D Display Technology

Chapter five presents number of pixel mapping techniques to enhance spatial resolution of both unidirectional and omnidirectional H3D displays. In particular, it proposes novel distributed smart pixel mapping for improving 3D resolution and 3D pixel per inch in space, which enrich visual details of reconstructed H3D scene.

1.5.6   Chapter six – Conclusions and Future Work

This chapter presents conclusions of the research findings and development. In addition, it discusses the potential future work in the area of H3D display, camera and processing.

1.5.7   Appendix A – Holoscopic 3D Displays

Appendix A presents development of multiple unidirectional and omnidirectional H3D displays including pixel mapping techniques.

1.5.8   Appendix B – Holoscopic 3D Computer Graphics

Appendix B presents development of virtual H3D camera plugins for commercial CAD tools such as 3Ds MAX including open-source ray-tracing rendering tools.

1.5.9   Appendix C – Holoscopic 3D Image Resampling

Appendix C presents resampling method for H3D images.

1.6   Conclusion

Contributions of H3D camera technology chapter includes omnidirectional H3D computer graphic rendering techniques, which simplifies the rendering process to a single step and smart microlens array architecture of H3D camera, which doubles spatial resolution of H3D camera.

The contributions in the field of H3D imaging processing consists microlens array border noise correction and H3D image conversion algorithm.   In addition, it includes H3D image stitching algorithm, which widens overall viewing angle of H3D camera.

The contributions made in the field of H3D display technology include introduction of pixel mapping to omnidirectional H3D display which enhances the spatial resolution by doubling 3D pixels per inch in space and achieves HD equivalent holoscopic spatial.

1.7   References

[1] J. Hong, Y. Kim, H.J. Choi, J. Hahn, J.-H. Park, H. Kim, S.-W. Min, N. Chen, and B. Lee, "Three-dimensional display technologies of recent interest: principles, status, and issues" Applied optics, vol. 50, no. 34, pp. H87–115, Dec. 2011.

[2] K. W. Bowyer, K. Chang, and P. Flynn, "A survey of approaches and challenges in 3D and multi-modal 3D+2D face recognition," Computer Vision and Image Understanding, vol. 101, no. 1, pp. 1–15, Jan. 2006.

[3] H.J. Choi, "Current status of stereoscopic 3D LCD TV technologies," Journal of 3D Research, vol. 2, no. 2, p. 4, Nov. 2011.

[4] N. VALYUS, Stereoscopy, 1st Edition. London: Focal Press, 1996.

[5] S. Kratomi, "Stereoscopic Apparatus Having Liquid Crystal Filter Viewer", US patent US3737567, 1972.

[6] H. Urey, K. V Chellappan, E. Erden, and P. Surman, "State of the Art in Stereoscopic and Autostereoscopic Displays," Proceedings of the IEEE, vol. 99, no. 4, pp. 540–555, Apr. 2011.

[7] A. Yöntem and L. Onural, "Integral imaging based 3D display of holographic data", Optics express, vol. 20, no. 22, pp. 2359–2375, 2012.

[8] A. Aggoun, "3D Holoscopic video content capture, manipulation and display technologies," 2010 9th Euro-American Workshop on Information Optics, pp. 1–3, Jul. 2010.

[9] T. Okoshi "Three-Dimensional Imaging Techniques", Academic Press, Inc., ISBN-10: 0982225148, London, UK. 1976

[10]   D. Gabor "A new microscope principle", Nature – Journal of science, no. 161, pp. 777-779, doi:10.1038/161777a0, 1948.

[11]   D. Gabor "Microscopy by reconstructed wavefronts", Proceedings of the Royal Society of London. Series A. Mathematical and Physical Sciences,Proc. Phys. Soc., no. A194, pp. 454-487, 1949.

[12]   E. N. Leith, J. Upatnieks "Reconstructed wavefronts and communication theory", Journal of the Optical Society of America, vol. 52, no.10, pp. 1123-1130, 1962.

[13]   E. N. Leith, J. Upatnieks "Wavefront reconstruction with continuous-tone objects", Journal of the Optical Society America, vol. 53, no.12, pp. 1377-1381, 1963.

[14]   E.N. Leith, J. Upatnieks, "Wavefront reconstruction with diffused illumination the three-dimensional objects", Journal of the Optical Society America, vol. 54, no.11, pp. 1295-1301, 1964.

[15]   G. Lippmann, "La Photographies integrals," Comptes Rendus de l'Académie des Sciences, pp. 446-451, 1908

[16]   H. E. Ives, "Optical properties of a Lippmann lenticulated sheet," Journal of the Optical Society America, 21, 171-176 (1931).

[17]   N. Davies, M. McCormick, and L. Yang "Three dimensional imaging systems: A new development", Appl. Optics, 27, pp. 4520-4528, 1988.

[18]   N. Davies, and M. McCormick "Holoscopic Imaging with True 3-D Content in Full Natural Colour", Journal of Photographic Science, vol. 40, pp.46-49, 1992.

[19]   J.H. Park, K. Hong, and B. Lee, "Recent progress in three-dimensional information processing based on integral imaging." Applied optics, vol. 48, no. 34, pp. H77–94, Dec. 2009.

[20]   Y. Kim, K. Hong, and B. Lee, "Recent researches based on integral imaging display method," Journal of 3D Research, vol. 1, no. 1, pp. 17–27, Aug. 2010..

[21]   A. Aggoun, E. Tsekleves, **M.R. Swash,** D. Zarpalas, A. Dimou, P.Daras, P. Nunes, L.D. Soares "Immersive 3D Holoscopic Video System," MultiMedia, IEEE , vol.20, no.1, pp.28-37, Jan.-March 2013

[22]   J. Makanjuola, A. Aggoun , **M.R. Swash** , P. Grange , B. Challacombe, P. Dasgupta "3D-Holoscopic Imaging: A New Dimension to Enhance Imaging in Minimally Invasive Therapy in Urologic Oncology", Journal of Endourology, May 2013, Vol. 27 Issue 5, p535

[23]   J. Makanjuola, P. Grange, A. Aggoun, P. Rouse, P. Lanigan, **M.R. Swash**, H. Yamamoto Compound Bionic Eye: A revolutionary dimension in imaging and minimal access therapy. Journal of Endourology. November 2011, 25(S1): P1-A373. doi:10.1089/end.2011.2001.supp.

[24]   **M.R. Swash,** A. Aggoun, O. Abdulfatah, B. Li, J. C. Jacome, E. Alazawi, E. Tsekleves "Pre-Processing of Holoscopic 3D Image For Autostereoscopic 3D Display", 5th International Conference on 3D Imaging (IC3D). 2013

[25]   **M.R. Swash,** A. Aggoun, O. Abdulfatah, E. Alazawi, E. Tsekleves, "Distributed Pixel Mapping for Refining Dark Areas in Parallax Barriers

Based Holoscopic 3D Displays", 5th International Conference on 3D Imaging (IC3D). 2013

[26]   **M.R. Swash,** A. Aggoun, O. Abdulfatah, B. Li, J. C. Jacome, E. Alazawi, E. Tsekleves, "Moiré-Free Full Parallax Holoscopic 3D Display based on Cross-Lenticular", 3DTV-CON: Vision beyond Depth AECC, Aberdeen, Scotland, 7-9th October 2013

[27]   O. Abdulfatah, A. Aggoun, **M.R. Swash** , B. Li, J. C. Jacome, E. Tsekleves, "Holoscopic 3D Image Re-formatting for stereoscopic 3D Displays", 3DTV-CON: Vision beyond Depth AECC, Aberdeen, Scotland, 7-9th October 2013

[28]   E. Alazawi, A. Aggoun, **M. R. Swash**, O. Abdulfatah, M. Abbod and J. Fernandez "Scene Depth Extraction From Holoscopic Imaging Technology", 3DTV-CON: Vision beyond Depth AECC, UK, 2013

[29]   **M.R. Swash**, A. Aggoun, O. Abdulfatah, B. Li, J. C. Jacome, E. Tsekleves, "Holoscopic 3D Image Rendering for Autostereoscopic Multiview 3D Display", IEEE International Symposium on Broadband Multimedia Systems and Broadcasting, London, UK, June 2013.

[30]   **M.R. Swash**, A. Aggoun, O. Abdulfatah, B. Li, J. C. Jacome, E. Tsekleves, "Dynamic Hyperlinker for 3D Search and Retrieval", IEEE International Symposium on Broadband Multimedia Systems and Broadcasting, London, UK, June 2013.

[31]   **M.R. Swash**, A. Aggoun, O. Abdulfatah, B. Li, J. C. Jacome, E. Tsekleves, "Omnidirectional Holoscopic 3D Content Generation using Dual Orthographic Projection", IEEE International Symposium on Broadband Multimedia Systems and Broadcasting, London, UK, June 2013.

[32]   A. Mehanna, A. Aggoun, O. Abdulfatah, **M. R. Swash**, E. Tsekleves, "Adaptive 3D-DCT based compression algorithms for Integral Images", IEEE International Symposium on Broadband Multimedia Systems and Broadcasting, London, UK, June 2013

[33]   E. Alazawi, A. Aggoun, O. Abdulfatah , **M.R. Swash**, "Adaptive Depth Map Estimation from 3D Integral Images", IEEE International Symposium on Broadband Multimedia Systems and Broadcasting, London, UK, June 2013.

[34]   O. Abdulfatah , P. Lanigan, A. Aggoun , **M.R. Swash**, E. Alazawi, B. Li, J. C. Jacome, D. Chen, E. Tsekleves, "Three-Dimensional Integral Image

reconstruction based on viewpoint interpolation", IEEE International Symposium on Broadband Multimedia Systems and Broadcasting, London, UK, June 2013.

[35]   P. Lanigan, **M.R. Swash**, J. J. Fernandez, A. Aggoun, "Integral Imaging system for capture and display of 3D content", Advances in imaging and displays symposia, Photon12, Durham University, Durham, UK, 3th Sep 2012

[36]   O. Abdul Fatah, A. Aggoun, M. Nawaz, J.Cosmas, E.Tsekleves, **M. R. Swash**, E. Alazawi, "Depth mapping of Integral images using a hybrid disparity analysis algorithm", IEEE International Symposium On Broadband Multimedia Systems and Broadcasting 2012, Seoul, Korea 27th Jun 2012

[37]   J. Makanjuola , A. Aggoun **, M.R. Swash** , P. Grange , B. Challacombe, P. Dasgupta "3D-Holoscopic Imaging: A New dimension to Enhance Imaging in Minimally Invasive Therapy in Urological oncology", 27th EUS annual meeting, engineering and Urology society, 19th May 2012

[38]   J. Makanjuol, P. Grange, A. Aggoun, P. Rouse, P. Lanigan, **M.R. Swash**, H. Yamamoto. "Compound Bionic Eye: A revolutionary dimension in imaging and minimal access therapy", The Cheselden Club: St Thomas' Hospital, London UK. 6th December 2011

[39]   J. Makanjuola, P. Grange, A. Aggoun, P. Rouse, P. Lanigan, **M.R. Swash**, H. Yamamoto. "A Revolutionary Dimension in Imaging and minimal access therapy", 29th World Congress of Endourology and SWL, Kyoto, Japan, 30th Nov. 2011

2   Chapter Two - Exploitation of Existing 3D Imaging Technology

This chapter presents exploitation of existing 3D imaging technology in the research area. It covers overview of state of the art 3D imaging technology, which includes stereoscopic, multiview, holographic, compressive and holoscopic imaging. In addition, it presents depth studies of holoscopic 3D imaging technology. The layout of the chapter is as follows: 2.1 Introduction, 2.2 Stereoscopic 3D Imaging Technology, 2.3 Autostereoscopic 3D Imaging Technology, 2.3.1 Multiview, 2.3.2 Holographic, 2.3.3 Volumetric, 2.3.4 Compressive, 2.3.5 Holoscopic and 2.4 Conclusion.

2.1   Introduction

Three-dimensional (3D) imaging technology [1] is a success story of digital imaging as it replicates real world effects such as 3D depth and motion parallax. It enables observers to experience the real world 3D effects. It also overcomes some of other 2D imaging limitations such as object size "depth measurement" because it offers more low-level features and cues compared to 2D imaging technology.   In fact, there are several types of 3D imaging system, which offer real-world 3D effect(s) but their concepts are different. They are divided into two major types [2]:

   I.   Stereoscopic 3D imaging
  II.   Autostereoscopic 3D imaging

Stereoscopic 3D imaging technology [3] is the early version that utilises two perspective images, which are for the left and right eye respectively to achieve the 3D depth effect. It requires the observers to wear special apparatus to channel the images to the corresponding eye. This is a human eye technique.

Autostereoscopic 3D imaging technology [4] pursues real-world 3D experience and viewing by enabling observers to perceive 3D effect(s) with the naked eyes. In fact it offers both 3D depth and motion parallax. There are numerous autostereoscopic 3D imaging systems such as multiview [6], holographic [7], compressive [47] and holoscopic [7].

2.2   Stereoscopic 3D Imaging Technology

Wheatstone stereoscope 3D (S3D) system was the early version that was proposed by Sir Charles Wheatstone in 1838 [2][4]. It requires bulky optical components for each viewer to perceive 3D depth effect. Later the technology was further developed to replace bulky optical components with a pair of glasses. The left and right images are projected by projectors/LCDs either alternatively or overlaid. The special glasses such as anaglyph, polarized or shutters glasses "also known as time multiplexed" [5] enable observers to see the left eye image with the left eye and to see the right eye image with the right eye.
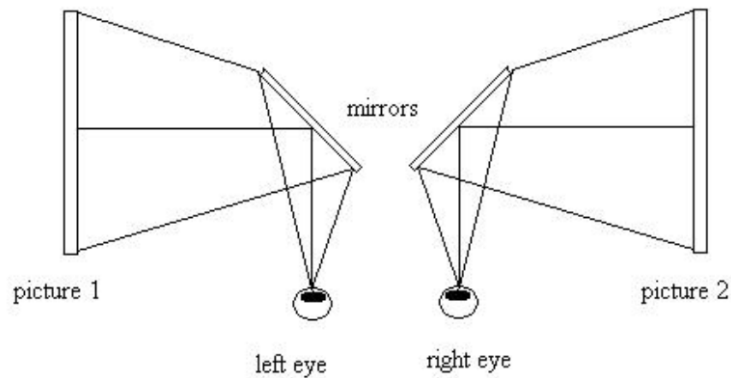
Figure 2.1 – Illustration of concept of Wheatstone's stereoscope [2]

Anaglyph method use colour coded image projection to separate the views with colour glasses from left eye and right eye. The viewer observes the opposite colour of the images projected to the viewer glasses colour to the left and right eye simultaneously. The glasses shown in Figure 2.2 (a) are mainly used for the separation of the views to give the perception of depth to the viewer [10].

(a) Anaglyph glasses   (b) polarized glasses   (c) shutter glasses
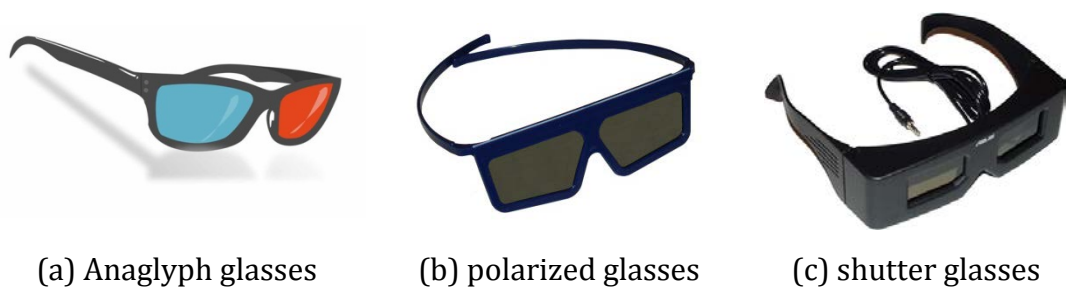
Figure 2.2 - Stereoscopic 3D glasses [11]

The most modern version of 3D system in the entertainment industry used is the perpendicular polarization technique where, it projects the two separate views simultaneously and the observers wears the specially made polarised glasses to perceive the left/right images. The polarised glasses as shown in Figure 2.2(b) are used to filter views to deliver the correct view to the eyes [12]. Both linear and circular polarisation works in the same principle but the only benefit of circular polarisation have over linear is to allow the viewer to tilt their head without disturbing the effect of 3D perception [13][14].

The Time division technique "Shutter glasses" is highly recognised as 'active shutter' in commercial industry, and it works in such a way that left and right frames are displayed in sequence one after the other in a very high frame rate [15]. The active shutter glasses shown in Figure 2.2(c) is required to

synchronise with the display, in a way that one of the eye to sees nothing while the other eye sees the correct image and few microseconds later the situation is reversed [5].

Stereoscopic 3D imaging systems have their own disadvantages besides that they require observers to wear special glasses. They cause eye stress after prolong time of viewing, fail to achieve full natural colour intensity as the glasses cause the image lightings. In addition, there is no motion parallax, which means the observer(s) see a 3D scene of a single fixed perspective [16][17].

2.3   Autostereoscopic 3D Imaging Technology

Although all autostereoscopic 3D imaging techniques offer observers perceiving 3D effects with naked eyes, their concept and mechanism are different.

2.3.1   Multiview 3D Imaging Technology

Multiview 3D imaging technology [6] mimics the stereoscopic concept and it is based on the human eye technique. It was first proposed to window multiple perspective view-windows using parallax barrier technology [18]. It targets to pursue real world 3D perception, which offers infinite convenient views as shown in Figure 2.3 (a) whereas multiview 3D technology offers finite views and one perceives the closed convenient views as shown Figure 2.3 (b).
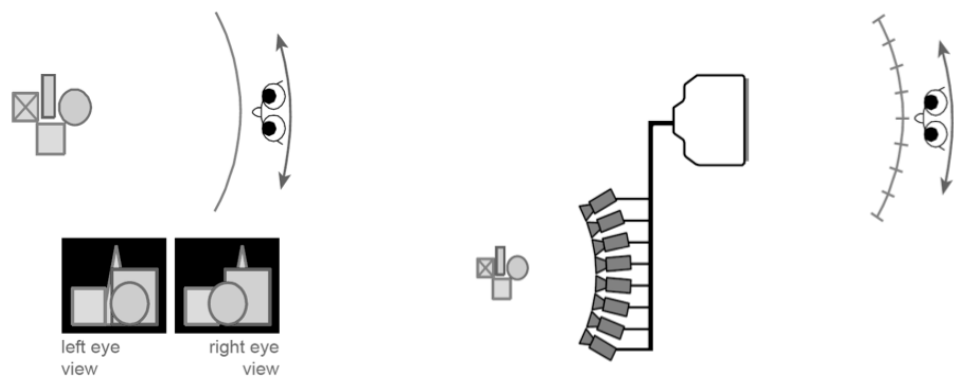
(a) Real world 3D perception   (b) Multiview 3D perception

Figure 2.3 - Illustration of principle of multiview 3D imaging vs. real world [19]

Later the concept's functional apparatus was developed by Frederic Ive in 1901 that uses the parallax barrier technology to create multiple view-windows and the observer sees two neighbouring view-windows e.g. 1 and 2 or 2 and 3 view-

windows to perceive 3D effects without using any headgear device as shown in Figure 2.4. As the observer moves horizontally, the view-windows are changed respectively which creates motion parallax. It was a great development however it has its own limitations e.g. motion sickness, eye fatigue, minimum and maximum viewing distance and unnatural 3D effects.
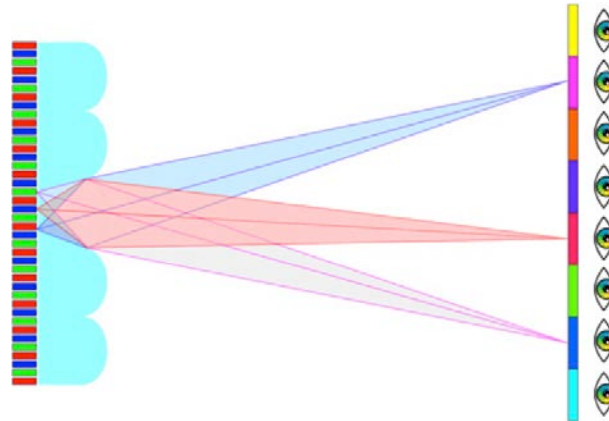
Figure 2.4 – The concept of windowing multiple views in multiview 3D technology [19]

The observer has to be within a defined distance range to perceive 3D effects as shown in Figure 2.4. In the case where the observer is not viewing from the recommended distance and standing point(s), the 3D effect is lost and the observer sees noised image e.g. ghost / cross-talk noise due to viewing from confusion or unsupported zone. Later head-tracking [20] concept was proposed to resolve this issue, which in fact resolves the issue but for a single user. However, the proposed head-tracking concept was not successful in supporting multiple users simultaneously.

In addition, Parallax barrier technology suffers from lighting, as it is based on occlusion of light as shown in Figure 2.5(a). As a result it was dim due to dark areas between pinholes, which separate and create view-windows. Later the concept was further developed and improved to resolve the lighting issue with lenticular technology [21] as shown in Figure 2.5(b). Lenticular technology was introduced to use index of refraction to separate and create multiple left eye and right eye images. However, it works the same way as parallax barrier technology but offers a better image lighting quality.
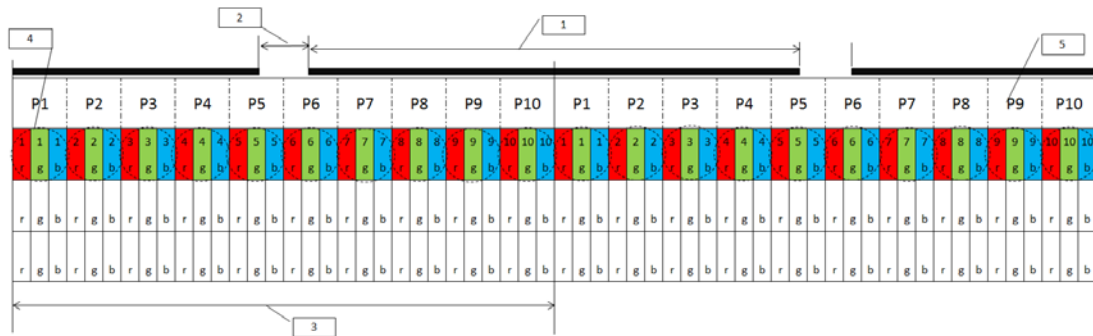
(a) Parallax Barriers: View pixels representation: (1) dark distance between pinholes, (2) pinhole which shows one pixel from a particular angle, (3) lens pitch, (4) view pixel for one perspective view, (5) view pixel numbers
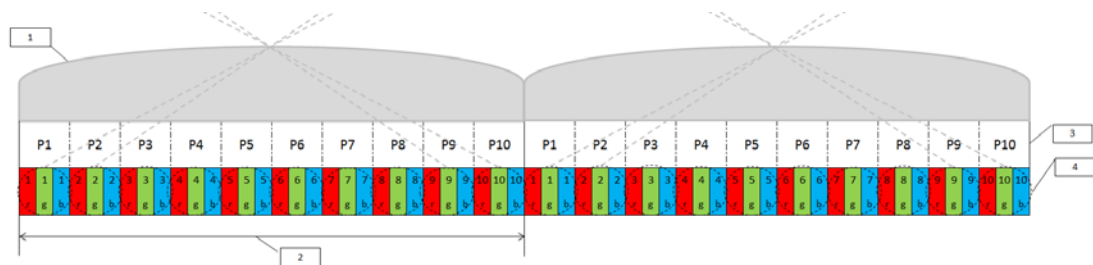
(b) Lenticular Sheet: Viewpoint pixels representation (1: Microlens array, 2: Microlens-pitch size, 3: Pixels per lens, 4: Viewpoint pixel structure)

Figure 2.5 – 3D Display pixel mapping: (a) Parallax barriers and (b) Lenticular sheet
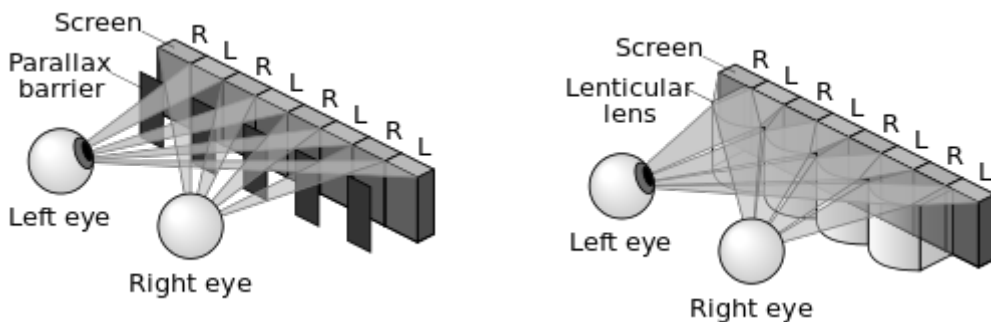
(a) parallax barrier technology   (b) lenticular technology

Figure 2.6 - Principle of multiview 3D display based on parallax barrier and lenticular [1]

Lenticular technology achieved much brighter image lighting quality, which was the only advantage in comparison to the parallax barrier technology whereas lenticular technology suffers from moiré effect.   Generally, moiré effect is a natural interference phenomenon that occurs when two separate patterns are overlapped.   In this case, the lenticular sheet's pattern matches with the LCD

pixel sheet, which causes moiré effect [22]. The moiré effect was reduced / removed by slanting either LCD pixel sheet as shown in Figure 2.7.
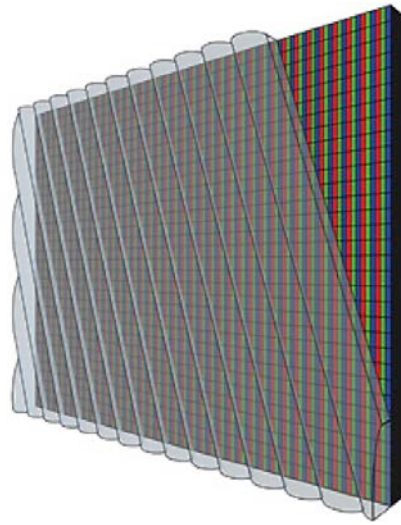
Figure 2.7 - Slanted lenticular sheet illustration on the LCD pixel sheet [26]

The slanting approach opened a new direction of the research for more investigations. Philips 3D research team proposed different multiview pixel mapping methods [23][24], which remaps multiview 3D images in such a way to achieve slanting angle of 9.46° degrees which reduces the moiré effect at a reasonable level for viewing and improves 3D resolution by trading-off horizontal and vertical resolutions.

The pixel mapping techniques separate sub-pixels (Red, Green, Blue sub-pixel) of a view pixel in vertical direction that uses the vertical resolution to enhance the horizontal resolution. Because a sub-pixel size is used to project a single pixel data, more 3D pixels can be fitted compared to the traditional approach. In addition, the lens array gets slanted as the sub-pixels are distributed in vertical direction. In particular, the pixel mapping techniques have been applied to state of the art multiview 3D displays available commercially [25].

The Alioscopy pixel mapping [26] method spreads a viewpoint pixel into 3 rows by shifting horizontally as illustrated in Figure 2.8-(a). This process creates 18.43 degrees slanting thus the lens array needs to be slanted by 18.43 degrees. As it fits a pixel into a subpixel, it triples the horizontal 3D resolution where the vertical resolution is reduced to 1/3 and the 3D-DPI remains unchanged.

However the Philips pixel mapping enhances 3D-DPI by two as shown in Figure 2.8-(b). Because it reduces the distance of two consecutive viewpoint pixels, it offers rich depth parallax with smooth transition between viewing zones.
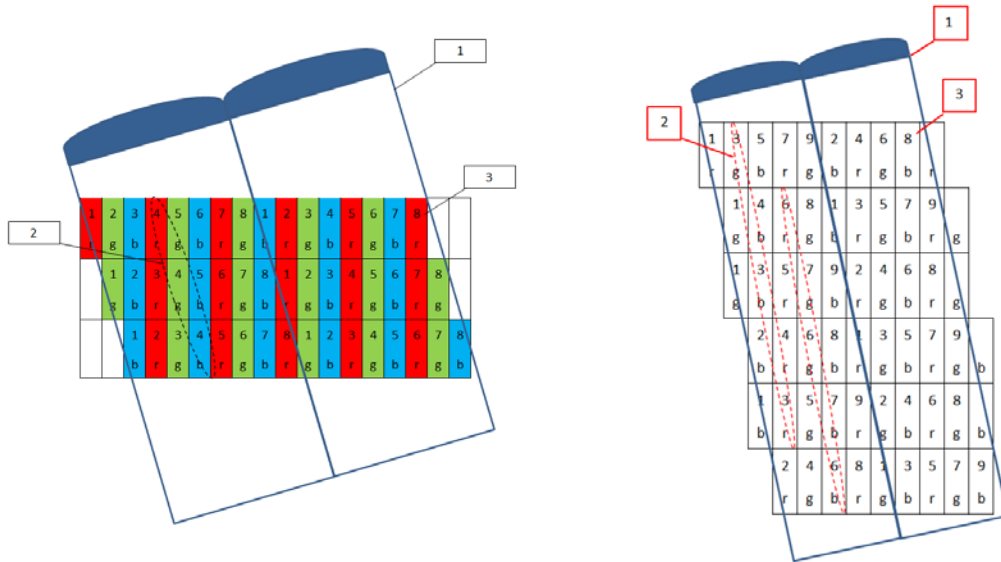
(a) Alioscopy pixel mapping [26]   (b) Philips pixel mapping [23]

Figure 2.8 - State of the art pixel mapping techniques: (a) Alioscopy pixel mapping [26], (b) Philips pixel mapping [23] (1: microlens lens array, 2: construction of a single viewpoint pixel, 3: number of pixels per lens)

The pixel mapping methods reduce vertical 3D resolutions and enhance horizontal 3D resolutions. For instance, the Figure 2.8-(a) is the pixel mapping which is implemented in Alioscopy displays that divides the vertical 3D resolutions by 3 and multiplies the horizontal 3D resolutions by 3 because it uses a physical subpixel size to project a pixel. On the other hand, the Philips pixel mapping technique doubles the 3D resolution because it maps subpixels in to two layers thus half of a physical subpixel is used to project a full pixel as shown in Figure 2.8-(b). This pixel mapping method divides the vertical 3D resolutions by six and multiplies the horizontal 3D resolutions by six.

There have been good developments in multiview 3D technology and also 2D content migration to multiview 3D content is much easier compared to any other autostereoscopic 3D technology such as holographic and holoscopic. As a result, multiview 3D technology is considered to be the technique with the easy integration with stereoscopic 3D (S3D) as virtual view images can be rendered from S3D content [27].

Multiview 3D content is generated using multiple perspective 2D cameras. Traditionally, number of cameras is defined by number of views supported by the multiview 3D display. For instance, Alioscopy multiview 3D display has 8 views or 8 pixels per lens. Thus its 3D content shall be generated using 8 2D cameras. It has been simplified by generating view-images e.g. 8 views from 2D-Plus-Depth or stereoscopic pair images [28]. In fact, most of multiview 3D displays have embedded 3D rendering engine, which generates required view-images from 2D-Plus-Depth image and there have been different techniques that are applied to improve the result for real time 3D content streaming [28]. In addition, the algorithms were proposed for converting 2D images to 3D images by generation a depth map of the 2D image [29].

However, the multiview 3D images generated from 2D-Plus-Depth / stereoscopic pair images are not as effective as generating from multiple cameras because there is not enough angular visual information.
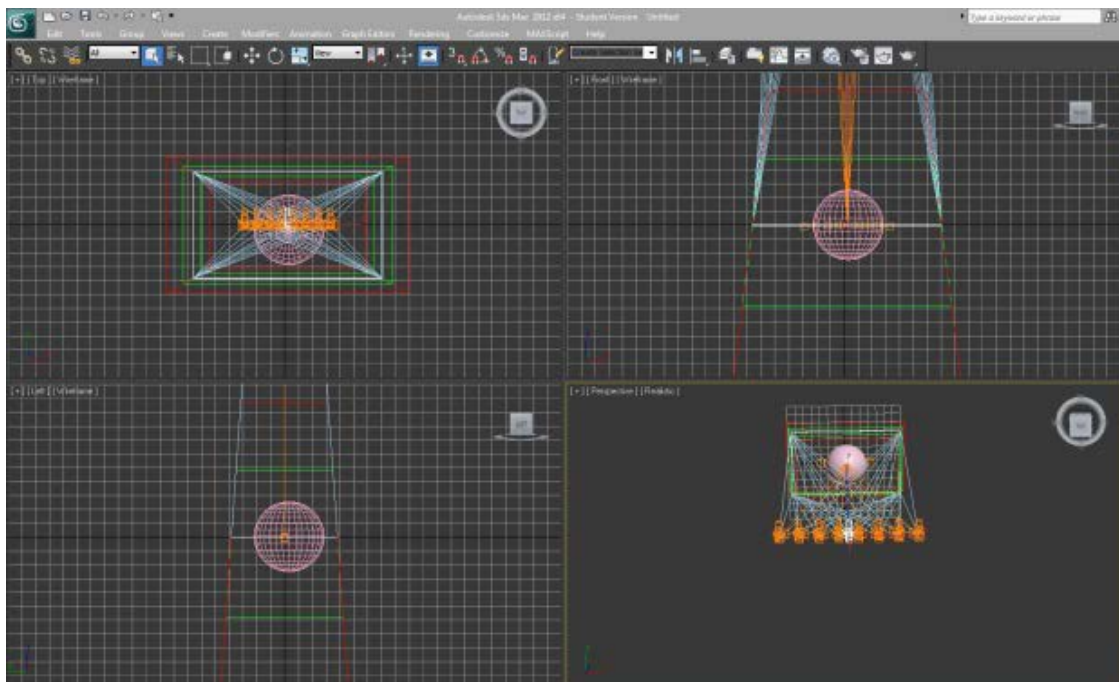
Figure 2.9 – Camera setup for rendering virtual multiview 3D content using Alioscopy plugin in 3Ds MAX [26]

Multiview 3D computer graphic images are made easy by having multiple 2D virtual cameras in three-dimensional scene which pursue the same concept as generating real multiview 3D content. In fact, almost all multiview 3D displays

have virtual 3D camera plugins for CAD tools such as 3Ds MAX and Maya as shown in Figure 2.9 [26]. However, it is rather computationally expensive due to rendering all view images. Therefore there is not a real time virtual 3D rendering tool instead virtual multiview 3D image generation is carried out offline.

Multiview 3D content creation is rather complicated due to the synchronisation of multiple 2D cameras and 2D-plus-depth images do not offer sufficient spatial information; therefore there is a need of a better 3D imaging technology which offers easier and simpler recording with acceptable 3D visualisation.

2.3.2 Holography 3D Imaging Technology

Holographic 3D imaging technology "also known as holography" is the complete three-dimensional imaging system that offers 3D depth and motion parallax in complete directions by constructing a 3D scene in space. The principle of holographic was established by Denis Gabor in 1948 [30][31]. The idea is recording light wave interference patterns which later illuminated with suitable light for re-producing the scene.
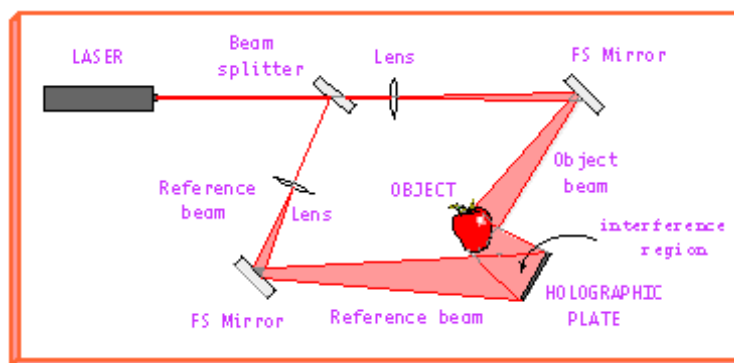
Figure 2.10 – Illustration of holography principle [36]

Figure 2.10 illustrates the basic principle of holographic 3D imaging. One way of recording hologram is to split the laser beam into two. One beam aimed directly to the film passing through the lens spreading the beam on the film plate and the other reflects off the object onto a film, causing a beam to reflect light off the object with slight delay on the film.

During the replay process, a 3D image of the original object appears when the hologram is illuminated from the original direction of the reference beam. The

produced 3D images are virtually indistinguishable from real objects. By shifting position, the viewer can look around or over objects in the foreground to see what is behind them.

The distinctive characteristic is the idea of recording both the phase and the amplitude of the light waves from an object. Since all recording materials respond only to the intensity in the image, it is necessary to convert the phase information into variations of intensity. Holographic 3D technology performs this by interfering coherent light from the object and the reference beams derived from the same source.

There have been good developments and enhancements to the foundation in both viewing conditions and fabrication techniques [32]-[36]. Depending on the precise materials and technique used in the capture process, reconstruction may take place under coherent or incoherent illumination. The white light reflection hologram, which can be found on credit cards, magazine covers and recording packaging [35]. These are perhaps one of the best known developments from the earlier hologram. However, problems exist when attempting to transfer the holographic technique to the display of moving spatial images. An additional problem is the capture of natural scenes as there are the requirements in making hologram for coherent light sources, dark room conditions and high mechanical stability during recording. These considerations reduce the practical utility of the holography technique for general 3D spatial video imaging applications. On the other hand, there has been a great development on holographic 3D display technology.

Figure 2.11 - Holografika HoloVisio 3D Display [38]

Recently, Holografika [38] managed to deploy a holographic flavored 3D display "HoloVisio display" which offers only 180° degrees viewing angle. HoloVisio

display [38] is based on holographic geometrical principles with special focus on reconstructing the key elements of spatial vision [37]. It pursues traditional LCD display approach and looks like a 2D LCD monitor from outside. However, it requires a cluster of 4 or 12 PCs to run the display.

The technology is still computationally expensive and commercially unaffordable. Having said that, it could be a candidate for medical and military application as it can offer flicker-free 180° degrees viewing zone and the quality of constructed 3D object looks real and immersive as shown in Figure 2.11.

Recently, holographic image reformatting algorithm has been proposed which converts holographic 3D image to holoscopic 3D image [39]. The reformatting method converts a diffraction pattern into an elemental image set in order to display the image on a holoscopic 3D display. It was achieved by generating elemental images based on diffraction calculations as an alternative to commonly used ray tracing methods.

2.3.3 Volumetric 3D Imaging Technology

Volumetric 3D imaging technology offers complete parallax as wide as 360° degrees; most volumetric displays are portrayed as large transparent spheres with imagery seeming to hover inside [40]. It allows the generation, absorption or scattering of visible radiation from a set of localized and defined regions within a physical volume [41].

The most common architectures use a rotating projection screen, a gas or a series of liquid crystal panels and Figure 2.12 shows a demo of swept-screen volumetric display system. In this system, a three-dimensional data set is first converted into a series of "slices," similar to thin slices of an apple around its core i.e. tomographic oriented. The slices are stored in a memory bank. A high-speed digital projector illuminates a rotating screen with hundreds of slices of voxel data at a reasonable frequency. Viewers perceive a sharp 3D image due to the fusion caused by the persistence of vision in the eye.

The unique benefit of volumetric 3D technology is that it offers large fields of view such as 360 degrees around the display. The constructed 3D scene is

viewable simultaneously by a number of people which fits around the display. On the other hand, the technology is always difficult to design and manufacture which limits its application areas. However, it is highly adapted and applicable in medical, military and mechanical medical aid design [42].
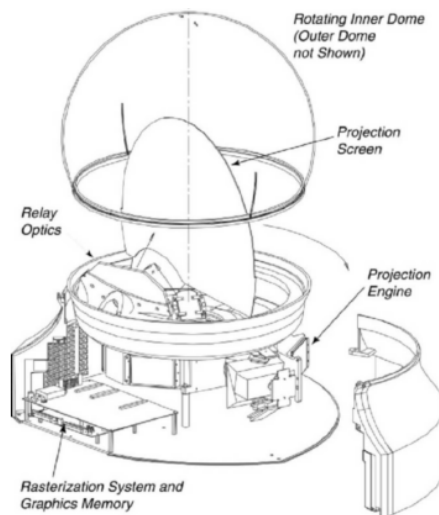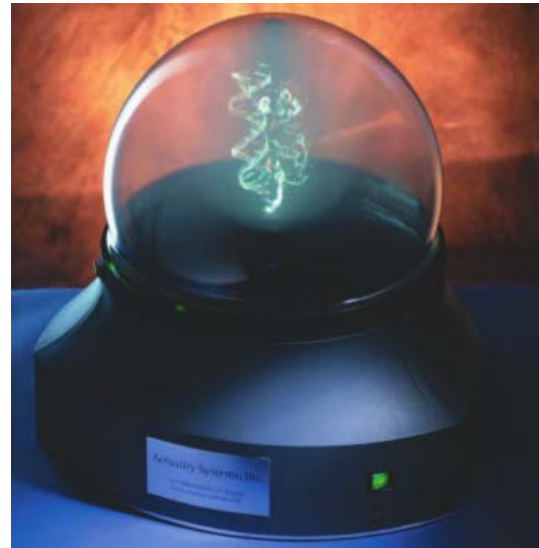
<div align="center">(a) Systematic   (b) Product</div>

Figure 2.12 – Illustration of concept of volumetric 3D imaging technology: (a) the display design designated to project a series of 2D patterns in rotation manner which construct's volumetric 3D scene: (b) playback of volumetric image in 360 angles [42]

2.3.4 Compressive Imaging Technology

Compressive imaging technology [47] was first proposed by MIT research team in 2010. The motivation of this technology is the generation of holographic 3D video content which requires capturing, storing, transmitting, and decoding terabytes of data per second. With the current technology, this is not being efficient. Therefore, tensor display was proposed to target the bandwidth limitations.

MIT research team has invented a series of techniques [43]-[47] to exploit the coherence in nearby views of 3D scenes. Various techniques were proposed to depict 3D scenes, without the need for any head-gear device. It was achieved with optimised optical hardware and co-designed "compressive" image-encoding algorithms. So far, variations of compressive displays techniques have been explored that are primarily composed of multiple layers of high-speed LCDs. The List of different variations of compressive 3D imaging technology is as follows:

High-Rank 3D [43][44] was assembled with a pair of modified LCD panels is stacked. Rather than using heuristically-defined parallax barriers, it was proposed to generate 2 flat 2D images "front LCD and back LCD images" from the 3D image and parallax barriers respectively. Both LCD layers can be simultaneously optimized for the multi-view content. It improves and increase brightness and refresh rate.
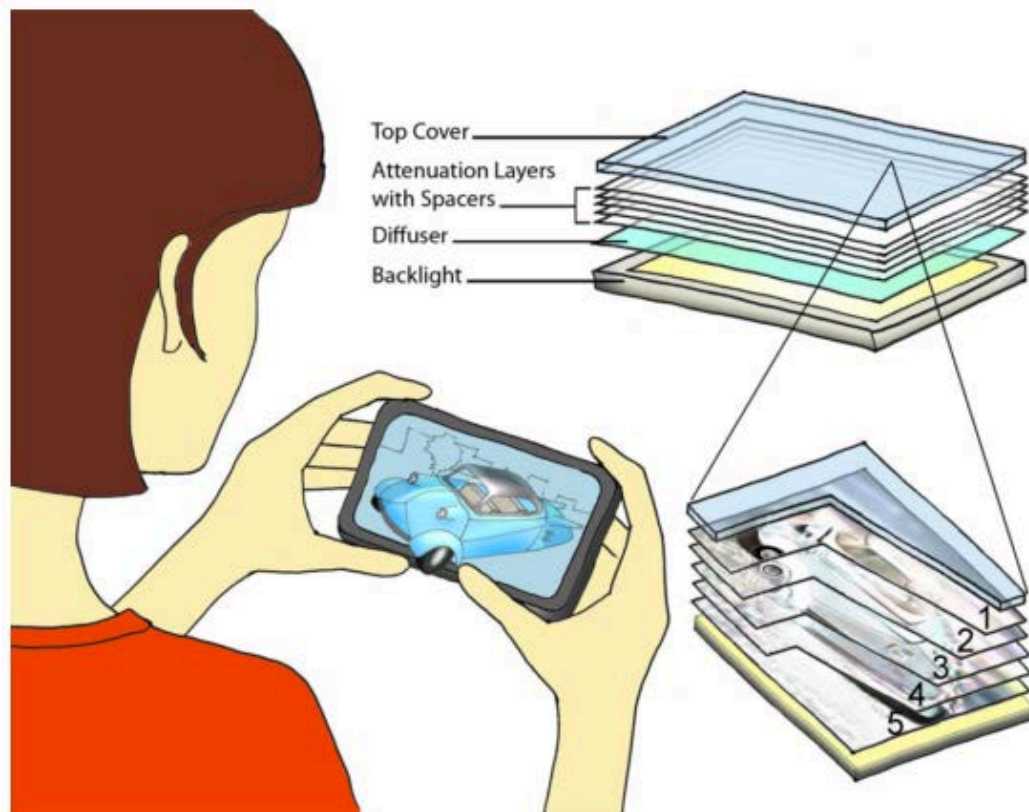
Figure 2.13 – Illustration of compressive Layered 3D Display [45]

Layered 3D display [45] was composed of compact volumes of light-attenuating material. It uses flat 2D images by creating transparence layers and attenuators to recreate a light field when back-illuminated as shown in Figure 2.13. As it simulates tomographic technique, tomographic optimisation was employed to resolve inconsistent views and to improve the resolution with greater depth of field.

Polarisation field display [46] was introduced as an optically-efficient construction for light field display with layered LCDs. Thus, it contains a stack of LCDs with a single pair of crossed polarisers, with layers acting as spatially-controllable polarization rotators as shown in Figure 2.14.

Figure 2.14 shows direct comparison of layered 3D and polarization field display whereas polarisation field display [46] is improved version of Layered 3D display [45] as it uses a single pair of crossed polarizers which improved optically.

Tensor displays [47] was latest compressive light field displays comprising all architectures employing stacks of time-multiplexed, light-attenuating layers illuminated by uniform or directional backlighting.
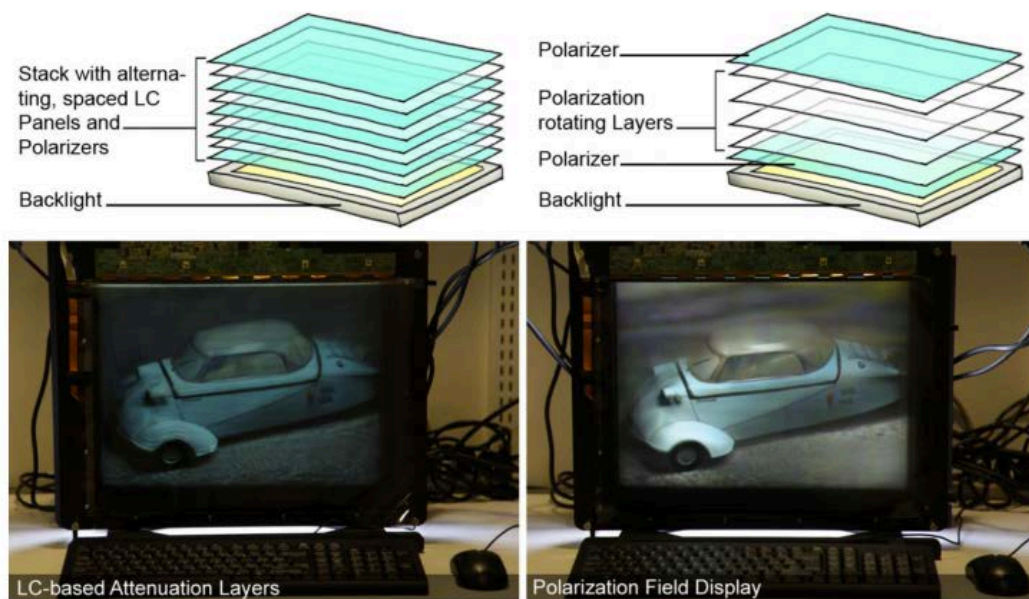
Figure 2.14 – Illustration of compressive polarisation field 3D display [46]

The most recent tensor displays [47] is a family of compressive 3D displays embracing all architectures by employing a stack of time-multiplexed, light-attenuating layers illuminated by directional backlighting as shown in Figure 2.15 [47]. It represents the set of viewpoint images of the 3D scenes using tensor algebra. Tensor algebra [48] is a mathematical framework previously applied to compress complex, high-dimensional data sets. In fact, this fundamental representation was used to introduce a unified optimization framework, based on nonnegative tensor factorization by encompassing all tensor display architectures and aimed at leading the autostereoscopic 3D displays with current LCD technology.
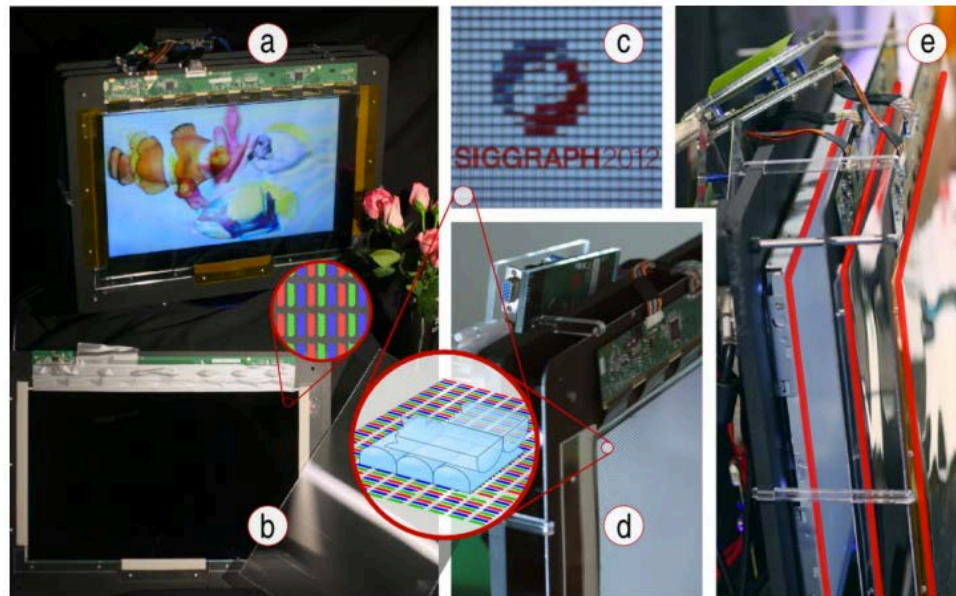
Figure 2.15 – The tensor display prototype: (a) The prototype configured as a three-layer display, (b) a LCD layer mounted on an aluminum frame (left) and a lenticular sheet (right), (c) the directional backlight, consisting of two crossed lenticular sheets on top of the rear LCD, (d) the single-layer directional backlight configuration. (e) The three-layer configuration, with layers highlighted in red [47]

It has multilayered complex computationally expensive modules and a 3D scene is created by number sliced imaging layer e.g. LCDs and to get an acceptable 3D resolution requires adding more layers which increases the complexity exponentially. In addition, it shows stack of spaced flat images and observer's brain generates depth illusion. However, it does not simulate true 3D-imaging technique and it is computationally expensive. In fact, it will be a bulky display if many of LCDs are packed together.

One of the major drawbacks of the technology is that it's computationally impossible to design and manufacture a display with acceptable resolution. In addition, compressive layered 3D display [45] has been experimented by viewing random numbers from different angle to compare it with a traditional parallax barriers 3D display. As shown in Figure 2.16, it failed to separate views when it was attempted to display the scene at highest possible resolution due to crosstalk noise.
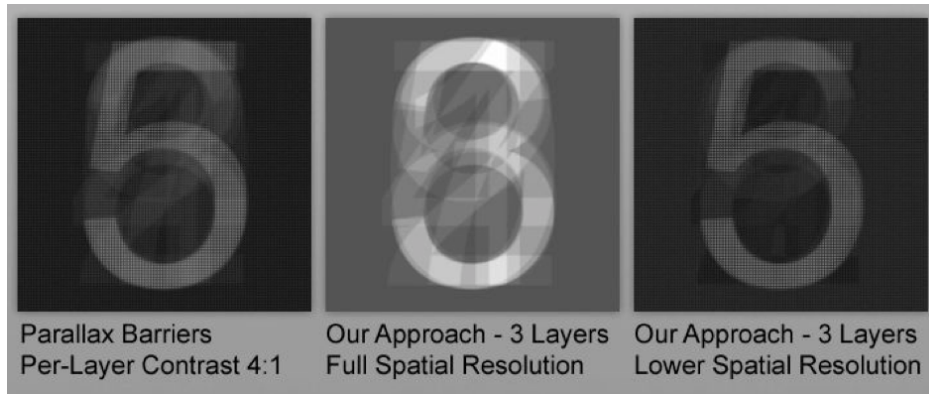
Figure 2.16 – Playback result of random number on compressive layered 3D display, failed to perform @ Full Spatial Resolution [45]

It requires more layers to increase sharpness of the constructed object as shown in Figure 2.17. The rendering process of each layer is mathematically rich, requires complex computation. As a result, the technology is computationally complex whereas it does not offer or create a 3D scene in the space instead layered spaced flat images are displayed where the spacing technique makes human brains to kick off depth illusion. Further visual analysis of the technology has been reported in [49].
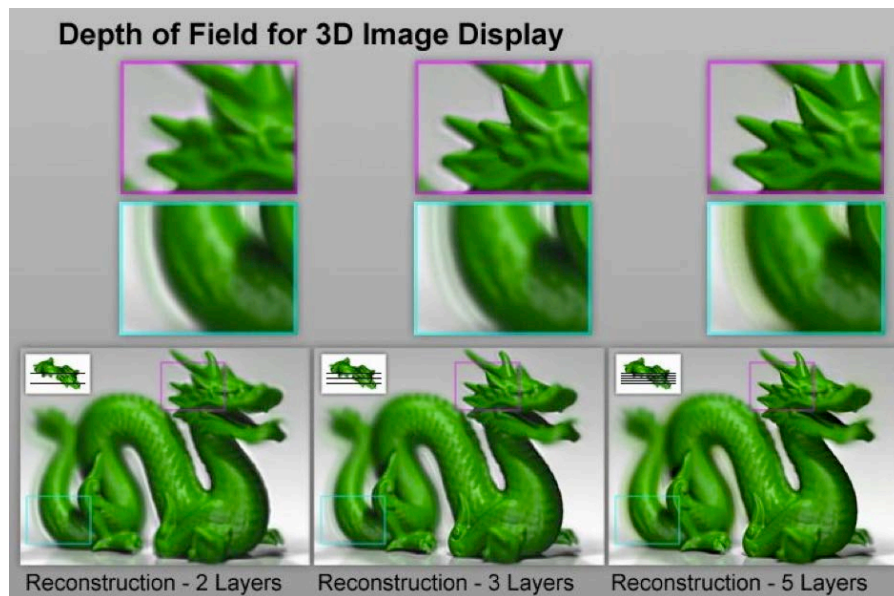
Figure 2.17 – Illustration of depth of field in compressive layered 3D display [45]

Figure 2.17 shows the experiment result of 3-layered which does not have acceptable resolutions whereas 5-layered gives a very small sharpness in the area closed to the display panel. It clearly illustrates that the compressive approach(s) require more than 5-layers to produce acceptable resolutions. It is still unclear number of required layers for getting the whole scene in focused

and sharp. On the other hand, adding more layers increases bulkiness as each layer could be a traditional 2D monitor as well as increases its complexity.

It is concluded that the compressive tensor approach is computationally very expensive even though it was shown with real-time image generation for 3-layerd display in [50]. This makes it not suitable for any real time / online processing applications e.g. gaming, TV, and real time data visualization. Yet its application areas remain undefined due to its computational complexity as well as its size.

2.3.5 Holoscopic 3D Imaging Technology

Holoscopic 3D imaging (H3D) technology [51] also known as integral imaging is a true 3D imaging technology. It offers the simplest form that is capable of recording and replaying the true light field 3D scene in the form of a planar intensity distribution, by employing MLA [52]. Despite it uses the same characteristics of holographic, it records the 3D information in 2D form and display in full 3D with optical component, without the need of coherent light source and confine dark fine. In addition, it facilitates post production processing such as refocusing [53]. This makes it more practical approach for real-time 3D image capture and display.

It was first proposed by G. Lippmann as integral photography (IP) in 1908 [54]. It simulates fly's eye technique which uses coherent replication of light to construct a true 3D scene in space. Therefore, it offers side effect free 3D depth and motion parallax in either continuous unidirectional or omnidirectional parallax depending on the MLA type.

In Lippmann's approach, 3D scene is reproduced with a fly's-eye lens array as encoding and decoding devices in the recording and replaying process respectively. As seen the recording process in Figure 2.18 (a), Rays from the objects are recorded by emulsion as 2D planar image at the recording plane through the fly's-eye lens sheet. In the process of playback as shown in Figure 2.18 (b), a suitable lens array is placed in front of the recorded image and aligned with the micro-lens image as the recording process and the diffused rays from the image reconstruct the 3D scene in space. It is a simple method

however the main problem with this approach is that the image is constructed with wrong depth i.e. it is pseudoscopic. What the observers see is the other side of the object instead of the side of the object which is near the observer. The depth of the reconstructed image is inverted.

(a) recording
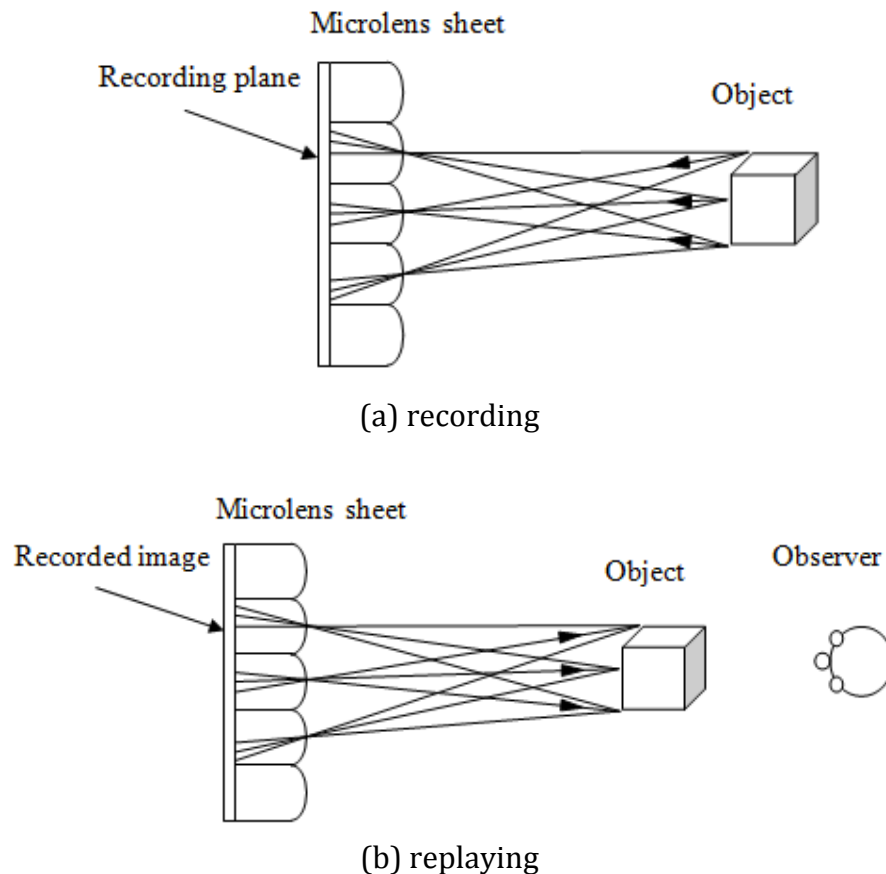
(b) replaying

Figure 2.18 - Illustration of single-step recording and replying of holoscopic imaging [55]

The pseudoscopic "inverted depth" problem was solved by modifications proposed by Okoshi and Ives [2][57]. The method employed two-step depth inversion recording, which produce the orthoscopic images. Figure 2.19 illustrates the principle of recording and replaying. Two-step approach added an optical component to reverse the depth. In this approach, the image recorded with the single-step is used as an imaging source as shown in Figure 2.19 (a), which reverse the depth of 3D information. Then the recorded image with depth inversion is ready for replay. The playback is the same way as single-step method. The recorded image is replayed by placing an appropriate lens array in front of it as shown in Figure 2.19 (b). It clearly shows that the

depth is reversed from the point of view of a viewer staring at the screen. Recently, the method has been simulated on computer graphics [58].
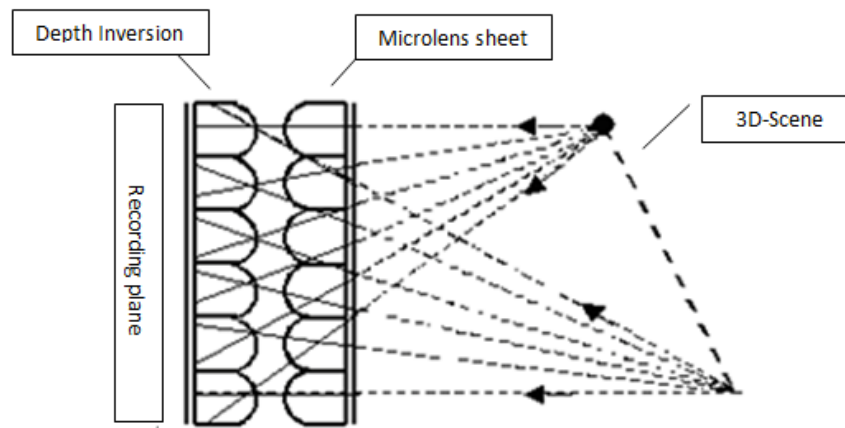
(a) recording
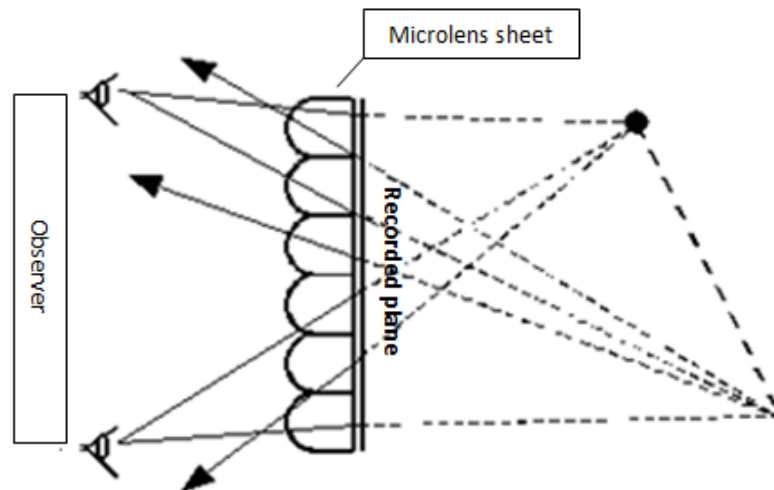
(b) replaying

Figure 2.19 – Illustration of two-step recording (a) and replaying (b) of H3D imaging [63]

Although the two-step system proposed by Ives could produce orthoscopic image, it has its own drawbacks because optical rays can be affected by smallest noise/error. Therefore the optical properties of the MLA affect the quality of the image significantly. The added second lens array introduces more noises, distortions and even moiré interference due to the sampling effect, aberration and manufacturing precision [59].

In this particular case, reducing number of components reduces the noise level in the system. Therefore, it was pursued with the one-step approach and it was proposed to use a gradient-index (GRIN) lens array as shown in Figure 2.20. It

has been experimented in real-time 3D imaging system to acquire inverted image in one-step [60][61].

| (a) Inverted image by conventional lens | (b) Erected image by a gradient-index lens |
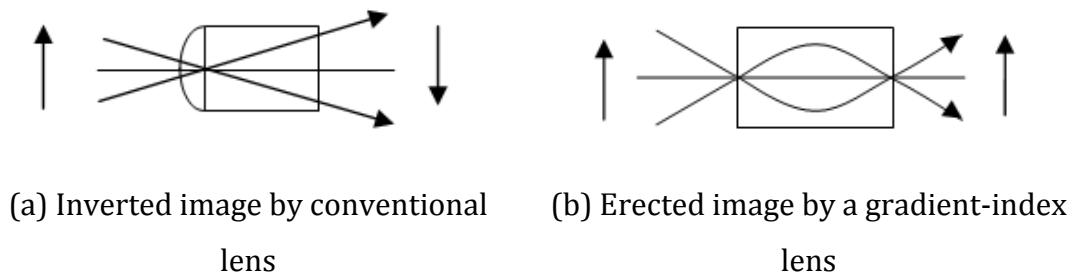
Figure 2.20 – Illustration of concept of gradient-index lens [60][61]
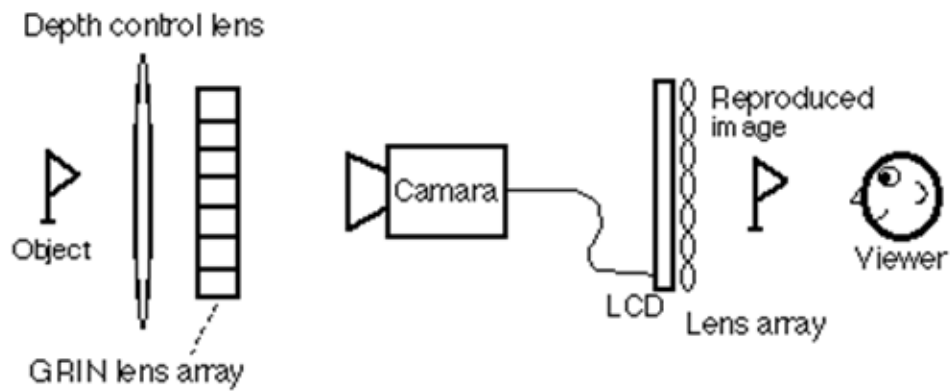
Figure 2.21 – Illustration of one-step system by gradient-index array [60][61]

A gradient-index lens has a radially varying refraction index that causes an optical ray to follow a sinusoidal propagation path through the lens. It combines refraction at the end surfaces along with continuous refraction within the lens. By defining appropriate gradient-index lens, the output image of the lens can be an erected version of the input as shown in Figure 2.20 (b). Block diagram of the system is illustrated in Figure 2.21. The major drawback of such system is that the replayed image is always inside the replaying screen.

There have been good developments in the area of holoscopic imaging technology. In particular the imaging research team at De Montfort University has a new variation of holoscopic imaging system that can directly capture H3D images without the two-step depth inversion processes [59]- [64]. The newly proposed two-tier holoscopic imaging system architecture is illustrated in Figure 2.22. As seen, it has a network of arrays. There are two MLAs, which are

put back-to-back at their joint focal distance. The encoding screen on the right is a MLA. The two-tier network works as an optical "transmission inversion screen" allowing a direct capturing of correct 3D image spatial for orthoscopic replay. The modification of optical element as shown in Figure 2.22., to illustrate the two-tier network consisting of two pair of micro-lens array place back to back to generate spatial inversion
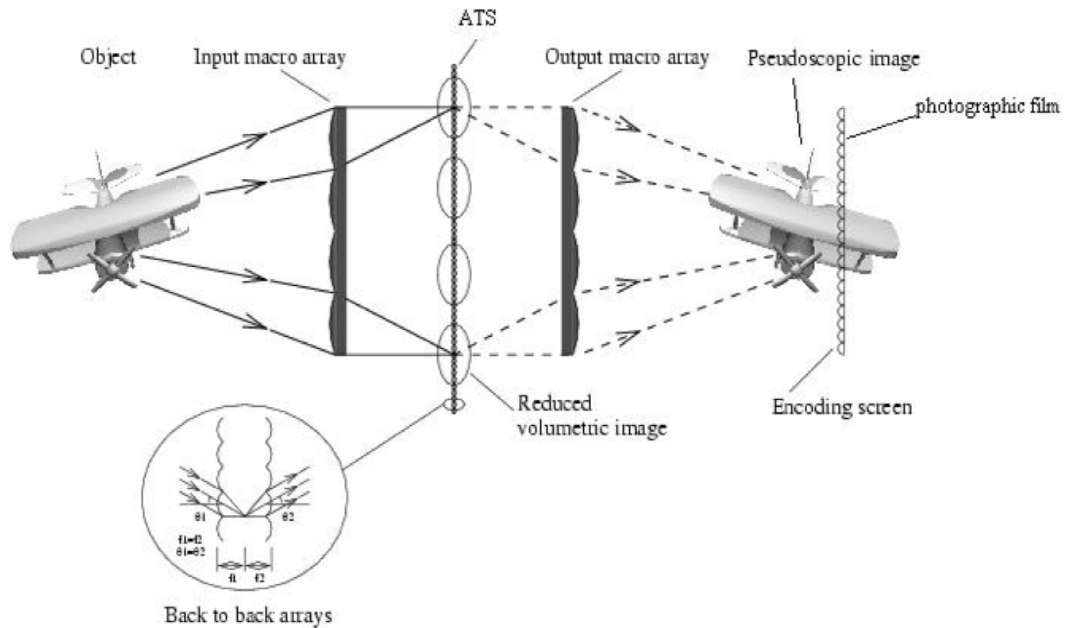
Figure 2.22 – Illustration of Two-tier holoscopic 3D imaging system [64]

As a whole, the system has the ability of transmitting 3D model(s) of a scene from the left to the right at a 1:1 scale and reconstruction a pseudoscopic aerial image for recording. Since the image for recording is pseudoscopic, after recording, the replayed image is orthoscopic. The benefit of the transmission is its flexibility to put the encoding screen and recording media. It offers the scalability of the 3D depth control i.e. the replayed image can be inside, in front of or straddling the screen.

Recently, 3DVIVANT project team made good developments on H3D imaging technology. In particular, a H3D camera has been prototyped by employing a normal 2D camera sensor as shown in Figure 2.23. This pursues a single camera aperture approach [7][65][66][67].
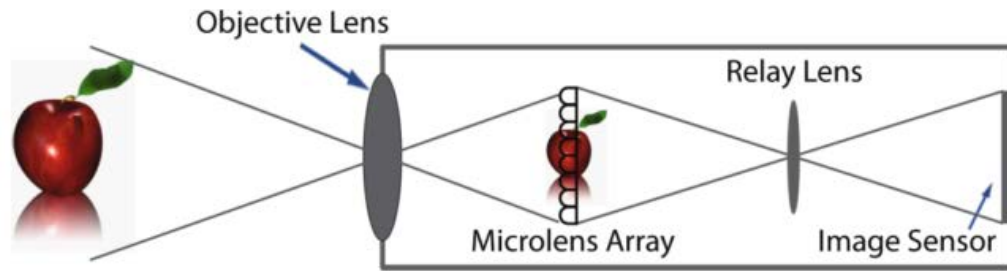
Figure 2.23 – Illustration of H3D camera design with a relay and objective lens [7]

2.3.5.1 Holoscopic 3D image rendering

H3D image rendering has been computationally complex because there has not been a simpler or greener approach for constructing a MLA in three-dimensional scene virtually. H3D imaging rendering has been reported in several literatures [68]- [71], which proposed variations of the same concept e.g. replicating a pinhole to constructed a lens array and the pinhole cameras were rendered individually which creates the actual complexity as it requires rendering of every microlens in the MLA.

There have been improvements on rendering H3D image from 3D models [71] as well as different techniques to improve the rendering process by pixel grouping and shadow caching technique [72]. In addition, researchers have been carried out for achieving maximum viewing zone in H3D computer graphics [73].

A patent [74] on H3D image rendering has been filed by BBC research team in 2001 that proposed a reverse approach [74] as shown in Figure 2.24. The concept proposed to render viewpoint images using orthographic projection type cameras and then interlace the viewpoint images to form a H3D image.
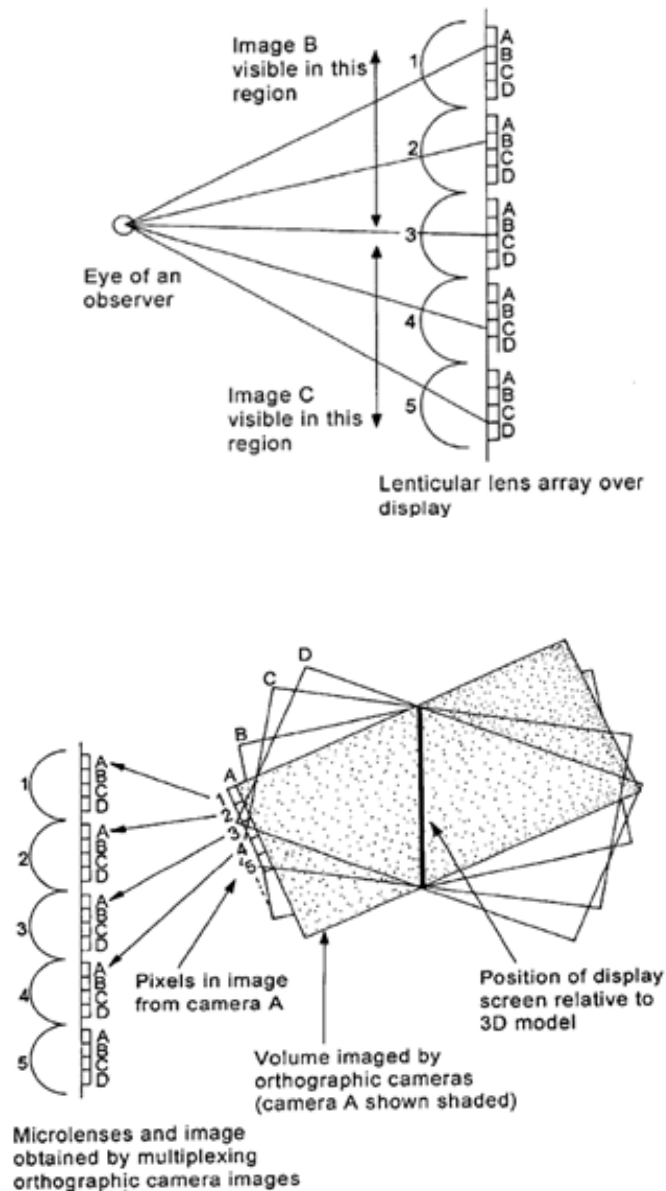
Figure 2.24 - Relationship of microlens images with viewpoint orthographic images [74]

As seen in Figure 2.24, it does a reverse engineering because traditionally a viewpoint image is formed by collecting a pixel from a particular location of every microlens image in the lens array. It renders one particular pixel of all microlens images at once. For instance, if there are 5 microlenses and every micro-lens covers 4 pixels then it renders 4 orthographic viewpoint images with resolution of 5 pixels. Empirical studies of state of art 3D displays shows a

normal 3D display has between 700 – 1000 microlenses and each microlens covers up to 28 pixels.

As a result, the orthographic projection type method reduced the complexity from O(r) = O(MLA size) to O(r) = O(PPL) where r = rendering cycle, MLA size = size of MLA i.e. between 700 – 1000, PPL = pixels per lens i.e. between 8 – 28 pixels per lens. As a result, it is rather fast and simplified technique for rendering H3D computer graphics because traditionally these hundreds of microlens images are rendered using a perspective pinhole hundreds of time to form a H3D image [71], which is computationally rich, time consuming and complex for end users. However, it has been applied to unidirectional H3D images by shifting the orthographical cameras in a single direction.

2.3.5.2 *Holoscopic 3D image Features*

Three-dimensional imaging technologies offer depth information. In particular, H3D imaging technology offers a unique feature, useful for post-production. The most unique feature "refocusing" is the ability to produce image(s) of different plane in post-production stages.

H3D imaging technology enables researchers to pursue a different way to render 2D images by doing pixel manipulation of 3D images after the 3D image is captured. The first digital refocusing was addressed in 1995 from two views each focused at different depth [75], which is called "depth from defocus" in computer vision. However, the process generates high artifacts in the final image when changing the virtual plane closer to image plane [75][76][77]. As a result, it failed to attract much of attention from researchers or users.

The first functional digital refocusing on light field 3D image "H3D image" was illustrated and reported in 2000 [78][79]. Later, the technology was further developed that offers better cues for processing [80][81]. Researchers used Plenoptic cameras "H3D camera" for refocusing in photography and the images rendered in low resolution initially [81]. Recently the refocusing algorithms have been improved that renders HD equivalent images [82][83].

2.3.5.3 Micro-Image and Microlens Array

As H3D imaging simulates fly's eye technique, it consists of a lens array "fly's lens array". The lens array is made of up hundreds of micro-lenses which generate micro-images also known as elemental image. The lens array is generally categorised into two major types (1) unidirectional and (2) omnidirectional.

D: focal length, P: lens pitch

(a) lenticular lens structure   (b) spherical lens array
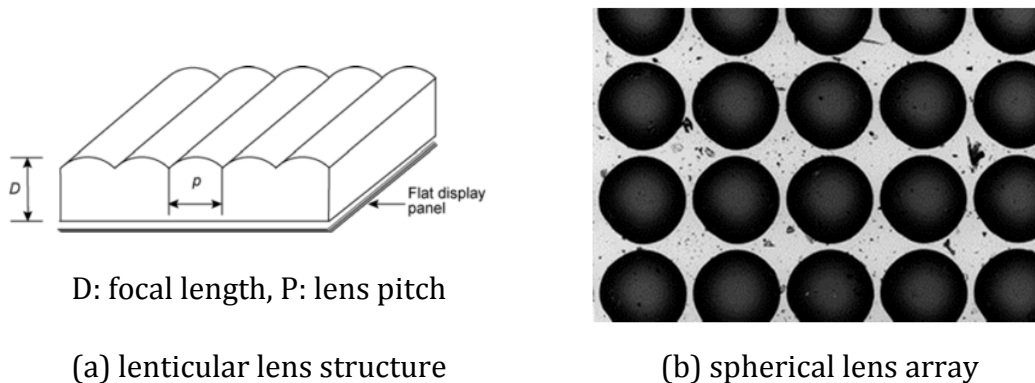
Figure 2.25 - Microlens structure of unidirectional (a) and omnidirectional (b) [84]

Unidirectional lens array shown in Figure 2.25 (a) offers a single direction 3D depth and motion parallax. It is implemented with cylindrical lens type i.e. lenticular sheet and parallax barrier technology whereas omnidirectional lens array type shown in Figure 2.25 (b) offers full parallax 3D depth and motion parallax.

These lens array types can be used to build a H3D display based on application requirements. H3D imaging has a great flexibility in terms of different lens array types. Traditionally, a H3D image contains complete 3D depth and motion parallax i.e. the constructed 3D scene is view-able in all directions. On the other hand, unidirectional one is a simplified version which contains only one direction 3D depth and motion parallax.

There have been different pattern of MLAs to achieve good imaging quality as the packing density or fill factor is an important design criterion. The packing density of a MLA is defined as the total percentage of area occupied by the microlenses. It determines the efficiency of the lens array. Since the configuration pattern of unidirectional H3D imaging lens array has only one

type i.e. lenticular / parallax barrier technology and its packing density can be achieved normally 100% as it has a simple structure.

On the other hand, there are numerous lens array types of omnidirectional H3D imaging. MLAs of various element shapes such as square, circular and hexagonal, various arrangement grids such as orthogonal and hexagonal, and various elements and sheet sizes have been manufactured as shown in Figure 2.26 [85].

| (a) Square | (b) Spherical | (c) hexagonal |
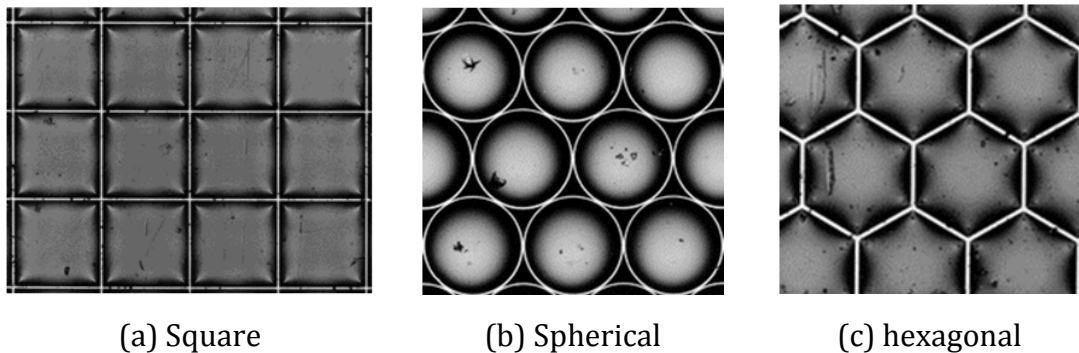
Figure 2.26 –Different shapes/types of omnidirectional lens array [84]

As seen in Figure 2.26, the square MLA can offer 100% fill factor. However, the main problem with this type is that the equal vertical and horizontal dimensions which limit the lateral angle of view, while larger horizontal viewing angle is desirable in omnidirectional H3D imaging. Whereas the other lens array types offer less fill factor e.g. The circular lens array type can have a packing density of 78.5% with orthogonal grid arrangement, and a greater value with hexagonal grid arrangement [86].
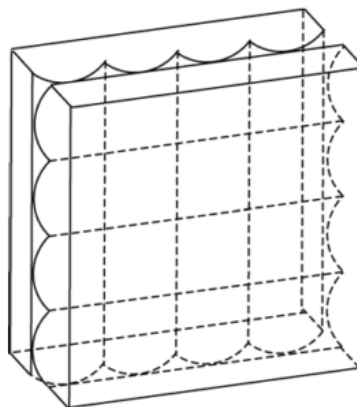
Figure 2.27 - Square aperture MLA construction with cross-lenticular [86]

As manufacturing omnidirectional lens types is very costly and yet not ready for mass market, cross-lenticular approach [86] is proposed for designing square aperture lens array type as shown in Figure 2.27. The cross-lenticular lens array is formed by two lenticular sheets overlapped orthogonally. It offers reasonable a spatial image quality and comparable to the conventional MLA.

2.3.5.4 Holoscopic 3D Display Technology

Incremental developments have been made on H3D display technology from unidirectional [87] to omnidirectional display [89] as shown in Figure 2.28, which illustrates the summary of the technology developments for the past 100 years [88].

In addition, moiré reduction methods [90] were developed for reducing moiré effect by introducing color filter as shown in Figure 2.29. Yet it is not an optimal approach because color filter fails to produce natural color image(s).
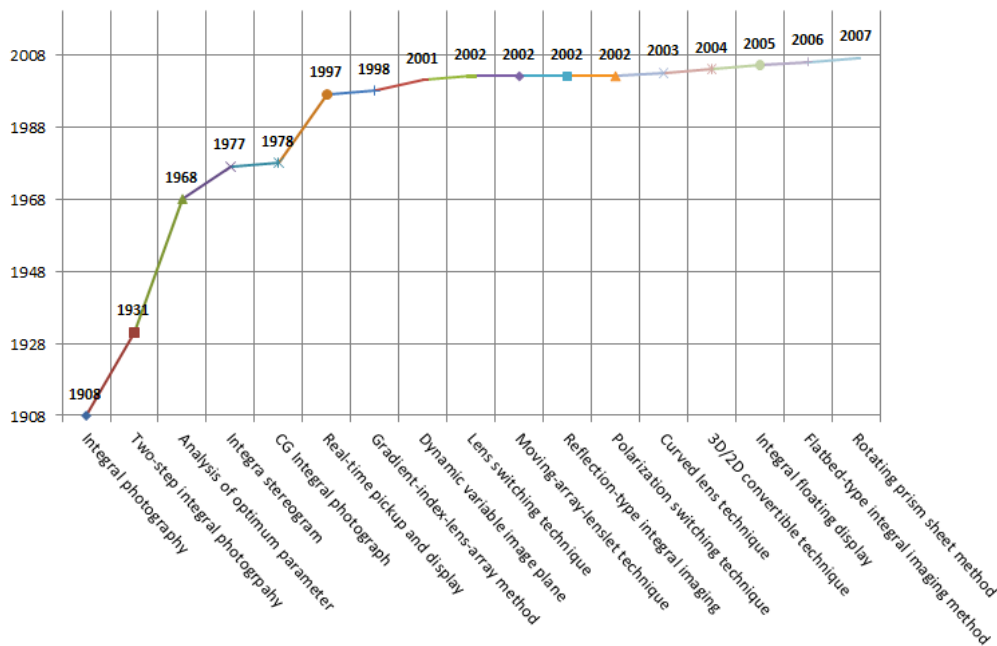
Figure 2.28 - Development timeline of holoscopic 3D imaging technology [88]
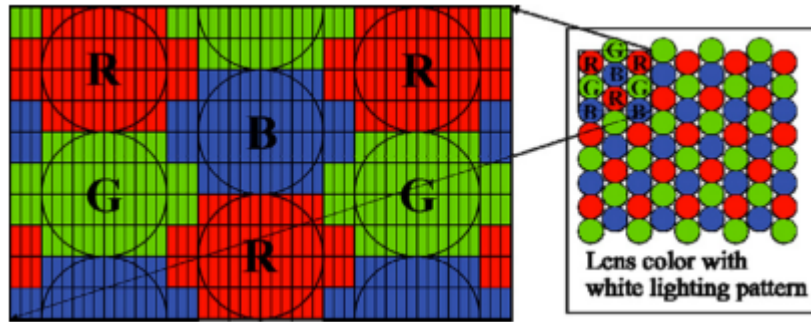
Figure 2.29 - Layout of color filter and lens to reduce color moiré [90]

In addition, there have been different approaches for designing H3D display such as using polymer-dispersed liquid crystal (PDLC) in which parallel layered PDLC films and a projector were adopted as a display system and the ability to vary the location of image plane. The transparency of PDLC films was controlled electrically by making each film diffuse the projected light successively with different depth from lens array as shown in Figure 2.30 [91].
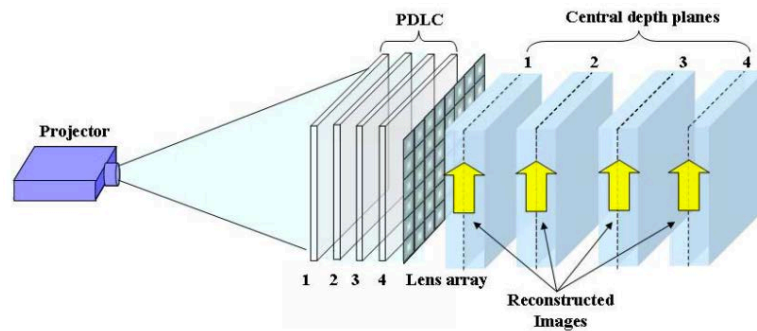
Figure 2.30 - Concept of the PDLC based 3D display [91]
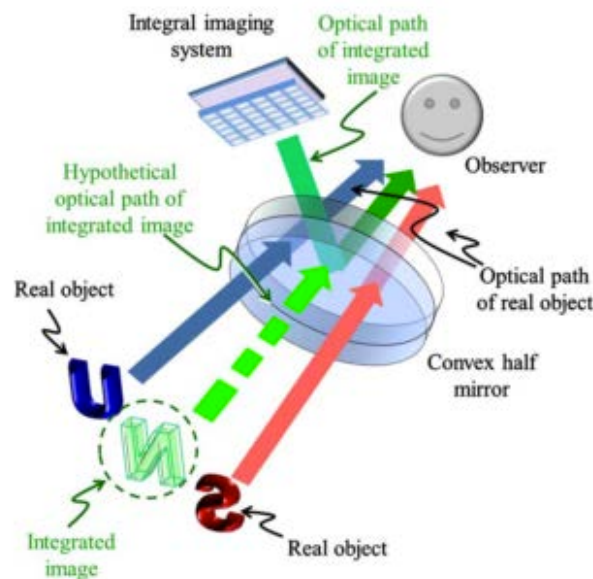
Figure 2.31 - Concept of integral floating scheme adopting a convex half mirror [91]

Augmented reality 3D display was proposed that requires a long-range focus depth and a see-though property. It adopted a concave lens instead of a convex lens for realizing the 3D floating display with a long working distance using a reduced pixel pitch of the elemental image as shown in Figure 2.31. An optical see-through system was built with a convex half mirror for providing 3D images with a proper accommodation response [92].
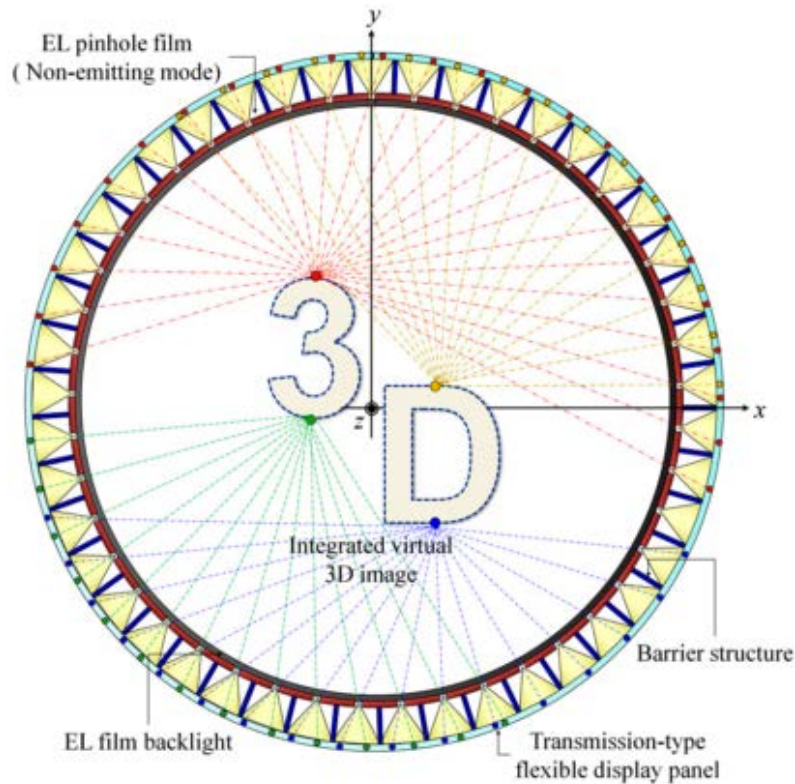
Figure 2.32 - Principle of 360 view-able 3D displays [93]

Due to high interest in H3D imaging,   A 360° degree viewable 3D display was built based on H3D imaging [93] that offers only unidirectional 3D depth and motion parallax. The 360° display was composed of a cylindrically arranged electroluminescent pinhole film, an EL film backlight, a barrier structure, and a transmission-type flexible display panel as shown in Figure 2.32.   It also supported 3D/2D switch-ability which was achieved by switching of EL pinhole film by using a point light source to a surface light source.

2.4   Conclusion

This chapter presented background studies and state of the art developments of 3D imaging and display technologies, namely stereoscopic and autostereoscopic imaging systems.

S3D technology simulates human eye technique to achieve stereo parallax effect which is done by viewing right and left images in a specific way; the observer sees left-eye image with the left eye and sees right-eye image with the right eye by using a special head gear device. However, it has its own limitations such as unnatural image colour, eye fatigue, and motion sickness. Therefore it is not suitable for prolonged operations.

Autostereoscopic 3D technology pursues natural 3D experience by enabling observers to perceive 3D effects with the naked eye. It has different concepts and mechanisms such as multiview, holographic, volumetric, compressive, and holoscopic, which offer natural 3D viewing experiences.

Multiview 3D technology is an advancement of S3D that creates discrete view-windows which observers perceive convenient left/right view-windows. However, it requires observer to stand in particular place to perceive 3D effects thus, it still suffers from eye fatigue, motion sickness and viewing distance range.

Holographic and volumetric 3D imaging technologies are true 3D imaging techniques that reconstructs objects in space. These technologies are very costly to manufacture for mass market; therefore, their application areas are focused to medical imaging and military applications where user experience is highly desired.

Compressive display was rather very recent invention that is proposed by MIT research team in 2010. It simulates tomographic technique to reconstruct 3D scene with layers of LCDs. It targets to resolve data size in terms of transmission of 3D images for autostereoscopic imaging technology. However, the results were not impressive due to many reasons i.e. it is not a true 3D imaging technique as it uses flat 2D images to form a 3D scene "tomographic technique"; therefore, more layers of LCDs are required for reconstructing a 3D scene with acceptable resolution; It is computationally complex as iterative tensor optimisation algorithm is required for a better result. The experimental results illustrated that the compressive display failed to differentiate between viewpoints of 3D image due to increasing noise [45].

H3D imaging technology is a true 3D imaging technique that mimics fly's eye technique for reconstructing 3D scene in space by utilising replication of light. It offers side effect free 3D experience i.e. 3D depth and motion parallax on the either continuous unidirectional or omnidirectional parallax depending on the choice of MLA.

There have been incremental developments on H3D imaging technology, which offers natural 3D effect. This put the technology in one of the most promising future imaging technique. In addition, it enhances 2D imaging technology for instance images captured with H3D camera can be refocused in different planes in the post-production and H3D images can be reformatted to S3D, multiview 3D image or HD 2D image format.

The distinctive advantage is that H3D imaging offers scalable solution for 3D displays and it pursues rather a simplified approach for recording a H3D image. Presently, there have been some limitations due to existing technology i.e. lens array and LCD to build a HD equivalent H3D display. In addition, the omnidirectional lens array offers the same ratio 1:1 depth and motion parallax in both horizontal and vertical directions. Realistically, more 3D effects are required horizontally than vertically.

2.5 References

[1] J. Hong, Y. Kim, H.J. Choi, J. Hahn, J.H. Park, H. Kim, S.W. Min, N. Chen, and B. Lee, "Three-dimensional display technologies of recent interest: principles, status, and issues," Applied optics, vol. 50, no. 34, pp. H87–115, Dec. 2011.

[2] T. Okoshi "Three-Dimensional Imaging Techniques" Academic Press, UK. 1976.

[3] H.J. Choi, "Current status of stereoscopic 3D LCD TV technologies," 3D Research, vol. 2, no. 2, p. 4, Nov. 2011.

[4] I. Sexton and P. Surman, "Stereoscopic and autostereoscopic display Systems," Signal Processing Magazine, IEEE, 1999.

[5] H. Urey, K. V Chellappan, E. Erden, and P. Surman, "State of the Art in Stereoscopic and Autostereoscopic Displays," Proceedings of the IEEE, vol. 99, no. 4, pp. 540–555, Apr. 2011.

[6] A. Yöntem and L. Onural, "Integral imaging based 3D display of holographic data," Optics express, vol. 20, no. 22, pp. 2359–2375, 2012.

[7] A. Aggoun, E. Tsekleves, M. R. Swash, D. Zarpalas, A. Dimou, P. Daras, P. Nunes, and L. D. Soares, "Immersive 3D Holoscopic Video System," MultiMedia, IEEE, vol. 20, no. 1, pp. 28–37, 2013.

[8] N. VALYUS, Stereoscopy, 1st Edition, Focal Press. London, 1996.

[9] S. Kratomi "Stereoscopic Apparatus Having Liquid Crystal Filter Viewer", US patent US3737567, 1972.

[10] E. Dubois "A projection method to generate anaglyph stereo images", Acoustics, Speech, and Signal Processing, Proceedings, IEEE International Conference, pp. 1661. 2001

[11] 3DStereo, "3D Stereo." [Online]. Available: www.3dstereo.com. [Accessed: 01-Sep-2013].

[12] B. Toperverg, O. Nikonov, V. Lauter-Pasyuk, and H. Lauter "Towards 3D polarization analysis in neutron reflectometry", Physica B: Condensed Matter, vol. 297, no. 1, pp. 169-174. 2001

[13] P. Boher, T. Leroux, T. Bignon and V. Collomb-Patton "Multispectral polarization viewing angle analysis of circular polarized stereoscopic 3D displays", Proc. SPIE, pp. 75240R. 2010

[14]   S.A. Benton "Holographic Displays: 1975-1980", Optical Engineering, vol. 19, no. 5, pp. 195686-195686. 1980

[15]   A.W. Divelbiss, D.C. Swift and W.V. Tserkovnyuk "3D stereoscopic shutter glass system" US Patent No: 6727867, 2004

[16]   M. McCormick, Davies. N., "3-D worlds", Physics World, pp.42-46, June 1992.

[17]   M. McCormick, N. Davies and E. Chovanietz, "Restricted parallax images for 3D TV", Proc. IEE Conf. Pub. No. 172, London, 1992.

[18]   W. Funk "History of autostereoscopic cinema", IS&T/SPIE Electronic Imaging International Society for Optics and Photonics, pp. 82880R, 2012

[19]   N. A. Dodgson, "Autostereoscopic 3D Display," IEEE Computer Society, pp. 31–36, 2005.

[20]   N. Tetsutani, K. Omura and F. Kishino "Wide-screen autostereoscopic display system employing head-position tracking", Optical Engineering, vol. 33, no. 11, pp. 3690-3697, 1998

[21]   R. B. Johnson and G. A. Jacobsen, "Advances in lenticular lens arrays for visual display," Proc. SPIE, vol. 5874. pp. 587406, 2005

[22]   V. Saveljev, "Characteristics of moiré spectra in autostereoscopic three-dimensional displays," Journal of Display Technology, vol. 7, no. 5, pp. 259–266, 2011.

[23]   C. Van Berkel and J. A. Clarke, "Autostereoscropic Display Apparatus," US Patent No: 6064424, 2000

[24]   C. Van Berkel and D. W. Parker, "Autostereoscopic Display Apparatus," US Patent No: 61185842002. 2000

[25]   Y. Takaki, O. Yokoyama, and G. Hamagishi, "Flat panel display with slanted pixel arrangement for 16-view display," vol. 7237, pp. 723708–723708–8, Feb. 2009.

[26]   Alioscopy, "Alioscopy 3D Display Pixel Mapping Principles," Alioscopy, 2013. [Online]. Available: http://www.alioscopy.com/en/principles.php. [Accessed: 01-May-2013].

[27]   J.Y. Son and B. Javidi, "Methods for Displaying Three-Dimensional Images," Proceedings of the IEEE, vol. 94, no. 3, pp. 502–523, Mar. 2006.

[28]   C. Riechert, F. Zilly, P. Kauff, J. Güther, and R. Schäfer, "Fully Automatic Stereo-to-Multiview conversion in Autostereoscopy Displays," International Broadcasting Convention (IBC2012), 2012.

[29]   Y. Lai, Y. Lai, and Y. Chen, "An Effective Hybrid Depth-Generation Algorithm for 2D-to-3D Conversion in 3D Displays," Journal of Display Technology, vol. 9, no. 3, pp. 154–161, 2013.

[30]   D. Gabor, "A new microscope principle", Nature, no. 161, pp. 777-779, 1948.

[31]   D. Gabor. "Microscopy by reconstructed wavefronts", Proc. Phys. Soc., no. A194, pp. 454-487, 1949.

[32]   S.A. Benton "Holographic Displays: 1975-1980", Optical Engineering, vol. 19, no. 5, pp. 195686-195686, 1980

[33]   C. Wu, A. Aggoun, M. McCormick and S. Kung "Depth measurement from integral images through viewpoint image extraction and a modified multibaseline disparity analysis algorithm", Journal of Electronic Imaging, vol. 14, no. 2, 2005

[34]   J. Casper and S. Feller "The Complete Hologram Book", 1987

[35]   D. C. Weber and J. D. Trolinger, "Holographic labeling and reading machine for authentication and security applications." Google Patents, 1999.

[36]   P. Hariharan, Basics of holography, Cambridge University Press, 2002

[37]   P. Kovács and T. Balogh, 3D Visual Experience. Springer Berlin Heidelberg, pp. 391–410, 2010

[38]   Holografika, "HoloVisio Light Field Display," 2013. [Online]. Available: http://www.holografika.com/. [Accessed: 01-Jul-2013].

[39]   A. Yöntem and L. Onural, "Integral imaging based 3D display of holographic data," Optics express, vol. 20, no. 22, pp. 2359, 2012

[40]   J. Lewis, C. Verber, and R. Mcghee, "a True Three-Dimensional Display," Electron Devices, IEEE, 1971.

[41]   B. Blundell and A. Schwarz, Volumetric Three- Dimensional Display Systems, John Wiley & Sons, 2000.

[42]   G. Favalora, "Volumetric 3D Displays and Application infrastructure," Computer, pp. 37–44, 2005.

[43]   D. Lanman, M. Hirsch, Y. Kim, and R. Raskar, "Content-adaptive parallax barriers: Optimizing dual-Lauyer 3D Displays using Low-Rank Light Field Factorization," ACM SIGGRAPH Asia 2010 papers on - SIGGRAPH ASIA '10, vol. 29, no. 6, p. 1, 2010.

[44]   D. Lanman, G. Wetzstein, M. Hirsch, W. Heidrich, and R. Raskar, "Beyond parallax barriers: applying formal optimization methods to multilayer automultiscopic displays," Proc. SPIE 8288, 2012.

[45]   G. Wetzstein, D. Lanman, W. Heidrich, and R. Raskar, "Layered 3D: Tomographic Image Synthesis for Attenuation-based light Field and High Dynamic Range Displays," ACM SIGGRAPH 2011 papers on - SIGGRAPH '11, vol. 1, no. 212, p. 1, 2011.

[46]   D. Lanman, G. Wetzstein, M. Hirsch, W. Heidrich, and R. Raskar, "Polarization fields: Dynamic Light Field Display using Multi-Layer LCDs," Proceedings of the 2011 SIGGRAPH Asia Conference on - SA '11, vol. 30, no. 6, p. 1, 2011.

[47]   G. Wetzstein, D. Lanman, M. Hirsch, and R. Raskar, "Tensor displays: compressive light field synthesis using multilayer displays with directional backlighting," ACM Transactions on Graphics, Volume 31, Issue 4, 2012.

[48]   T. Kolda and B. Bader, "Tensor Decompositions and Applications," Society for industrial and applied mathematics (SIAM) Review, vol. 51, no. 3, pp. 455–500, 2009.

[49]   D. Lanman, G. Wetzstein, M. Hirsch, and R. Raskar, "Depth of Field Analysis for Multilayer Automultiscopic Displays," Journal of Physics: Conference Series, vol. 415, p. 012036, Feb. 2013.

[50]   G. Wetzstein, D. Lanman, M. Hirsch, and R. Raskar, "Real-time Image Generation for Compressive Light Field Displays," Journal of Physics: Conference Series, vol. 415, p. 012045, Feb. 2013.

[51]   A. Aggoun, E. Tsekleves, M. R. Swash, D. Zarpalas, A. Dimou, P. Daras, P. Nunes, and L. D. Soares, "Immersive 3D Holoscopic Video System," MultiMedia, IEEE, vol. 20, no. 1, pp. 28–37, 2013.

[52]   A. Aggoun, "3D Holoscopic Imaging Technology for Real-Time Volume Processing and Display," in in High-Quality Visual Experience, M. Mrak,

Marta and Grgic, Mislav and Kunt, Ed. Springer Berlin Heidelberg, pp. 411–428, 2010

[53]   R. Ng, M. Levoy, and M. Brédif, "Light field photography with a hand-held plenoptic camera," Stanford University Computer Science Tech Report CSTR 2005-02, pp. 1–11, 2005.

[54]   G. Lippmann, "Photographies integrals," ComptesRendus de l'Academic des Sciences, 146, pp. 446-451, 1908

[55]   J. Ren, A. Aggoun, and M. McCormick, "Computer generation of integral 3D images with maximum effective viewing zone," Proc. SPIE 5006, Stereoscopic Displays and Virtual Reality Systems X, 65 (May 29, 2003); doi:10.1117/12.474128

[56]   H. Arimoto and B. Javidi, "Integral three-dimensional imaging with digital reconstruction," Opt. Lett., vol. 26, no. 3, pp. 157–159, Feb. 2001

[57]   H. E. Ives, "Optical properties of a Lippman lenticulated sheet," J. Opt. Soc. Am., vol. 21, no. 3, p. 171, Mar. 1931.

[58]   H. Deng, Q. Wang, and D. Li, "The Realization of Computer Generated Integral Imaging Based on Two Step Pickup Method", Symposium on Photonics and Optoelectronic (SOPO), pp. 4–6, 2010.

[59]   N. Davies and M. McCormick, "Holoscopic imaging with true 3-D content in full natural color," The journal of photographic science, vol. 40, pp. 46–49, 1992.

[60]   F. Okano, J. Arai, H. Hoshino, and I. Yuyama, "Real-time three-dimensional pickup and display system based on integral photography," Proc. SPIE, vol. 3430. pp. 70–79, 1998.

[61]   F. Okano, J. Arai, H. Hoshino, and I. Yuyama, "Three-dimensional video system based on integral photography," Optical Engineering, vol. 38, no. 6, pp. 1072–1077, 1999.

[62]   N. Davies, M. McCormick, and L. Yang, "Three-dimensional imaging systems: a new development," Appl. Opt., vol. 27, no. 21, pp. 4520–4528, Nov. 1988.

[63]   N. A. Davies, M. Brewin, and M. McCormick, "Design and analysis of an image transfer system using microlens arrays," Optical Engineering, vol. 33, no. 11, pp. 3624–3633, 1994.

[64]   M. Mccormick and N. Davies, "Full natural colour 3D optical models by integral imaging," Holographic Systems, Components and Applications, 4th International Conference on , vol., no., pp.237,242, 13-15 Sep 1993.

[65]   A. Aggoun, "3D Holoscopic video content capture, manipulation and display technologies," 9th Euro-American Workshop on Information Optics, pp. 1–3, Jul. 2010.

[66]   A. Aggoun, "3D Holoscopic Imaging Technology for Real-Time Volume Processing and Display," in High-Quality Visual Experience, Springer Berlin Heidelberg, pp. 411–428, 2010

[67]   M.R Swash, A. Aggoun, O. Abdulfatah, B. Li, J.. Fernández, and E. Tsekleves, "Holoscopic 3D image rendering for Autostereoscopic Multiview 3D display," IEEE international Symposium on Broadband Multimedia Systems and Broadcasting, 2013.

[68]   S.W. Min, S. Jung, J.-H. Park, and B. Lee, "Three-dimensional display system based on computer-generated integral photography," Proc. SPIE, vol. 4297. pp. 187–195, 2001.

[69]   T. Naemura, T. Yoshida, and H. Harashima, "3-D computer graphics based on integral photography." Optics express, vol. 8, no. 4, pp. 255–62, Feb. 2001.

[70]   G. Milnthorpe, M. McCormick, A. Aggoun, N. Davies, and M. Forman, "Computer generated content for 3D TV displays," International Broadcasting Convention, Amsterdam, Netherlands. 2002.

[71]   M. Eljdid, A. Aggoun, and H. Youssef, "Computer Generated Content for 3D TV," 3DTV Conference, pp. 1–4, 2007.

[72]   O. H. Youssef, A. Aggoun, W. Wolf, and M. McCormick, "Pixels grouping and shadow cache for faster integral 3D ray tracing," Proc. SPIE 4660, Stereoscopic Displays and Virtual Reality Systems IX, 123 (May 24, 2002); doi:10.1117/12.468025.

[73]   J. Ren, A. Aggoun, and M. McCormick, "Computer generation of integral 3D images with maximum effective viewing zone" Proc. SPIE 5006, Stereoscopic Displays and Virtual Reality Systems X, 65 (May 29, 2003); doi:10.1117/12.474128..

[74]   G. A. Thomas and R. F. Stevens, "Processing of Images for 3D Display," U.S. Patent US6798409B22004, 2004

[75]   M. Subbarao, S. Member, T. Wei, and G. Surya, "Focused image recovery from two defocused images recorded with different camera settings", IEEE Transactions on Image Processing, vol.4, no.12, pp.1613,1628, Dec 1995, doi: 10.1109/83.475512.

[76]   E. Krotkov, "Focusing", Intl. Journal of Computer Vision, vol. 237, pp. 223–237, 1982.

[77]   AP. Pentland, "A new sense for depth of field.," IEEE transactions on pattern analysis and machine intelligence, vol. 9, no. 4, pp. 523–31, Apr. 1987.

[78]   J. C. Yang, M. Everett, C. Buehler, and L. McMillan, "A real-time distributed light field camera," in Proceedings of the 13th Eurographics workshop on Rendering, pp. 77–86, 2002

[79]   W.C. Chien, D. S. Dilworth, E. Liu, and E. N. Leith, "Synthetic-aperture chirp confocal imaging.," Applied optics, vol. 45, no. 3, pp. 501–10, Jan. 2006.

[80]   A. Lumsdaine and S. Jose, "The focused plenoptic camera," IEEE International Conference on Computational Photography (ICCP), 2009.

[81]   A. Lumsdaine and T. Georgiev, "Full resolution lightfield rendering," University and Adobe Systems, Tech. Rep, no. January, pp. 1–12, 2008.

[82]   T. Georgiev and A. Lumsdaine, "Focused plenoptic camera and rendering," Journal of Electronic Imaging, vol. 19, no. 2, pp. 21106–21111, 2010.

[83]   T. Georgiev and a. Lumsdaine, "Reducing Plenoptic Camera Artifacts," Computer Graphics Forum, vol. 29, no. 6, pp. 1955–1968, Sep. 2010.

[84]   S. Manolache, A. Aggoun, M. Mccormick, and N. Davies, "Analytical model of a three-dimensional integral image recording system that uses circular- and hexagonal-based spherical surface microlenses," Opt. Soc. Am., vol. 18, no. 8, pp. 1814–1821, 2001.

[85]   R. Stevens and T. Harvey, "Lens arrays for a three-dimensional imagine system," Journal of Optics A: Pure and Applied, vol. 17, 2002.

[86]   D. Daly, R. F. Stevens, M. C. Hutley, and N. Davies, "The manufacture of microlenses by melting photoresist," Measurement Science and Technology, vol. 1, no. 8, p. 759, 1990.

[87]   C.G. Luo, C.C. Ji, F.-N. Wang, Y.-Z. Wang, and Q.-H. Wang, "Crosstalk-Free Integral Imaging Display With Wide Viewing Angle Using Periodic Black Mask," Journal of Display Technology, vol. 8, no. 11, pp. 634–638, Nov. 2012.

[88]   Y. Kim, K. Hong, and B. Lee, "Recent researches based on integral imaging display method," 3D Research, vol. 1, no. 1, pp. 17–27, Aug. 2011.

[89]   H. Deng, Q.H. Wang, L. Li, and D.-H. Li, "An integral-imaging three-dimensional display with wide viewing angle," Journal of the Society for Information Display, vol. 19, no. 10, p. 679, 2011.

[90]   T. Koike, K. Utsugi, and M. Oikawa, "Moiré-reduction methods for integral videography autostereoscopic display with color-filter LCD," Society for Information Display, pp. 678–685, 2010.

[91]   Y. Kim, H. Choi, J. Kim, S.W. Cho, and B. Lee, "Integral imaging with variable image planes using polymer-dispersed liquid crystal layers," vol. 6392, pp. 639204–639204–8, Oct. 2006.

[92]   J. Hong, S.W. Min, and B. Lee, "Integral floating display systems for augmented reality.," Applied optics, vol. 51, no. 18, pp. 4201–9, Jun. 2012.

[93]   J. Jung, K. Hong, G. Park, I. Chung, and B. Lee, "360° viewable cylindrical integral imaging system using a 3-D / 2-D switchable and flexible backlight," Journal of the Society for Information Display, pp. 527–534, 2010.

3   Chapter Three - Holoscopic 3D Camera Technology

This chapter presents novel methods for rendering omnidirectional holoscopic 3D (H3D) computer graphics using 2-dimensional (2D) orthographic camera array or by constructing a virtual lens array in the virtual world.   It also presents smart microlens array architecture for H3D camera that doubles the spatial resolution. The layout of the chapter is as follows: 3.1 Introduction, 3.2 Omnidirectional H3D Computer Graphics, 3.3 Single Stage H3D Computer Graphics Rendering, 3.4 Smart Microlens Array Architecture, and 3.5 Conclusion.

3.1 Introduction

In this chapter, omnidirectional H3D [1] computer graphics rendering method is proposed and developed using 2D array of orthographic cameras [2]. The proposed method simplifies and improves the 3D rendering performance enormously compared to the traditional approach. As it requires multiple orthographic cameras for rendering, H3D computer graphics rendering remains as multistep pre-processing.

To overcome the multistep 3D rendering issue, we proposed a single stage H3D image rendering method which simulates the single aperture H3D camera principle. The proposed method virtually constructs a fly's eye lens array in the scene using constructive solid geometry objects. It renders the virtual lens array with orthographic projection camera. It pursues 2D computer graphic rendering style as it renders a H3D image in a single rendering step.

In addition, smart microlens array architecture is proposed that doubles and triples horizontal spatial resolution. As MLA is slanted some degrees, a smart pixel mapping technique is applied to pre-process the image before extracting viewpoint images.
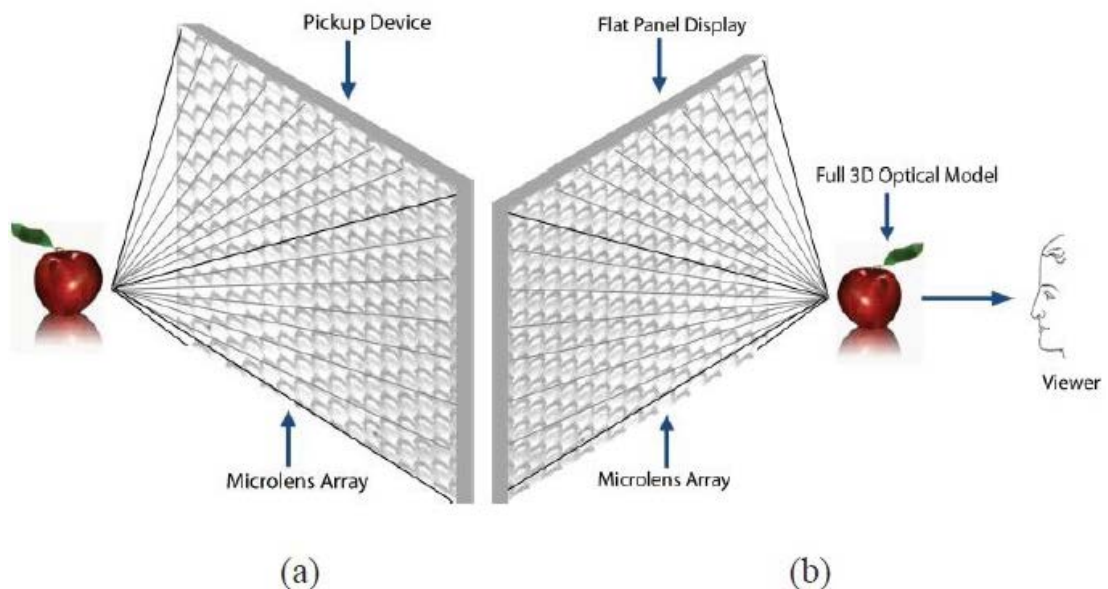
Figure 3.1 - H3D imaging system - (a) Recording and (b) replaying [1]

3.2   Omnidirectional H3D Computer Graphics

In this section, a novel method is proposed for rendering omnidirectional H3D images using 2-Dimensional array of orthographic cameras [2]. It utilises rather a simpler technique in order to simulate the single aperture H3D imaging system shown in Figure 3.1.

A H3D image is presented under an array of spherical or lenticular microlenses as shown in Figure 3.2. Different 2D viewpoint images are projected from different angles to construct a true 3D scene in space as shown in Figure 3.2; these 2D viewpoint images are orthographic images. Therefore, this process can be repeated using an array of orthographic projections with correct shifting and rotating angles. The shifting and rotation values are calculated from the microlens pitch and focal length. The number of required orthographic cameras is defined by the number of pixels per lens. Therefore, the viewpoint image resolution is the total number of microlenses and can be defined as the 3D resolution.

Figure 3.3 shows the construction of a 2-Dimensional array of orthographic projections for rendering omnidirectional H3D images. It avoids creation of hundreds or thousands of perspective pinhole cameras in order to form a H3D camera. Therefore it removes the intensive processing such as from O(number of lenses) to O(pixels per lens).

In the proposed approach, the number of orthographic cameras is defined by the number of pixels under each spherical lens. For instance, rendering a H3D image of 3 x 3 pixels per lens with the resolution of 300 x 300 requires 3 x 3 = 9 orthographic cameras. The resolution of orthographic cameras/images is 300 × 300 pixels. On the other hand, the traditional approach would require 300 × 300 = 90000 perspective pinhole cameras of 3 × 3 pixels resolutions

As a result, the proposed method reduces complexity enormously. It improves the performance significantly and makes it an appropriate solution for interactive 3D gaming and real-time 3D interactive applications. In fact, every row of 2D array of orthographic cameras is independent of each other so they can be multi-threaded easily to boost up the performance. The only shared

object is the 3D model which can be replicated for every camera row and then the rows will be rendered simultaneously. This will achieve a possible best performance required in building interactive 3D applications.

Figure 3.2 shows construction of 3 orthographic camera images from 5 lenticular lens array whereas Figure 3.3 shows the steps for constructing 2D array of orthographic cameras from a spherical lens of 3 × 3 pixels.
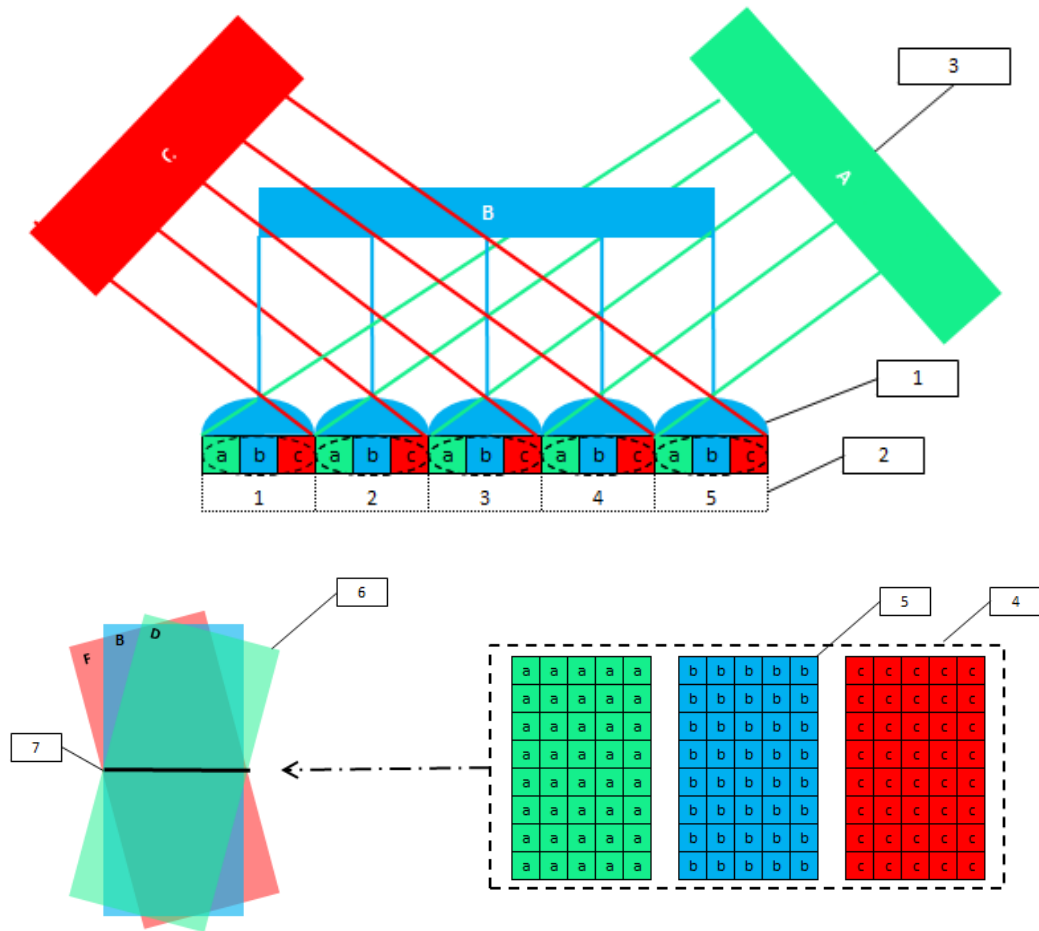
Figure 3.2 - Lenticular lens array relationship with orthographic projection

Figure 3.2's descriptions: 1 – number of microlenses, 2 – number of pixels per lens, 3 – orthographic viewpoint image, 4 – set of orthographic cameras, 5 - a single constructed orthographic image, 6-set of orthographic cameras, 7-postion of display screen relative to 3D model
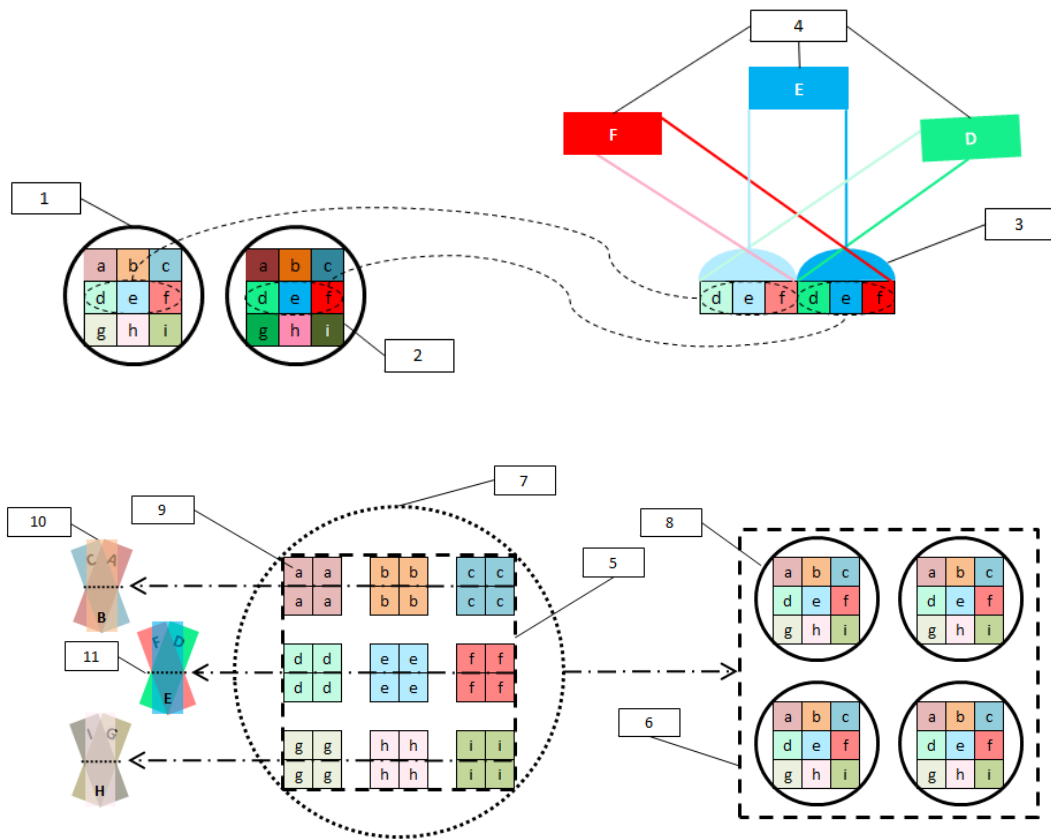
Figure 3.3 - Spherical lens array relationship with dual orthographic projection

Figure 3.3's label descriptions: 1 – spherical lens array, 2 – number of pixels per lens, 3- cylindrical lens construction from spherical lens, 4-orthographic projection of cylindrical lenses, 4- 2D array of orthographic cameras, 6- spherical lens array of label 5, 7-array of orographic cameras, 8 – a single spherical lens, 9 – a single orthographic camera which captures a single pixels of each spherical lens, 10- a set of 3 orthographic cameras for row 1 pixels, 11- a set of 3 orthographic cameras for row 2 pixels.

3.2.1   H3D Image Rendering

The Omnidirectional H3D image rendering method is developed using omnidirectional array of orthographic cameras. The proposed method utilises multilayer of unidirectional H3D camera module implemented in POV-Ray [8] as shown in Figure 3.3.   There are $N \times M$ orthographic cameras where N is horizontal pixels per lens (row) and M is vertical pixels per lens (column). For instance the rendered H3D image shown in Figure 3.7 has 10 × 10 pixels per

lens. In this case, there are 10 × 10 = 100 orthographic cameras aligned in 10 rows × 10 columns for forming a single omnidirectional H3D camera.

The camera module uses the POV-Ray [8] system clock, which works like a counter to renders all viewpoint images on a user click. Afterwards, the orthographic images are used to created elemental images, which are interwoven to form an omnidirectional H3D image. The interweaving of viewpoint images into elemental images is implemented in .NET framework using C sharp.

It is fully customisable to render H3D images with different lens array specifications. The lens array parameters such as lens per pixels, lens pitch, lens array size, and lens focal length are reconfigurable in the configuration file. These parameters are vital to take under consideration during the rendering because the H3D image should be the display-compatible in order to construct 3D scene in space.

Pseudo Code for rendering H3D computer graphics

Input a 3D model of supported format
Converts the input 3D model to a pov-ray 3D model
Configure MLA parameters i.e. PPL and LP
Loop until end of PPL
       Render viewpoint image of PPL[i]
End loop
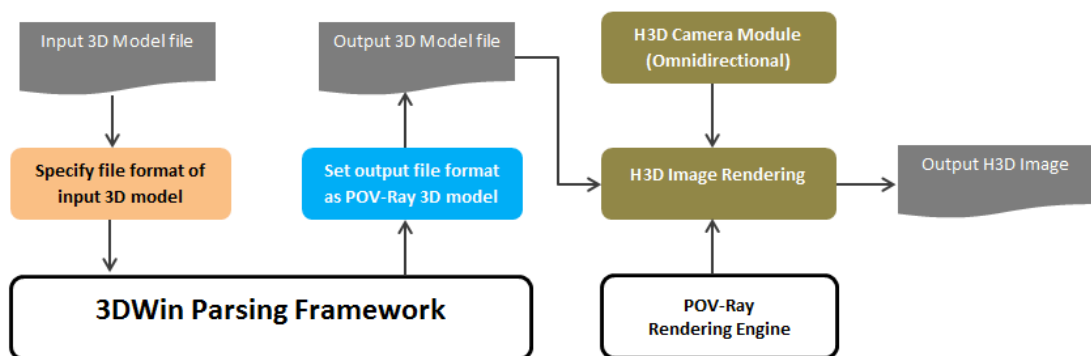
Figure 3.4 - Block diagram of proposed omnidirectional H3D camera module

Figure 3.4 shows Block diagram of the proposed H3D camera module which is integrated with the 3D model re-formatting add-on. The 3D model re-

formatting add-on enables users to generate omnidirectional H3D image from 3D models of any format supported by the convertor. As it is built on open-source rendering engine, there is no licensing if it is made available to public or web-interfaced to enable public for rendering omnidirectional 3D content online.

3.2.2 Playback Results

The rendered omnidirectional H3D images are replayed on both lens array [Figure 3.6] and parallax barriers [Figure 3.7] based omnidirectional 3D displays. The H3D displays are custom built in the lab at Brunel University because there is no omnidirectional H3D display available in the commercial market. The experiments confirm the complete depth and motion parallax of the proposed method is superb. Indeed, the 3D depth and motion parallax are adjustable as the user can set depth of objects in the scene. In addition rendering for different lens arrays / 3D displays is made a joy as it is the matter of changing couple of values in the settings.
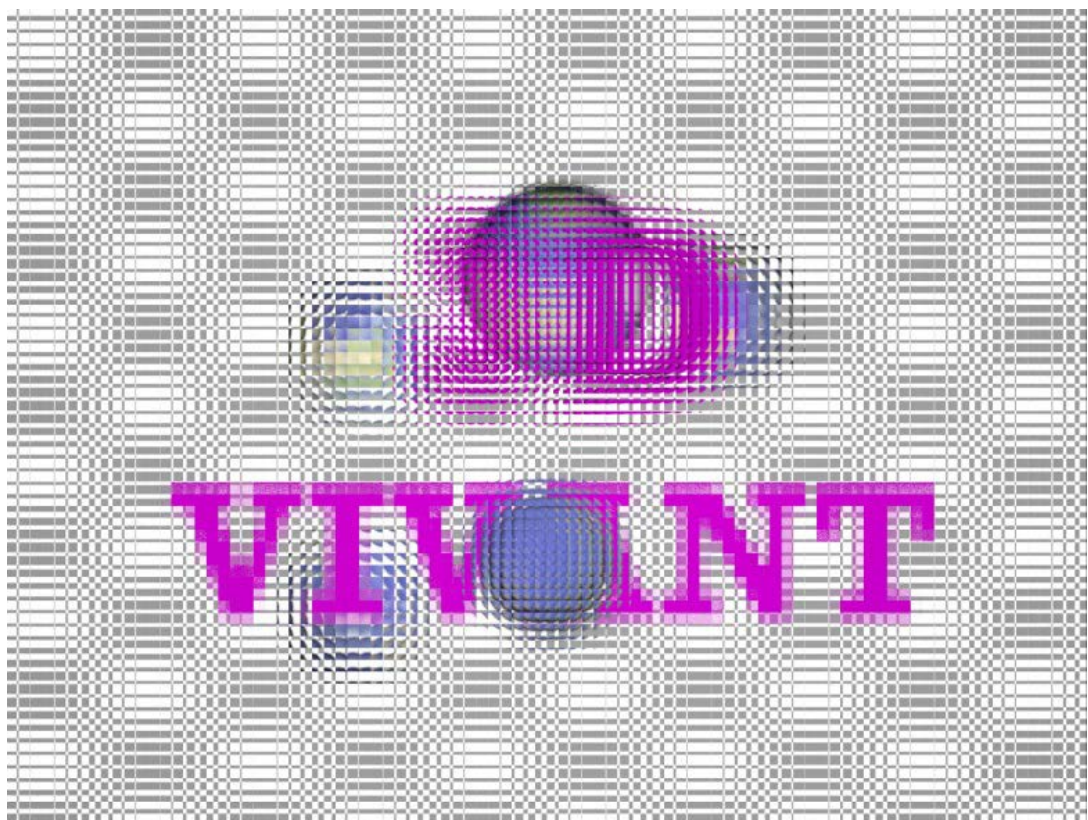
Figure 3.5 – The omnidirectional H3D image is rendered with the proposed method

Figure 3.5 shows the rendered omnidirectional H3D image where Figure 3.6 shows its playback result. The prepared image is replayed using cross-lenticular based omnidirectional iPad 3D which was proposed in [6]. The cross-lenticular technique is done by putting two lenticular sheets back-to-back to form a square aperture lens array. In fact it simulates the proposed principle.

The playback results of cross-lenticular based H3D display are shown in Figure 3.6. As seen in the captured images, a superb horizontal and vertical motion parallax is achieved including rich depth parallax.

Figure 3.6 - Playback results of the rendered H3D image on omnidirectional H3D iPad

Figure 3.7 - Playback results of rendered H3D image on parallax barriers based omnidirectional H3D display

Figure 3.7 shows the playback result of the rendered H3D image on parallax barriers based omnidirectional 3D display. As seen the resulting images contain motion parallax in the horizontal and vertical directions and there is 10

× 10 pixels per lens. The display is built with a normal LCD with rather larger pixel pitch. The important point to consider is that the experiment illustrates a wide angle of complete 3D depth and motion parallax.

3.3   Single Stage Omnidirectional H3D Computer Graphics Rendering

3D computer graphics rendering remains as a multi-step process such as rendering orthographic viewpoint images [2] or perspective microlens images [4].   In fact, in section 3.2 we proposed omnidirectional H3D image rendering using 2-dimensional array of orthographic cameras which reduced the rendering steps from thousands to hundreds i.e. it does reverse engineering by rendering orthographic viewpoint images which are later interlaced to form a H3D image.

These pre-processing steps become a challenge when deploying interactive 3D displays.   Therefore, we propose a single stage H3D computer graphic rendering method which simplifies the 3D rendering as it pursues traditional 2D rendering style.   The proposed method simulates single aperture H3D camera principle [3]. It virtually constructs a fly's eye lens array in the virtual world using constructive solid geometry technique [7] and then the virtual lens array is rendered with orthographic projection camera in a single step and there is no additional step involved.

3.3.1   Constructive Solid Geometry Technique

Constructive Solid Geometry (CSG) [8] is the most powerful 3D modelling technique that is to combine basic three-dimensional shapes shown in Figure 3.8 to form more complex shapes by Boolean operations such as union and intersection in 3D space.   Constructive solid geometry technique is well established and understood technique that offers fundamental Boolean operations such as union, intersection, difference, and merges which are used for constructing more complex solids by combining objects.

Figure 3.8 - Basic 3D objects used by CSG

Table 3.1 - Basic Boolean operations of Constructive solid geometry
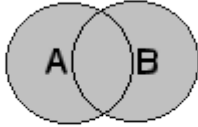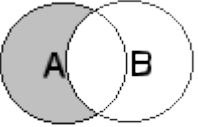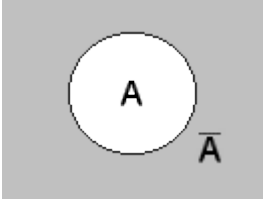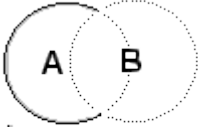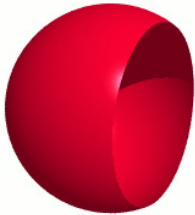
(1) Union of sets	= A ∪ B	
(2) Difference	= A \ B	
(3) Intersection	= A ∩ B	
(4) Complement		$A \setminus B = A \cap \overline{B}$
(5) Opening by cutting off	| = A clipped_by (B inverse)	

Table 3.1 demonstrates some of the fundamental principles of constructing more complex solids using constructive solid geometry technique. In this

particular case, we refer a solid as a special set of points in the 3D space. Therefore, CSG technique is applicable with all solids and all shapes which have a clear defined in/outside. The most commonly used solids are box, sphere, cylinder, cone and prism which offer fundamental structure of most designs.

Table 3.1 shows the basic operations, which are the most powerful ones in building different shapes. (1) Union operation: The resulting shape consists of all regions either in the first, in the second, or in both input objects. It basically combines two or more objects together to a new object, (2) Difference: The resulting shape is the region of the first object, reduced by the region of the second shape so it can be used to drill out holes and shape out any kind of notches, (3) Intersection: The resulting shape is the region common in or shared by both objects, (4) Complement: it is an inverse function and with two or more objects it results in an object which has an area that consists of the area common to all these objects, the area where the objects are overlapping, (5) opening by cutting off: result of this operation is similar to "intersection" and "difference".
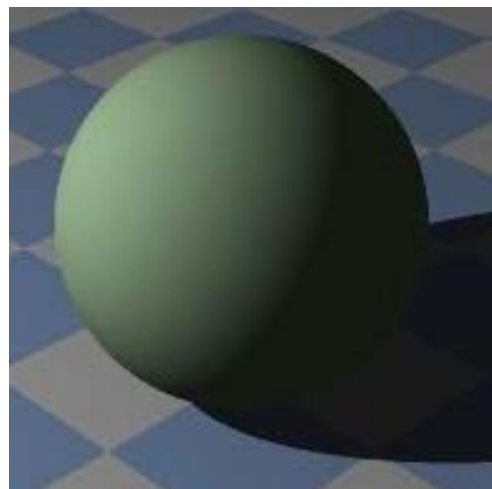
(a) photo-realistic rendering   (b) non-photo realistic rendering

Figure 3.9 – (a) Photo realistic rendering Vs. (b) Non-photo realistic rendering

In addition, CSG technique can be used to create true lens effects in Ray tracing technology. Ray tracing is an advanced computation technique that renders photo realistic graphic images as shown in Figure 3.9 (a) whereas non-photo realistic image is shown in Figure 3.9 (b). It depends on complex mathematics to mimic the optical behaviour of lenses, water, beams of light, and a very

specific diffuse glow one sees in natural environments. In this experiment, we choose to use POV-Ray which is an open-source ray-tracing engine. One of the useful features of POV-Ray [5] is the great ease with moving objects and replicating objects in script.

3.3.2   Lens Effect Simulation in Ray-tracing

As Ray-tracing is a photo realistic rendering [9] technique, it calculates an image of a scene by simulating the real world rays of light. On the other hand, like any other computer graphics, it traces rays in backwards compared to the real world. In the real world, rays of light are released from a light source. The light reflects of the objects and this reflected light hits our eyes or a camera lens whereas Ray-tracing applications e.g. POV-Ray start with their simulated camera and trace rays backwards out into the scene. Therefore the camera, light sources, objects locations are set in virtual three-dimensional scene. Pixels of the final image are viewing rays, which are shot from the camera, into the scene to see if it intersects with any of the objects in the scene.

In addition, it offers special features such as atmospheric effects and index of refraction (IOR). The IOR command is used to mimic the optical behaviour of glasses and lenses. Basically, a material's IOR describes how slowly light passes through it which means is that the light takes a more circuitous route through glass. In other word, it defines the objects transparency as shown in Algorithm 3.1 (Its resulting image is shown in Figure 3.9 (a))

```
sphere {
    <0, 0, 0>, 1
    interior {
        ior 1.5
        caustics 0.3
    }
    finish {
        specular 0.6
        roughness 0.05
        reflection {
            rgb <0.3, 0.3, 0.3>
        }
    }
```

Algorithm 3.1 - The code makes the sphere look like a transparent glass ball in POV-Ray

As seen in Algorithm 3.1, the IOR is set to the interiors of objects to simulate optical refraction property of glass. Therefore, a service-able lens can be designed virtually by two spheres using the CSG operator "union". The resulting lens is a combination of the two original objects. On the other hand, changing union Boolean to intersection Boolean composes a converging lens because it composes a lens only of those parts where both two objects intersect, or overlap as shown in Table 3.1 (3).

To conclude, the lens shape object is created using constructive solid geometry technique whereas the lens effect is created by advanced internal specification "interior" with a specified refraction. The combinations of these two techniques help us render a perfectly serviceable lens in a three-dimensional virtual scene.

| (a) 3D virtual scene | (b) construction virtual lens array |
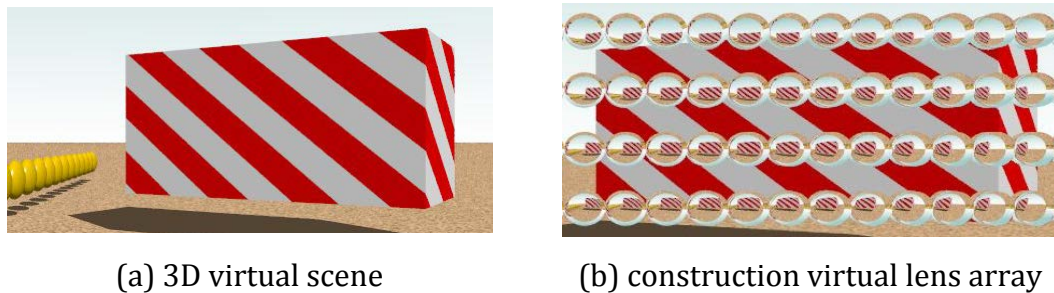
Figure 3.10 - Simulating of lens effect in 3D virtual scene

Figure 3.10 shows the experimental result of optical lens simulation where a virtual MLA is constructed in the three-dimensional virtual scene. Figure 3.10 (a) shows a virtual 3D scene rendered in 2D whereas Figure 3.10 (b) shows a virtual MLA constructed in the 3D scene. It clearly illustrates the lens effect which has index of refraction of 1.35.

A lens effect is defined by IOR; it causes light to change course by delaying the passage of light wave, which means it is related to the focal length of the lens. A typical lens shape is spherical which can be engraved using two sphere solid objects. In fact, the most basic equation of the lens-maker's art assumes two spheres, with ranges raduis1/raduis2 (r1/r2) and an IOR. These values can be used to calculate the focal length of a lens as shown Equation 3.1.

Equation 3.1 – Calculating focal length

$$\text{Focal length} = \frac{1}{(IOR - 1)\left(\frac{1}{r1} - \frac{1}{r2}\right)} \; where \; r1 \; \& \; r2 \; is \; the \; raduis$$

3.3.3   The Proposed Methodology

Novel single stage H3D computer graphics rendering is proposed.   It simulates and constructs optical lens effects in the 3D scene and it uses CSG to cut a microlens shape object using two primitive objects e.g. sphere and cylinder; it sits the lens's index of refraction to the interior of newly cut microlens object. The index of refraction is a special feature that defines how light goes through an object "interior".
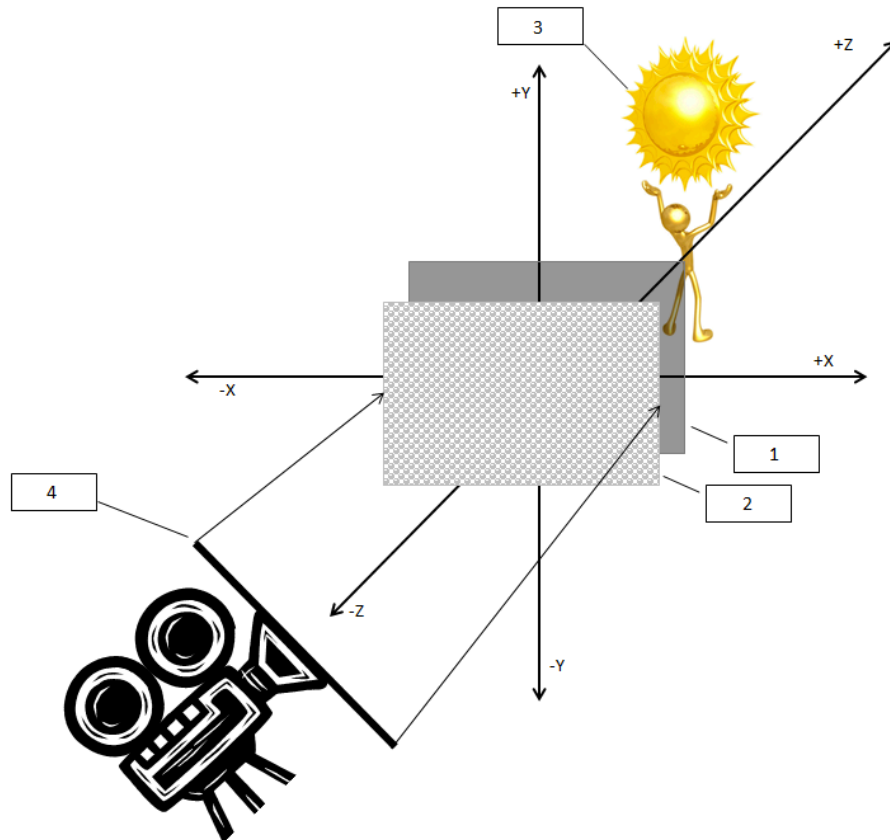
Figure 3.11 - Single stage H3D computer graphics rendering architecture: (1) imaging panel e.g. CCD, (2) virtual lens array, (3) three-dimensional virtual scene, (4) orthographic camera

Traditionally, a single perspective camera is replicated in X and Y directions to create a MLA. The micro-cameras are rendered in sequential manner so rendering a H3D image of 300 × 150 microlenses is rendered in 300 × 150 =

45,000 steps. The microlens images are then interlaced and stitched together to make up a H3D image.

In the proposed method, the MLA is constructed virtually in the 3D scene. The lens array is then imaged using an orthographic camera as shown in Figure 3.11 because orthographic camera projection type has all rays in parallel with no angular effect. Indeed, in this particular case, the orthographic camera acts like a CCD of a real camera in computer graphics. The image in Figure 3.12 is rendered to show a virtual lens array construction in three-dimensional scene in computer environment. In this case, a microlens pitch is ~0.85 mm. There are 120 × 75 microlenses which are clearly shown in the virtual scene.
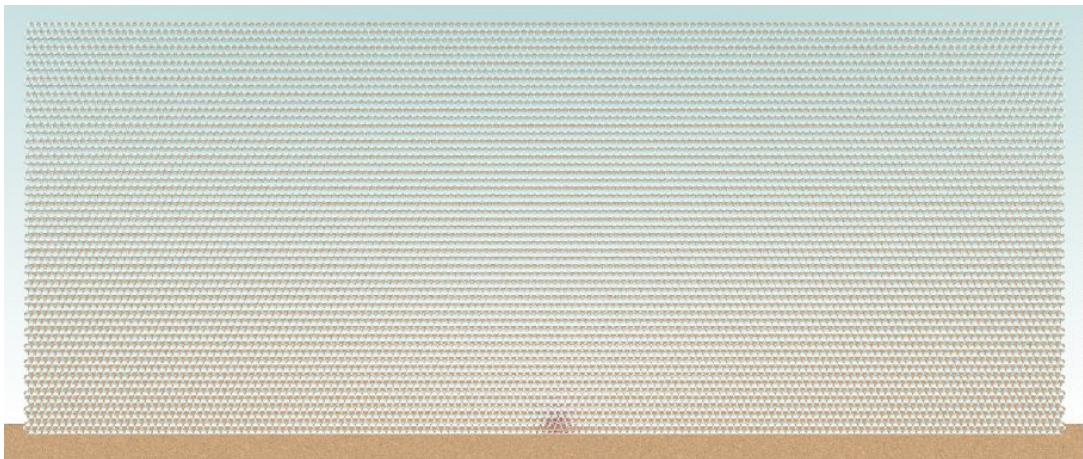
Figure 3.12 – Illustration of single stage H3D image rendering concept in virtual scene

Table 3.2 - Technical specifications of the omnidirectional H3D display

Description	Specification
Liquid Crystal display	*1280 × 800 pixels*
Active display dimension	*120.96 × 75.6 mm*
Pixel pitch	*0.0945(H) × 0.0945 (V) mm*
Lens array size	*142~ × 109~ lenses*
Pixels per lens	*9.5~ × 9.5~ pixels*
Microlens pitch	*0.850 mm*
Focal length	*1.0 mm*

To prove the proposed concept, an omnidirectional H3D display is assembled with a hexagonal lens array. Figure 3.13 shows the display components whereas Table 3.2 shows technical specifications of the display. The display LCD size is 120.96 × 75.6 mm which defines the orthographic camera aperture

size "acts like real camera CCD". It has 2D resolutions of 1280 × 800 pixels which define the orthographic camera resolutions. It also has a hexagonal style lens array of 142 × 89 microlenses and hexagonal lens array is illustrated in Figure 3.14.
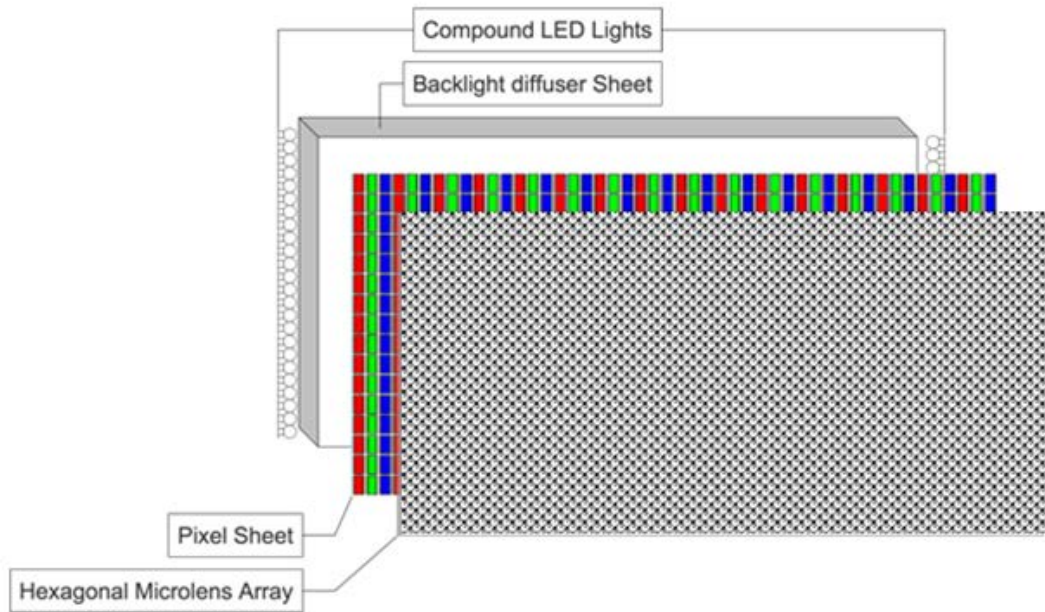
Figure 3.13 - Components of omnidirectional H3D field display

(1) microlens pitch, (2) number of microlens in vertical direction of lens array, (3) number of microlens in horizontal direction of lens array
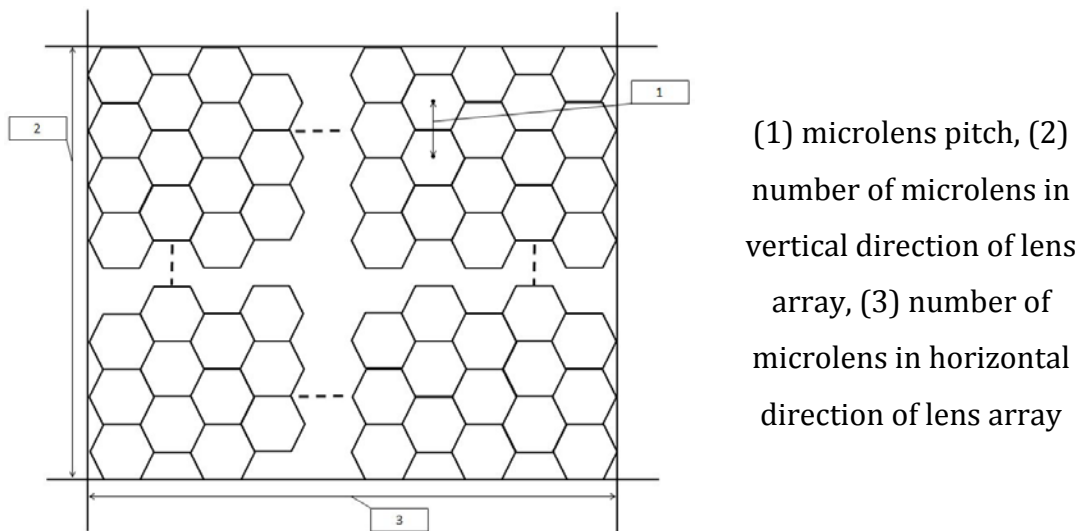
Figure 3.14 - Hexagonal lens array structure

As the display has a hexagonal lens array, an almost perfect hexagonal lens shape is engraved from cylinder and sphere object using difference Boolean function of CSG; the syntax is presented in Algorithm 3.2. The objects are created with the microlens size 0.85 mm, difference as illustrated in Table 3.1 (2).

Experiments were carried out with different IOR values in order to find optimal IOR value of the lens array used in the display. As seen, the IOR value is set to 1.283 as it produces the optimal result.

```
#declare Lenslet =
        difference {
                cylinder { 0*z, (0.85/2)*z, 0.85/2}

                sphere { <0,0,0> 0.85/2}
                }


object {Lenslet
        material {
                texture {
                        pigment{
                                color rgbf<1,1,1,1>
                                }
                        }
                interior {
                        ior 1.283
                        }
                }
}
```

Algorithm 3.2 - Engraving hexagonal microlens from cylinder and sphere objects
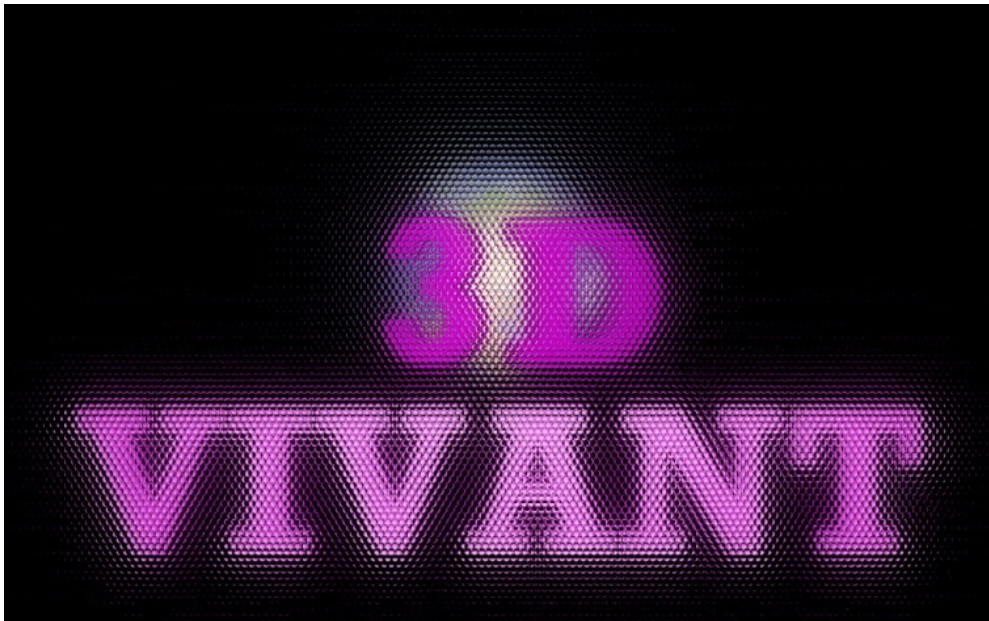
Figure 3.15 - The resulting image of the proposed single stage H3D image rendering

Once the microlens is constructed with correct shape and index of refraction, the virtual microlens is replicated 143 times in horizontal direction and 109 times vertical direction, which make up a lens array in the virtual scene. Afterwards, the scene is rendered with an orthographic camera with resolution of the 3D display in this case the resolution is 1280 × 800 pixels. The resulting image is an omnidirectional H3D image with 3D resolutions of 143 × 109 3D-pixels as shown in Figure 3.15.

3.3.4   Playback Result

The H3D image is rendered from a 3D model using a virtual H3D camera developed using the proposed method. It has ~10 × ~10 pixels per lens in POV Ray [5]. Figure 3.16 shows the playback result of rendered H3D image by single stage H3D camera.   As seen in the playback result, there is good immersive 3D effects in both directions even the display lens array does not cover digital number of 10 pixels (because the microlens pitch is 850 microns whereas the display pitch is 94.5 microns). The experiment proves that the concept of single stage H3D image rendered is a good candidate for interactive 3D displays.

| Top-right view | Bottom-left view |

| Top view | Top-right-corner view |

Figure 3.16 - Playback Results of single stage H3D image rendering method

The display has H3D resolutions of 143 × 109 3D-pixels, which is the same as the lens array size. A H3D pixel is the intersection of two viewpoint pixels in space.   The lens array does not cover integer number of pixels because we use off the shelf lens array and display to reduce the cost of the experiment. Most importantly, the setup confirms the proposed principle.

3.4   Smart Microlens Array Architecture

In this section, we propose smart microlens array architecture with smart pixel mapping to advance spatial resolution with definition in space. H3D imaging creates physical duplicates of light field to construct a true three-dimensional object in space by simulating the principle of "Fly's eye" using MLA as shown in Figure 3.17.
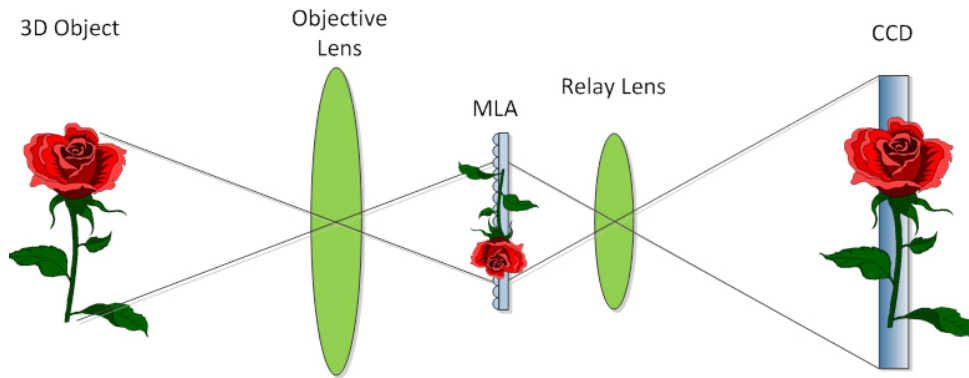
Figure 3.17 – State of the art architecture of the single aperture H3D camera [1]

(a) Square MLA   (b) Cylinderical MLA
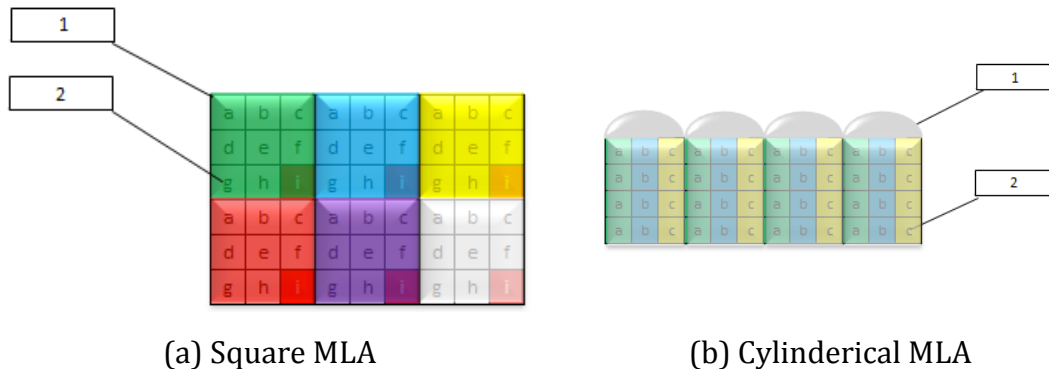
Figure 3.18 – Traditional MLA structure and pixel mapping under the microlens: (1) MLA, (2) pixels per lens

Traditionally, it uses different aperture types of MLA such as spherical, hexagonal and square as shown in Figure 3.18 (a) [10] which offer omnidirectional 3D effects of 3D depth and motion parallax, whereas, cylindrical lens array shown in Figure 3.18 (b) offers unidirectional 3D effects because it only captures 3D information in a single direction. However, the main issue with the traditional pixel structure under the microlens is that three-dimensional resolution and definition is bind to the charge coupled device (CCD) resolution and the MLA. In this section, we propose novel lens array

architecture for H3D camera with smart pixel mapping technique to double the three-dimensional resolution without need of new CCD and lens array.
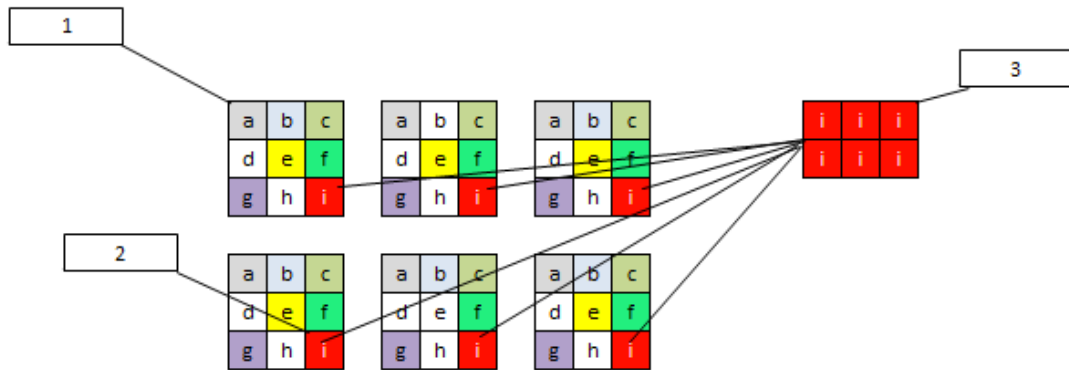
Figure 3.19 – Viewpoint image construction from an omnidirectional H3D image

Figure 3.19's description: (1) Elemental images, (2) Viewpoint pixels in elemental images, (3) Extracted viewpoint
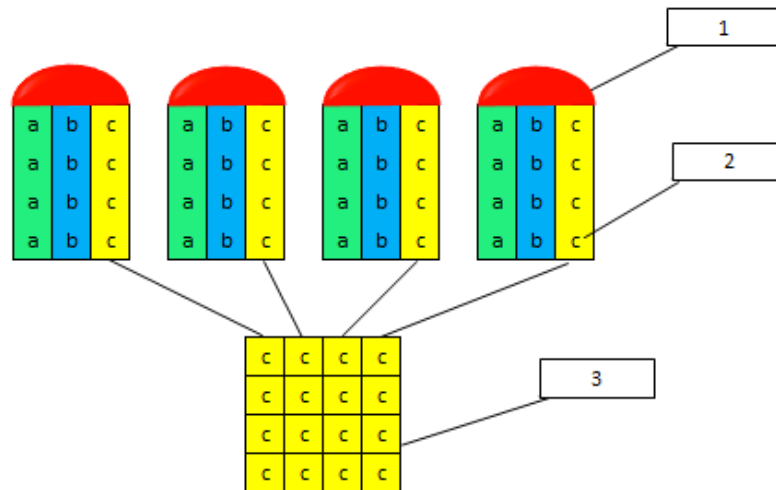
Figure 3.20 – Viewpoint image construction from a unidirectional H3D image

Figure 3.20's description: (1) Elemental images, (2) Viewpoint pixels in elemental images, (3) Extracted viewpoint

A viewpoint image is created by extracting a pixel from an exact location of all elemental images. Figure 3.19 shows the steps for creating a viewpoint image from an omnidirectional H3D image, whereas, Figure 3.20 shows a viewpoint image created from an unidirectional H3D image recorded using a cylindrical MLA. However, the issue with the cylindrical lens is that viewpoint images have

unbalanced pixel aspect ratio, which is caused by much higher vertical resolution compared to the horizontal resolution.

3.4.1   The Proposed Methodology

The proposed lens array architecture for H3D camera improves definition of 3D resolution that also achieves better accuracy in 3D depth calculation. Therefore, it is a suitable architecture for designing post-production 3D cameras such as refocusing, depth measurement as well as high resolution 3D content production applications e.g. shooting a single 3D content which can be used to produce stereoscopic 3D content as well as multiview 3D content in controlled 3D depth.
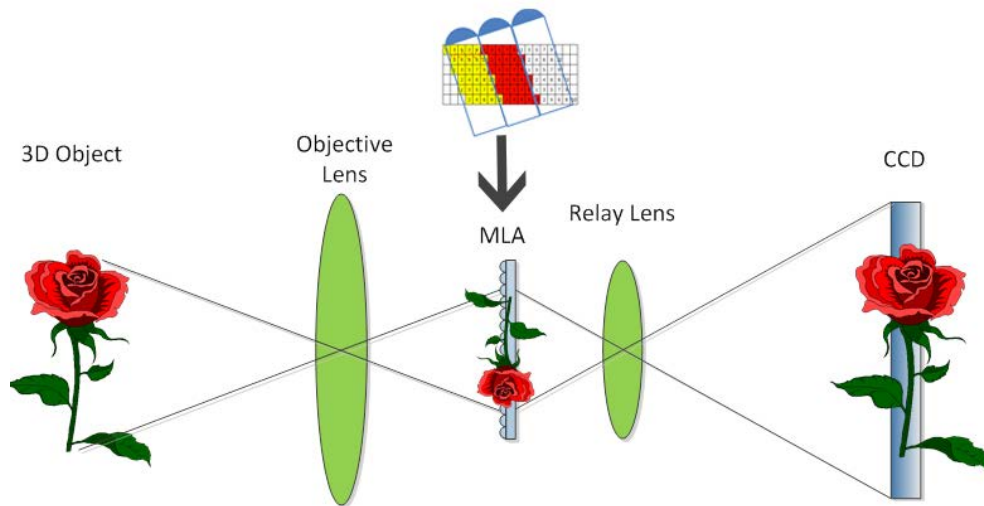
Figure 3.21 – Smart microlens array architecture of the H3D camera

The proposed architecture uses a smart pixel mapping method with slanted MLA as shown in Figure 3.21. In fact, it is a scalable architecture. The lens array slanting angle depends on the dimensionality of the pixel mapping. Figure 3.22 shows two flavours of smart pixel mapping methods which has different slanting angles. As seen in Figure 3.22(a), viewpoints are represented in zigzag manner. It is 2D pixel mapping so it doubles the 3D resolutions whereas Figure 3.22(b) shows 3D pixel mapping, which triples the 3D resolution. As a result, it offers scalable 3D resolutions which can be defined based on the applications. In addition, it resolves the issue "unbalanced pixel aspect ratio" of cylindrical lens array because it trades off horizontal and vertical resolutions in order to enhance the definition of horizontal 3D resolution.
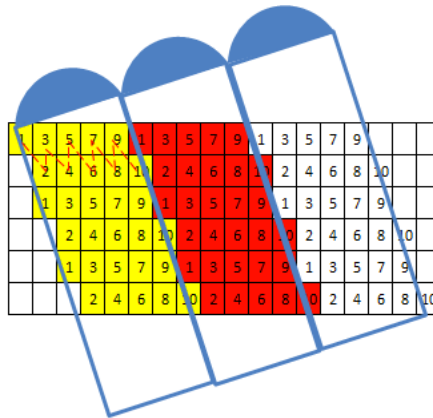
(a) 2-Dimensional Pixel Mapping
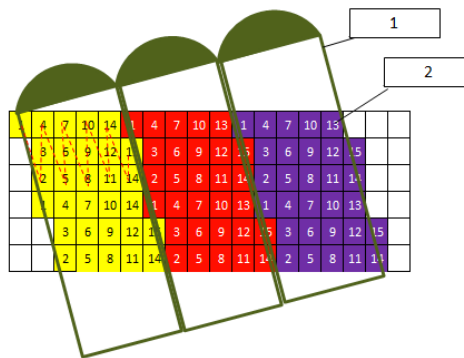
(b) 3-Dimensional Pixel Mapping

Figure 3.22 - The proposed 2D and 3D pixel mapping with smart MLA architecture applied on cylindrical MLA: (1) MLA, (2) Viewpoint pixels

The proposed method is applicable for both cylindrical and spherical lens arrays "uni/omnidirectional H3D images". However the slanting angle must be carefully defined because the pixel mapping is applied on elemental images, which is very low resolution in omnidirectional 3D images. Figure 3.23 shows how viewpoint images are constructed from the captured images using different slanting configuration.

In order to prove the concept, we integrate the proposed method in the H3D camera developed by 3DVIVANT Brunel team [11] using both cylindrical and square lens arrays. Figure 3.24 shows the camera design and layout. The camera is built with the 5.6k sensor of the Canon 5D Mark2 (C5D M2) DLSR. The captured images are presented in Figure 3.25 and Figure 3.26; the results are discussed later in the experiment.
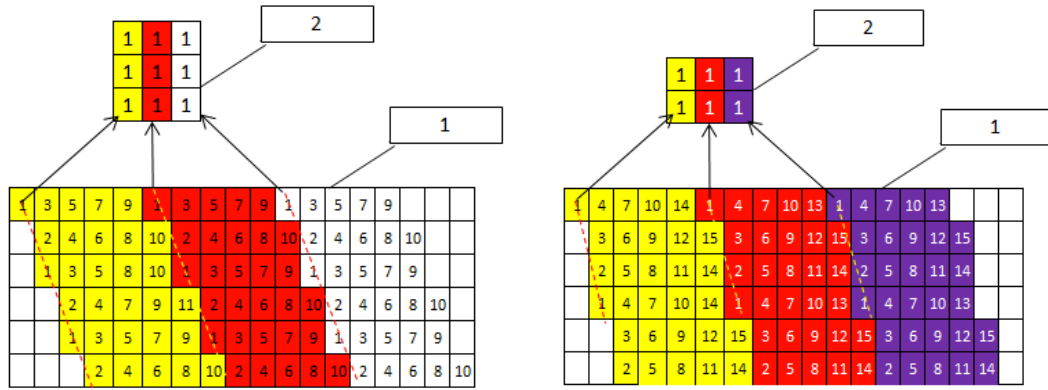
(a) Viewpoint image extraction from 2D-SPM

(a) Viewpoint image extraction from 3D-SPM

Figure 3.23- A viewpoint image extraction from H3D image captured using the proposed method: (1) H3D image, (2) constructed viewpoint image.
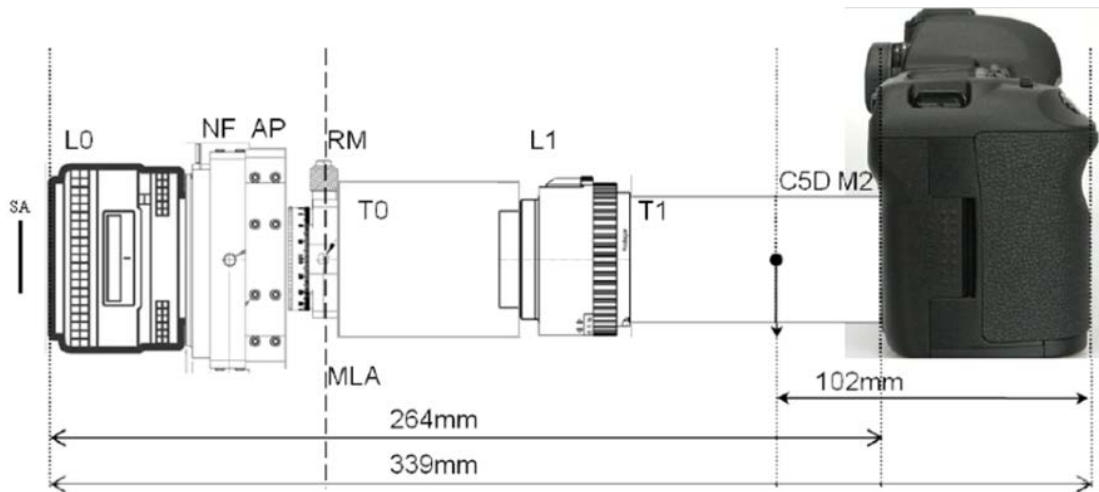
Figure 3.24 - Square Aperture Type 2 camera integration with canon 5.6k sensor [12]

Figure 3.24's description: L0 = Nikon 35mm F2 wide-angle lens, NF = Nikon F-mount, AP = adaptor plate, ER = 6mm diameter extension rods, RM = <5arcminute accuracy rotation mount, MLA = plane of MLA, which is slanted in the process method, T0-T2 = extension tubes, L1 = Rodagon 50mm F2.8 relay lens ×1.89, C5D M2 = Canon 5D Mark2 DSLR. Arrow shows position of center of gravity, SA = Square aperture mouthed to the L0.

Figure 3.25 shows the H3D image captured with square lens array which has a slanting angle of 6.34° degrees whereas Figure 3.26 shows the H3D image captured with cylindrical lens array which has a slanting angle of 9.46° degrees. The omnidirectional H3D image has smaller angle compared to the unidirectional one because the vertical resolutions of elemental images

(omnidirectional) is very low resolution therefore the slanting may distort elemental images.
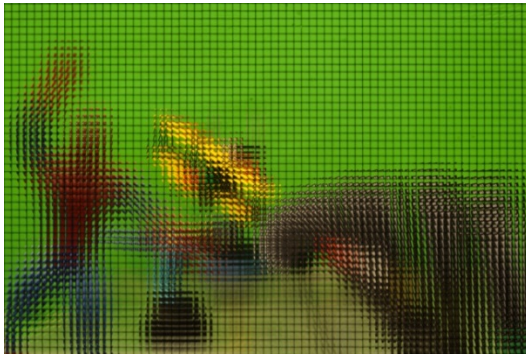
(a) Captured without slanting the MLA
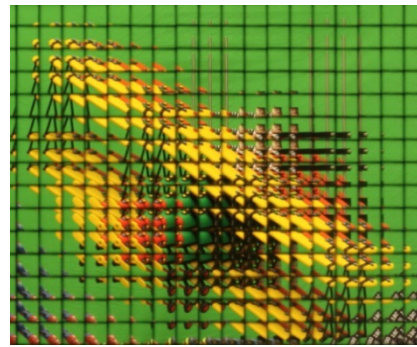
Zoom in view of (a)
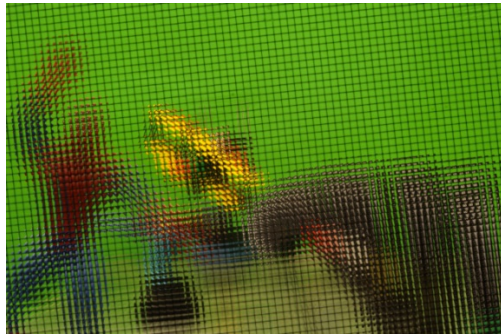
(b) Captured with slanted MLA
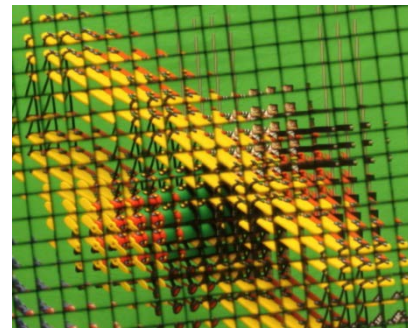
(Proposed method)

Zoom in view of (b)

Figure 3.25 - Captured images using square MLA of 250 microns, microlens image: 69 × 69 Pixels
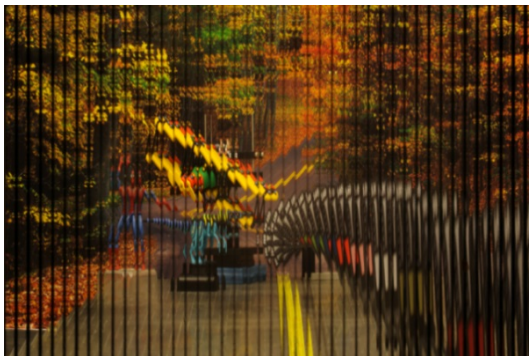
(a) Captured without slanting the MLA
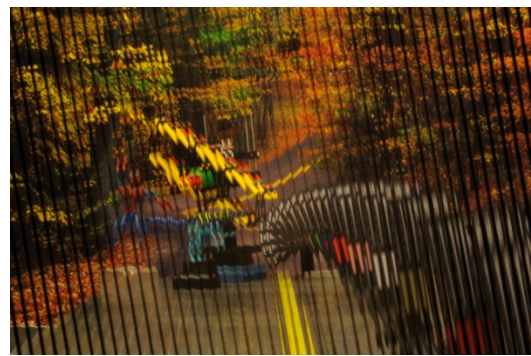
(b) Captured with slanted MLA
(Proposed method)

Figure 3.26 - Captured images using cylindrical lens array of 400 microns, microlens image: 128 × 3996 Pixels

3.4.2   The Experimental Results

The proposed approach doubles 3D resolutions and definitions of the H3D image. It is an appealing design for post-production applications such as

refocusing and 3D depth measurement. In addition, it gains balanced pixel aspect ratio, therefore, it is a potential design for producing multiview 3D content using lenticular based H3D camera. In order to illustrate the effectiveness of the design, the state of the art refocusing algorithm [13] is applied on H3D images, which were captured with traditional and proposed lens array architecture and the results are compared where the proposed method produces more refocusing panel.

In the first experiment, the H3D camera is configured with a square lens array which is slanted by 6.34° degrees. A H3D image is captured using slanted square lens array as shown in Figure 3.25 (b). An image is captured with the traditional approach as shown in Figure 3.25 (a). These two images are used to perform a like-to-like comparison using refocusing algorithm. The proposed method improves 3D pixels per inch in space, which doubles refocusing surface. As the square lens array is slanted 6.34° degrees in the recording stage, the H3D image is de-slanted by 6.34° degrees as shown in Figure 3.27 prior the refocusing algorithm is applied because it easies the process of extracting viewpoint pixels from the image.

As shown in Figure 3.28, there are 13 refocusing panels which are extracted from the traditional image shown in Figure 3.25 (a). The refocusing scene distance is ~3 meters so the distance between two consecutive refocusing panels is ~23cm. Any object within this region cannot be refocused so it is a blink region. In other word, the refocusing plane is rather large therefore the traditional approach cannot facilitate depth measurements very accurately. Figure 3.29 and Figure 3.30 show resulting images of the proposed method which improves depth of the field significantly. It reaches up to 30 refocusing planes within the given distance of 3 meters so the distance between two refocusing planes becomes 10 cm. This clearly shows the proposed method doubles the definition of spatial resolutions as shown in Table 3.3.

(a) Original captured image (slanted)

(b) Pre-processed image (deslanted)

Figure 3.27 - Illustration of de-slanting process

Table 3.3 - Comparison of the proposed smart microlens architecture

Description	Without Slanting MLA	Proposed with slanting MLA
Spatial Resolutions	Depends the employed CDD and MLA	Doubles the spatial resolution
Pixel aspect ratio	Unbalanced pixel aspect ratio	Achieved balanced pixel aspect i.e. wide screen
3D Depth	Depends the employed CDD and MLA	Doubles the depth accuracy

Refocused plane 1
(Focused on front)

Refocused plane 2

Refocused plane 3

Refocused plane 4

Refocused plane 5
(Focused on label 100)

Refocused plane 6

Refocused plane 7

Refocused plane 8

Refocused plane 9

Refocused plane 10

Refocused plane 11

Refocused plane 12

Refocused plane 13

(Focused on back)

The refocused images of the H3D image in Figure 3.25 (a) "without MLA slanting and smart pixel mapping"

Figure 3.28 - All refocusing planes of traditional H3D image shown in Figure 3.25 (a)

Refocused plane 1 (Focused on front)	Refocused plane 2	Refocused plane 3
Refocused plane 4	Refocused plane 5	Refocused plane 6
Refocused plane 7	Refocused plane 8	Refocused plane 9
Refocused plane 10	Refocused plane 11	Refocused plane 12
Refocused plane 13	Refocused plane 14	Refocused plane 15 *(Focused on label 100)*
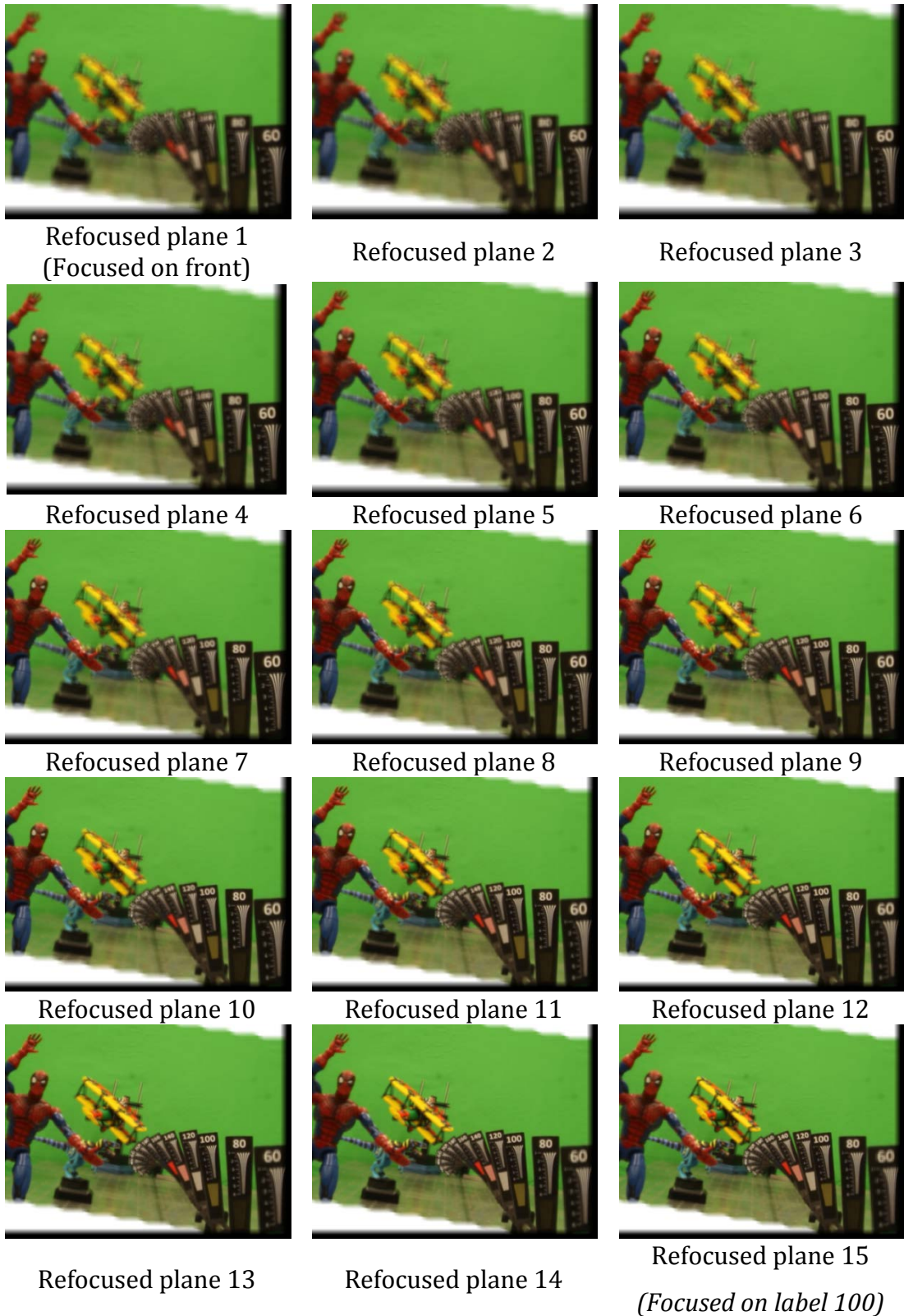
Figure 3.29 – 1 of 2: All refocusing planes of the new approach's H3D image shown in Figure 19 (b)

As the proposed method achieves better 3D depth, 30 refocusing images are generated using the focusing algorithm [13] from the H3D image shown in Figure 3.25 (b).

Refocused plane 16   Refocused plane 17   Refocused plane 18

Refocused plane 19   Refocused plane 20   Refocused plane 21

Refocused plane 22   Refocused plane 23   Refocused plane 24

Refocused plane 25   Refocused plane 26   Refocused plane 27

Refocused plane 28   Refocused plane 29   Refocused plane 30

(Focused on back)
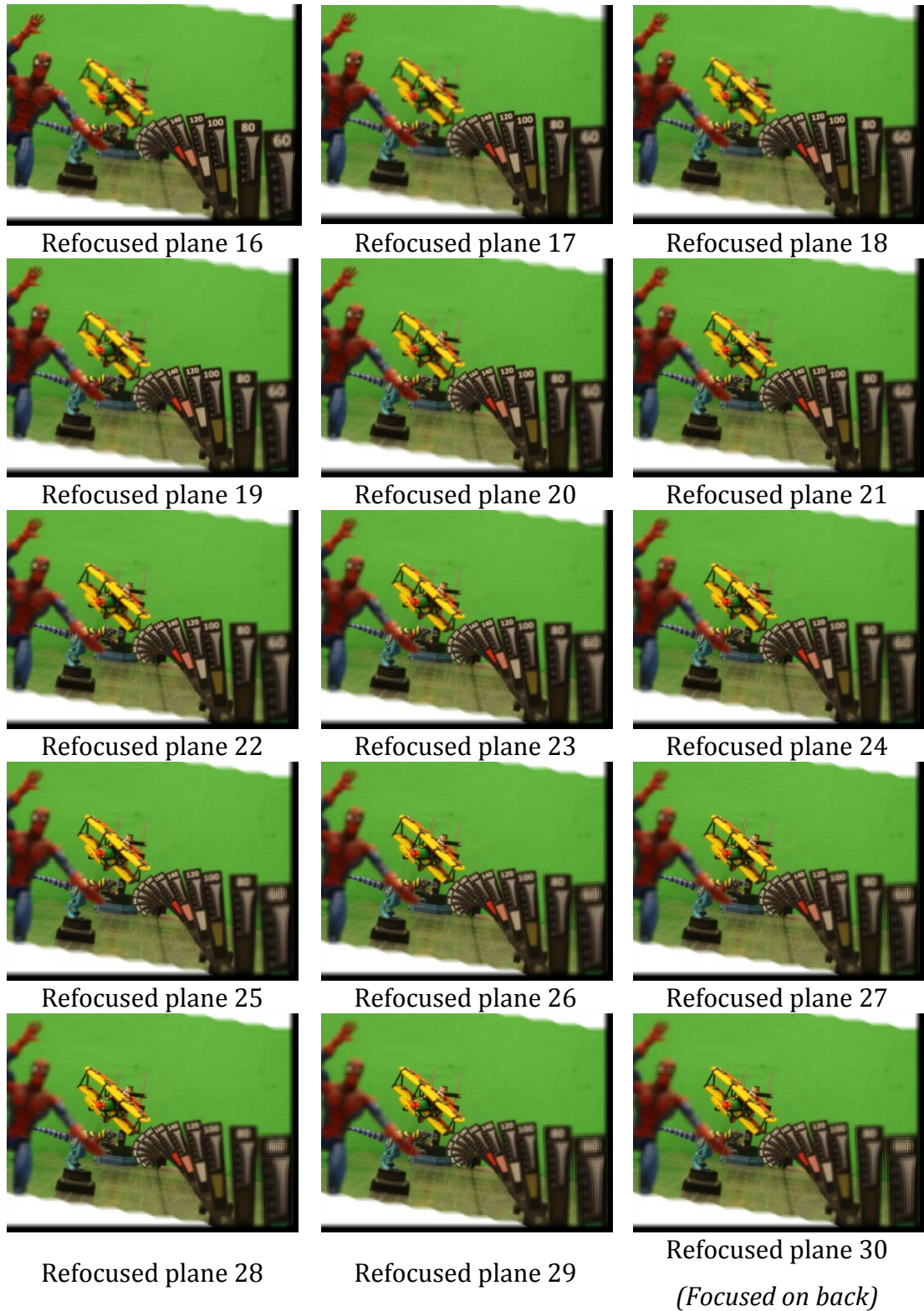
Figure 3.30 - 2 of 2: All refocusing plane of the new approach's H3D image in Figure 19 (b)

As seen in the traditional lens array architecture "Figure 3.28 (3)", the 80 cm-flag is in focused in the 3rd panel whereas in the proposed lens array architecture "Figure 3.29 (11)", it is in focused in 11th panel. Therefore, the

proposed method has the ability to refocus as small as ~10 cm distance. As stated, the proposed method resolves unbalanced pixel aspect ratio of unidirectional H3D image in lenticular technology. Figure 3.31 (a) shows the H3D image capturing with the proposed camera architecture which has a slanting lens array of 6.34° degrees. The 3Dimentional smart pixel mapping is applied to triple the horizontal resolutions as shown in Figure 3.31 (b) by trading off the vertical resolution. In addition, it achieves balanced aspect pixel ratio. As seen in Figure 3.31 (b), much better visual details are achieved.
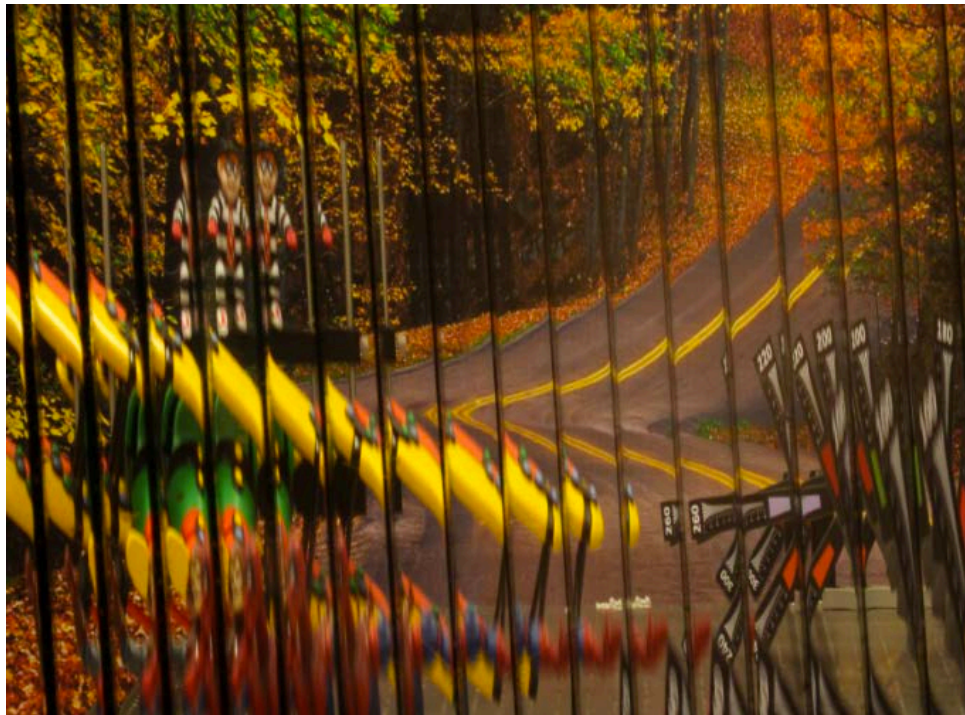
(a) Original H3D image captured with the proposed method

(b) The pre-procesesd H3D image in (a) for reconstruction of virtual pixels
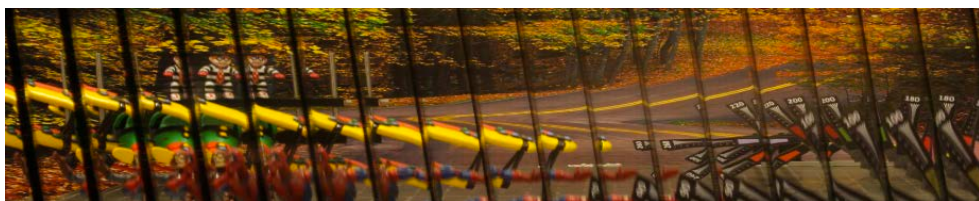
Figure 3.31 – 3Dimensional pixel mapping in unidirectional H3D image: (a) the original H3D image, (b) the pre-processed H3D image
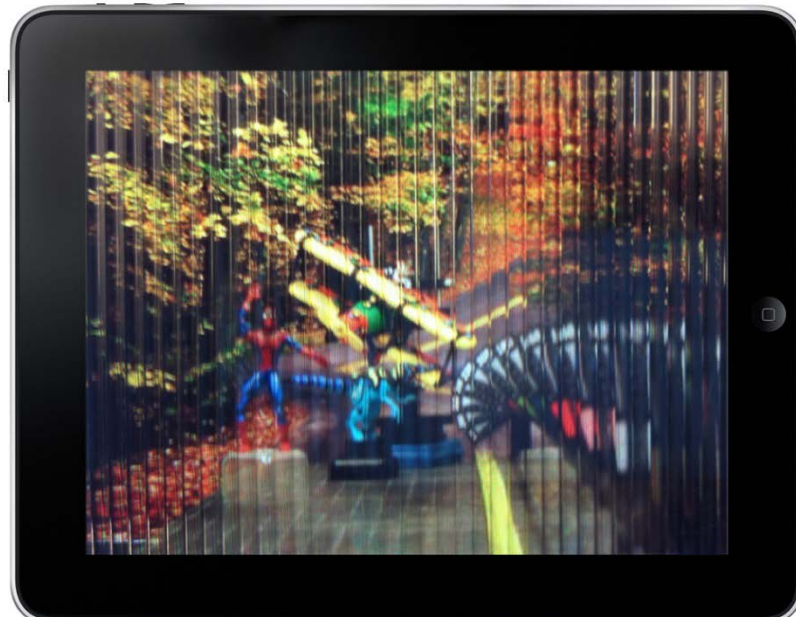
Figure 3.32 – Playback result of traditional H3D image on the H3D display

The proposed lens array architecture is approved and illustrated by 3D processing algorithms i.e. refocusing algorithm [13]. We further tested the captured images on the H3D display. Figure 3.32 shows the playback result of the traditional H3D image whereas Figure 3.33 shows playback results of the proposed approach. The proposed method clearly improves definition of the constructed 3D scene in space.
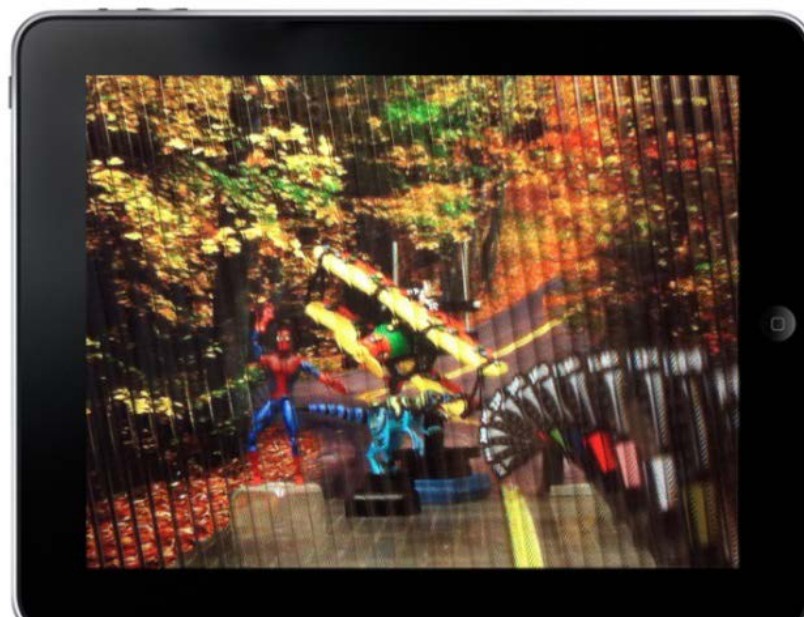
Figure 3.33 - Playback result of the image captured with proposed smart microlens array architecture

3.5   Conclusion

In this chapter, a novel omnidirectional H3D computer graphics rendering method was proposed that is based on 2D array of orthographic cameras.   It is rather simplified and superior approach compared to the traditional method. However, it remains a multi-step process as orthographic viewpoints need to be interwoven to reform a H3D image. Therefore, we proposed a single stage H3D computer graphics rendering method, which takes advantages of CSG. The IOR feature allows simulating the fly's eye technique in recording 3D computer graphics.   The proposed method generates a H3D computer graphic in a single step by constructing a virtual MLA in the virtual computer world and then an orthographic camera is used to render the virtual MLA.

In addition, we proposed smart microlens array architecture with smart pixel mapping for doubling spatial resolution of H3D camera.   In this approach, 3D images are recorded through a slanted lens array as the slanted lens array creates hexagonal oriented pixel structure. A smart pixel mapping method is applied to remap and create viewpoint images/pixels, which are extracted in zigzag style.   It improves the 3D resolutions as well as the definition by trading off horizontal and vertical images on elemental image level.   It also resolves unbalanced pixel ratio of unidirectional H3D images cylindrical lens array based H3D camera.

The smart microlens architecture concept has been proven and demonstrated successfully by replaying the images on the H3D display as well as by applying refocusing algorithm to illustrate the spatial resolution.   The experimental result confirmed the proposed approach doubles visual definition of spatial resolution. It stands a good candidate for future H3D camera architecture.

As H3D imaging technology is in the initial research phase, there are multiple areas such as barrel distortion, vignetting, lens array distortion, and H3D image stitching need improvements.   Indeed it's a great challenge for producing quality H3D images for displays and processing.   Next chapter is going to present pre-processing of H3D images for noise reduction including a stitching algorithm for widening overall viewing angle of H3D camera.

3.6 References

[1] A. Aggoun, E. Tsekleves, M. R. Swash, D. Zarpalas, A. Dimou, P. Daras, P. Nunes, and L. D. Soares, "Immersive 3D Holoscopic Video System", MultiMedia, IEEE, vol. 20, no. 1, pp. 28–37, 2013.

[2] M. R. Swash, A. Aggoun, O. Abdulfatah, B. Li, J. C. Jacome, and E. Tsekleves, "Omnidirectional Holsocopic 3D Content Generation Using Dual Orthographic Projection", IEEE International Symposium on Broadband Multimedia Systems and Broadcasting, 2013.

[3] A. Aggoun, "3D Holoscopic video content capture, manipulation and display technologies", 9th Euro-American Work. Inf. Opt., pp. 1–3, Jul. 2010.

[4] M. Eljdid, A. Aggoun, and O. Youssef, "Computer Generated Content for 3D TV", 3DTV Con-ference, 2007, pp. 1–4, 2007.

[5] Persistence of Vision Pty. Ltd. (2004), Persistence of Vision Raytracer (Version 3.6). [Online]. Available: http://www.povray.org/download/

[6] H. Morishama, H. Nose, N. Taniguchi, K. Inoguchi, and S. Matsumura, "32.3: An Eyeglass-Free Rear-Cross-Lenticular 3-D Display," SID Symposium Digest of Technical Papers, Volume 29, Issue 1, pages 923–926, May 1998.

[7] F. Kirsch and J. Döllner, "OpenCSG: A Library for Image-Based CSG Rendering", Proceedings of the annual conference on USENIX Annual Technical Conference, p.49-49, April 10-15, 2005

[8] A. A. G. Requicha and H. B. Voelcker, "Constructive solid geometry," 1977.

[9] K. Agusanto, "Photorealistic rendering for augmented reality using environment illumination", 2nd IEEE and ACM International Symposium on Mixed and Augmented Reality Proceedings, pp. 208–216, 2003

[10] S. Manolache, A. Aggoun, M. Mccormick, and N. Davies, "Analytical model of a three-dimensional integral image recording system that uses circular- and hexagonal-based spherical surface microlenses", JOSA A, vol. 18, no. 8, pp. 1814–1821, 2001.

[11] 3DVIVANT-Brunel Team, "Holoscopic 3D Camera", Brunel University, 2013. [Online]. Available: www.3dvivant.eu. [Accessed: 01-Jun-2013].

[12]   A. Aggoun, P. Nunes, J. Steurer, M. Meier, S. Theodoros, Z. Nagi, M. Muratori, and P. Nicolas, "Report on Integration issues and prototype system,", 3DVIVANT, 2013.

[13]   O. Abdul Fatah, P. M. P. Lanigan, a. Aggoun, M. R. Swash, E. Alazawi, B. Li, J. C. Fernandez, D. Chen, and E. Tsekleves, "Three-dimensional integral image reconstruction based on viewpoint interpolation," 2013 IEEE Int. Symp. Broadband Multimed. Syst. Broadcast., pp. 1–4, Jun. 2013.

4   Chapter Four - Holoscopic 3D Image Processing

This chapter presents a novel technique for widening overall viewing angle of H3D camera aperture including processing of H3D images for visual data alignment. In addition, it discusses H3D image conversion for H3D displays, medical tomographic image conversion and interactive H3D video content player. The layout of this chapter is as follows: 4.1 Introduction, 4.2 Barrel Distortion Correction, 4.3 Pre-processing of H3D Image, 4.4 Micro-image Equaliser, 4.5 H3D Image Stitching, 4.6 H3D Image Conversion for Multiview 3D Displays, 4.7 Medical Tomographic Image conversion, 4.8 Interactive H3D Content Search and Retrieval, and 4.9 Conclusion.

4.1 Introduction

One of the challenges in the reconstruction process for H3D display is nonlinear distortion in 3D image capturing. The nonlinear distortion in a H3D camera mainly includes lens radial distortion (intrinsic) and MLA perspective distortion (extrinsic) which can seriously affect the viewpoint extraction process. This chapter discusses automatically calibration grid generation for Barrel distortion correction.

A H3D camera uses lens array to record 3D information. A lens array consists of array of perspective microlenses firmly packed in non-overlapped manner thus dark borders noise get introduced in the recorded H3D image regardless of microlens aperture/shape. A MLA dark borders correction filter is presented that uses MLA to generate a grid and then uses the information to detect and to remove the border noise.

A micro-image equaliser algorithm is proposed for equalising micro-image sizes and correcting the unfilled microlens images. It defines a default size of micro-image by averaging size of all micro-images and then it resamples all micro-images to the defined size by down-sampling and up-sampling.

H3D cameras captures a very small scene as its overall viewing angle is limited and one way of improving overall viewing angle of H3D camera is shooting images by shifting the H3D camera in horizontal / vertical directions and then stitch the images to produce one larger view image. This is straight forward in 2D imaging systems but in H3D imaging system, the stitching process must be processed in micro-lens image to synchronise 3D information correctly from a micro-image to micro-image. To resolve this issue, a reference based H3D image stitching method is proposed that uses MLA information to perform the stitching in micro-lens level and the proposed method enlarge the holoscopic camera aperture. In addition, it can be used for shooting 360 degrees H3D images.

A H3D image conversion algorithm is presented that parses H3D images to multiview 3D displays by applying supported multiview pixel mappings. In

addition, medical tomographic image reformation is explored that enables to visualise tomographic image data on the H3D display.

Last but not least, an interactive H3D content browsing solution is proposed and developed. In fact, it is a joint work carried out in 3DVIVANT project [2] and my contribution includes development of dynamic hyperlinker, 3D content descriptive protocol schema and metadata engineering & synchronisation [3]. The proposed system advances 3D multimedia content navigability and search-ability by linking selectable objects in the scene while the H3D video clip is being replayed.

4.2   Barrel Distortion Correction

In this section, a barrel distortion correction algorithm is presented and it is a joint work carried out by 3DVIVANT team at Brunel University [1]. My contribution is the idea of using MLA as a reference point to correct the barrel distortions as well as the implementation of the calibration grid module, which generates a calibration grid from the camera MLA by simply capturing a white background.

H3D imaging is based on concurrent capture of many different views of 3D scene by using MLA as shown in Figure 4.1 (a). Under each micro-lens, there are certain pixels to depict different view point. During the reconstruction stage as shown in Figure 4.1 (b), an appropriate lens array is placed on top of the display equipment to reproduce the 3D scene [4]. However, nonlinear distortion will happens during the capturing stage. Both intrinsic and extrinsic factors in the integrated camera contribute to the distortion.

The lens radial distortion of the lens specific feature is the main intrinsic factor in the system. This will occur in two main effects which are barrel and pincushion. Second is the MLA perspective distortion which happens from the mounting procedure (extrinsic) of the MLA which can induce perspective errors. The nonlinear distortion is critical to the 3D scene reconstruction and must be corrected before display. In order to correct such distortion, people can either use third-party programs such as Photoshop or calibrate the real camera system. The third-party program cannot read real system parameters, so it is

not accurate. Therefore, calibrating the real camera system is more attractive. There are many methods for calibrating camera distortion [6][7][8][9]. Their basic concept is acquiring an image of the planar calibration target using the imaging setup. For the planer calibration target, the common patterns include square chessboard, square grid, circular grid, etc. Since the geometry of the calibration target is known, the camera distortion parameters can be estimated to a high level of accuracy. However, this method does not work with H3D imaging cameras because of the existence of the lens array. For this reason, developing a flexible method for correcting distortion in a H3D camera is necessary.
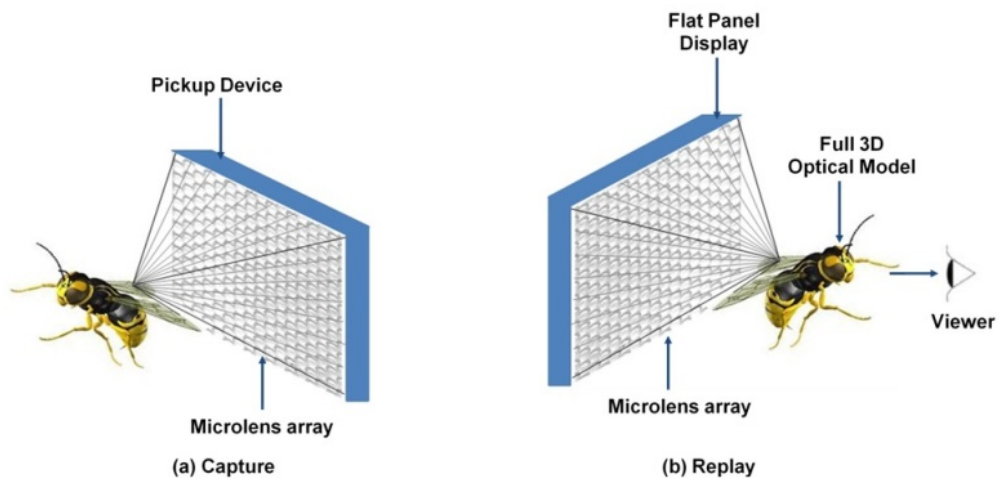
Figure 4.1 - (a) Recording and (b) replay process in the H3D Imaging System [4]

In here, a nonlinear distortion correction method for a H3D Imaging system is proposed for the first time. According to the calibration grid which is generated from the lens array, it is successfully demonstrated on a single aperture H3D camera developed in Brunel University [1]. The correction principle can also be applied to other H3D imaging system.

4.2.1   The Proposed Barrel Correction Method

As any changes in the H3D camera system will violate the nonlinear distortion, the calibration is valid only for the H3D camera system that is used to create the grid. Once a new camera system is setup, before capturing a H3D image, this camera system should be calibrated first. This allows compensating nonlinear distortion inherent in the system. In order to generate a calibration grid of

circular dots from the MLA, an image with plain background (e.g. white background) is captured (Figure 4.2 (a)).

The camera lens is manually focused at infinity which is the same as the 3D scene capturing plane. Applying threshold technique (enhancing the border intensity) to detect microlens borders (edges) [10][11], an image (Figure 4.2 (b)) with clear grid lines is achieved. Plotting circular dots at each microlens intersect (Figure 4.2 (c)) and removing all borders are the subsequent steps that need to be completed. This generated calibration grid (Figure 4.2 (d)) will contain all important parameters of the H3D camera.

The Brown's distortion model [12] is applied to calibrate the camera system. An application is developed based on NI Vision [13] to learn the calibrated information, which uses a list of pixel to real-world mappings and a nonlinear algorithm [13] to create a mapping for the entire image. The nonlinear algorithm computes pixel to real-world mappings in a rectangular region entered around each dot in the calibration grid. It estimates the mapping information around each dot based on its neighboring dots. The information obtained from the calibration process can be saved and used to correct nonlinear distortion of this system at any time.
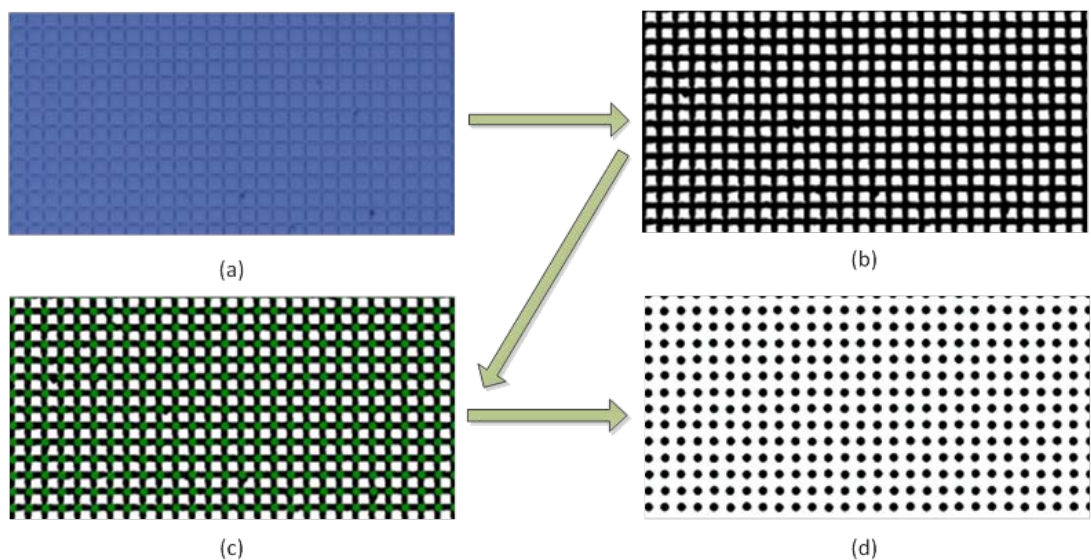
Figure 4.2 - Calibration grid generation for a 3D Integral Imaging camera (a portion from an image of 5616 x 3744 pixels), (a) captured 3D image with white background the grid lines are the borders of the MLA with 90μm pitch (b) the image after enhancing the border intensity

After calibrating the H3D camera system, the distortion of the captured image can be corrected by attaching the calibration information. Image correction involves transforming a distorted image acquired in this system into an image where nonlinear distortion is corrected. The image is corrected by applying the transformation from pixel to real-world coordinates for each pixel in the input image. Subsequently applying simple shift and scaling transformations to position the real-world coordinates into a new image.

The corrected H3D image can be used for the viewpoint extraction process and H3D display after some signal processing. In our demonstration, the captured pseudoscopic images are digitally processed and converted to orthoscopic images. The block diagram of the nonlinear correction procedure is shown in Figure 4.3.
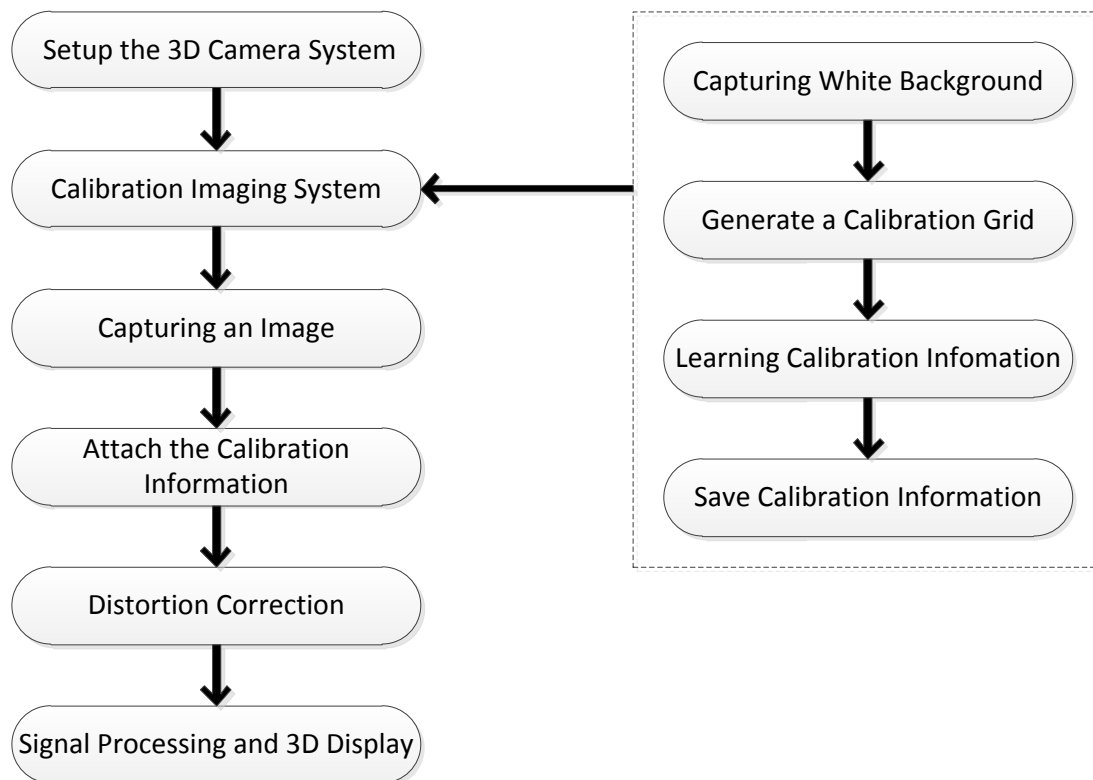
Figure 4.3 - Block diagram of the proposed barrel correction procedure [1]

4.2.2 Experimental Results

The first experiment is demonstrated using a S-90-0.25 pitch MLA (Epigem, Pitch = 90µm, f=1mm, square 100% fill). Under each microlens there are 29×29 pixels, so the effective resolution of the reconstructed image is 193×129 pixels.

After assembling the 3D integrated camera, it is calibrated using the above proposed method at the beginning. The comparison between the uncorrected and corrected H3D image is shown in Figure 4.4. The magnified section at different area is picked up individually. Using the MLA borders as the reference grid line, the nonlinear distortion from the uncorrected image it is obvious that the horizontal (vertical) lines are not straight (Figure 4.4(b)-(d)). Vertical lines are the same. This effect can be corrected after the nonlinear distortion correction procedure (Figure 4.4(f)-(h). The black areas which appear at the image borders are the objects outside the field-of-view (FOV) during the capturing process. In the reconstruction processing, the microlenses with black area are not considered.
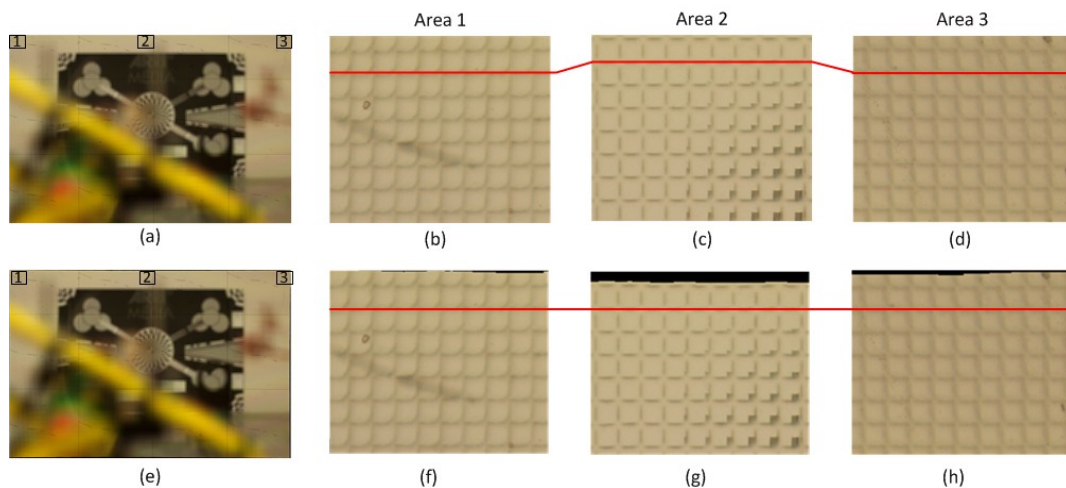
Figure 4.4 - (a) Uncorrected and (e) corrected 3D image (5616 x 3744 pixels) using 90μm pitch MLA with magnified section comparison in different area, (b) (c) (d): uncorrected magnified sections, (f) (g) (h) corrected magnified sections.

The reliability and accuracy of our correction method is further proved by the comparison of the single viewpoint extraction between an uncorrected and corrected H3D image. The basic idea of the viewpoint extraction is shown in Figure 4.5. A single viewpoint image is constructed by extracting one pixel from each lens. For example, assembling of every first pixel (1, 1) of each lens generates the viewpoint image (1, 1). A viewpoint image is formed by extracting a pixel of extract location from every microlens in MLA. Three different viewpoints from uncorrected and corrected image are selected respectively as shown in Figure 4.6. For the uncorrected image, undesirable distortions in reconstructed viewpoint images are noticeable. The viewpoint

images are blurry and inaccurate. However, after distortion correction, the reconstructed viewpoint images are sharp and accurate. This demonstrates that our proposed method can be used in real-time 3D display.
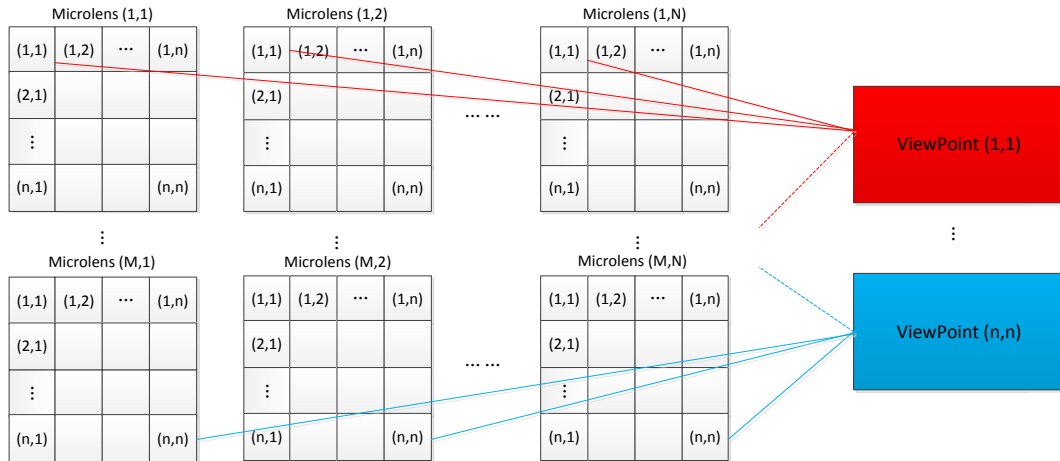
Figure 4.5 - Fig. 8. Viewpoint extraction from a 3D Integral image, (M, N): the number of MLA, (n, n): the pixels under a single microlens. The total of n^2 viewpoints can be generated. The resolution is M x N for each viewpoint image [1]
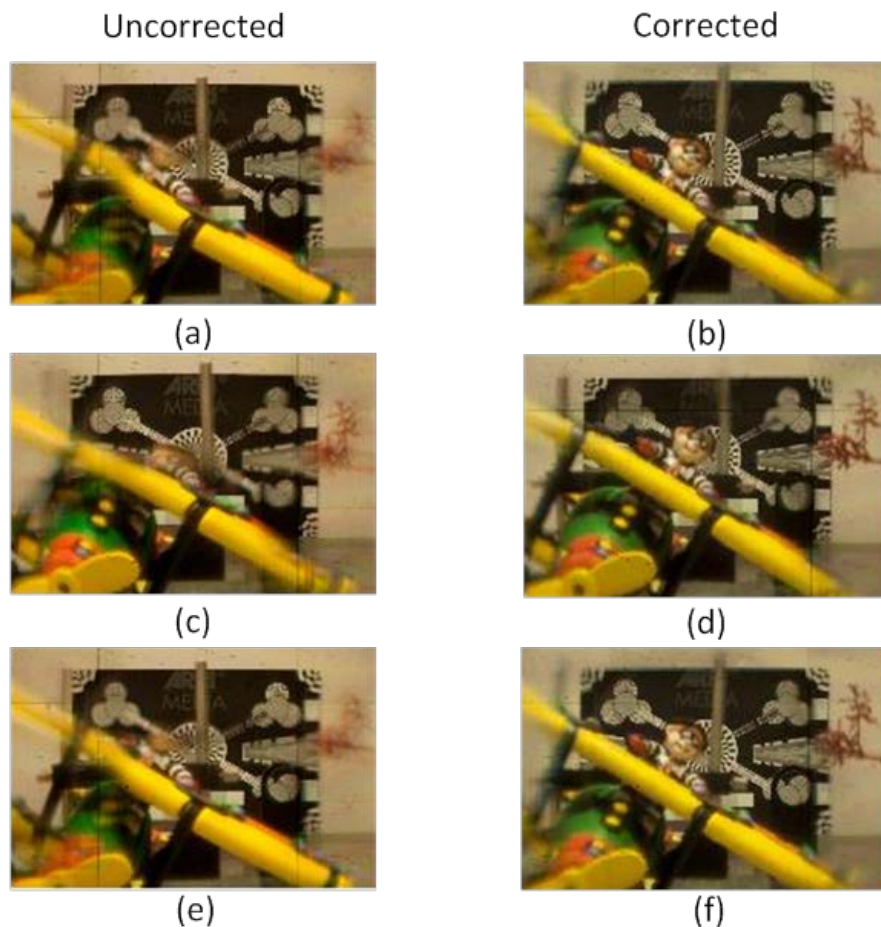
Figure 4.6 - Viewpoint extraction images of 193 × 129 resolution: (a) viewpoint image (1, 1), (c) viewpoint image (20, 20), (e) viewpoint image (29, 29) from an uncorrected 3D image; (b) viewpoint image (1, 1), (d) viewpoint image (20, 20), (e) viewpoint image (29, 29) from a corrected 3D image
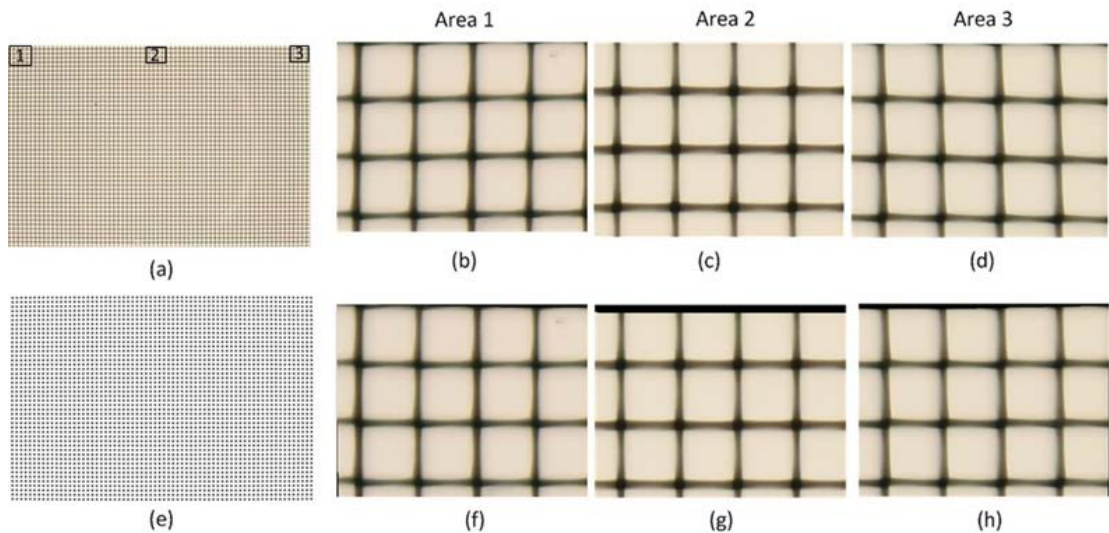
Figure 4.7 - (a) Captured 3D image (5616 x 3744 pixels) using 250μm pitch MLA with white background, (e) an image with circular calibration grid from image (a). Magnified section comparison in different area, (b) (c) (d): uncorrected magnified sections, (f) (g) (h) corrected magnified sections.

Another testing was performed using a 250-1.0-S MLA (Adaptive Optics Associates, Pitch = 250μm, f=1mm square 100% fill). The effective resolution is 70×46 pixels as there are 80×80 pixels under each microlens. Because the 3D camera system is changed, the calibration of 90μm MLA is not valid for this setup. Another circular calibration grid (Figure 4.7 (e)) is generated from the captured white background image (Figure 4.7 (a)). The calibration should be implemented according to the generated grid for this setup. Correction results are shown in Figure 4.7 (f)-(h) with a comparison to the uncorrected image in Figure 4.7 (b)-(d). The distortion from the captured image is removed after correction. The method is not only valid for the square MLA, but also hexagonal and other regular distributions. As the border information of the MLA is obtained, it's not difficult to generate a proper calibration grid for the camera with the specified MLA.

4.3 Pre-processing of H3D image

In this section, a referenced based MLA border reduction algorithm is proposed and presented that reduces the dark borders introduced by MLA in H3D images [14]. A H3D image is captured through a MLA, which is made of multiple lenses of the same specification formed in a one-dimensional or two-dimensional array on a supporting substrate. The microlenses are not allowed to overlap therefore there are gaps between the microlenses which introduce dark border

noise. Such distortions are scaling errors which, if not corrected, will cause noises and dark moiré effect on the playback and in the final image even in processing.

Images are captured with the H3D camera developed by 3DVIVANT team at Brunel University [1]. The captured H3D image is illustrated in Figure 4.8 and there are noticeable dark borders in the image.

The barrel distortions of the image are corrected prior to the proposed method is applied. The proposed MLA borders correction algorithm uses MLA as a reference point to detect the amount of dark borders. This is done by simply capturing a white background.
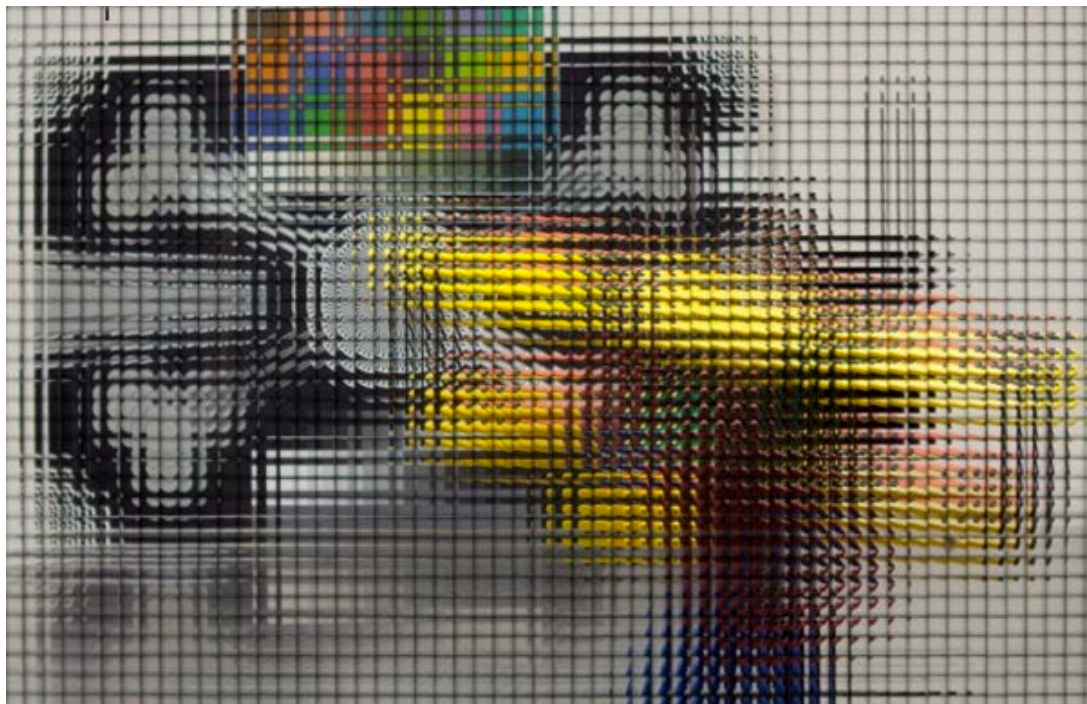
Figure 4.8 – Resulting captured H3D image with H3D camera at Brunel University [1]

Figure 4.9 shows block diagram of the proposed method. As seen the process is rather simple and fast compared to any other visual data processing because it references the MLA information i.e. grid to filter out dark borders in the image. (1) once the camera is setup, (2) the dark borders are detected and learnt by generating a grid of the lens array as shown in Figure 4.10, (3) capture your desire H3D image, then (4) the proposed algorithm is applied on the captured images that uses the information learnt during the calibration to filter out the dark borders in the image.
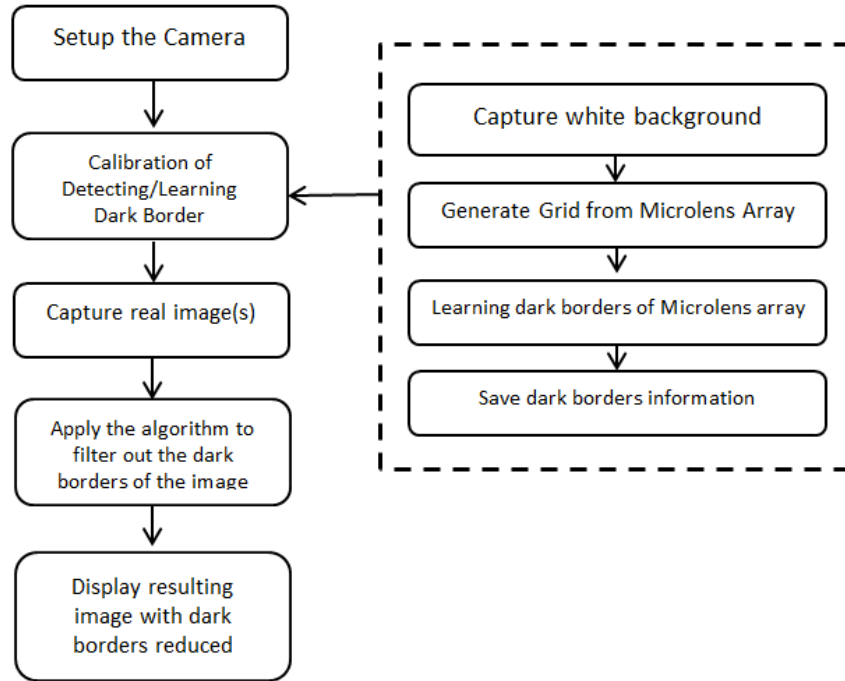
Figure 4.9 - Block diagram of proposed MLA dark borders correction algorithm

The MLA grid information helps to extract elemental images and filter out dark borders as shown in Figure 4.11. The proposed method filters out only extra dark borders thus it does not remove the lens array border completely. Instead it refines them further as shown in Figure 4.12 as it will align well with the playback lens array. Removing the borders completely will also remove visual details which should be avoided.

The proposed method works dynamically as it is calibrated with the H3D camera's MLA dynamically every time the camera is setup. The dark border noise could vary as the camera setup changes. As a result, it has a self-tuning method which is valid for all type of H3D cameras.

| (a) White background | (b) MLA Grid |
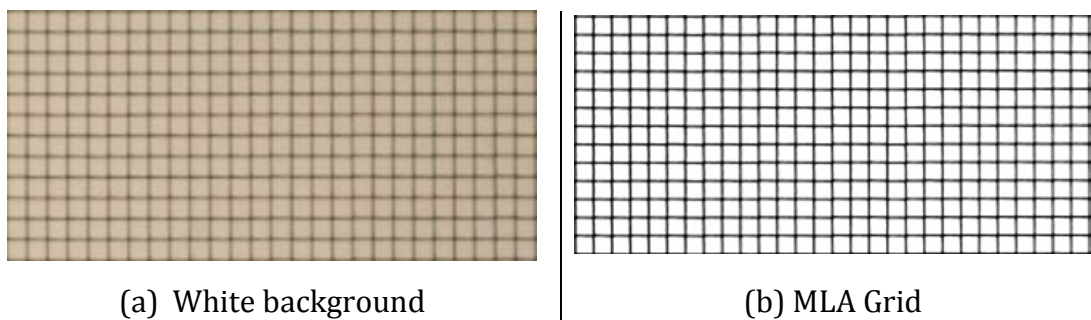
Figure 4.10 - Generated microlens grid from H3D image of a white background

(a) Generated microlens dot grid (b) H3D image prior to correction
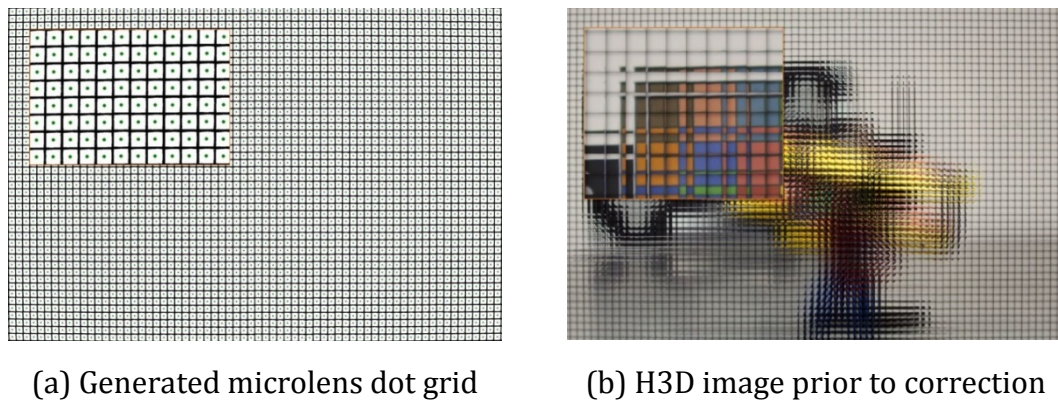
Figure 4.11 - MLA grid and the original image before applying the proposed algorithm

4.3.1 Experimental Results

The proposed method is applied to an omnidirectional H3D image (Figure 4.8) and its resulting image is shown in Figure 4.12 which also illustrates the removed bordered. It makes an educated decision in removing the dark border that is based on microlens grid information which is learnt prior to the operation.

(a) The resulting image (b) The removed dark borders
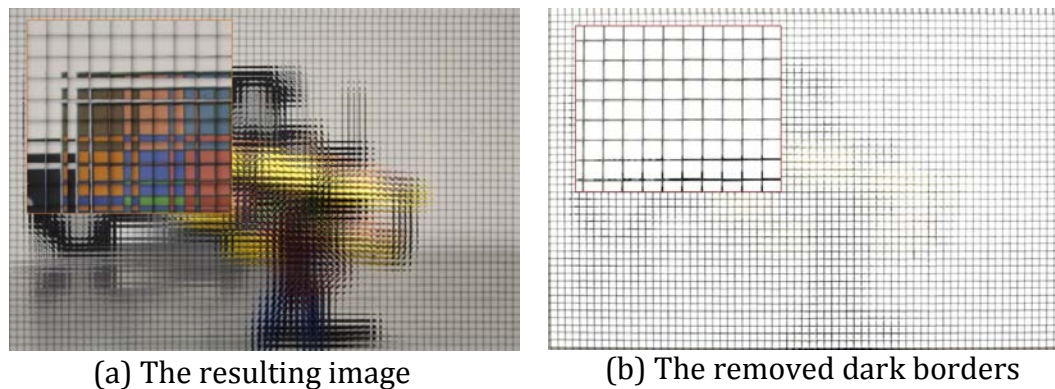
Figure 4.12 - The resulting image of the proposed method

It is scalable and applicable to unidirectional H3D images. In fact, it can be applied to any image, captured with a light field 3D camera, because it is not dependent on any fixed parameters or threshold values. Instead, it is just a matter of capturing an image of white background, which is used to detect and filter out the undesirable dark borders without affecting the visual data. As the algorithm uses MLA information without carrying out exhaustive signal processing, its execution is computationally light therefore it can be implemented on the camera to filter images on the capture.

4.4   Micro-image Size Equaliser

This section presents a micro-image size equaliser algorithm.   The barrel distortion in H3D image also causes vignetting distortions, unfilled micro-image and unbalance micro-image size which are random errors that need to be considered for different systems. Figure 4.13 (a) shows a distortion free 3D image whereas Figure 4.13 (b) illustrates an image with distortions caused by barrel distortion and in this case, each cell represents a micro-image. As seen in Figure 4.13 (b), the micro-images have different sizes, and also the micro-images in the edges are unfilled due to failing to record visual information. This section proposes a micro-image size equaliser algorithm for balancing out microlens-images size which reduces noise in the replay and processing.

(a)   (b)
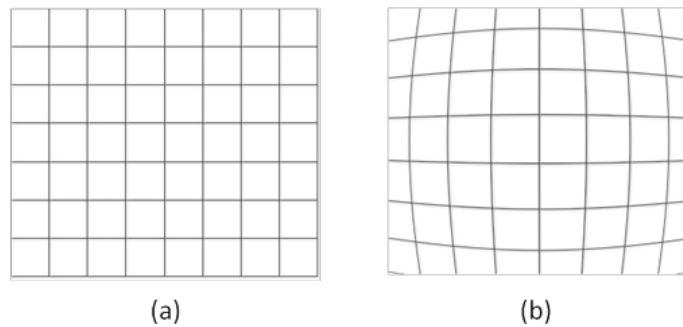
Figure 4.13 – (a) Image without distortion, (b) Image with distortions: each cell represents an elemental image also known as micro-image

Such distortions varies due to H3D camera configurations, for instance, the distortions will be different for a wide angle and a narrow angle lens array in the H3D camera setup. The proposed method is applicable to all type of lens array of H3D camera as it takes advantages of MLA for defining a default size for micro-images. As seen in Figure 4.14, micro-images are not equal and noise varies from micro-image to micro-image depending on its location. For instance, the micro-images at the edges have more noise and are smaller than the micro-images in the middle areas.
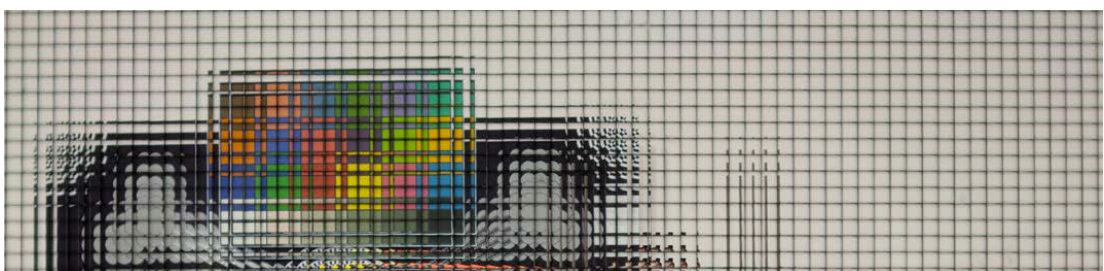
Figure 4.14 – Small segment of original image before applying the micro-image equalizer

4.4.1   Defining a Default Size for Micro-Images

The proposed method calculates the default size of micro-images from a holoscopic image of white background. It references and uses MLA grid to define a default size for micro-images. It uses the grid as a reference source to average height/width of micro-images vertically and horizontally for defining the default size as illustrated in Figure 4.15. Indeed, it runs once in each direction from the middle of the image, because middle micro-images of both directions carry valid error size distributions. The grid (Figure 4.15 - (c)) is generated by histogram thresholding technique (enhancing border/background intensity) to detect microlens borders (edge) [10][11] on a white background image shown in Figure 4.15 (a).
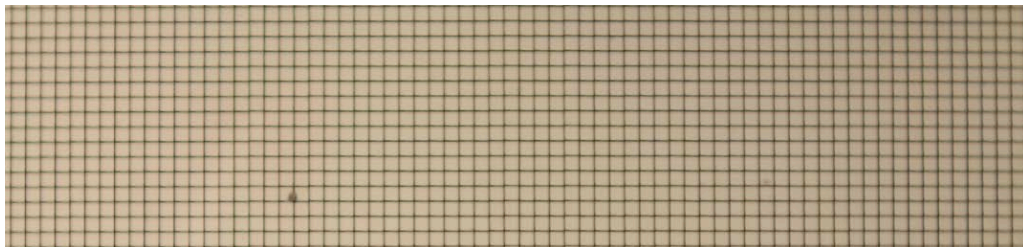
(a) Small top portion of zoom H3D image of a white background
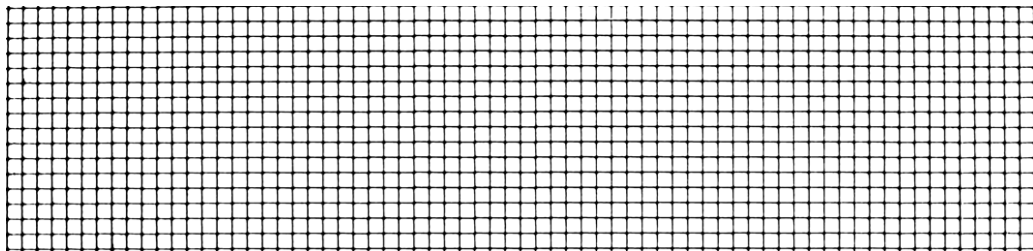
(b) Small top portion of zoom lens array grid generated from a white background image
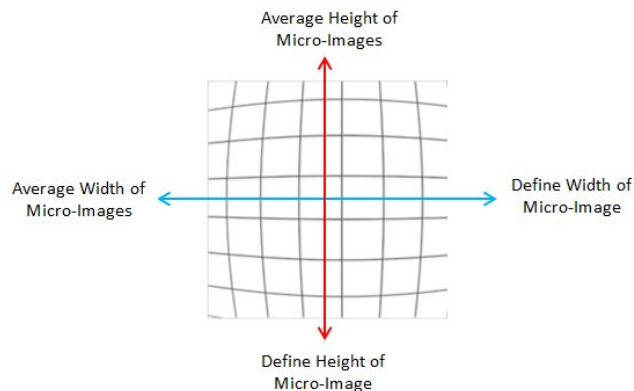
(c) Averaging process of micro-images

Figure 4.15 – Illustration of defining the default micro-image size (height/width)

4.4.2   The Micro-image Size Equaliser Process

The proposed method requires a quick calibration for every camera setup which is performed by just capturing a white background. A white background 3D image is used to generate the MLA grid, which is used to define a default micro-image size and later for extracting micro-images from the H3D images as shown in Figure 4.16.
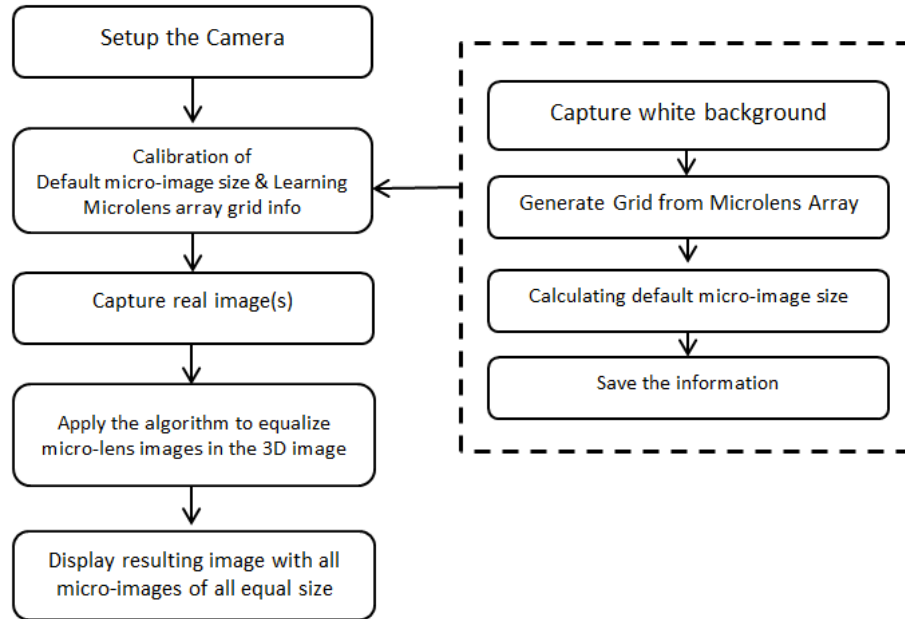
Figure 4.16 - Block diagram of the proposed micro-image size equaliser algorithm

4.4.3   Experimental Results

The test images are captured using the H3D camera [1] developed by 3DVIVANT team at Brunel University. The proposed method is applied offline after H3D images are captured; however, the algorithm is computationally efficient so it can be implemented on-camera in order to apply captured images in real time. As seen in the resulting image in Figure 4.17 (b), the resulting image's quality is improved compared to Figure 4.17 (a). The resulting image does not have distortions as micro-images are picked by referencing MLA grid information and then a new H3D image is rendered from resampled micro-images. The zoom-in version of the input and output H3D images is presented in Figure 4.18 which clearly shows the improvement e.g. equalised micro-image size. Yet the method does not recover the lost data, which is part of future work, as it will be further developed to be able to recover the lost data from neighboring micro-images.
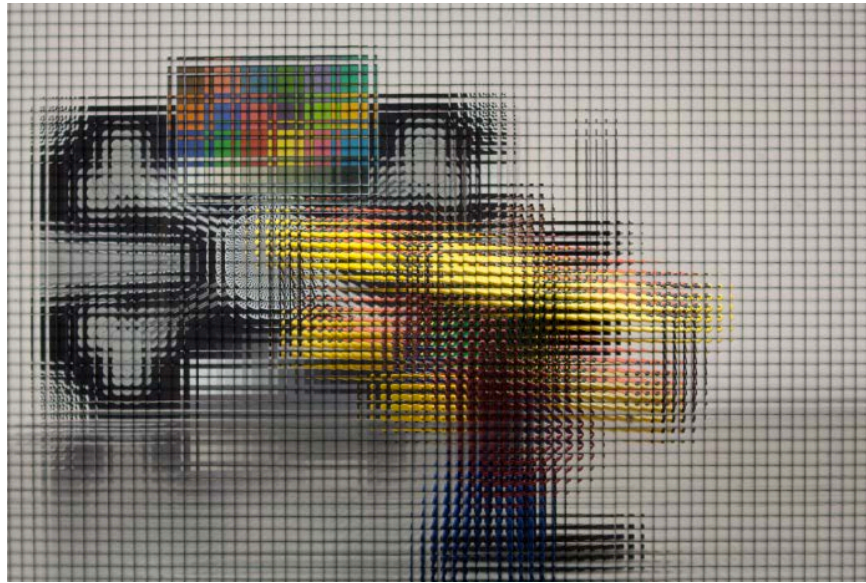
(a) input original image
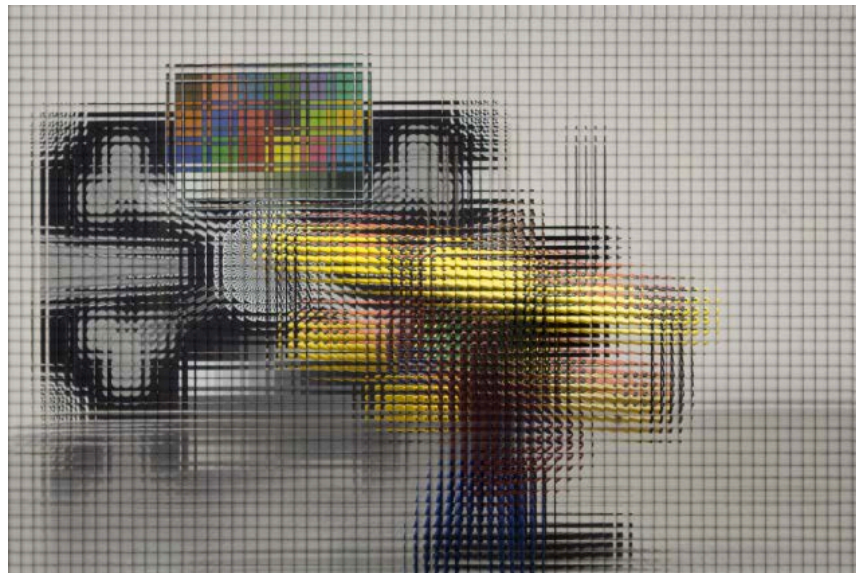
(b) output resulting image

Figure 4.17 - The resulting image of micro-image equaliser for noise reduction method

(a) input original image (zoom version of small portion in top)
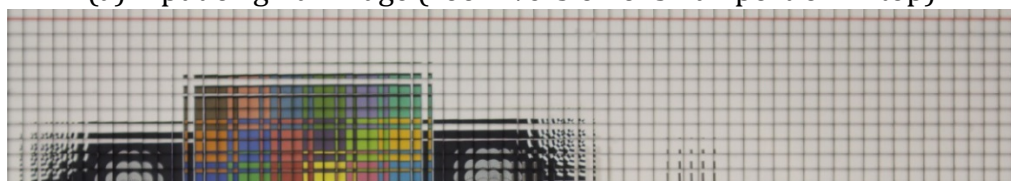
(b) output resulting image (zoom version of small portion in top)

Figure 4.18 - The resulting image of micro-image equaliser algorithm

4.5   H3D Image Stitching

A digital image stitching has been intensively used in 2D imaging systems for capturing 360° images, shooting panoramic scenes, enlarging a camera aperture and stitching two or more images of the same scene. In 2D imaging system, the stitching is perform by matching low level visual feature [15][16] however the problem is that these 2D stitching algorithms are not applicable for stitching H3D images [5] because A H3D image consists of micro-images which contribute to construction of a 3D scene in space with full 3D depth and motion parallax.   If micro-images are not propagated correctly it will cause error in construction of 3D scene on 3D display, thus it is essential to synchronize micro-images.

As a result, a reference based H3D image stitching method is proposed and presented for improving the overall viewing angle of H3D camera aperture. It enables stitching two or more H3D images without effecting 3D information that reside in the micro-images as microlens specification is considered during the process.

The lens correction algorithm is applied to correct nonlinear distortions to ensure the images are distortion free and the nonlinear distortion is mainly contributed from the lens radial distortion and MLA perspective distortion, which can seriously affect the reconstruction processing for the 3D scene. In this section, lens correction algorithm is not going to be discussed because the main focus is on H3D image stitching algorithm.

The proposed reference based H3D image stitching is computationally light and fast compare to 2D image stitching or any other visual data processing because it does not do any low level visual comparison; instead it takes advantages of MLA for referencing stitching points/locations in stitching 2 H3D images. Also it takes fewer steps for stitching two images as shown in Figure 4.19 because (1) once the camera is setup, (2) a simple histogram filtering algorithm generates MLA grid from a H3D image of white background as shown in Figure 4.20. (3) The first image is captured then (4) the camera is moved, which is discrete to digital number of microlenses, otherwise elemental images (represent a

microlens image) will be integrated with false information. (5) The second image is captured and then (6) MLA grid information is used to stitch the two images.
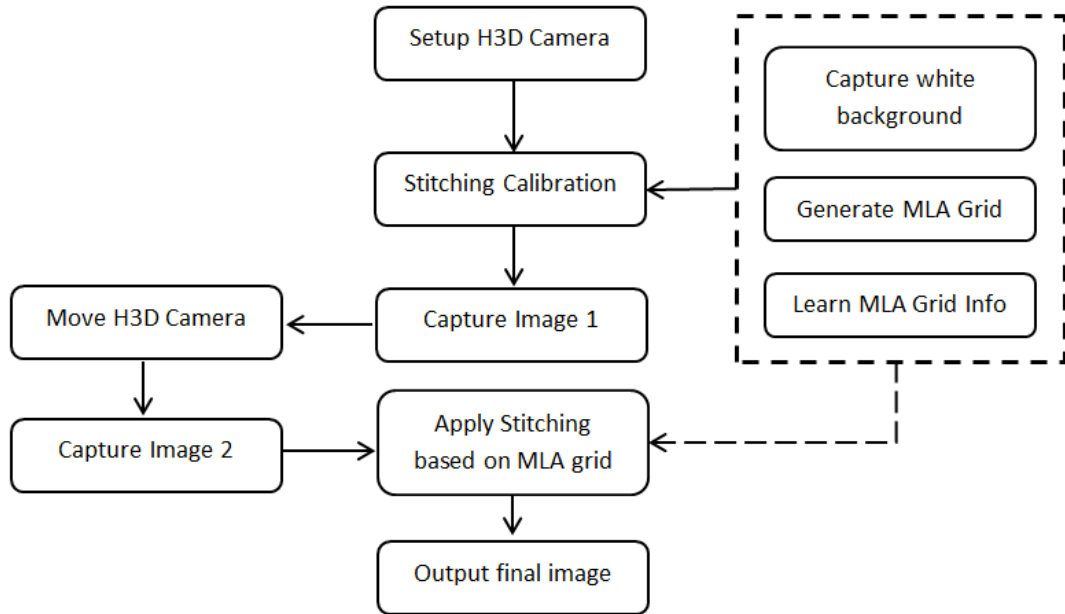
Figure 4.19 - Block diagram of proposed reference based H3D image stitching method

Once a white background image is captured, a simple histogram filtering algorithm is applied to improve intensity of MLA borders, and to enhance contrast of background (white) and the border (black). The resulting image of this process is presented in Figure 4.20. It is vital to generate a clean MLA grid with minimum noises because this grid is referenced for aligning and stitching elemental images. There is no low level visual processing except using this grid information.

(a) White background   (b) MLA Grid
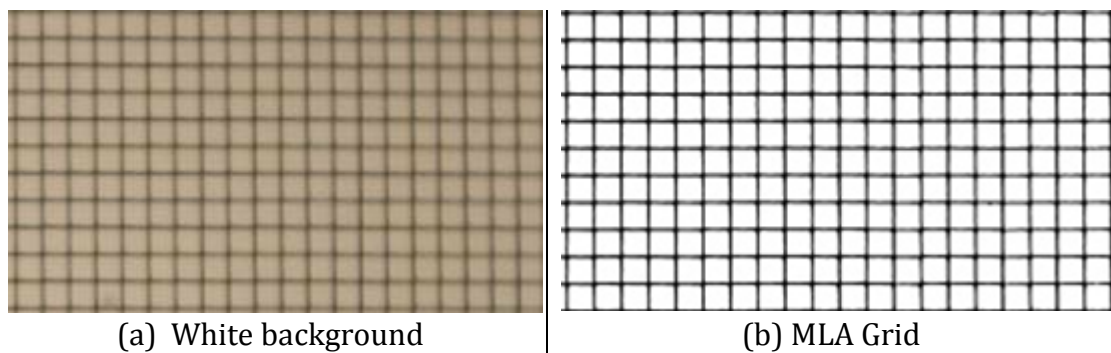
Figure 4.20 - Generated MLA grid from H3D image of a white background

The critical step is shifting the H3D camera from location of image 1 to the location for shooting image 2. The H3D camera has to be shifted by digital number of microlens due to synchronizing 3D depth and motion parallax "highlighted in green in Figure 4.21 - (1)" between two H3D images as shown Figure 4.21 in which two H3D camera movements are illustrated. This is because a microlens "micro-image" is representation of a pixel in H3D image if it is compared to 2D images. In fact, an intersection point of two viewpoint pixels creates a H3D pixel in space and all 3D pixels collectively construct a 3D scene in space.
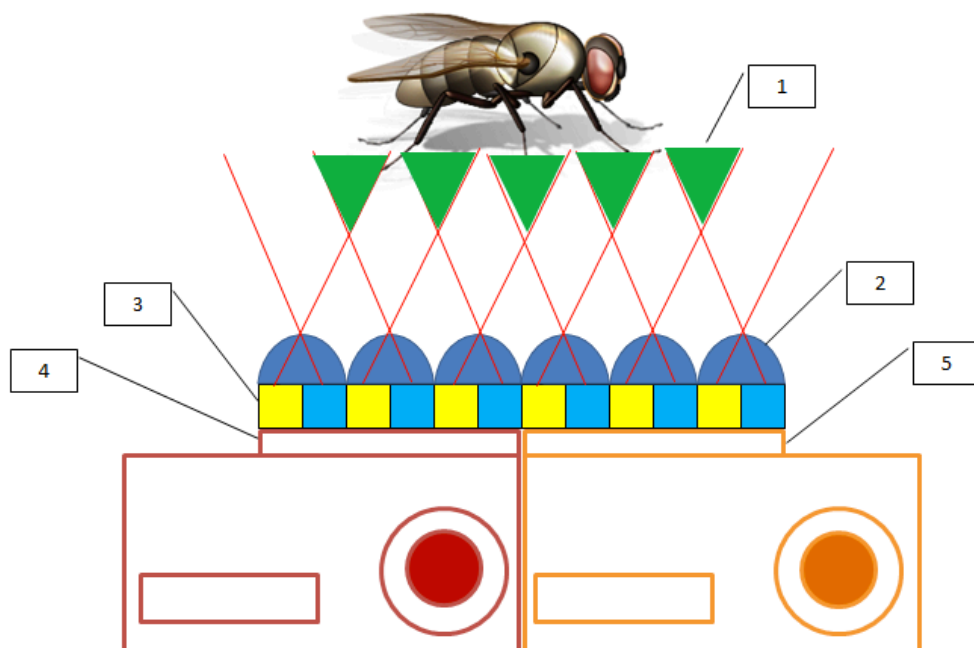
Figure 4.21 – Illustration of H3D camera shifting for H3D image stitching: (1) overlapping of two neighboring microlenses, (2) MLA, (3) pixels behind a microlens, (4) camera 1 sensor, (5) camera 2 sensor

4.5.1 Experimental Results

The illustrated H3D camera setup in Figure 4.21 is used to shoot two images as shown in Figure 4.22. This is a simple scenario of shooting a scene, in which the H3D camera viewing angle is not large enough to shoot the image in a single shot, therefore the scene is captured in two images. The proposed referenced based H3D image stitching algorithm is implemented in .NET so these two images are feed into the application which produces a single stitched H3D image shown in Figure 4.23.
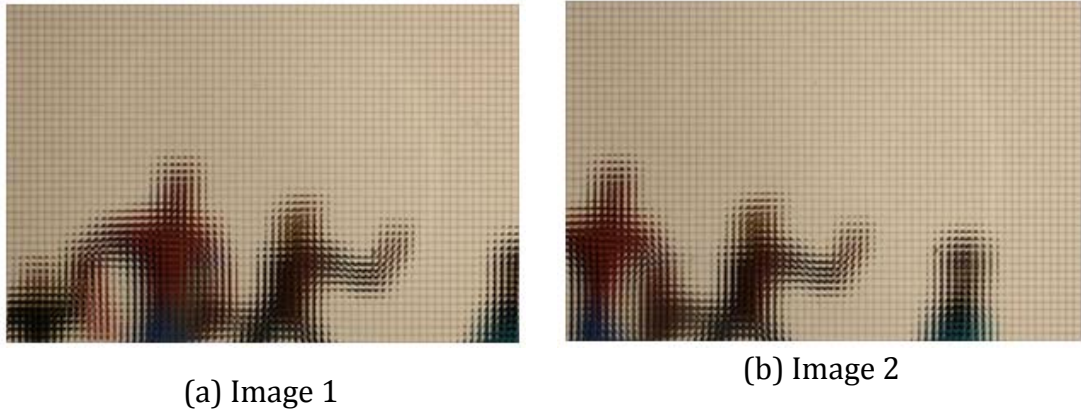
(a) Image 1   (b) Image 2

Figure 4.22 – Input H3D images for stitching
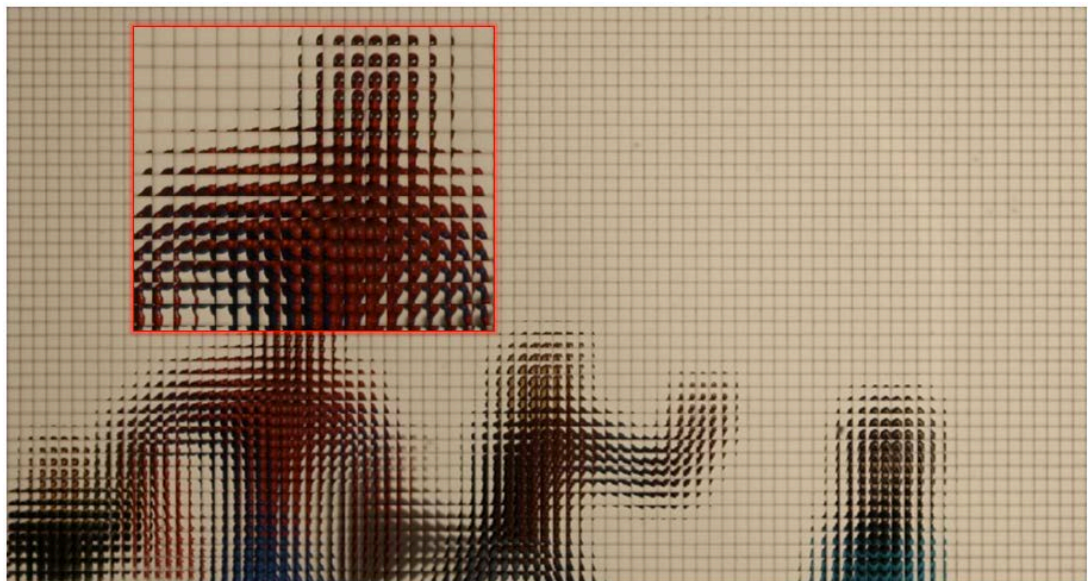
Figure 4.23 – The resulting stitched H3D image of (a) image 1 and (b) image 2

4.5.2   Discussion

A reference based H3D image stitching algorithm is proposed for stitching H3D images that is computationally light and fast because it uses the H3D camera MLA as a reference point by generating a calibration MLA grid which is later used to perform stitching images. The MLA information is vital as H3D imaging is made up of micro-images which are generated from the MLA. Therefore, the most importantly micro-images need to be stitched together without modify the parallax that reside in them because the micro-images contribute to the construction of a true 3D scene in space.

As a result, the critical step is the H3D camera distance between capturing image 1 and 2. This distance has to be an integer number of microlenses otherwise the spatial information cannot be integrated or stitched correctly.

The resulting H3D image is produced without any errors in integration of micro-images. In addition, the proposed method does not require intensive visual data processing; therefore, it can be implemented on camera in real time stitching. It, therefore, stands a good candidate for shooting 360° or shooting a large scene with multiple cameras.

The proposed method improves the overall H3D camera viewing angle for the first time. According to the calibration grid, which is generated from the MLA, it is successfully demonstrated on a single aperture H3D camera developed at Brunel University [5]. The stitching principle can also be applied to other H3D cameras / light field 3D cameras.

4.6   H3D Image Conversion for Multiview 3D Displays

This section proposes 3D image reformatting algorithm [17], which reformats H3D image to support 3D image format of multiview 3D displays. The necessary steps are describes in parsing H3D image parsing for autostereoscopic multiview 3D display.

Multiview 3D displays [18] use special pixel mapping methods [19][20] to improve horizontal 3D resolution and pixel aspect ratio by trading off horizontal and vertical resolution. The multiview pixel mapping methods are implemented to remap H3D images into the supported pixel representation format. H3D camera is developed to render H3D images with correct pixels per lens which is supported by the 3D displays.

The proposed method solves the issues of H3D content compatibility with state of the art multiview 3D displays as it reformats H3D images into multiview 3D images by parsing H3D image pixels format into the format supported by multiview 3D display and to achieve the correct slanting.

The experiment is conducted on multiview 3D displays of leading 3D display manufacturers e.g. Philips and Alioscopy displays which pursue two different approaches for multiview 3D content creation. They also use different pixel mapping methods as well as slanting angle.

The rendered and prepared H3D images by the proposed method are replayed on the multiview 3D displays without invoking the embedded 3D rendering engines. Good comparable playback results are achieved on both 3D displays. It opens a new door for content producers who can reformat any type of H3D image to be replayed on multiview 3D displays or H3D image rendering approach can be used for generating 3D content for any type of multiview 3D display. The proposed approach is an ideal candidate for sequence type content and real-time content interaction applications as it removes some pre-processing steps such as generating view images virtually from 2D-plus-depth image.

4.6.1 H3D Image Reformatting for Philips 3D Display

The 20-inch Philips autostereoscopic 3D display is designed using lenticular lenses to create a variety of distinct autostereoscopic views. The display has an embedded 3D rendering hardware that accepts 2D-plus-depth image and renders 9 viewpoint images and interlaces them in to a single 3D image to display so that multiple viewers can perceive a 3D experience at the same time.

The display has a plug-in for commercially available 3D modeling software such as Maya and 3Ds MAX. The plug-in is used to generate compatible 3D content "2D-plus-depth" which is used by the embedded 3D renderer to generate a Multiview 3D image/scene. Figure 4.24 illustrates the steps of generating 3D content from a 3D model using the camera plugin which renders a 2D-plus-depth image with resolution of 1600 x 600 pixels. The depth map pixel intensity defines the position of 3D pixel e.g. behind/in-front-of the display panel. For instance the depth map pixel intensity value of zero (0) places the 3D pixel behind the display, whereas the depth pixel intensity value of 255 places it in front of the display and 128 places it on the display panel. The generated 2d-plus-depth image is processed by the embedded 3D renderer to generate 9 distinct perspective images which are interlaced to form a 3D image.

The technical specifications of the display are as follows:

- 9 view autostereoscopic 3D display
- Embedded 3D rendering/processing hardware

- 2D RGB Resolution 1600 × 1200 pixels
- 3D mode the screen resolution 800 × 600 pixels
- 2D-plus-depth input in 3D mode
- 2D-plus-depth resolution 1600 × 800 pixels (side by side)
- RGB Pixel Pitch: 0.255×0.255 mm
- Optimal viewing distance: 80 cm

In the traditional approach, the embedded 3D rendering engine generates (1) 9 viewpoint images, (2) interlaces the view images "Perspective", (3) maps pixels and (4) slants remapped 3D image.   The display resolution is changed to 800 x 600 pixels in the 3D mode.
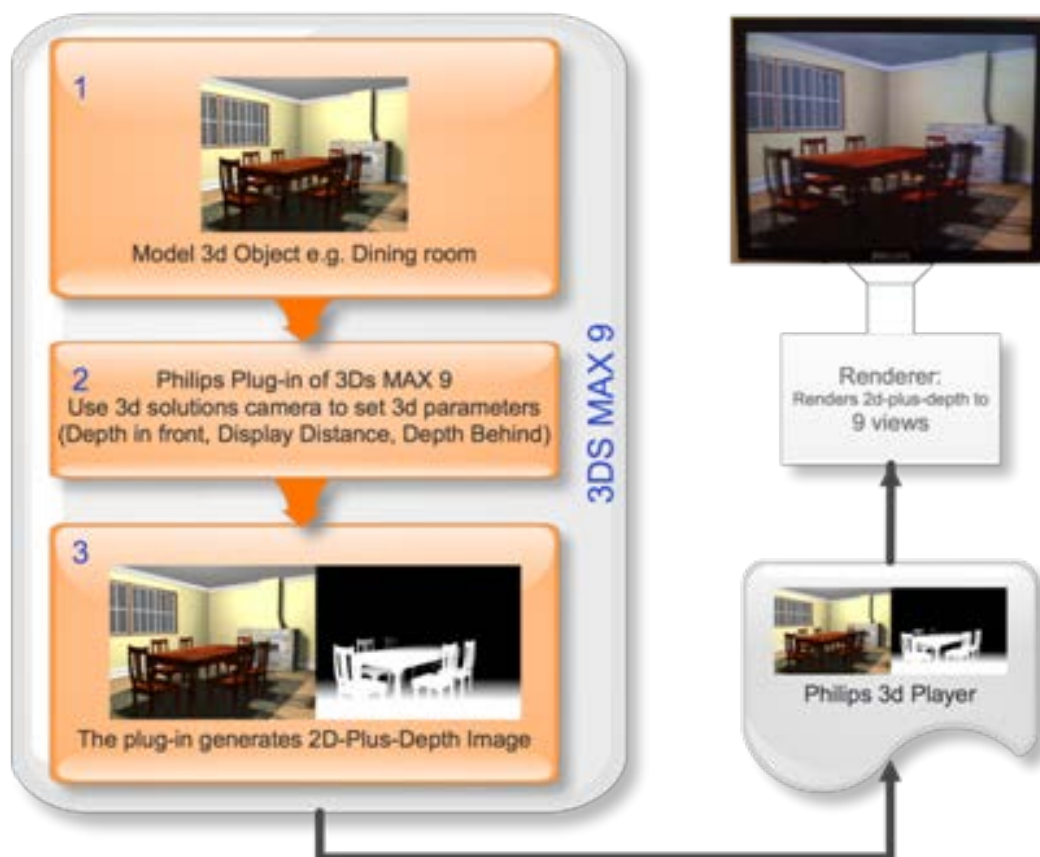
Figure 4.24 – The Philips display approach for multiview 3D image generation

4.6.1.1   The Pixel Mapping

Philips 3D display is built with slanted lenticular technology which has a slanted angle of 9.46° degrees as shown in Figure 4.25. This is due to moiré effect of lenticular sheet that is removed by slanting the lenticular sheet. Hence, the pixel

mapping method synchronised with the slanting angle of 9.46° degrees and Figure 4.25 shows the support pixel structure [19].

The viewpoint pixels are spread in columns as well as rows unlike a classical RGB pixel structure; this pixel mapping method achieves almost 2D pixel ratio and smooth transition between two distinct views because it reduces the distance between two consecutive 3D pixels [19]. A single viewpoint RGB pixel construction is shown in red dot lines in Figure 4.25.
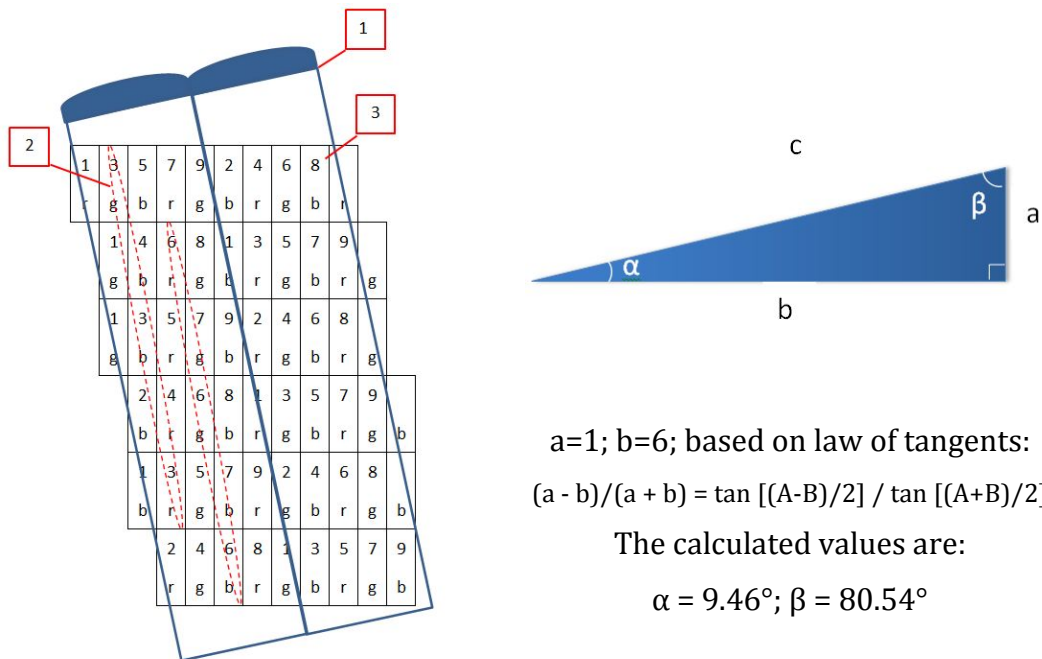
a=1; b=6; based on law of tangents:

$$(a - b)/(a + b) = \tan [(A-B)/2] / \tan [(A+B)/2]$$

The calculated values are:

$$\alpha = 9.46°; \beta = 80.54°$$

Figure 4.25 - The 3D display slanted lenticular lens array and pixel structure: (1) slanted MLA; (2) construction of a single viewpoint RGB dot pixel RGB, (3) viewpoint pixels per lens [19]

There are 9 pixels under each microlens which shields 4.5 physical subpixels because viewpoint pixels are mapped in vertical direction. The pixel mapping method fits one RGB viewpoint pixel to a single physical subpixel in horizontal direction whereas it uses 3 subpixels in vertical direction; therefore, it trades off horizontal and vertical resolution to achieve a balance pixel aspect ratio.

4.6.1.2 *Holoscopic Pixel Preparation*

Holoscopic pixels/subpixels are remapped according to the supported pixel mapping method and slanted by 9.46° degrees to achieve a compatible 3D image. One of the main differences is the holoscopic viewpoint images are orthographic unlike the multiview 3D image which has perspective viewpoint

images. In the preparation stage, holoscopic pixels are distributed vertically by shifting the subpixels in horizontally.

1) $\text{Pixel1} \Rightarrow R^{r,\,c} + G^{r+2,\,c+1} + B^{r+4,\,c+2}$

2) $\text{Pixel2} \Rightarrow R^{r-1,\,c} + G^{r+1,\,c+1} + B^{r+3,\,c+2}$

3) $\text{Pixel3} \Rightarrow R^{r-2,\,c} + G^{r,\,c+1} + B^{r+2,\,c+2}$

4) $\text{Pixel4} \Rightarrow R^{r-4,\,c} + G^{r-2,\,c+1} + B^{r,\,c+2}$

5) $\text{Pixel5} \Rightarrow R^{r-4,\,c} + G^{r-2,\,c+1} + B^{r,\,c+2}$

6) $\text{Pixel6} \Rightarrow R^{r,\,c+3} + G^{r+2,\,c+4} + B^{r+4,\,c+5}$

7) $\text{Pixel7} \Rightarrow R^{r,\,c+3} + G^{r+2,\,c+4} + B^{r+4,\,c+5}$

8) $\text{Pixel8} \Rightarrow R^{r-2,\,c+3} + G^{r,\,c+4} + B^{r+2,\,c+5}$

9) $\text{Pixel9} \Rightarrow R^{r-2,\,c+3} + G^{r,\,c+4} + B^{r+2,\,c+5}$

Where r = row number ; c = column number; R = red; G=green; B = blue; cell=subpixel

Figure 4.26 - The pixel mapping method and illustration of subpixels distribution

Figure 4.26 illustrates the distribution of the holoscopic pixels in vertical and horizontal direction under each microlens. This process creates new compatible pixels. For instance the first pixel: R sub-pixel is placed in row 1, column 1; G sub-pixel is placed in row 3, column 2; and B sub-pixel is placed in row 6, column 3 according to Figure 4.27 This subpixel distribution process also creates 9.46 degrees slanting shape which matches to the lens array slanting in Figure 4.25.

$\text{Pixel}^{r,\,c} \Leftarrow R^{\text{Pixel}[i]} + G^{\text{Pixel}[i+2]} + B^{\text{Pixel}[i+4]}$

Where r = row; c = column; R = red; G=green; B = blue;

Figure 4.27 - Newly created a 2D pixel contains subpixels of 3 different 3D pixels

The display has 4800 subpixels in horizontal direction where each microlens has 9 pixels which are mapped to 4.5 physical subpixels and it has 1066 lenses in total. Equation 4.1 shows the 3D pixel resolution which is 533×400 pixels; these parameters are taken under consideration while rendering a H3D image.

Equation 4.1 – The Philips display 3D pixels counts

$$\frac{1600 \times 3}{4.5 \times 2} = 533 \; pixels \; in \; horizontal \; direction$$

$$\frac{1200}{3} = 400 \; pixels \; in \; vertical \; direction$$

4.6.1.3   H3D Image Rendering

A H3D camera model is developed using 9 orthographic cameras that is implemented in POV-Ray [21] and then the viewpoint images are interlaced to form a H3D image.

The common parameters are not stated in the display specification as these can be calculated from hardware specification shown in Equation 4.2. The lens pitch size is calculated from RGB dot pixel pitch and pixels per lens and Table 1 shows the calculated parameters. There are 1066 lenses and 9 pixels per lens with lens pitch of 0.3825 mm. The parameters are mandatory to be considered while a 3D image is being rendered for an adaptable H3D image.

Table 4.1 – Philips 3D Display lens array parameters

Description	Value
Lens array size	1066 lenses
Lens Pitch	0.3825 mm
Lens Focal length	0.5~1.0
Number pixels per lens	9 pixels
Number of physical subpixels per lens	4.5 subpixels
Number of horizontal 3D pixels	533 pixels
Number of vertical 3D pixels	400 pixels
2D viewpoint image resolution	1066x200 pixels

Equation 4.2 – Calculated lens pitch of Philips 3D display's lens array

$$\frac{0.255 \; mm \; (RGB \; Size)}{3} \times 4.5 = 0.3825 \; mm$$
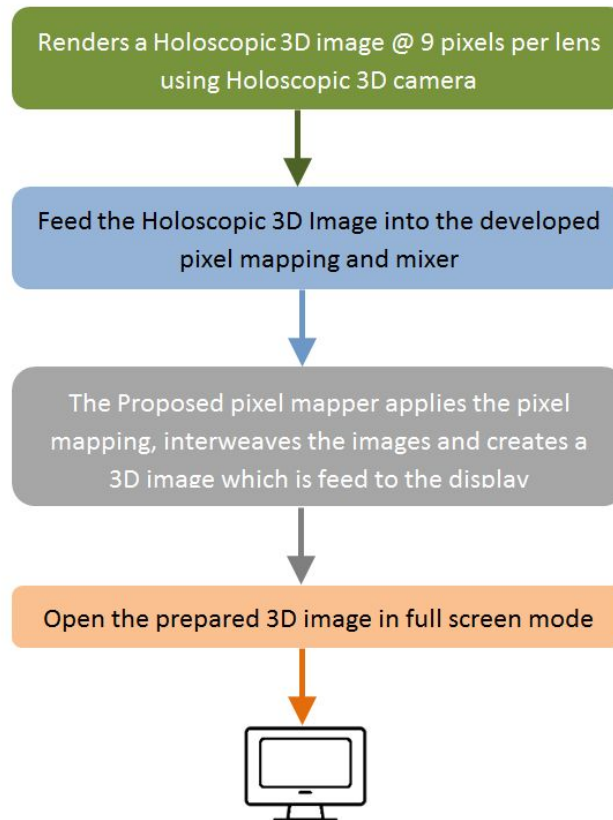
Figure 4.28 - Block diagram of the proposed method "H3D image rendering for Philips Multiview 3D display"

A H3D image is rendered by taking into account of the lens array specifications. Figure 4.28 illustrates the rendering steps which are as follows:

- Render 9 orthographic viewpoint images with resolution 1066 × 200 pixels.
- Apply Interlacing algorithm to interweave 9 viewpoint images to create a H3D image with resolution 9594 × 200 pixels.
- Apply the developed pixel mapping algorithm to remap the H3D image pixels to the compatible pixel representation and create a 3D image with resolution 1600 × 1200 pixels.

In the standard approach, a 2D-plus-depth image is fed into the 3D player which invokes the embedded 3D rendering engine to create a multiview 3D image (9 perspective viewpoint images). In the proposed method, the embedded 3D rendering engine is bypassed because the rendered converted H3D image is a

ready-to-play 3D image on the display. As a result, it saves the pre-processing computational power and speeds up for 3D playing response.

(a) Top-centre view   (b) Top-Right view

Figure 4.29 - Playback result of H3D image on Philips 3D display

4.6.1.4   Playback Result

Figure 4.29 shows the playback results of converted 3D images on Philips 3D display. There is a rich depth parallax as well as comparable motion parallax. There are enough images captured from various angles to illustrate the 3D experience.

The converted 3D images are opened in full screen mode which can be done by any media player. This is purely to not invoke the display 3D rendering engine. The display size and parameters are taken into consideration so when the 3D image is opened in full screen mode, it gets aligned well with the lens array patterns. The alignment is very important to avoid crosstalk noise and other errors in 3D scene construction process.

4.6.2   H3D Image Reformatting for Alioscopy 3D Display

Alioscopy is one of the market leaders in multiview 3D displays which are widely available in US, Europe and Asian digital display market thus we choose to test the proposed algorithm on their 3D display. In this case the wide screen 42-inch Alioscopy autostereoscopic multiview 3D display is designed to offer distinct autostereoscopic views using lenticular technology.

The 3D display has an embedded 3D rendering hardware that accepts 8 camera images and renders a 3D image by remapping viewpoint pixels according its

pixel mapping structure [20] and then interlacing them in correct format. The rendered 3D scene offers 8 distinct views, thus multiple viewers can perceive a 3D experience at the same time without changing viewing-zone.

The 3D display has a camera plug-in tool for 3Ds MAX which eases 3D content generation from a 3D model. The camera plug-in renders compatible 3D content "8 Perspective Camera Images" and then the embedded 3D renderer uses the 8 images to generate a multiview 3D image/scene. Figure 4.30 (i) illustrates the traditional approaches for generating 3D content for the 3D display. In Figure 4.30 (i), 8 cameras are used to produce 3D content, on the other hand Figure 4.30 (ii) shows using the display plug-in in 3Ds MAX for rendering 3D content.

Hardware — *Software*

Renders images 8 perspective images from a 3D model in 3Ds MAX

Acquire images from 8 perspective cameras and then feed them in to Alioscopy 3D MIXER

Acquire images from 8 perspective virtual cameras in 3Ds MAX, feed them in to Alioscopy 3D MIXER

Alioscopy 3D MIXER applies the pixel mapping, interweaves 8 perspective images and creates a 3D image which is feed to the Alioscopy player

Alioscopy 3D MIXER applies the pixel mapping, interweaves 8 perspective images and creates a 3D image which is feed to the Alioscopy player

Alioscopy player plays the 3D content

Alioscopy player plays the 3D content

  (i)   8 real cameras   (ii)   Virtual camera plugin

Figure 4.30 – The normal approach for generation 3D content for the Alioscopy 3D display

The camera plug-in renders 8-camera images with the 2D resolution of 960 x 540 pixels and the depth (scene e.g. behind/in-front-of the display panel) is adjustable in the camera plugin settings where the z-reference point is shown in the virtual scene. As the display's MLA specifications e.g. lens pitch/focal length

are known to the camera plugin, it puts 8 cameras side-by-side in correct distances to give the optimum 3D experience. The technical specifications of 42-inch Alioscopy multiview 3D display:

- Multiple users experience 3D at the same time – offers 8 views
- Embedded 3D rendering/processing hardware plus mixer and player
- 2D RGB Resolution 1920 × 1080 pixels @ 16:9 pixel aspect ratio
- 8-Camera images input in 3D mode
- RGB dot pixel pitch: 0.4845 mm × 0.4845mm

4.6.2.1   The Pixel Mapping

The 3D display is built based on cylindrical lens array technology "known as lenticular technology" which has a slanting angle of 18.43° degrees for removing the moiré effect [20].   As a result the pixels/subpixels are remapped in such a way to create a slanting angle of 18.43° degrees shown in Figure 4.31. The viewpoint pixels are spread in columns as well as rows unlike a classical RGB pixel structure. It achieves 3 times better 3D resolution (720 × 360 3D-pixels) compared to the traditional approach where the 3D resolution is 240 × 1080.   It sacrifices the vertical resolution to gain more horizontal resolution and it also balances the aspect pixel ratio as it achieves a wide screen aspect ratio 2:1 with good 3D motion and depth parallax. More details about the pixel mapping algorithm can be found on the site [20]. Figure 4.31 illustrates a single viewpoint pixel constructed from 3 different consecutive rows and columns which creates an angle of 18.43° degrees.

a=1; b=3; based on law of tangents:

$$(a - b)/(a + b) = \tan[(A-B)/2] / \tan[(A+B)/2]$$

The calculated values are:

α = 18.43°; β = 71.57°
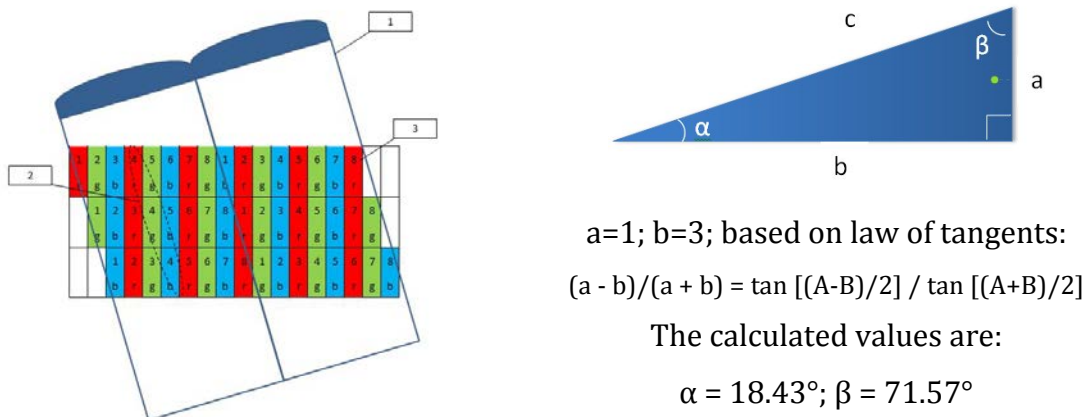
Figure 4.31 - The pixel mapping pixel structure and slanting angle calculation: (1) lens array | 8 subpixels, (2) a RGB dot pixel construction, (3) LCD pixel sheet [20]

4.6.2.2   Holoscopic Pixel Preparation

Once a H3D image is rendered with the correct lens array information, the viewpoint pixels are remapped according to the supported pixel mapping method described in Figure 4.31. The necessary steps are mentioned to achieve a compatible H3D image for Alioscopy multiview 3D display.   The only difference is that in H3D image, viewpoint images are orthographic (fly's eye technique) unlike the multiview 3D image which has perspective viewpoint images (human's eye technique). In the processing stage, holoscopic pixels are distributed vertically by shifting the subpixels both horizontally and vertically shown in below.

As illustrated in Equation 4.3, a viewpoint RGB dot pixel is distributed into 3 rows (which is 3-subpixel columns). H3D image pixels are remapped to this format to generate a compatible H3D image. The pixel mapping process twists the shape of the objects as it slants by 18.43° degrees, which is resolved by applying de-slanting algorithm on the viewpoint images before applying the pixel mapping.

Equation 4.3 – The pixel mapping subpixels distribution

$\text{Pixel1} \Rightarrow R^{r, c} + G^{r+1, c+1} + B^{r+2, c+2}$

$\text{Pixel2} \Rightarrow R^{r-1, c} + G^{r, c+1} + B^{r+1, c+2}$

$\text{Pixel3} \Rightarrow R^{r-2, c} + G^{r-1, c+1} + B^{r, c+2}$

$\text{Pixel4} \Rightarrow R^{r, c+3} + G^{r+1, c+4} + B^{r+2, c+5}$

$\text{Pixel5} \Rightarrow R^{r-1, c + 3} + G^{r, c+4} + B^{r+1, c+5}$

$\text{Pixel6} \Rightarrow R^{r-2, c+3} + G^{r-1, c+4} + B^{r, c+5}$

$\text{Pixel7} \Rightarrow R^{r, c+6} + G^{r+1, c+7} + B^{r+2, c+8}$

$\text{Pixel8} \Rightarrow R^{r-1, c+6} + G^{r, c+7} + B^{r+1, c+8}$

Where r = row number ; c = column number; R = red; G=green; B = blue;
cell=subpixels

The display has full HD resolution which makes 5760 subpixels (1920 Pixels × 3 RGB) and it has 8 pixels per lens and by applying the pixel mapping technique, a

wide screen pixel aspect ratio is achieved with stunning 3D resolution of 720 × 350 pixels as shown in Equation 4.4.

Equation 4.4 - The Alioscopy display 3D pixels counts

$$\frac{1920 \times 3}{8} = 720 \; pixels \; in \; horizontal \; direction$$

$$\frac{1050}{3} = 350 \; pixels \; in \; vertical \; direction$$

4.6.2.3   H3D Image Rendering

A H3D image is rendered by H3D camera, which is built using 8 multiple orthographic cameras in POV Ray [21] that renders 8 orthographic viewpoint images which are interlaced to form a H3D image.

The lens array details are calculated from the display hardware specifications e.g. the lens pitch size is calculated from RGB dot pixel pitch and pixels per lens as shown in Equation 4.5. There are 1066 lenses, 9 pixels per lens with lens pitch of 1.292 mm; the display including lens array parameters are shown in Table 4.2. Indeed these parameters are mandatory to be considered while rendering a H3D image for the display in order to have a compatible image.

Equation 4.5- Calculating microlens pitch of the display

$$\frac{0.4845 \; mm \; (RGB \; Size)}{3} \times 8 = 1.292 \; mm$$

Table 4.2 The Display lens array parameters

Description	Value
Lens array size	720 lenses
Lens Pitch	1.292 mm
Lens Focal length	~2.0
Number pixels per lens	8 pixels
Number of physical subpixels per lens	8 subpixels
Number of horizontal 3D pixels	720 pixels
Number of vertical 3D pixels	350 pixels
2D viewpoint image resolution	720x350 pixels

Figure 4.32 shows the steps for converting a H3D image into supported 3D image of the 3D display. The 3D display and its lens array specifications are taking into account while preparing, rendering and converting a H3D image. This includes the following steps:

- Render 8 orthographic viewpoint images with resolution of 720×350 pixels
- Apply Interlacing algorithm to interweave 8 viewpoint images to create a H3D image with resolution 5760×350 pixels
- Apply the developed pixel mapping algorithm to remap the H3D image pixels to the compatible pixel structure and create a 3D image with resolution 1920×1050 pixels
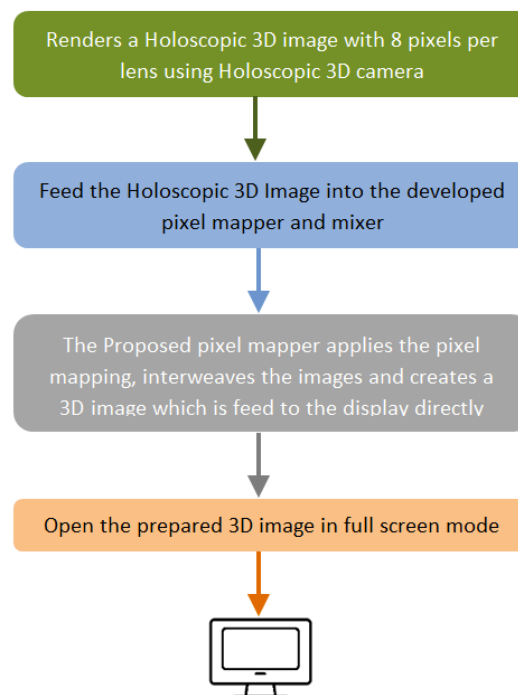
Figure 4.32 – Action flow diagram of proposed H3D image parsing for multiview 3D display

In the traditional approach, 8 perspective images are feed into the 3D mixer and player which invoke the embedded 3D rendering engine to create a multiview 3D image. In the proposed method, the embedded 3D rendering engine is bypassed because the rendered converted H3D image is a ready-to-play 3D image on the display. As a result, it saves the preprocessing computational power and speeds up for 3D playing response time. Last but not least the

proposed method simply converts multiview 3D display into H3D display by parsing H3D image in supported pixel mapping.

4.6.2.4 Playback Result

Figure 4.33 shows the playback results of reformatted 3D images. As seen in Figure 4.33, there is a rich depth parallax as well as wider motion parallax with naturalness which means there is no minimum and maximum distance to perceive 3D images. In the playback resulting images, the 3D scene is constructed in space and objects exist in our real world. This gives the users feeling of immersive 3D effect.

(a) Front view   (b) with hand reference
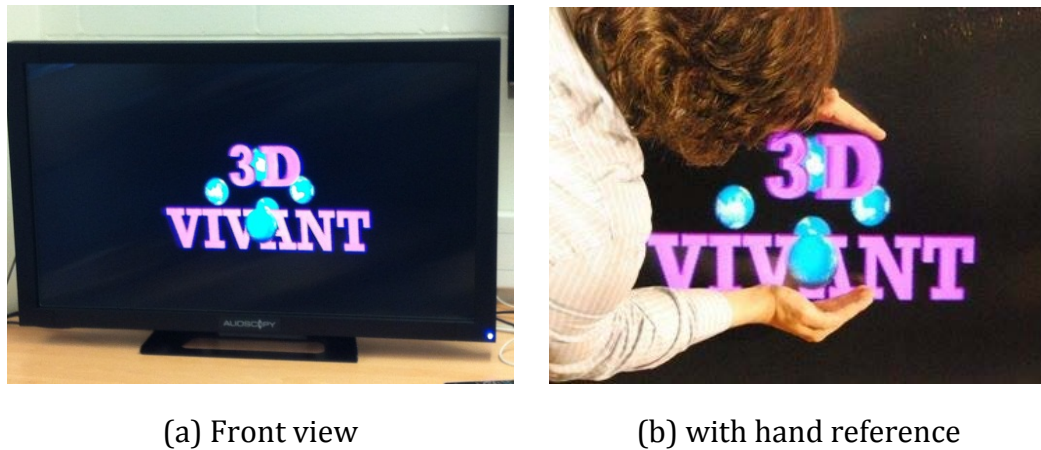
Figure 4.33 – Playback result of H3D image on the Alioscopy multiview 3D display

The converted 3D images achieved a very good result as there is a rich depth parallax as well as wider motion parallax with naturalness which means there is no minimum and maximum distance to perceive 3D effect. As seen in the playback resulting images, the 3D scene is constructed in the space and objects exist in our real world. This gives the users feeling of immersive 3D effect.

The converted 3D images are opened in full screen mode which can be done by any media player. This is purely to not invoke the display's 3D rendering engine. The display size and parameters are taken into consideration so when the 3D image is opened in full screen mode, it get aligned well with the lens array patterns.

4.7   Medical Tomographic Image Conversion

The medical data obtained through CT and magnetic resonance imaging (MRI) is exported in DICOM (Digital Imaging and Communications in Medicine) format. A segmentation process is then applied to manually highlight the regions of interest in each slice as shown in Figure 4.34 using commercially available software a 3D representation of the medical image data from the resulting sliced images is generated.

The 3D model is then passed through the developed software creating a virtual H3D camera [23] made of MLA, with the data being rendered into full H3D medical grade images shown in Figure 4.35. We build a proof of concept display models using a commercially available high-definition autostereoscopic 3D display.
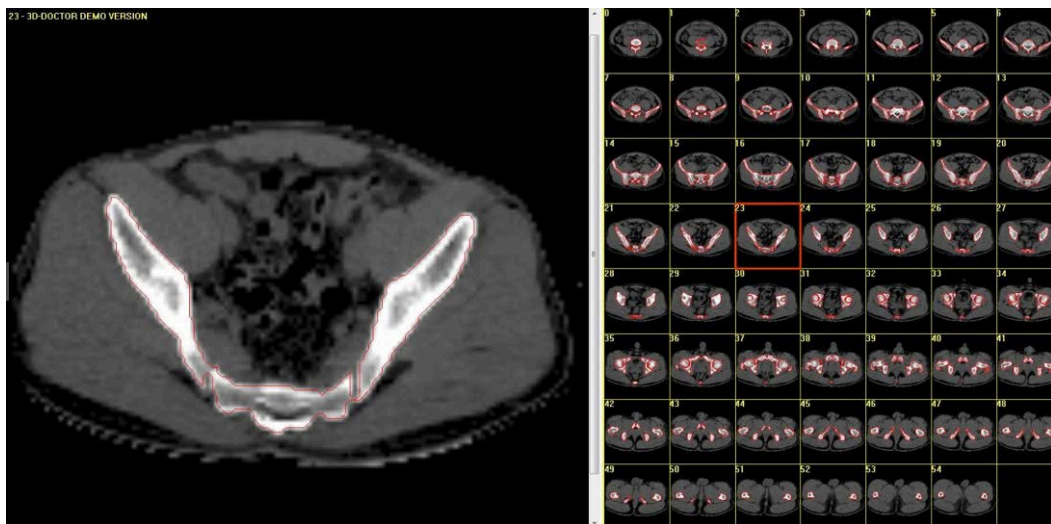
Figure 4.34 - Region segmentation using 3D-Doctor to construct a 3D model from CT images

The limitation of the current prototype is that the virtual 3D-Holoscopic camera is made of 8 orthographic cameras with the capability to generate 8 orthographic images. We are able to generate 8 images because the high definition (HD) auto-stereoscopic display (1920 × 1080) used currently only accommodates 8 horizontal views through parallel projections. The virtual 3D-Holoscopic camera model has 8 pixels under each lenticular (long strips of cylindrical lenses) giving a good motion parallax range. The quality of the images produced is limited by the display 3D resolution.
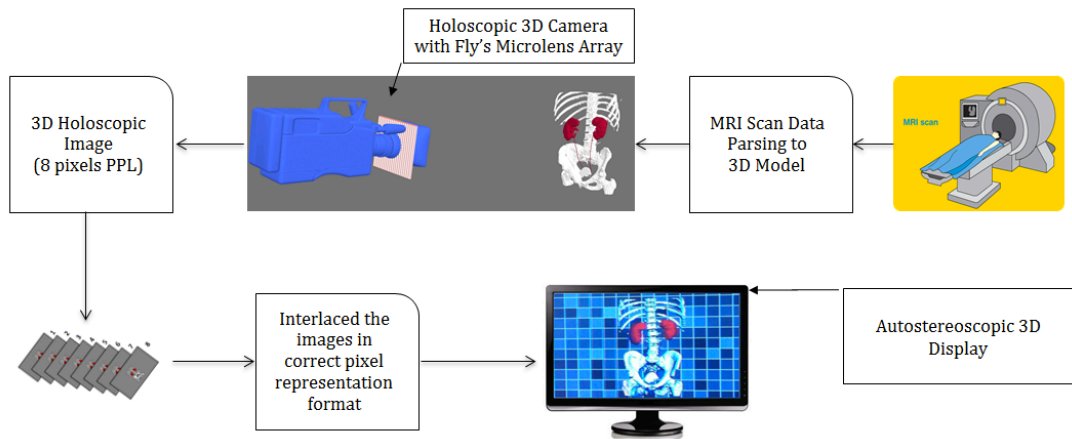
Figure 4.35 - Block diagram of CT scan data reformatting and rendering H3D images for data visualization on the autostereoscopic 3D display
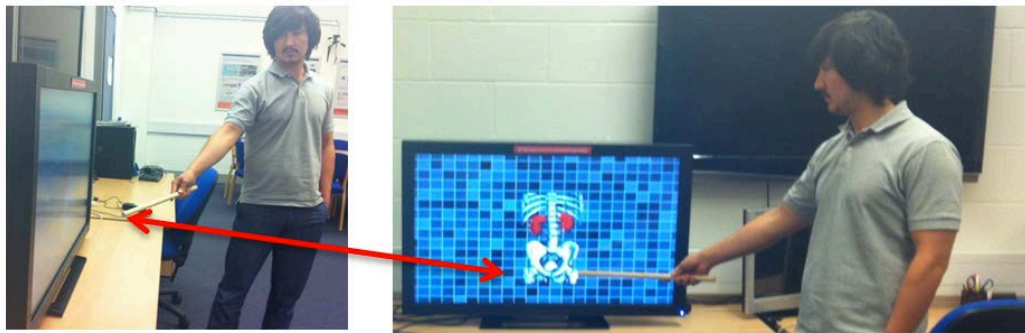
(a) Depth Parallax
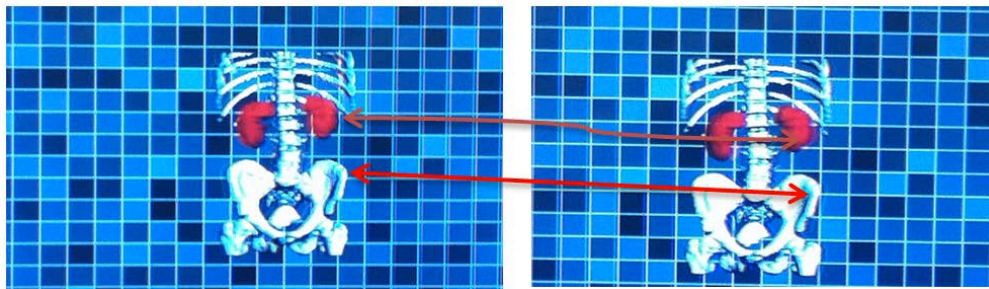
(b) Motion Parallax (Horizental viewing zone)
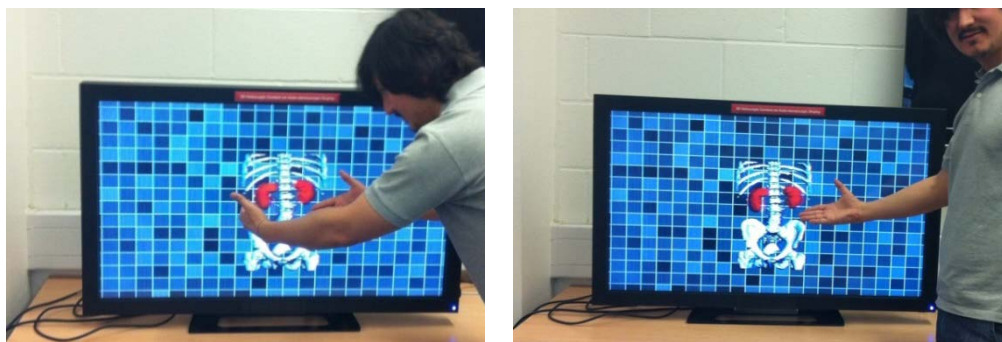
(c) Illustration of the virtual object/scene in the space (immersive)

Figure 4.36 – Playback result of CT data on the autostereoscopic 3D display

4.7.1   Playback Result

Figure 4.36 shows the playback result of the holoscopic image in a number of viewing angles with the pointer representing the actual time location of the image.   In order to perceive 3D effect such as depth and motion parallax, the viewer must not need to wear any head gear device. As seen there are number of images captured to illustrate different 3D effects e.g. Figure 4.36 (a) shows depth of 3D objects in space whereas Figure 4.36 (b) illustrates the motion parallax within the viewing zone.

In particular, this experiment proves that the technology has a lot to offer as it has a benefit over true 3D reconstruction in space.

4.8   Interactive H3D Content Search and Retrieval

This section presents development of interactive 3D video content search and retrieval that advances 3D multimedia navigability and search-ability by creating dynamic hot links for selectable / clickable objects in the scene. The proposed system uses metadata to perform interactive tasks so it has off-line 3D operators namely Centric-view extraction, Depth map extraction, object segmentation, content based search and retrieval, which were developed and reported by the 3DVIVANT project team in the project deliverable [2].

This is part of a joint work carried out in 3DVIVANT project [2] and my contribution includes development of dynamic hyperlinker, 3D content descriptive protocol schema and metadata engineering and synchronisation, which are discussed in this section.

4.8.1   Dynamic Hyperlinker

The Dynamic hyperlinker module is one of my contributions in the system. It is an advanced H3D video player that has hyperlinking capability to ease the 3D search and retrieval. It links objects in the scene to similar / matching object(s) in the repository, while the video clip is being played. The user clicks on an object in the scene to search for similar objects in the repository. Also it allows professional users to add a new annotation such as object description and relevant video links. The changes are synchronized throughout the video clip

for the selected objects so the user does not need to repeat the process for every frame.

As hyper-video generation involves multiple intensive 3D processing, it does off-line processing for creating hyper-videos that is analysing and annotating H3D video content and then creating and synchronization metadata to prepare a header of H3D videos in following steps:

- Generation of centric viewpoint images and 3D depth map images of H3D video images that are used by the object segmentation module to generate a segmentation mask with its bounding box
- Generation of metadata of H3D video images using a segmentation mask and bounding box in the content based search and retrieval module
- Synchronization of the generated metadata files to create an xml-header file, which is associated with the H3D video to produce a hyper-video
- Apply the hyper-video in the hyperlinker tool, which creates hyperlinks to facilitates 3D content search and visualization
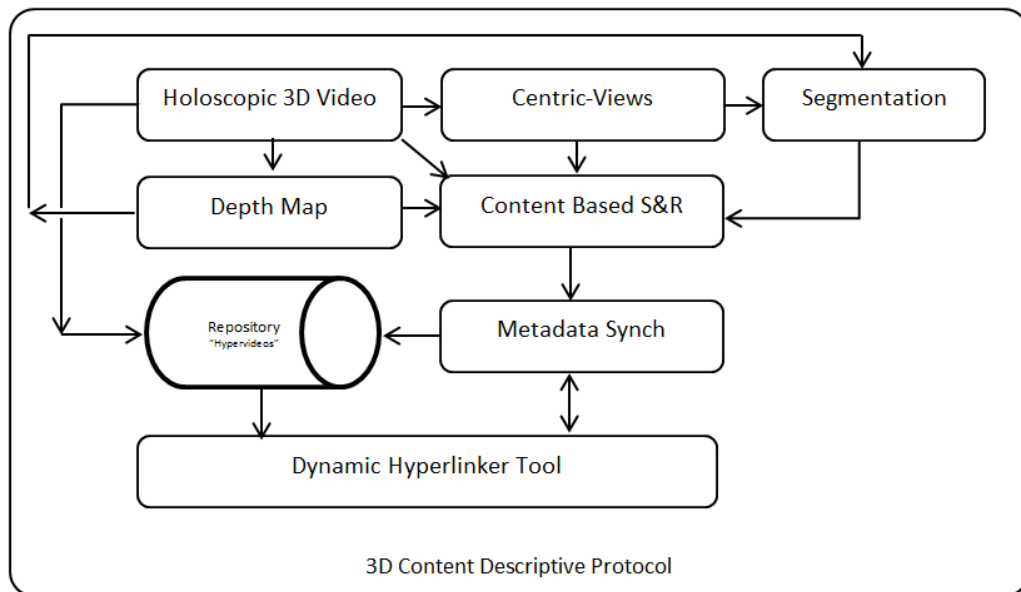
Figure 4.37 - Architecture of Hyperlinker tools for 3D Content search and retrieval

All the above processes are performed offline for creating hyper-videos using 3D content descriptive protocol as shown in Figure 4.37. The components communicate and exchange meta-messages using the 3D content descriptive

protocol, which enables to describe H3D objects in the scene using metadata descriptive languages. The metadata is later used to create a hyper-video.

Centric-views and 3D depth map are generated from H3D videos that are used for segmenting 3D objects as well as creating bounding boxes for 3D objects. Then these 3D depth maps, segmentation masks, and bounding boxes related information are used to perform a content based search to associate or create linking information "Metadata" for identical objects in the H3D videos as shown in Figure 4.37.

The content based search and retrieval module generates a single xml-indexed for every H3D video frame. The index xml file holds complete information of each frame, such as the position of objects in the scene, including object search results, as well as search result descriptions and target URL/paths. All these metadata files are fed into the metadata synchronization module, which reprocesses and merges the metadata files to create a single optimized xml-header file for the input H3D video clip. The xml-header file with H3D video are combined together to create a hyper-video, which is replayed by the Hyperlinker tool to facilitate interactive 3D content search and retrieval as well as visualization shown in Figure 4.37.
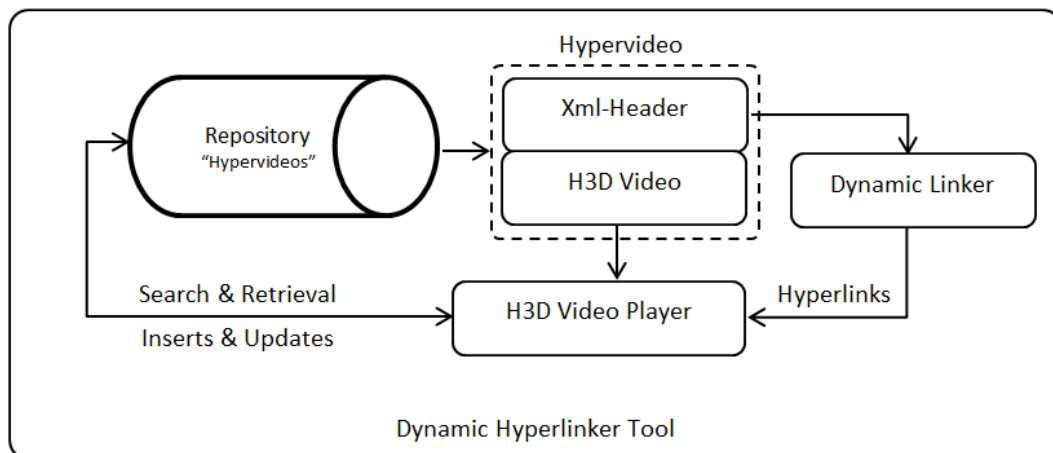
Figure 4.38 - Block diagram of Dynamic hyperlinker tool

A hyper-video is a complete meta-tagged H3D video clip, which is created by associating an xml-header with a H3D video clip as shown in Figure 4.38. It is

fed into the hyperlinker tool that facilitates interactive 3D multimedia search, retrieval and annotation.

The Dynamic hyperlinker player loads the H3D video clip with the associated xml-header file. The dynamic linker module uses xml-header file to create hot links on the screen, while the H3D video is being played. It highlights clickable 3D objects with a redline box if the highlight feature is enabled in the settings. In addition, it monitors the mouse cursor movements and when a region of selectable or clickable objects are hovered over, the cursor icon is changed from the default to the hand icon to alert the user that the object is clickable or hyperlinked as shown in Figure 4.39. On a mouse click event, it captures the mouse cursor position (X, Y) and matches it with a bounding box in the xml-header file and then it performs a search for identical objects in the repository, passing the bounding box region and content based search and retrieval batched processed the search result. These can be found in the xml-header file, therefore, it is just a matter of matching the bounding box region to pull out the result and display it in the search result screen.

The hyperlinker tool supports user feedback and offers a semi-automatic solution for annotating H3D video clips.   It enables users to create a new hyperlink to an external source or remove an existing hyperlink if it finds an irrelevant result.   It performs a bulk-synchronization so that in the case the user needs to modify any one of the H3D video frames, the system synchronizes the changes to the whole scene automatically.

The basic functionality of the system is as follows:

- Open and play a hyper-video
- Play/pause/stop H3D video clip
- Add/remove/update the xml-header file that is automatically updated
- Add/remove/update title of bounding boxes
- Export/import/save/save-as the xml-header file
- Highlight selectable objects
- Show search and retrieval results including thumbnail
- Link selectable objects to any destination resource

- Play search result items on user click from the particular scene/frame
- Preview hyperlinked video
- User feedback e.g. adding/deleting search results
- Create a new bookmark for selectable objects that is automatically synchronized to the whole scene
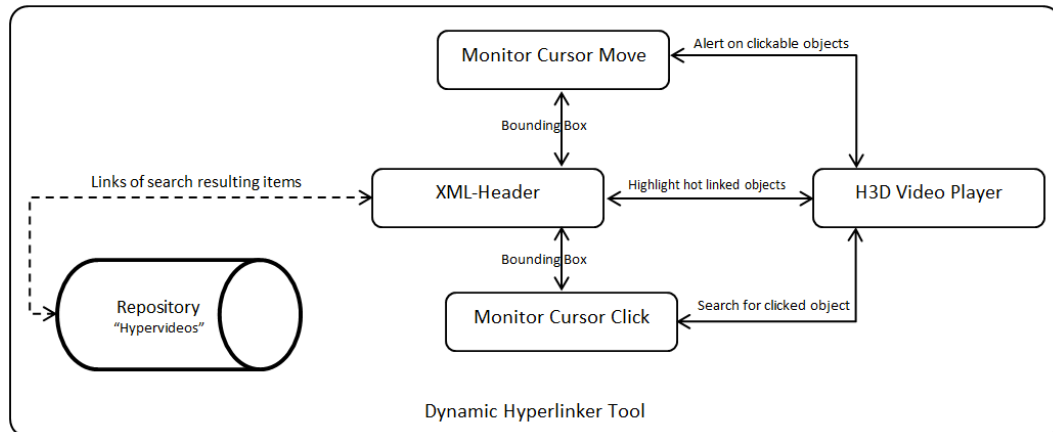
Figure 4.39 - Action flow diagram of dynamic hyperlinker

The H3D video gets paused automatically when a selectable object is clicked, as the system invokes the content based search and retrieval and the found results appear in the list box. At this stage, the user can remove any irrelevant results from the result list if necessary or add a new bookmark for the selected object. The changes are synchronized to the xml-header automatically and saved which overwrites any existing ones, unless the "save as" feature is selected. The system re-indexes the whole sequence of frames.

The re-indexing works only on objects in the scene. It is valid until the object disappears from the scene. If the object goes away from scene and then comes back, the system treats it as a new object. This is because the content based search and retrieval module retrieves objects based on their visual information.

All the components process H3D video offline including the metadata engineering and synchronization. The hyperlinker tool plays a hyper-video and performs a real-time hyperlinking using the xml-header. The hyperlinker's performance is monitored and analysed.

Table 4.3 shows the time taken to perform various actions such as playing, linking, loading, searching, listing, adding and removing hot links. This shows that in terms of performance requirement point of view, the hyperlinker system can be executed on of any today's PCs/laptops without the need for special powerful computer.

Table 4.3 - The performance sheet of the hyperlinker tool

Description	Time in sec.
Bounding Box Loading time	0.0009766
A single object highlighting time	0.0019531
Adding new item – re-indexing time	0.0742187
Removing an item – re-indexing time	0.0019532
Loading/playing first frame play	0.2792969
Loading/playing first frame play with highlighting enabled	0.2841797
Search and retrieval time on an object click	0.0175782

4.8.2   3D Content Descriptive Protocol Schema

The 3D content descriptive protocol "3DCDP" is one of my contributions in the system. It is a descriptive meta-language that describes and annotates holoscopic video images content using Extensible Markup Language "XML". It is used for 3D video content indexing including tagging selectable objects in the video clip.

In addition, it is used for annotating H3D video content as well as meta-information exchange between components e.g. segmentation, content based search & retrieval, and hyperlinker tool which use it to exchange action-message in a single format in the system.

The proposed 3D content descriptive protocol has enough elements and attributes shown in Table 4.4 to describe 3D video contents in a structured manner in xml tag. It uses minimal elements to annotate all possible cases

which may appear in indexing a 3D video clips. More importantly, it seamlessly integrates the system components of batch and real-time operators as well as improving 3D search & retrieval performance with interactive navigability features due to the fact that objects in the scene are easily described including annotations, bounding boxes and search results. As seen, Table 4.4 shows all elements of 3DCDP that are used to fully describe both still and video H3D image content as well as embedding object(s) search results.

Table 4.4 - All elements of 3D Content Descriptive Protocol

Element	Description
CDP	*3D Content descriptive protocol element*
ContentInfo	*Content information*
SearchResultItem	*Research result item*
Max	*Maximum x,y values of bounding box*
Min	*Minimum x,y values of bounding box*
BoundingBox	*Bounding box values*
Operator	*Operator / classifier*
OperatorDesc	*Operator description*
Annotation	*Annotation element*
Scene	*Scene element*
Content	*Content element*
SearchResult	*Search result item*
UUID	*Unique ID*

Figure 4.40 shows the hierarchical structure of 3D content descriptive protocol from its root element. It is associated with a H3D video clip that has a UUID which is unique for the video in the repository and then it's content with content-info element. A content element can have a single or multiple scene(s) which is given an ID and defined by start-frame and end-frame. As seen, it also allows one to add a description to the scene. A scene can have no or more annotation(s) because a scene could contain no or more clickable objects.
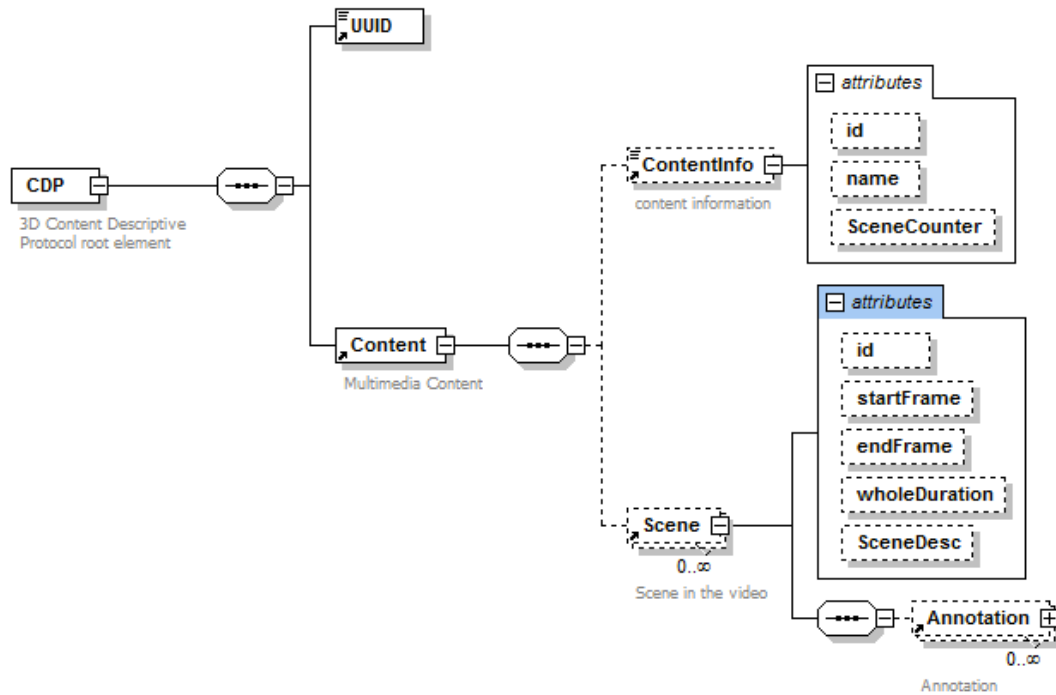
Figure 4.40 - Hierarchical structure of 3D content description protocol @Root

An annotation has a given ID as well as start-frame and end-frame which is its validity. The attributes are used to identify the annotation if there is more than one annotation. As seen in Figure 4.41, an annotation is created by operator(s) "Operator-Desc", which has multiple attributes to describe the particular annotation and associate its bounding-Box of one or more. An operator is not restricted to a single Bounding-box because there could be two of the same object in the scene so it allows binding multiple bounding-boxes if necessary.

Every object in the scene is located and annotated by a bounding-box element of minimum (X,Y) and maximum (X,Y) attributes. Its URL and description attributes are used to bookmark the bounding-box with a URL and add its description. As seen, each bounding-box has embedded search result list/item and search-result-items have a minimum information of hyperlinked destination such as content-type attributes (image, video, file), relevance (of destination source in percentage) and Item-Desc, which allows one to tag a tip to it.
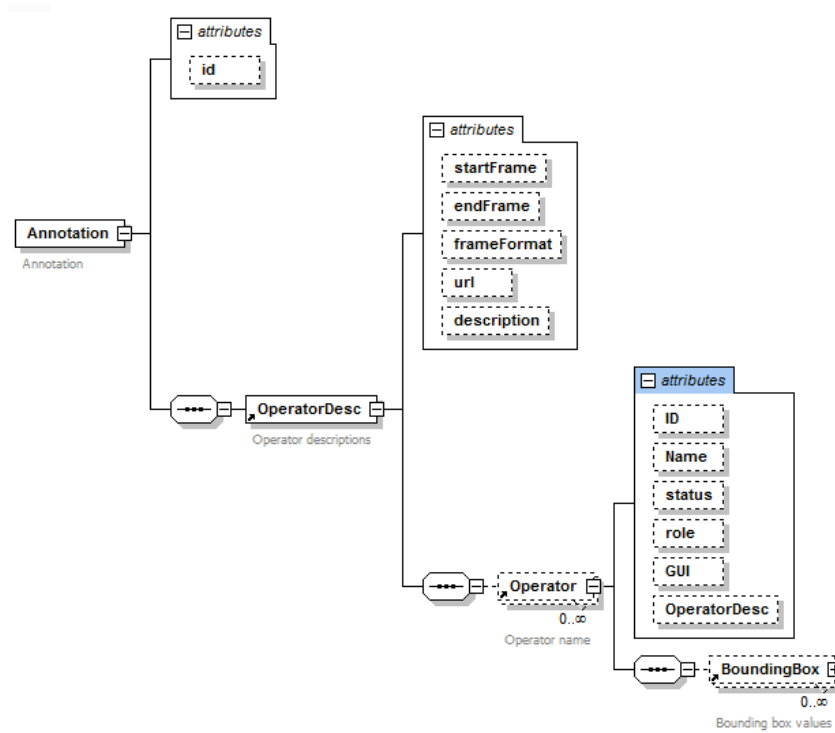
Figure 4.41 - Annotation element hierarchical structure of 3DCDP
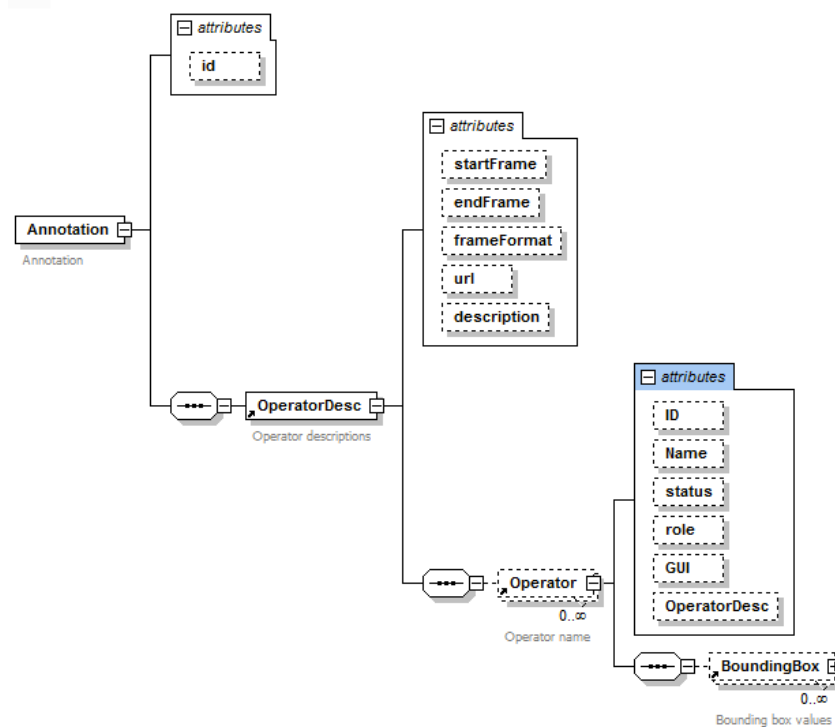
Figure 4.42 - Bounding-Box element hierarchical structure of 3DCDP

The proposed 3D content descriptive protocol is going to be submitted to MPEG7 as an extension to cover H3D imaging formatting once it is further developed to include H3D imaging features, such as pixels per lens, microlens information, and viewpoint images.

The proposed approach is effective for indexing, searching and navigating a video content. In addition, the metadata can be used for creating statistical reports for the visualization of the video clip e.g. number of selectable objects, number of scenes and in the same manner as reported in [22].

4.8.3 Metadata Engineering and Synchronisation

Metadata engineering and synchronization is one of my contributions in the system. H3D videos frames are analyzed and processed by the segmentation and content based search & retrieval module, which generate a metadata file [22]. That describes H3D video frames in structured manner using 3D-CDP meta-language. At this stage, a single metadata file is generated for every frame of the H3D video. The metadata file structure is presented in Figure 4.43 that contains a single annotation with one or more bound-boxes of the scene. The bounding-box contains the search result item of this particular object "bounding-box".

The bounding-box is valid for a single frame as it is for video objects. Therefore object positions are in constant change from frame to frame. In addition, 3D objects in the scene will appear differently from different perspectives so the content based search and retrieval system may do the matching with the particular perspective of the object.
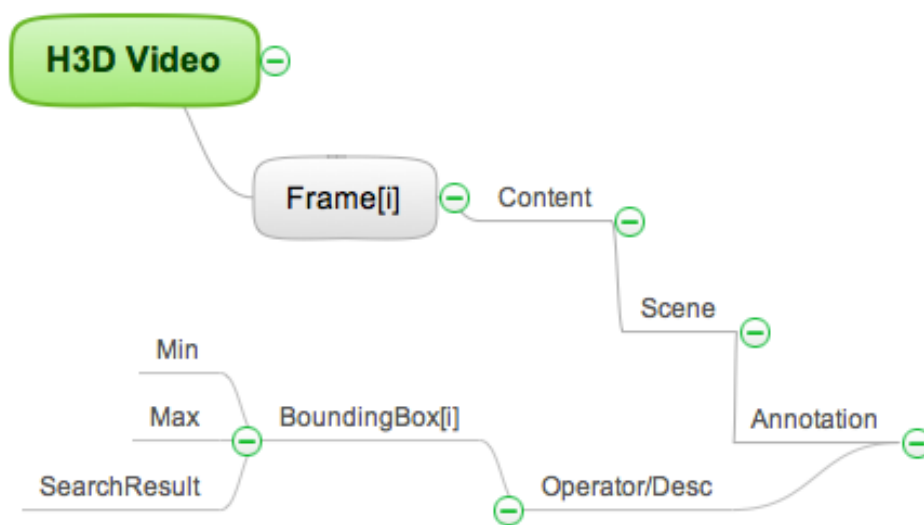
Figure 4.43 - Metadata file structure generated by segmentation and S&R

As a result, there are hundreds of metadata files containing meta-description of scenes. To overcome this issue exhausted and complex metadata files management, we propose a multimodal metadata synchronization technique for re-engineering the metadata file to create a single optimized xml-header of H3D video.

The proposed metadata synchronisation aims at merging all metadata files by removing redundant sections and then putting meta-nodes in a structured way, which will not overlap each other. It also structures the meta-nodes in such way that is more manageable in terms of re-manipulating it. The process creates a single xml-header file of the H3D video and its file structure is shown in Figure 4.44.
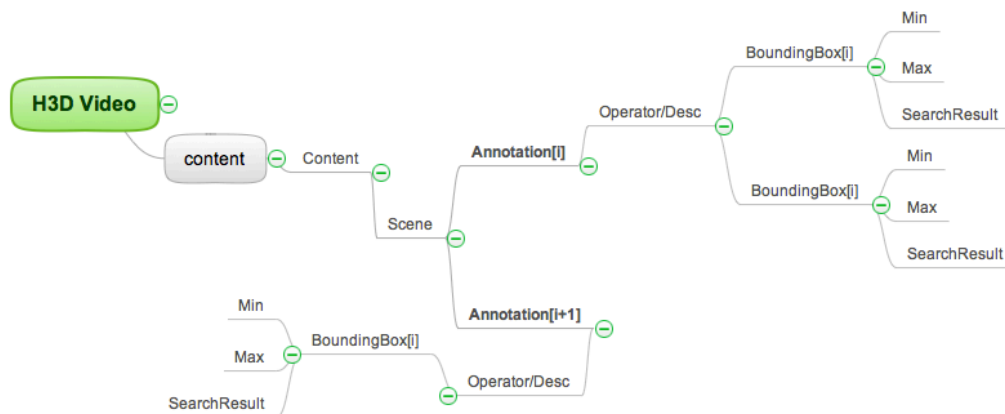
Figure 4.44 - The xml-header file's structure generated by metadata synchronisation

It imports all frames metadata files and decomposes the file nodes as low level as annotation. It then creates a new metadata file (xml-header), which has a single scene with multiple annotations. Each frame metadata file has a single annotation; therefore it is treaded as an annotation node in a newly created file. It reforms a new scene and a new annotation with correct frame locations, which also presents statistical data such as scene-duration, and annotation start/end-frame. The statistical data can be easily processed to generate a visualization graph e.g. a particular object (bound-box) live on the scene and number of objects in the scene/video as well as complexity of the video content. Also this can be used for navigating the video content without replaying the video and such video summarization techniques are widely adopted by

consumers who like to view the summary of the video before they start watching it, such as movie trailer.

```xml
<?xml version="1.0" encoding="utf-8"?>
<CDP xsi:noNamespaceSchemaLocation="THREEDCDP.xsd" xmlns:xsi="http://www.w3.org/2001/XMLSchema-instance">
    <UUID>UUOD_String</UUID>
    <Content>
        <ContentInfo SceneCounter="1" id=" RBB_001_01_X1" name="seq_1">RBB sequences</ContentInfo>
        <Scene id="1" startFrame="0" endFrame="325" wholeDuration="326" SceneDesc="">
            <Annotation id="1">
                <OperatorDesc startFrame="0" endFrame="0" frameFormat="png" description="" url="./sequences_Vivant/RBB
                    <Operator ID="0" Name="String" status="String" role="String" GUI="String" OperatorDesc="">
                        <BoundingBox ID="1" BoundingBoxDesc="" URL="">
                            <Min X="1435" Y="629" />
                            <Max X="1479" Y="682" />
                            <SearchResult SearchResultCounter="20">
                        </BoundingBox>
                        <BoundingBox ID="2" BoundingBoxDesc="" URL="">
                            <Min X="1336" Y="703" />
                            <Max X="1479" Y="898" />
                            <SearchResult SearchResultCounter="20">
                        </BoundingBox>
                    </Operator>
                </OperatorDesc>
            </Annotation>
            <Annotation id="2">
                <OperatorDesc startFrame="1" endFrame="1" frameFormat="png" description="" url="./sequences_Vivant/RBB
                    <Operator ID="0" Name="String" status="String" role="String" GUI="String" OperatorDesc="">
                        <BoundingBox ID="1" BoundingBoxDesc="" URL="">
                        <BoundingBox ID="2" BoundingBoxDesc="" URL="">
                    </Operator>
                </OperatorDesc>
            </Annotation>
            <Annotation id="3">
            <Annotation id="4">
            <Annotation id="..">
            </Annotation>
            <Annotation id="326">
            </Annotation>
        </Scene>
    </Content>
</CDP>
```

Figure 4.45 - A sample of xml-header created by metadata synchronization

A sample of newly created xml-header file is shown in Figure 4.45 that shows the meta-content. It is a complete meta-descriptive file, which contains the video objects including its location and search result including statistical data. As seen, the scene has the duration of 325 frames, annotations with other properties.

4.8.4   Experimental Result and Demo

The proposed tool supports H3D videos and Figure 4.46 shows a H3D video clip playback result. The selectable objects are highlighted in red rectangles. This means the objects are hyperlinks. The user can click on any of the objects to search for similar objects in the repository. The search results are listed in the list box. The user can view/play the result by selecting it from the list box.

It is further developed to support editing metadata of xml-header file as well as importing/exporting and saving it as a new project, which can be later opened

without losing the changes and without having to save it on its original version. In addition, it has been revised to support center-views of H3D videos because H3D content requires a special "H3D display", which is not available widely and also it opens to those who want to replay 2D version of H3D content. A screenshot of this is presented in Figure 4.47 and as seen objects in the scene are highlight and titled if the object(s) has an associated title.

As it allows editing metadata of the H3D video, the user can select an object and add a new associated search result or delete a search result. The system propagated the changes to the whole scene automatically so next when one click on the object, the updated search result is shown. In addition, the user can back-up the changes by exporting the metadata without saving it to the original file. The exported file can be imported later if necessary.
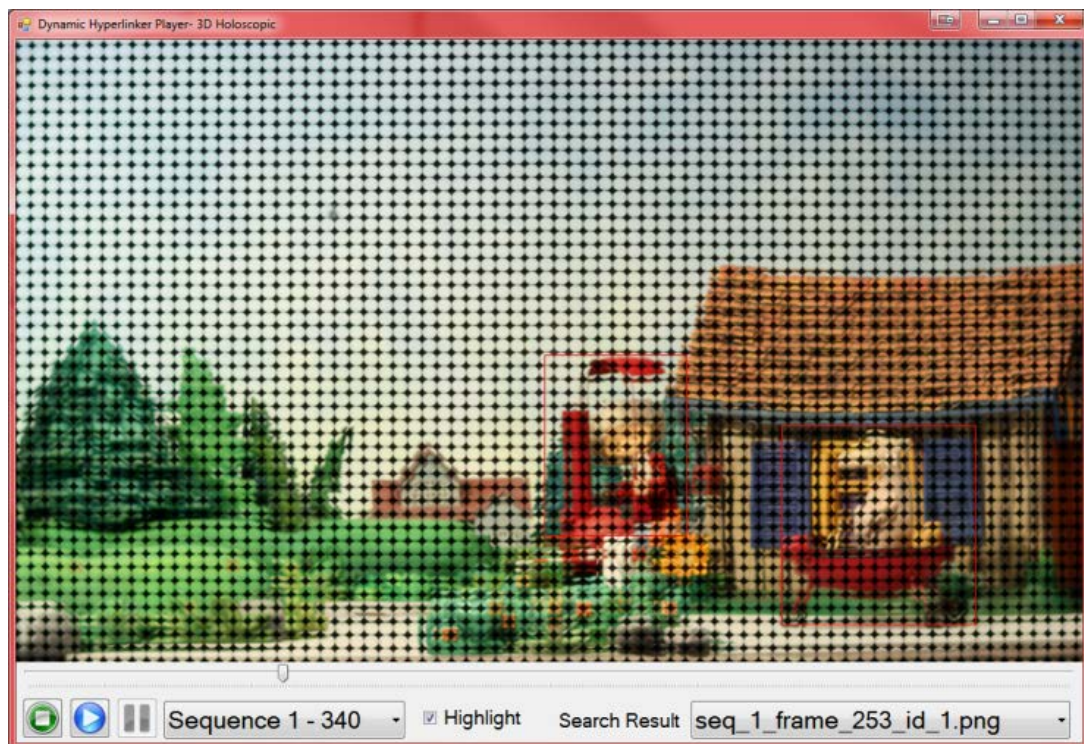
Figure 4.46 - The proposed dynamic hyperlinker player
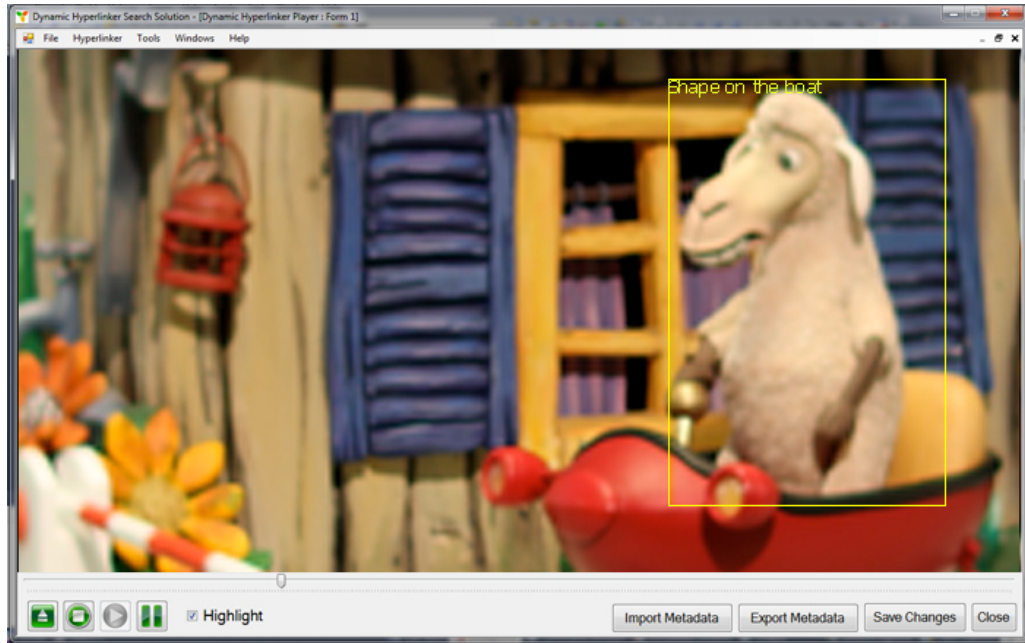
Figure 4.47 - The screenshot of hyperlinker replaying centric-view of H3D videos

Figure 4.48 shows the screenshot of search result screen that shows list of similar objects in the repository excluding the current video. It also shows the search results descriptions, video names and the scene frame number in which the object is found. At this stage, any of the search result items can be clicked to play it and the system will start playing the video from this particular scene/frame.
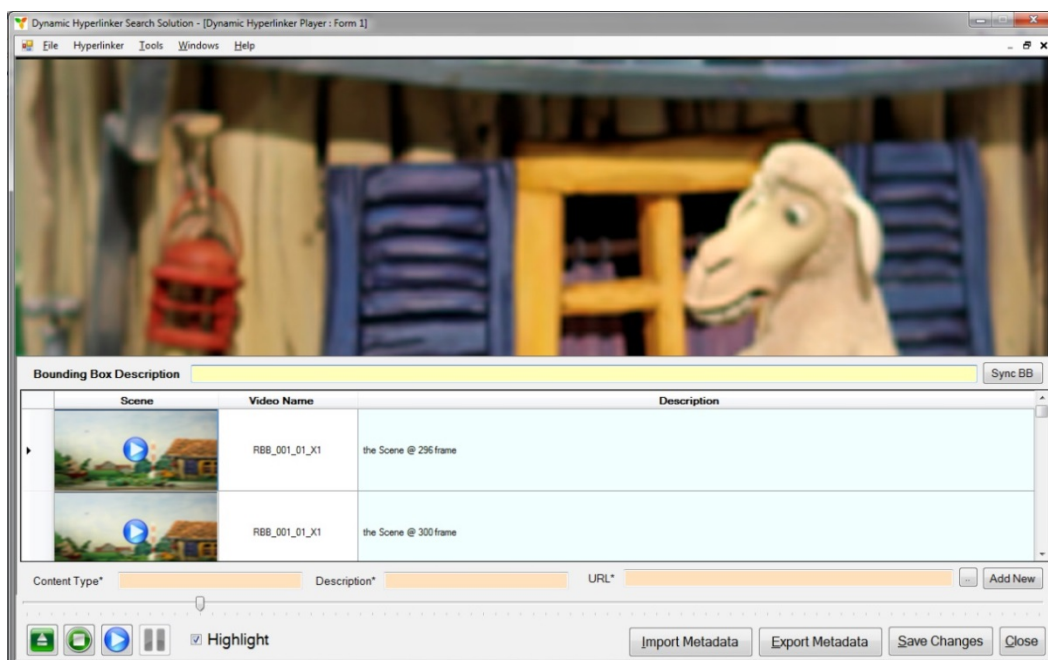
Figure 4.48 - Search result screen of hyperlinker tool

4.9   Conclusion

This chapter presented pre-processing of micro-images "elemental image" for correcting different distortions as well as conversions of H3D image to multiview 3D images and medical CT data to H3D images.

A barrel correction algorithm was presented that offers effortless calibration and mountable solution to any 3D camera because it takes advantages of MLA for generating calibration grid that is later used for correcting barrel distortions in H3D images.   The algorithm was implemented in LabWindows that performed efficiently in generating a grid from microlens grid and then in correcting barrel distortions.   This can be extended and implemented on-camera to process H3D images for video recording.

The H3D camera's MLA introduces dark borders in the captured images. If such noise is not corrected, it adds black moiré in constructed H3D scene. A MLA dark borders correction algorithm was proposed and presented that uses the MLA as a reference point for detecting dark borders and for removing the noise from the image. It is a self-calibrated and an effortless solution as capturing a white background image calibrates and corrects dark borders of final images.

A reference based micro-image equaliser algorithm was proposed that dynamically defines a default size of micro-images by generating grid of the lens array and calculating a default micro-image size. Later it uses the lens array grid to extract micro-images and resample them to the default size.

A H3D images stitching algorithm was proposed that widen overall viewing angle of the H3D camera. The current generation of H3D cameras trade off a great deal of sensor and 3D image resolution in order to obtain information on the angular directions of the incoming light rays with limited aperture. The resulting stitched image proved the H3D images were stitched together at micro-image level using MLA information and grid.

A H3D image conversion algorithm was presented that converts H3D images to multiview 3D image. It has been successfully illustrated with two multiview 3D

displays and the resulting playback results were impressive with great immersive 3D depth with reasonable movement parallax.

In addition, we proposed and built a medical image visualization system based on H3D imaging system that enables the visualization of CT scan tomographic data on H3D display. The experiment was conducted on real CT scan data provided by king's college hospital achieving promising playback results.

Last but not least, this chapter presented the development of an interactive H3D video content search and retrieval system, which offers an interactive search and annotation facilities. In addition, it offers metadata engineering and synchronization for creating hyper-videos. The proposed system has pre-processing 3D operators such as centric-view extractor, depth map extractor, object segmentation, content based search & retrieval and metadata engineering & synchronisation, which communicate and exchange action-message using 3D content descriptive protocol.

4.10 References

[1] A. Aggoun, P. Nunes, J. Steurer, M. Meier, T. Semertzidis, Z. Nagi, M. Muratori, N. Patz, "Deliverable: Report on Integration issues and prototype system" 3DVIVANT, 2013

[2] N. Pereira, O. Pidancet, P. ThoPesch, T. Semertzidis, M. R. Swash, and O. Abdulfatah, "Deliverable: 3D Hypervideo Service," 3DVIVANT, 2013

[3] M.R. Swash, A. Aggoun, O. Abdulfatah, B. Li, J. C. Jacome, E. Tsekleves, "Dynamic Hyperlinker for 3D Search and Retrieval", IEEE International Symposium on Broadband Multimedia Systems and Broadcasting, London, UK, June 2013.

[4] A. Aggoun, E. Tsekleves, M.R Swash, "Deliverable: Microlens array based 3D Holoscopic monitor" 3DVIVANT, 2013

[5] A. Aggoun, E. Tsekleves, M. R. Swash, D. Zarpalas, A. Dimou, P. Daras, P. Nunes, and L. D. Soares, "Immersive 3D Holoscopic Video System," MultiMedia, IEEE, vol. 20, no. 1, pp. 28–37, 2013

[6] S.W. Park and K.-S. Hong, "Practical ways to calculate camera lens distortion for real-time camera calibration," Pattern Recognition, vol. 34, no. 6, pp. 1199–1206, Jun. 2001.

[7] L. Alvarez, L. Gómez, and J. R. Sendra, "An Algebraic Approach to Lens Distortion by Line Rectification" Journal of Mathematical Imaging and Vision, vol. 35, no. 1, pp. 36–50, May 2009.

[8] W. Yu, "An embedded camera lens distortion correction method for mobile computing applications," IEEE Transactions on Consumer Electronics, vol. 49, no. 4, pp. 894–901, Nov. 2003.

[9] T. Stanescu, H. S. Jans, K. Wachowicz, and B. G. Fallone, "Investigation of a 3D system distortion correction method for MR images" Journal of applied clinical medical physics / American College of Medical Physics, vol. 11, no. 1, p. 2961, Jan. 2010.

[10] A. Aggoun, "Pre-Processing of Integral Images for 3-D Displays," Journal of Display Technology, vol. 2, no. 4, pp. 393–400, Dec. 2006.

[11] X. Jiang and H. Bunke, "Edge Detection in Range Images Based on Scan Line Approximation," Computer Vision and Image Understanding, vol. 73, no. 2, pp. 183–199, Feb. 1999.

[12]   D. C. Brown, "Decentering Distortion of Lenses," Photometric Engineering, vol. 32, no. 3, pp. 444–462, 1966.

[13]   NI Vision - NI Vision Concepts Manual, 2013

[14]   M. R. Swash, A. Aggoun, O. Abdulfatah, B. Li, J. C. Jacome, E. Alazawi and E. Tsekleves, "Pre-Processing of Holoscopic 3D Image for Autostereoscopic 3D Displays," IEEE International Conference on 3D Imaging, 2013.

[15]   A. Zomet, A. Levin, S. Peleg, and Y. Weiss, "Seamless image stitching by minimizing false edges.," IEEE transactions on image processing : a publication of the IEEE Signal Processing Society, vol. 15, no. 4, pp. 969–77, Apr. 2006.

[16]   M. Brown and D. G. Lowe, "Automatic Panoramic Image Stitching using Invariant Features," International Journal of Computer Vision, vol. 74, no. 1, pp. 59–73, Dec. 2006.

[17]   M. R. Swash, A. Aggoun, O. Abdulfatah, B. Li, J. Fernández, and E. Tsekleves, "Holoscopic 3D image rendering for Autostereoscopic Multiview 3D display," IEEE international Symposium on Broadband Multimedia Systems and Broadcasting, 2013.

[18]   Y. Zhang, Q. Ji, and W. Zhang, "Multi-view autostereoscopic 3D display," Optics Photonics and Energy Engineering (OPEE), vol. 1, pp. 58-61, 2010

[19]   V. Berkel and J. A. Clarke, "Autostereoscropic Display Apparatus," U.S. Patent number: 6064424, 2000.

[20]   Alioscopy, "Alioscopy Pixel Mapping," Alioscopy, [Online]. Available: http://www.alioscopy.com/en/principles.php. [Accessed: 01/02/2013].

[21]   Persistence of Vision Pty. Ltd. (2004), Persistence of Vision Raytracer (Version 3.6). [Online]. Available: http://www.povray.org/download/

[22]   O. Schreer, I. Feldmann, I. A. Mediavilla, P. Concejero, A. H. Sadka, M. R. Swash, S. Benini, R. Leonardi, T. Janjusevic, and E. Izquierdo, "RUSHES—an annotation and retrieval engine for multimedia semantic units," Multimedia Tools and Applications, vol. 48, no. 1, pp. 23–49, Oct. 2009.

[23]   M.R. Swash, A. Aggoun, O. Abdulfatah, B. Li, J. C. Jacome, E. Tsekleves, "Omnidirectional Holoscopic 3D Content Generation using Dual Orthographic Projection", IEEE International Symposium on Broadband Multimedia Systems and Broadcasting, London, UK, June 2013.

5 Chapter Five - Holoscopic 3D Display Technology

This chapter presents core techniques, which enhances spatial resolution of unidirectional and omnidirectional holoscopic 3D display. In addition, it presented development of a moiré-free omnidirectional H3D display based on cross-lenticular technology. The layout of the chapter is as follows: 5.1 Introduction, 5.2 Pixel Mapping Techniques, 5.2.1 Adopting Multiview Pixel Mapping in H3D Display, 5.2.2 Novel Triangular Pixel Mapping, 5.2.3 Novel Distributed Pixel Mapping, 5.2.4 Novel Smart Pixel Mapping, 5.2.5 Novel Distributed Smart Pixel Mapping, 5.3 Moiré-Free Omnidirectional H3D Display and 5.5 Conclusion.

5.1   Introduction

In this chapter, the design aspect of holoscopic 3D (H3D) displays is investigated and options are discussed by proposing multiple pixel mapping methods for both omnidirectional and unidirectional H3D displays. In fact, it is the first attempt ever to apply pixel mapping on omnidirectional H3D images.

Multiview pixel mapping techniques [1][2][26] are adopted and implemented in H3D display for advancing the H3D resolutions and a good result is achieved. Also a novel alternative triangular pixel mapping (TPM) method are proposed that does not require the slanting and highly applicable for parallax barrier technology [4].

In addition, novel distributed pixel mapping (DPM) is proposed for separating R, G, B channel images for a better 3D image quality. It enables creation of R, G, B elementals and project them separately from independent microlens e.g. R elemental image is created from all R subpixels of a microlens image (RGB elemental images). It is applicable for both lens array and parallax barriers technology and more importantly it can further refine lens array in front of 3D displays to make the lens array unnoticeable to viewers. The state of the art pixel mapping grows in vertical direction whereas the proposed distributed pixel mapping allows growth in both vertical and horizontal directions. It is applicable and works with different pixel mapping methods and slanting angles.

To date, there is not a pixel mapping method which targets to improve 3D visual definition. In this chapter, novel smart pixel mapping (SPM) and distributed smart pixel mapping (DSPM) are proposed for designing high definition 3D display such as SPM and DSPM enhance 3D pixels per inch by bringing 3D pixels closer to each other in the space. The slanting technique is applied to eliminate moiré effect of omnidirectional H3D displays [5].

5.2   Pixel Mapping Techniques

Pixel mapping is a pixel arrangement in digital LCDs which have rectangular subpixels and square RGB pixels in array style shown in Figure 5.1 (a).   This particular pixel structure is proposed and implemented in existing 2D display technology in different resolutions and pixel aspect ratio standards, such as the widely known Full-HD 1920 × 1080 pixels @16:9. Some of widely used pixel aspect ratios and standards in 2D imaging systems are presented in Figure 5.1 (b).

(a) Traditional Pixel Structure

Standard	5:4	4:3	3:2	16:10	16:9
CGA				320 x 200	
QVGA		320 x 240			
VGA		640 x 480			
NTSC			720 x 480		
PAL		768 x 576			
SVGA		800 x 600			
WVGA					854 x 480
XGA		1024 x 768			
-			1152 x 768		
-		1280 x 960			
HD 720					1280 x 720
SXGA	1280 x 1024				
-			1280 x 854		
SXGA+		1400 x 1050			
-			1440 x 960		
UXGA		1600 x 1200			
WSXGA+				1680 x 1050	
HD 1080					1920 x 1080
WUXGA				1920 x 1200	
QXGA		2048 x 1536			
WQXGA				2560 x 1600	
QSXGA	2560 x 2048				

(b) State of the art pixel aspect ratio standards

Figure 5.1 – Pixel structure of liquid crystal display and standard pixel aspect ratios

Autostereoscopic 3D displays with flat panel LCD and lenticular sheets (or parallax barriers) have been received much attention after the moiré effect issue was resolved by slanting the lenticular sheet [1][2]. In addition, Pixel

mapping techniques [1][2] were proposed for unidirectional 3D displays that enabled viewers to achieve 2D like pixel aspect ratios by trading off horizontal and vertical 3D resolutions.
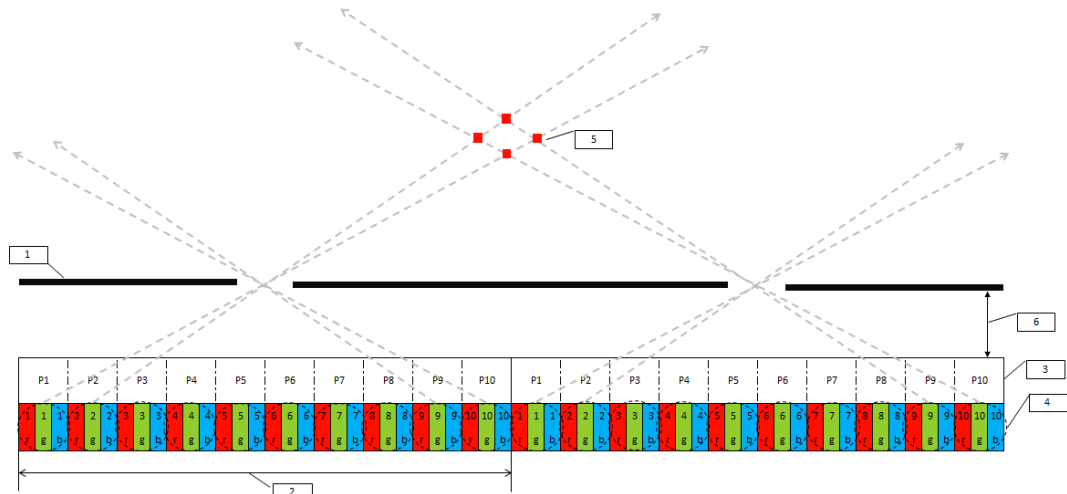
(a) Unidirectional holoscopic pixel mapping (1) Pinhole array, (2) Pinhole pitch size = 1 Pixel, (3) Pixels per pinhole = 10 pixels, (4) Viewpoint RGB dot pixel structure, (5) 3D pixel 'viewpoint pixels Intersections', 6: Focal length
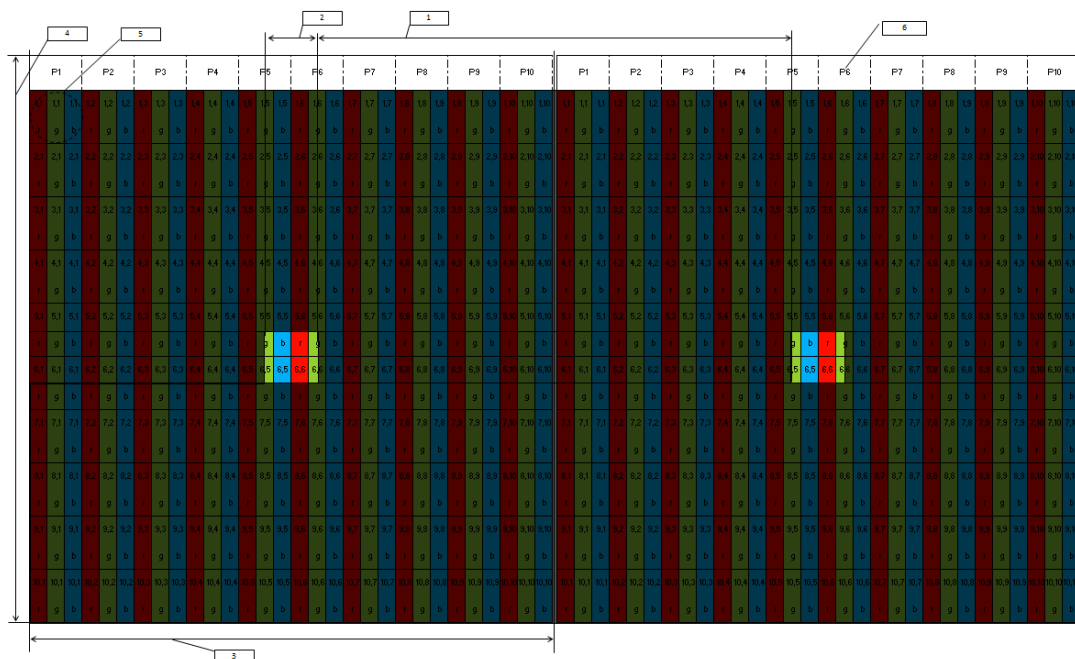
Figure 5.2 – H3D display pixel mapping in (a) unidirectional and (b) omnidirectional

Figure 5.2's label description: (B) Omnidirectional holoscopic pixel mapping: (1) distance between pinholes = 9 pixels, (2) pinhole pitch = 1 pixel, (3, 4) lens pitch = 10 pixels, (6) pixel index under the microlens.

Presently, the main target is making the viewing experience as natural as possible with natural enough 3D effects and 3D resolution are of prime importance. The challenges are to design FULL HD equivalent autostereoscopic 3D displays using available LCDs technology for mass digital market. In this section, multiple pixel mapping techniques and smart pixel distributions are proposed to improve 3D resolutions and 3D definition of both unidirectional and omnidirectional H3D displays.

H3D imaging also known as integral imaging [6] utilises microlens array (MLA) to construct a true 3D scene and the microlenses presents perspective micro-images whereas viewpoint pixels are projected successively into space as representation shown in Figure 5.2. Therefore in traditional approach, increasing number of 3D pixels growths horizontal size of the 3D display in unidirectional one and in omnidirectional, both horizontal and vertical pixels must be equal whereas vertical movement parallax is less relevant compared to the horizontal movement. In addition, number of 3D pixels per inch depends on physical 2D LCD pixel pitch.

5.2.1 Adopting Multiview Pixel Mapping in H3D Display

The Multiview 3D display [9] is developed based on the human eye technique and to date, all multiview 3D displays are unidirectional for instance an 8-view Multiview 3D display will have 3D resolution of 2D width resolution / 8 × 2D height resolution which creates a very unbalanced pixel aspect ratio problem. Also accommodating more views/viewers will increase the unbalanced pixel aspect ratio further. This problem is overcome by applying pixel mapping techniques [2][26], which are adopted for H3D displays in this section.

The pixel mapping techniques separate sub-pixels (Red, Green, Blue sub-pixel) of a view pixel in vertical direction that use the vertical resolutions to enhance the horizontal resolution. Because a sub-pixel size is used to project a single pixel data, more 3D pixels can be fitted compared to the traditional approach.

In addition, the lens array gets slanted as the sub-pixels are distributed in vertical direction. In particular, the pixel mapping techniques have been applied to multiview 3D displays. This section focus is to adopt and implement the multiview pixel mapping techniques such as Alioscopy [26] and Philips pixel [2] techniques in unidirectional and omnidirectional H3D displays.

The Alioscopy pixel mapping method [26] spreads a viewpoint pixel into 3 rows by shifting horizontally as illustrated in Figure 5.3-(a). This process creates 18.43 degrees slanting thus the lens array needs to be slanted by 18.43 degrees. As it fits a pixel into a subpixel, it triples the horizontal 3D resolution where the vertical resolution is reduced to 1/3 and the 3D-DPI remains unchanged. However the Philips pixel mapping enhances 3D-DPI by two as shown in Figure 5.3-(b). Because it reduces the distance of two consecutive viewpoint pixels, it offers rich depth parallax with smooth transition between viewing zones.

In H3D imaging, a 3D scene is constructed by collective microlenses, which project viewpoint pixels where intersection point of two viewpoint pixels creates a 3D pixel as shown in Figure 5.2. The only difference between the multiview 3D display and the H3D display is that the multiview 3D display has viewpoint images are perspective (based on human imaging system "present a diagram") and the H3D display's viewpoint images are orthographic (based on fly's eye technique "present a diagram")

(a) Alioscopy pixel mapping [26]   (b) Philips pixel mapping [1][2]
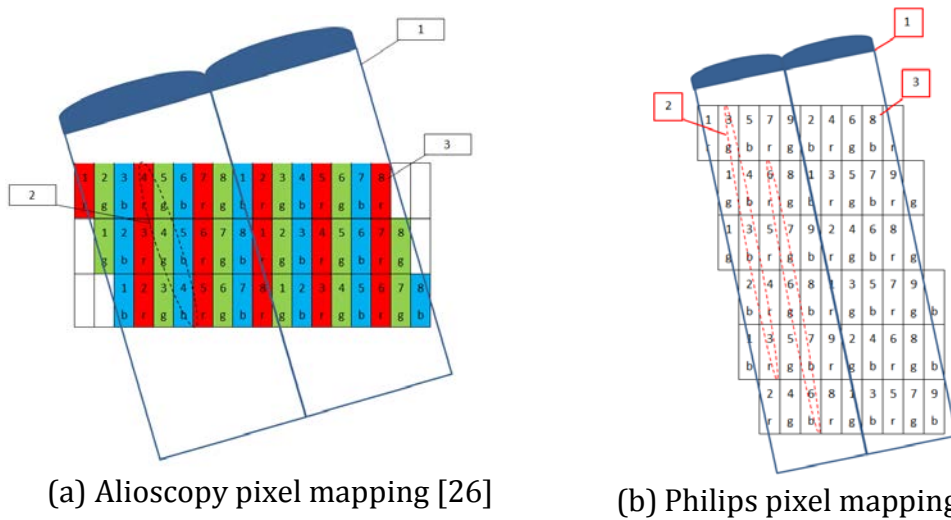
Figure 5.3 – State of the art pixel mapping techniques: (a) Alioscopy pixel mapping [26], (b) Philips pixel mapping [2] (1: MLA, 2: Viewpoint pixel construction, 3: Pixels per lens)

The pixel mapping techniques [2][26] are adopted and implemented in H3D display. It inherits the advantages, for example, it makes the 3D display size to grow in both horizontal and vertical directions. When more 3D pixels are added to a microlens, which enhances the horizontal 3D resolution compared to the traditional method. However 3D pixel distance or the number of 3D pixels per inch remains unchanged before and after applying the pixel mapping method (a) however the method (b) enhances the visual definition of spatial resolution by reducing the distance of two viewpoint pixels. Figure 5.3 illustrates the state of the art pixel mapping methods implemented in commercial multiview 3D displays and adopted in the H3D display. The distance between two viewpoint pixels is 1 in Figure 5.3-(a) while it is ½ in Figure 5.3-(b) pixel mapping method which fits two times more pixels per lens "double number of 3D pixels per inch in the space" compared to Figure 5.3-(a).

The pixel mapping methods reduce vertical 3D resolutions and enhance horizontal 3D resolutions. For instance, Figure 5.3-(a) is the pixel mapping which is implemented in Alioscopy displays that divide the vertical 3D resolutions by 3 and multiply the horizontal 3D resolutions by 3 because it uses a physical subpixel size to project a pixel. On the other hand, the Philips pixel mapping technique doubles the 3D resolution because it maps subpixels in to two layers thus half of a physical subpixel is used to project a full pixel as shown in Figure 5.3-(b). This pixel mapping method divides the vertical 3D resolutions by 6 and multiplies the horizontal 3D resolutions by 6. This section presents implementation of Alioscopy multiview pixel mapping methods in parallax barriers based H3D display. This proves that any multiview pixel mapping methods are applicable to H3D displays. The experimental results demonstrate that pixel mapping techniques are implemented in H3D display successfully.

5.2.1.1   *Pixel Preparation for Omnidirectional H3D Display*

This section illustrates adaptation of Alioscopy pixel mapping [26] in omnidirectional H3D display. Philips pixel mapping is not considered in omnidirectional pixel mapping. It is not suitable for omnidirectional 3D display as Philips pixel mapping [2] trades it off by 6 times which creates unbalance elemental images.

The pixel mapping technique is applied on elemental images. It separates sub-pixels (Red, Green, Blue sub-pixel) of a view pixel in vertical direction that use the vertical resolutions to enhance the horizontal resolution. Because a sub-pixel size is used to project a single pixel data, more 3D pixels can be fitted compared to the traditional approach as shown in Figure 5.4. It is a fixed pixel mapping method which trades off horizontal and vertical resolution of elemental images by 3. Therefore it triples horizontal resolution by losing vertical resolution of the elemental image. For instance, Figure 2.2.19 shows a microlens of 9 × 9 pixels; we apply the pixel mapping method to fit 27 × 3 pixels which is replayed using the same lens array.
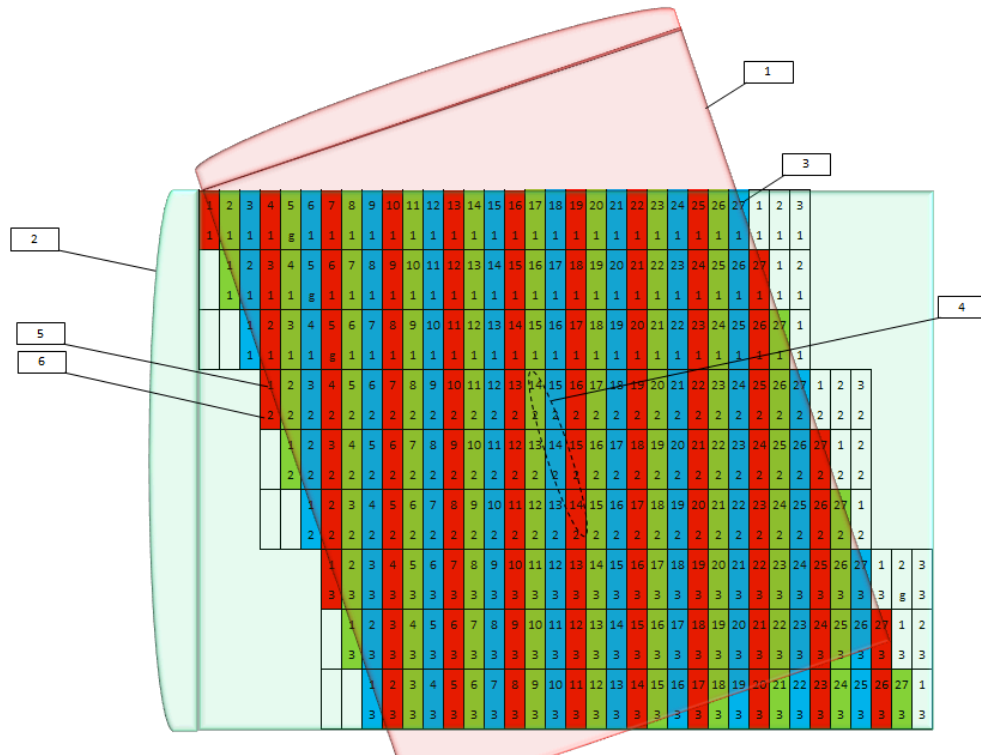
Figure 5.4 - Omnidirectional pixel structure of multiview pixel mapping method: (1) horizontal lenticular sheet, (2) vertical lenticular sheet, (3) pixels per lens = 27 × 3 pixels, (4) construction of a RGB pixel dot, (5) horizontal viewpoint pixel index, (6) vertical viewpoint pixel index

More importantly, lenticular sheets should be carefully designated for this pixel mapping to support the trade-off if not then lens pitches and focal length of both lenticular sheets should be compatible. On the other hand, it can be easily implemented in parallax barrier technology which is easy to manufacture /

print in any style and size. Figure 5.5 shows an example of mapping 10 × 3 pixels occupying 3.33 pixels horizontally 4.5 pixels vertically.
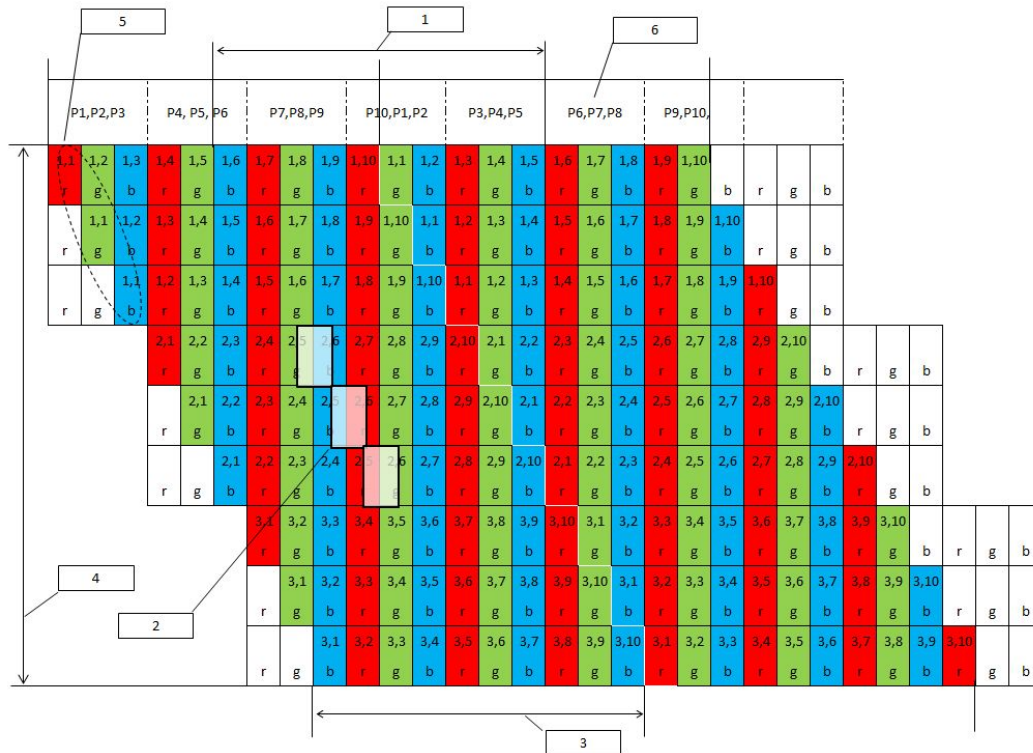
Figure 5.5 - Omnidirectional pixel structure of multiview pixel mapping method in parallax barriers: (1) distance between pinholes = 9 subpixels, (2) pinhole pitch = 1 subpixel, (3) horizontal lens pitch = 10 subpixels, (4) vertical lens pitch, (5) construction of a RGB pixel dot, (6) pixel index number under the microlens

5.2.1.2 *Pixel Preparation for Unidirectional H3D Display*

In preparation stage, pixels of H3D image are distributed vertically by shifting the subpixels in horizontally. Figure 5.6 shows the distribution of the pixels in vertical and horizontal directions under each pinhole to create new compatible pixels. For instance, the first pixel: R sub-pixel is placed in row 1, column 1; G sub-pixel is placed in row 2, column 2; and B sub-pixel is placed in row 3, column 3 according to Equation 1. This subpixel distribution process also creates a slanting angle of 18.43° therefore the display has the lenticular sheet slanted by 18.43 degrees as shown Figure 5.3 (a).

The pixel mapping requires the pinhole array to be slanted then mapped viewpoint sub/pixels are projected correctly however the slanting introduces crosstalk noise as small portions of neighbouring subpixels are projected too as

illustrated in Figure 5.6 (b). The crosstalk noise is removed by creating strip subpixel shape pinhole array in slanted manner shown in Figure 5.6 (a).
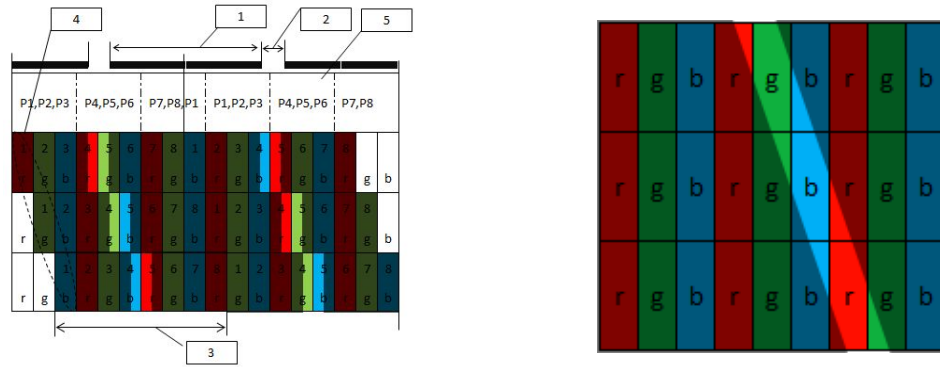
(a) Shifted stripe subpixel shape "Proposed"

(b) Slanting pinhole array

Figure 5.6 – Systematic of Alioscopy pixel mapping in parallax barriers based H3D display: (1) dark spacing distance between pinholes | 7 Subpixel size, (2) pinhole pitch | 1 Subpixel size, (3) lens pitch | 8 subpixels, (4) a single viewpoint pixel construction and (5) pixels per lens

Equation 5.1 - A newly created pixel contains subpixels of viewpoint pixels

$$\textbf{Pixel}^{\,r,\,c} <= \textbf{R}^{\,\text{Pixel[i]}} + \textbf{G}^{\,\text{Pixel[i + 1]}} + \textbf{B}^{\,\text{Pixel[i + 3]}}$$

Where r = row; c = column; R = red; G=green; B = blue;

The display has 5040 subpixels in the horizontal direction where each microlens has 8 pixels that are mapped to 8 physical subpixels and it has 630 pinholes in total. Equation 5.2 shows a 3D pixel resolution of 630 × 350 3D pixels with aspect pixel ratio of 1.80 which is almost wide screen aspect pixel ratio standard. These parameters are taken under consideration during rendering a H3D image.

Equation 5.2 - 3D pixels counts in the proposed approach

$$(1680 * 3) / (10) = 630 \text{ pixels in horizontal direction}$$
$$1050 / 3 = 350 \text{ pixels in vertical direction}$$

A H3D camera model is developed using multiple orthographic projection cameras which is patented by BBC [7]. In this setup, the H3D camera is built

using 8 multiple orthographic cameras which renders 8 orthographic viewpoint images in POV-Ray [8]. The viewpoint images are then interlaced to form a H3D image in .NET.

As shown in

Table 5.1, by taking into account the parallax barriers parameters including the display, a H3D image is rendered and the steps are:

1. Render 8 orthographic viewpoint images with resolution of 630 × 350 pixels
2. Apply Interlacing algorithm to interweave 8 viewpoint images to create a H3D image with resolution of 5040 × 350 pixels
3. Apply the developed pixel mapping algorithm to remap the H3D image pixels into a compatible pixel representation and to create a 3D image of resolution 1680×1050 pixels

The prepared H3D images are opened in full screen mode, which can be replayed by any media player without a need for 3D players. The LCD and pinhole array parameters are taken into consideration during the rendering and preparation. Therefore when the H3D image is opened in full screen mode, it fits well to the display resolution. The pinhole array alignment is carried out manually (human hand). As a result, a small noise is expected as the alignment accuracy is +/-20 microns. The alignment is very important to avoid crosstalk noise and other errors in 3D scene construction process.

5.2.1.3 *Playback Result*

A H3D display [Appendix A] is built in the lab at Brunel University as there is no H3D display available commercially in the consumer market yet. Both proposed and traditional 3D displays have been built with exact hardware specifications including pixel pitch size, pixels per pinhole, and focal length as show in

Table 5.1. The proposed method (3D Display) has 3 times more pinhole arrays than the traditional one because it fits 8 pixels (24 Subpixels) in the size of 8

physical subpixels sizes. The constructed H3D image is sharper and finer compared to the traditional one.

Table 5.1 – Parallax barriers based H3D display with proposed pixel mapping method

Items	Without Pixel mapping	With Pixel Mapping
Pixel pitch	0.282(H) × 0.282 (V) mm	0.282(H) × 0.282 (V) mm
2D Resolution	1680 × 1050 pixels	1680 × 1050 pixels
Backlight source	250 cd/m2	250 cd/m2
Pixels per pinhole	8 pixels	8 pixels
Pinhole pitch	*8 × 0.282 mm = 2.256 mm*	*8 × (0.282mm/3) = 0.752 mm*
Pinhole sheet	*168 pinholes*	*630 pinholes*

Parallax Barrier Sheet
without pixel mapping

Parallax Barrier Sheet
with pixel mapping
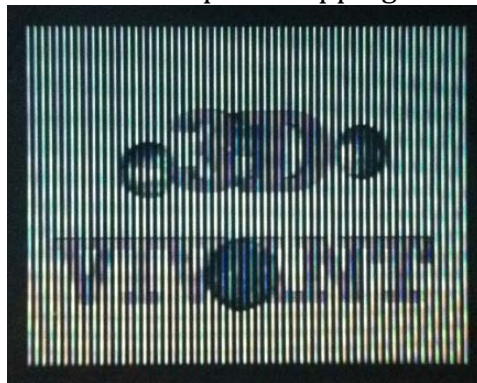
210 × 1050 3D-Pixels
Without pixel mapping

630 × 350 3D-Pixels
With pixel mapping "Proposed"

Figure 5.7 - Playback result of proposed approach

H3D images are prepared and rendered for traditional and proposed approach. They are replayed on the custom built H3D display and as seen in Figure 5.7 the resulting images playback, the outcome is very promising. The dark spacing barriers between pinholes is refined further as they get invisible for human eyes. It also improves the quality of constructed H3D scene (see the visual

richness quality of earth in both images). It is worth mentioning that lighting remains unchanged but the pinhole arrays are well refined to give stunning 3D scene quality.

5.2.2 Novel Triangular Pixel Mapping

All existing pixel mappings [2][26] are slanting as they have been targeted lenticular technology which must be slanted to remove the moiré. As noticed in the previews section not all existing pixel mappings e.g. Philips pixel mapping [2] are applicable to omnidirectional 3D display. In addition, parallax barrier technology [4] does not need to be slanted. This section presents a Triangular pixel mapping (TPM) for parallax barriers based H3D displays as it does not require slanting and also it is applicable for both unidirectional and omnidirectional H3D display. Viewpoint pixels are in triangular style to adapt existing LCDs without need for a bespoke LCD.

The proposed TPM achieves the same result as existing pixel mapping but the most importantly it does not require a bespoke LCD as it is applicable with existing LCDs. In other word, it is an equivalent of Alioscopy pixel mapping [26] without crosstalk error of slanting. Also it is computationally efficient compare to Alioscopy pixel mapping [26] because the pixel mapping process does not change shape of the image therefore no need for a de-slanting process.

This particular pixel mapping is proposed for parallax barriers technology because triangular style pinhole is possible and subpixels are propagated correctly without crosstalk error. An excellent sharp and crisp playback result is achieved in parallax barriers technology. In addition, it is tested on lens array technology without slanting it and the playback result is comparable. In theory, a small error is expected in lenticular technology, which has strip cylindrical microlens, therefore, a subpixel of neighbouring viewpoint pixel is used for construction of a 3D scene. However, the error is not there because using subpixel of neighbouring pixel is almost the same as the original one. Particularly, there will be almost no difference in high resolution digital images.
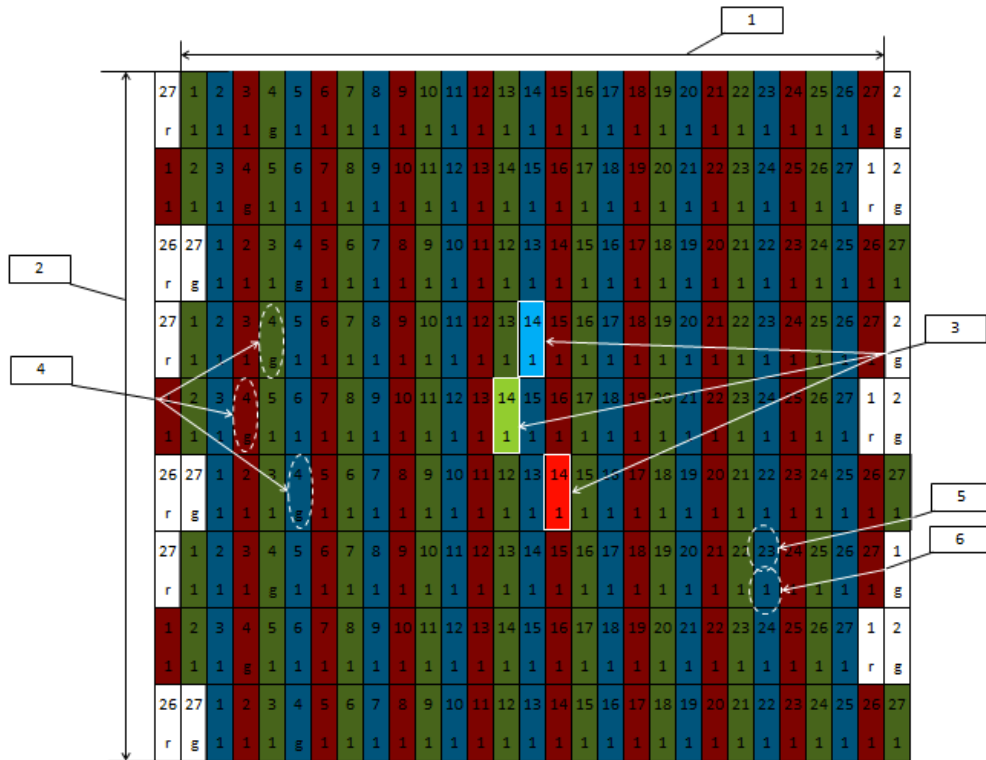
Omnidirectional triangular pixel mapping: (1,2) lens pitch = 27 × 3 pixels, (3) pinhole pitch, (4) construction of a RGB dot pixel, (5) horizontal pixel index number, (6) vertical pixel index number
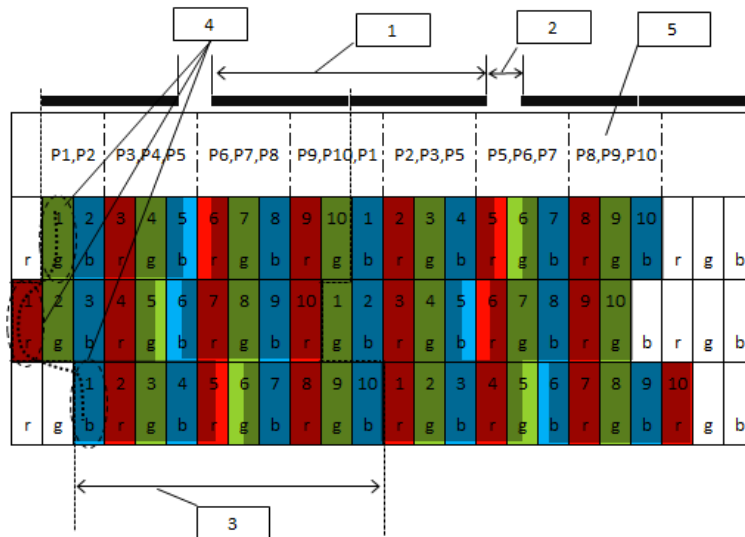
(B) Unidirectional Triangular Pixel Mapping: (1) distance between pinholes = 9 Subpixels, (2) pinhole pitch | 1 Sub pixel size, (3) pixels per lens = 10 subpixels per lens, (4) contruction of a viewpoint pixel, (5) viewpoint pixel index

Figure 5.8 – Proposed Triangular pixel mapping: (a) traditional pixel mapping, (b) Proposed triangular pixel mapping

5.2.2.1 Pixel Preparation

Figure 5.8 shows the proposed pixel mapping that illustrates the structure of subpixels as well as the construction of a RGB dot pixel in both unidirectional and omnidirectional H3D images. Figure 5.8 (a) illustrates how triangular pixel mapping is applied on omnidirectional 3D image.   In fact, the pixel mapping is applied on elemental images whose pixels are remapped to improve the horizontal resolution.

It improves 3D resolutions as well as 3D pixel aspect ratio by enhancing horizontal 3D resolutions three times better at the same pixels per lens. For Unidirectional H3D image, in the case of Figure 5.8 (b), there are 10 pixels per lens that is remapped in Figure 5.8 (b).   Viewpoint pixels are remapped in triangular style which is compatible with existing LCDs pixel structure and it trades off horizontal and vertical 3D resolution to balance 3D pixel ratio.

***504 × 350 3D-Pixels
With Pixel Mapping***
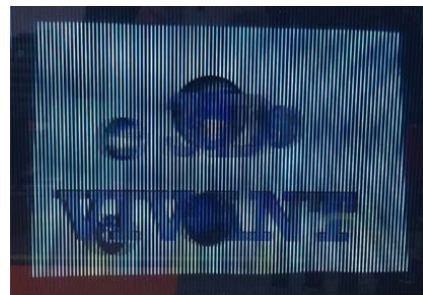
***168 × 1050 3D-Pixels
Without pixel mapping***

The playback on Parallax Barriers Technology @10PPL
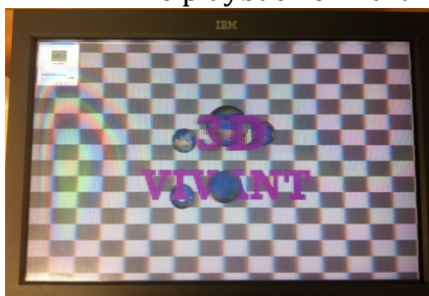
Top view
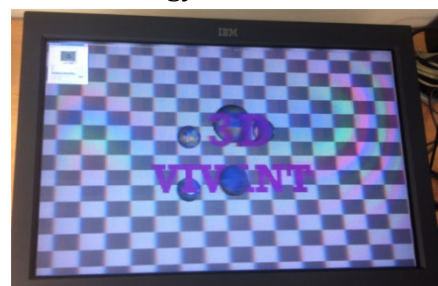
Top-right view

This pixel mapping has been testing on the Lenticular Technology @17PPL

Figure 5.9 - Playback result of TPM on (a) parallax barriers and (b) lenticular technology

5.2.2.2 Playback Result

The pixel mapping method is implemented in .NET that applies the proposed pixel mapping to H3D images to remaps viewpoint pixels.   The prepared H3D image is directly replayed on the H3D display as shown in Figure 5.9.

It has been tested on both parallax barriers and lenticular technology. Parallax barriers offers construction of H3D scene without any ghosting and crosstalk error as shown in Figure 5.9 (a) that has 10 pixels per lens. Also a comparable result is achieved in lenticular technology which offers an amazing 3D depth and motion parallax shown in Figure 5.9 (b). The experimental results prove the concept, which offers an alternative pixel mapping without ghosting / crosstalk errors and it is compatible with traditional LCDs.

5.2.3 Novel Distributed Pixel Mapping

Traditionally viewpoint pixels are replayed or projected by a single lens whose subpixels "R, G, and B" are organised in a successive manner. Also all existing pixel mapping methods [2][26] project a RGB dot pixel from a single lens. In this section, a novel distributed pixel mapping (DSP) method is proposed that distributes pixels in horizontal direction and subpixels "R, G, and B" of a dot pixel are projected from 3 different smaller lenses, as a result, it reduces the microlens size by 3 quarters. Figure 5.10 illustrates the distribution process of pixels remapping, where pixels from 1-coarse-lens are mapped to a 3-smaller-lens array which projects subpixels separately. The 3-smaller-lens array constructs a single coarse lens image.
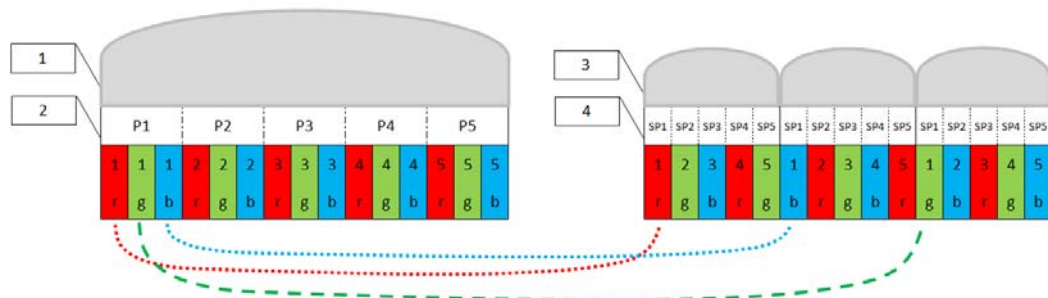
Figure 5.10 – Illustration of pixels distribution (1: Original coarse lens, 2: pixels per lens, 3: new refined lens array, 4: subpixels per lens)

The primary contribution is the introduction of pixel distributions to neighbouring lenses, which enables us to design and build 3D displays with refined and smooth MLA, using existing 2D pixel sheets. Furthermore, it refines large-dark areas in parallax barriers technology that improves quality of constructed 3D scene.
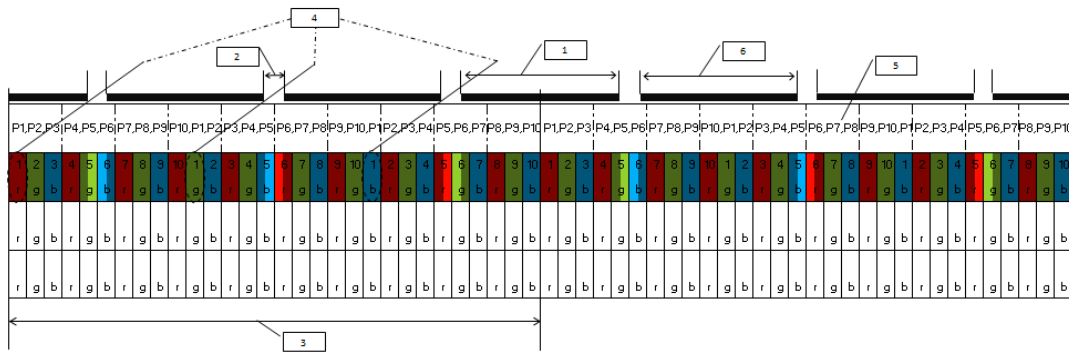
Figure 5.11 – Distributed pixel mapping pixel structure in unidirectional H3D image: (1) Dark spacing between pinholes = 9 Subpixels, (2) pinhole pitch size = one subpixel, (3) lens pitch size = 10 pixels, (4) construction of a single viewpoint RGB pixel, (5) number of pixels per pinhole, (6) dark spacing between created pinholes)
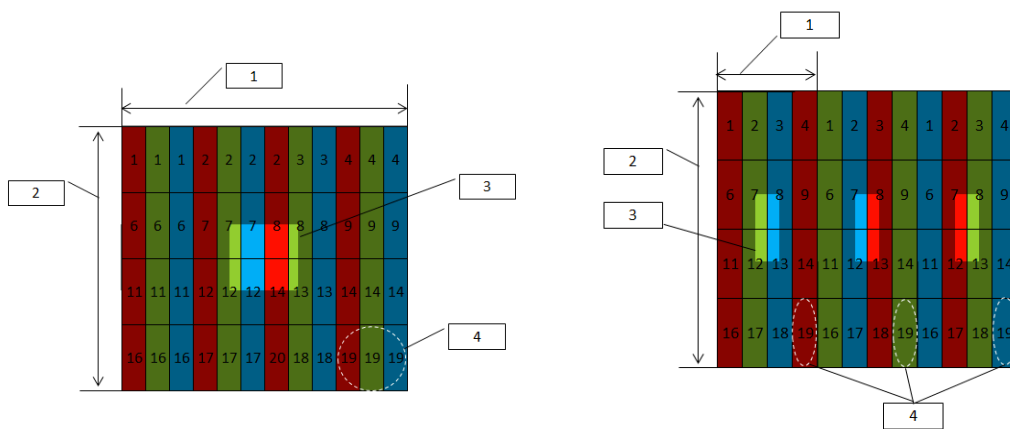
(a) without pixel mapping   (b) with proposed pixel maping

Figure 5.12 - Distributed pixel mapping pixel structure in omnidirectional 3D image (a): (1,2) lens pitch size = 4 × 4 pixels, (3) pinhole pitch = 1 pixel size, (4) construction of viewpoint pixel. (b): lens width size = 4 subpixels, (2) lens height size = 4 pixels, (4) construction of a RGB dot pixel

5.2.3.1 *Pixel Preparation*

Figure 5.11 illustrates how distributed pixel mapping remaps a unidirectional H3D image whereas Figure 5.12 shows the pixel mapping in omnidirectional H3D image. The advantages of the proposed pixel mapping method include:

- 3D images captured using a coarse lens array can be replayed using a finer lens array and the same applies to the parallax barrier technology
- It enables smart 3D pixels as viewpoint 3D pixels are mapped in vertical direction and 3D subpixels are mapped in horizontal direction
- It is compatible with all pixel mapping methods as well as any slanting angle can be achieved with it.

- It is a distortion free 3D pixel mapping method where the slanted image shape – caused by the vertical map in classical 3D pixel mapping methods – is resolved.

5.2.3.2 Playback Result

Figure 5.13 shows the playback result of both traditional and the proposed method. It shows that projecting RGB elemental images give a good quality 3D image as dark spacing are refined further for improving the viewer's visual perception. The proposed pixel mapping is superior when compared to the state of the art pixel mappings [2][26] because it enhances the quality of constructed image without introducing any noise or change the shape of the image. Instead it refines the dark spaces. In addition, it opens a door for further refinement of lens array on 3D displays.

Table 5.2 - The H3D display specifications of traditional and proposed method

Description	Without Pixel Mapping	Proposed Pixel Mapping
Pixel pitch	*0.282(H) × 0.282 (V) mm*	*0.282(H) × 0.282 (V) mm*
2D Resolution	*1680 × 1050 pixels*	*1680 × 1050 pixels*
Pixels per pinhole	*10 pixels*	*10 pixels*
Pinhole pitch	*10 × 0.282 mm= 2.82 mm*	*10 × (0.282mm/3)= 0.94 mm*
Pinhole sheet	*168 pinholes*	*504 pinholes*

As seen in Figure 5.13, from the resulting playback images it is realized that the result is very promising and the dark spacing barriers between the two pinholes is not visible with a naked eye. Also it does improve the constructed H3D image quality (see the visual richness quality of earth in both images). It is worthwhile of mentioning that lighting remains unchanged as shown in Figure 5.15 but pinhole arrays are well refined to give stunning 3D image quality.

We are using two liquid crystal displays and the pinhole LCD has 3 times smaller pixel pitch size than the image LCD. There is a noticeable moiré distortion, which can be removed by slanting the pinhole LCD. This paper does not focus on designing a, LCD and therefore it does cover that subject. LCDs are used to visualize the prepared 3D image to ensure 3D images are constructed

correctly (Figure 5.13). The proposed method improves the constructed 3D image quality significantly.

In addition, the proposed method is applicable with any pixel representation approach. For instance, it is successfully integrated with Alioscopy pixel mapping method and replayed on Alioscopy autostereoscopic 3D display successfully shown in Figure 5.14.

(a) 168 × 1050 3D-Pixels	(b) 168 × 1050 3D-Pixels
Without pixel mapping	With pixel mapping
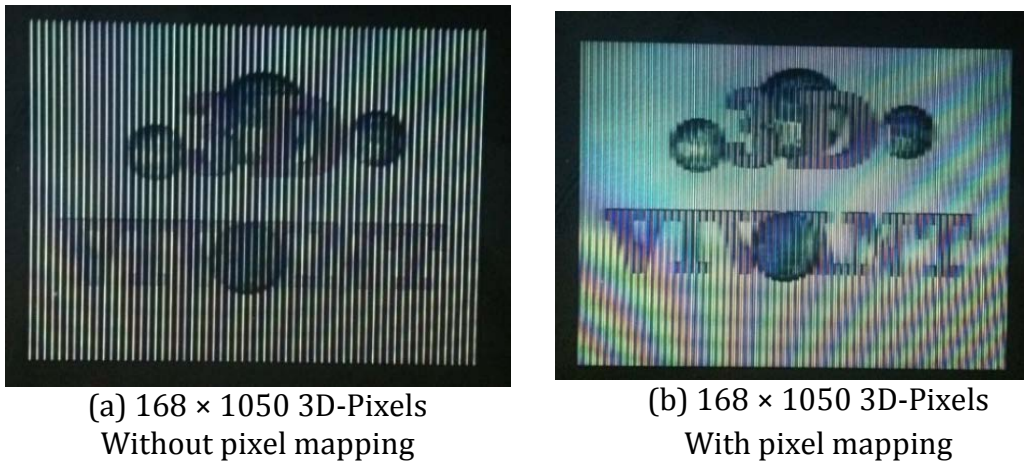
Figure 5.13 – Distributed pixel mapping playback result on parallax barriers H3D display

240 × 1080 3D-Pixels (Top view)   240 × 1080 3D-Pixels (Top-right view)
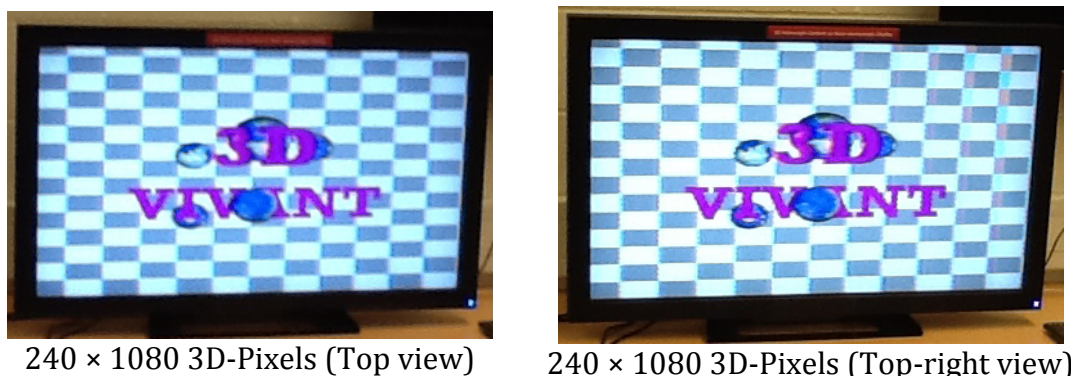
Figure 5.14 - Distributed pixel mapping playback results on lenticular based H3D display

(a) without pixel mapping   (b) with pixel mapping
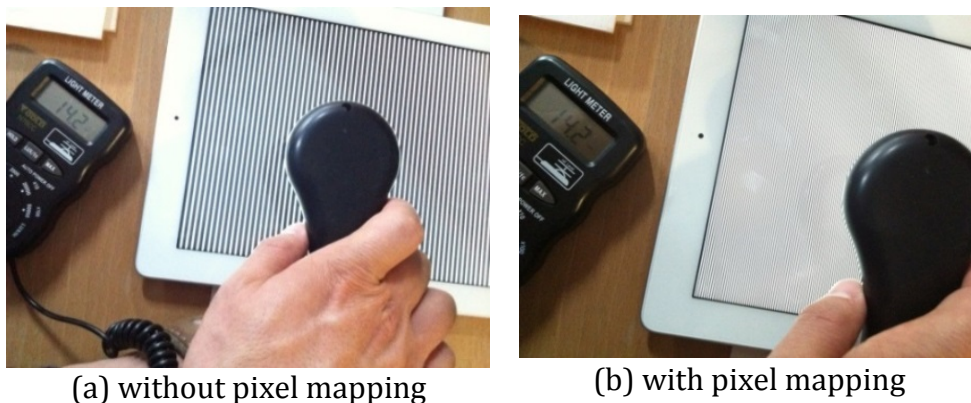
Figure 5.15 - Pinhole throughput light measurements of proposed method (b) vs. traditional pinhole method (a)

5.2.4   Novel Smart Pixel Mapping

In previews sections, a number of pixel mapping techniques have been proposed and discussed that trade off horizontal and vertical resolution in a fixed manner as they are limited to 3 times [26] or 6 times [2] for improving number of pixels in horizontal direction with a balanced pixel aspect ratio.   All state of the art pixel mapping methods allow the display size to grow in both horizontal and vertical directions while adding more 3D pixels in space resulting in improved 3D resolutions.
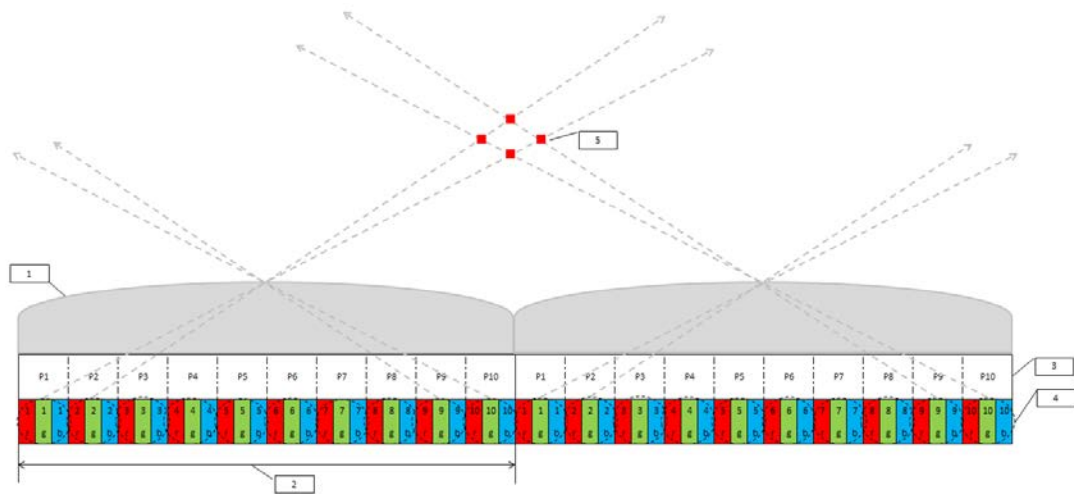
Figure 5.16 - H3D imaging of viewpoint pixels representation: (1) MLA, (2) Microlens-pitch size, (3) Pixels per lens, (4) Viewpoint pixel structure, (5) 3D pixel in the space 'viewpoint pixels Intersections')

However, the main issue is with the existing pixel mapping methods, which fail to increase the number of 3D pixels per inch in space; in other words, they do not enhance the definition of 3D resolution which has to be done by bringing 3D pixel closer in space as shown in Figure 5.16 with red coloured dot. Nevertheless, adding more 3D pixels does not make high definition 3D displays because the number of 3D pixels per inch remains unchanged. Taking this into consideration, we propose a novel Smart Pixel Mapping (SPM) method which overcomes this limitation. The propose pixel mapping is an ideal solution for designing HD 3D displays using existing LCD technologies.

5.2.4.1   Pixel Preparation

The proposed Smart Pixel Mapping (SPM) is a multidimensional pixel mapping technique that increases the definitions of 3D resolution by reducing 3D pixel

distance – which is the distance between two intersection points of viewpoint pixels. It fits more 3D pixels per inch using the same 2D LCD technology as its dimensionality defines the 3D pixel distance that makes it scalable and flexible. For instance, increasing the dimensionality reduces 3D pixel distance. Figure 5.17 shows four different dimensionality of smart pixel mapping methods where 3D pixel distance (3D-PD) size is 1/2, 1/3, 1/4 and 1/5 of the pixel size.

Figure 5.17 (i) shows 2Dimensional SPM method that is half the size of 3D pixel distance in space, because one pixel is added between two successive pixels. This is achieved by mapping viewpoint pixels in 2 rows, where row one contains odd viewpoint pixels, and row two contains even viewpoint pixels. This process doubles the definition of 3D resolution with smoother viewing zone transition, compared to the traditional approach.

The 3Dimensional smart pixel mapping method presented in Figure 5.17 (ii) reduces 3D pixel distance from 1 to 1/3 pixel because there are two viewpoint pixels between two successive neighbouring pixels. This is achieved by mapping the viewpoint pixels in 3 rows; where row one and two contain odd/even pixels and row three contains even/odd viewpoint pixels. This triples the definition of 3D resolution with even smoother viewing zone transition compared to the 2D-SPM.

Similarly the 4Dimensional smart pixel mapping method makes the 3D pixel distance one quarter, as it fits 4 viewpoint pixels in the size of a single pixel. It distributes viewpoint pixels in 4 rows as illustrated in Figure 5.17 (iii). The definition of 3D resolution is increased fourfold with this approach.

Moreover, the 5Dimenstaionl SPM further enhances the 3D resolution by refining the 3D pixel distance. In this case, viewpoint pixels are mapped in 5 rows. These smart pixel mapping methods reduce/refine noise to minimum, such as cross-talk, because viewpoint pixels are mapped in such a manner that avoid 3D construction errors; as seen in Figure 5.17, the viewpoint image construction is illustrated with a dotted line. It is worth mentioning that having smaller 3D pixel distance, in other words having more 3D pixels per

inch, makes transition between viewing zones smoother with richer stereo parallax. This is a very important factor in 3D imaging technology.

1	3	5	7	9		
	2	4	6	8		
	1	3	5	7	9	
		2	4	6	8	
		1	3	5	7	9
			2	4	6	8

i – 2Dimensional, 3D Pixel distance: $\frac{1}{2}$

1	4	7	10	13		
	3	6	9	12		
	2	5	8	11		
	1	4	7	10	13	
		3	6	9	12	
		2	5	8	11	

ii – 3Dimensional , 3D distance Pixel: $\frac{1}{3}$

1	5	9	13	17		
	4	8	12	16		
	3	7	11	15		
	2	6	10	14	18	
	1	5	9	13	17	
		4	8	12	16	
		3	7	11	15	
		2	6	10	14	18
		1	5	9	13	17

iii – 4Dimensional, 3D Pixel distance: $\frac{1}{4}$

1	6	11	16	21		
	5	10	15	20		
	4	9	14	19		
	3	8	13	18		
	2	7	12	17	22	
	1	6	11	16	21	
		5	10	15	20	
		4	9	14	19	
		3	8	13	18	
		2	7	12	17	22

iv – 5Dimensional, 3D Pixel distance: $\frac{1}{5}$

Figure 5.17 - Smart pixel mapping method of 2D, 3D, 4D and 5D pixel structure

In fact, the factors remain valid for mapping omnidirectional 3D images. For instance, Figure 5.18 shows 2Dimenstional smart pixel applied on microlens which is traditionally designated for 8 × 8 pixels. It doubles horizontal viewpoint pixels and fits 16 × 4 pixels per lens. The cross-lenticular used to replay the image of 8 × 8 pixels per lens, can be used to replay omnidirectional H3D image of 16 × 4 pixels per lens.
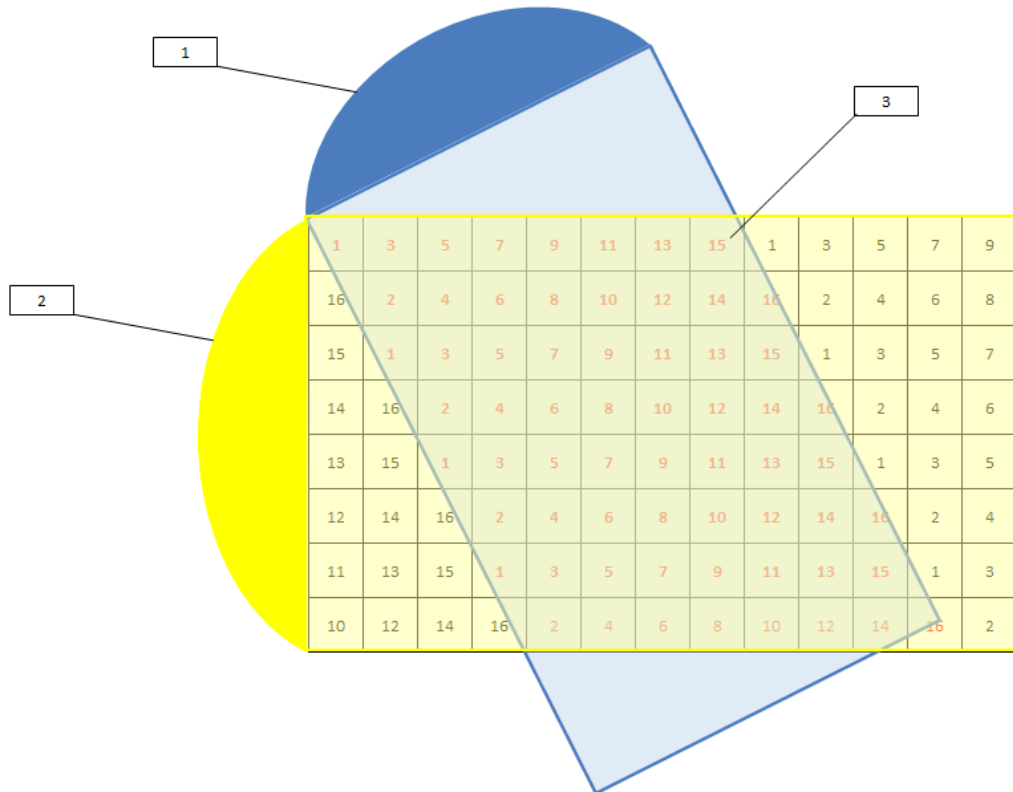
Figure 5.18 - 2Dimensional smart pixel method applied on omnidirectional 3D image: (1) horizontal lenticular sheet, (2) vertical lenticular sheet, (3) viewpoint pixels per lens

Likewise, Figure 5.19 shows 3Dimenstional smart pixel method on microlens designated for 10 × 10 pixels. It triples the horizontal 3D resolution by fitting 30 pixels for the place of 10 pixels.

The vital feature of SPM method is that it offers scalability in 3D pixel resolution. Chiefly, it allows users to achieve a necessary (required) 3D resolution for various 3D application areas such as medical and entertainment.
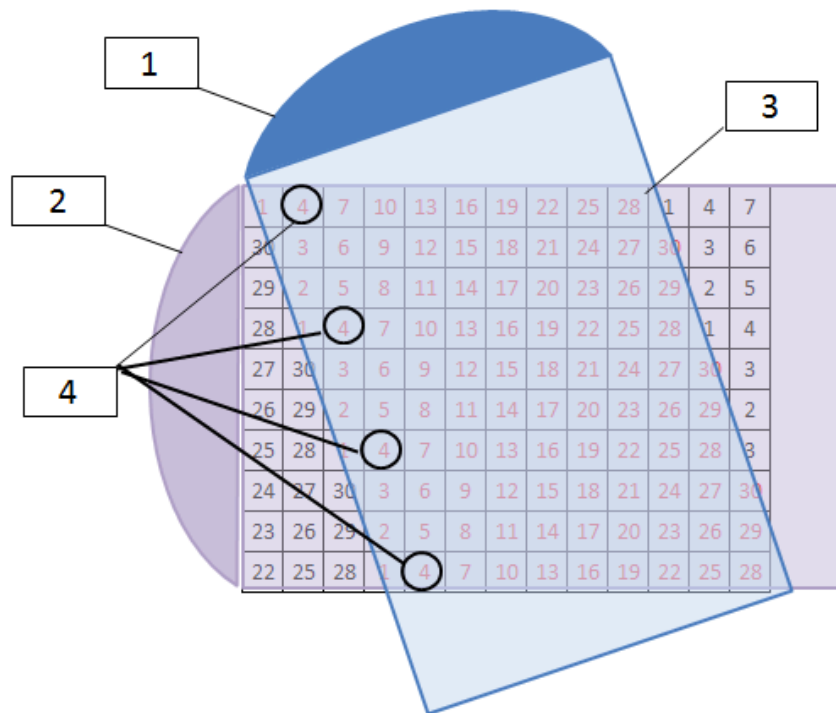
Figure 5.19 - 3Dimenstional smart pixel mapping method for omnidirectional 3D display: (1) horizontal lenticular sheet, (2) vertical lenticular sheet, (3) viewpoint pixels per lens, (4) vertical viewpoint pixels

The SPM contributions and its applicability can be summed up as follows:

- It is demonstrated that it is an ideal solution for designing high definition 3D displays without manufacturing custom pixel sheets.

- It is demonstrated that it is a scalable method of pixel mapping which makes it the perfect solution for any type of 3D displays.

- It can refine the coarse MLAs of 3D displays and make it more attractive 3D displays, as it can fit more viewpoint pixels into a smaller area, compared to the state of the art 3D displays. For instance, mobile devices may require a very fine MLA; this will require extremely small 2D pixel sheet which is currently not available or impossible to manufacture at present. The SPM overcomes this limitation.

- Firstly, it is applicable for both unidirectional and omnidirectional H3D displays and also it allows having different numbers of viewpoint pixels in horizontal and vertical directions, in an omnidirectional square MLA.

- It has the flexibility of achieving a square pixel ratio.

- It offers a natural movement parallax due to its smooth viewpoint transition.
- It improves depth parallax by enhancing the image definition

5.2.4.2 Playback Results

A Smart pixel mapping software tool is developed that applies SPM techniques on classical H3D images. In addition, a prototype 3D iPad [Appendix A] is developed, in order to conduct the experiment, by placing a MLA sheet in front of the iPad retina display. Table 5.3 presents the technical specifications as seen traditionally, the 3D iPad supports 22 viewpoint pixels per lens. Using SPM techniques, it is tested with 66, 88, 110, 132, 154 viewpoint pixels per lens. A rich 3D resolution with depth parallax and comparable viewing angles are achieved.

Table 5.3 – Holoscopic iPad 3D display technical specification

Title	Description
Display type	*Retina display*
2D Resolution	2048
3D Resolution	$93 \times 1536\ pixels$
Horizontal 3D pixel per	$12\ pixels$
Vertical 3D pixels per inch	$264\ pixels$
Lens array size	$93\ microlenses$
Viewpoint pixels per lens	$22\ pixels$
Microlens pitch	$2.11\ mm$
Microlens focal length	$3.16\ mm$

5.2.4.2.1 3Dimensional - SPM

Figure 5.20 shows playback of 3Dimensional-SPM images, which has 66 viewpoint pixels per lens. Therefore, it is triple the 3D resolution. Compared to the classical approach it gives a promising 279 × 512 spatial resolutions at 3D pixel distance size 0.032 mm which is 3 times smaller than the original one, as seen in Table 5.4.

Table 5.4 – 3D resolution comparison of 3Dimensional-SPM vs. Traditional H3D display

Descriptions	Without Pixel Mapping	3Dimensional-SPM
Pixels per lens	22 pixels	$66\ pixels$
Horizontal 3D pixel counts	$\dfrac{2048}{22} = 93\ pixels$	$\dfrac{2048}{22} \times 3 = 279\ pixels$
Vertical 3D pixel counts	$\dfrac{1536}{1} = 1536\ pixels$	$\dfrac{1536}{3} = 512\ pixels$
3D pixel distance	$\dfrac{0.096\ mm}{1}$ $= 0.096\ mm$	$\dfrac{0.096\ mm}{3} = 0.032\ mm$
3D Resolution	$93\ \times 1536\ pixels$	$279\ \times 512\ pixels$
Horizontal 3D pixel per inch	$12\ pixels$	$36\ pixels$
Vertical 3D pixels per inch	$264\ pixels$	$88\ pixels$

3D Resolution: 279 × 512 3D-Pixels
Top-left view

3D Resolution: 279 × 512 3D-Pixels
Top-center view

Figure 5.20 - Playback result of 3Dimensional-SPM pixel mapping

5.2.4.2.2 4Dimensional-SPM

SPM 4Dimensional achieves a 3D resolution of 372 × 384 at 48 3D pixels per inch in horizontal and 66 3D pixels per inch in vertical direction. The playback results are shown in Figure 5.21. It achieves almost a square pixel ratio n:n. There are 88 pixels per lens thus it enhances the 3D resolution four times. It gives a stunning stereo parallax and a smoother motion parallax because it reduces 3D pixel distance to ¼ which is 0.024mm in this configuration. Table 5.5 shows its detailed technical comparison.

Table 5.5 – Comparison of 4Dimensional-SPM approach vs. traditional H3D display

Descriptions	Without pixel mapping	4Dimensional-SPM
pixels per lens	22 pixels	88 $pixel$
Horizontal 3D pixel counts	$\frac{2048}{22} = 93\ pixels$	$\frac{2048}{22} \times 4 = 372\ pixels$
Vertical 3D pixel counts	$\frac{1536}{1} = 1536\ pixels$	$\frac{1536}{4} = 384\ pixels$
3D pixel distance	$\frac{0.096\ mm}{1} = 0.096\ mm$	$\frac{0.096\ mm}{4} = 0.024\ mm$
3D Resolution	$93 \times 1536\ pixels$	$372 \times 384\ pixels$
Horizontal 3D pixel per inch	$12\ pixels$	$48\ pixels$
Vertical 3D pixels per inch	$264\ pixels$	$66\ pixels$

3D Resolution: 372 × 384 3D-Pixels
Top-left view

3D Resolution: 372 × 384 3D-Pixels
Top-center view

Figure 5.21 - Playback result of 4Dimensional-SPM pixel mapping

5.2.4.2.3 5Dimensional-SPM

The 5Dimensional-SPM fits 110 viewpoint pixels per lens that reaches 60 3D pixels per inch by reducing 3D pixel distances to 1/5. Table 5.6 shows the 3D resolution and horizontal/vertical 3D pixels count where it achieves a pixel aspect ratio of 1.514, which is close to TV pixel aspect ratio – 1.333 (4:3). Figure 5.22 shows the playback resulting images which are captured from different angle of the display while the 3D image is being replayed. As 3D pixel distance is refined, crosstalk errors are reduced to minimum, illustrated in

Figure 5.17(iv) by the dot lines. The crosstalk error is introduced when viewpoint pixels are not well separated or differentiated in space.

Table 5.6 - Comparison of SPM-5Dimensional with the classical H3D display

Descriptions	Without pixel mapping	SPM-5Dimensional
pixels per lens	22 pixels	110 $pixels$
Horizontal 3D pixel counts	$\frac{2048}{22} = 93\ pixels$	$\frac{2048}{22} \times 5 = 465\ pixels$
Vertical 3D pixel counts	$\frac{1536}{1} = 1536\ pixels$	$\frac{1536}{5} = 307\ pixels$
3D pixel distance	$\frac{0.096\ mm}{1} = 0.096\ mm$	$\frac{0.096\ mm}{5} = 0.019\ mm$
3D Resolution	$93 \times 1536\ pixels$	$465 \times 307\ pixels$
Horizontal 3D pixel per inch	$12\ pixels$	$60\ pixels$
Vertical 3D pixels per inch	$264\ pixels$	$52\ pixels$

3D Resolution: 465 × 307 3D-Pixels
Top-center view

3D Resolution: 465 × 307 3D-Pixels
Top-left view

Figure 5.22 - Playback result of 5Dimensional-SPM pixel mapping (Demo IMG_0151.MOV)

5.2.4.2.4 6Dimensional-SPM

The SPM-6 Dimensional mapping is applied to 132 viewpoint pixels per lens that attains natural 3D perceptions such as motion and stereo parallax, as shown in Figure 5.23. It reduces the 3D pixel distance from 1 to 1/6 (0.016 mm in this 3D display setup). In essence, it achieves 3D resolution of 558 × 256 where 72 3D-PPI in horizontal direction and 44 3D-PPI in vertical direction. This method enables us to obtain a rectangular pixel aspect ratio of 2.17 which

is suitable for wide-screen displays. Detailed 3D resolution and horizontal/vertical 3D pixels counts are presented in Table 5.7.

Table 5.7 - 3D resolution comparison of 6Dimensional-SPM vs. traditional H3D display

Descriptions	Without Pixel Mapping	6Dimensional-SPM
Pixels per lens	22 pixels	132 *pixels*
Horizontal 3D pixel counts	$\frac{2048}{22} = 93\ pixels$	$\frac{2048}{22} \times 6 = 558\ pixels$
Vertical 3D pixel counts	$\frac{1536}{1} = 1536\ pixels$	$\frac{1536}{6} = 256\ pixels$
3D pixel distance	$\frac{0.096\ mm}{1} = 0.096\ mm$	$\frac{0.096\ mm}{6} = 0.016\ mm$
3D Resolution	$93 \times 1536\ pixels$	$558 \times 256\ pixels$
Horizontal 3D pixel per inch	$12\ pixels$	$72\ pixels$
Vertical 3D pixels per inch	$264\ pixels$	$44\ pixels$

| 3D Resolution: 558 × 256 3D-Pixels
Top-right view | 3D Resolution: 558 × 256 3D-Pixels
Top-center view |

Figure 5.23 - Playback result of 6Dimensional-SPM pixel mapping (Demo IMG_0161.MOV)

5.2.4.2.5 7Dimensional-SPM

The SPM 7Dimensional method is developed to fit 154 viewpoint pixels per lens that enhances the definition of the 3D resolution as well as 3D perception. It brings 3D pixels as close together as 0.013 mm (in the current 3D display setup) to obtain 3D resolution of 651 × 219 at 84 3D-PPI in horizontal direction and 37 3D-PPI in vertical direction; which is 7 times better than the traditional

approach of 93 x 1536 at 12 3D-PPI in horizontal direction and 264 3D-PPI in vertical direction. Its detailed comparison is presented in Table 5.8 and Figure 5.24 shows the replayed 3D scene images.

Table 5.8 - 3D resolution comparison of 7Dimensional- SPM vs. traditional H3D display

Descriptions	Without pixel mapping	7Dimensional-SPM
pixels per lens	22 pixels	154 $pixels$
Horizontal 3D pixel counts	$\frac{2048}{22} = 93\ pixels$	$\frac{2048}{22} \times 7 = 651\ pixels$
Vertical 3D pixel counts	$\frac{1536}{1} = 1536\ pixels$	$\frac{1536}{7} = 219\ pixels$
3D pixel distance	$\frac{0.096\ mm}{1} = 0.096\ mm$	$\frac{0.096\ mm}{7} = 0.013\ mm$
3D Resolution	$93\ \times 1536\ pixels$	$651\ \times 219\ pixels$
Horizontal 3D pixel per inch	$12\ pixels$	$84\ pixels$
Vertical 3D pixels per inch	$264\ pixels$	$37\ pixels$

3D Resolution: 651 × 219 3D-Pixels
Top-center view

3D Resolution: 651 × 219 3D-Pixels
Top-left view

Figure 5.24 - Playback result of 7Dimensional-SPM pixel mapping (Demo IMG_0156.MOV)

5.2.4.3 Summary

All existing pixel mapping techniques trade off horizontal and vertical resolution to improve horizontal 3D resolution and achieve an acceptable pixel aspect ratio but the problem is that they fail to enhance the definition of 3D resolution or in other words, the existing pixel mapping methods does not improve 3D pixels per inch; hence 3D pixels per inch remain unchanged. The

presented novel smart pixel mapping method improves 3D pixels per inch in space which improves the definition of 3D resolution.

The proposed method is the only pixel mapping method to date that advances the definition of 3D resolution i.e. 3D-PPI and also 3D depth is improved by the proposed method because it allows more 3D pixels in space for construction of a 3D scene. It is demonstrated that the proposed SPM is the most scalable pixel mapping to date because it offers a number of benefits listed below:

- Offers adjustable horizontal and vertical 3d resolution
- Offers flexible pixel aspect ratio
- Offers variable 3D pixels per inch
- Most importantly, an ideal approach for enhancing parallax barriers lighting [10]
- Applicable for omnidirectional 3D displays

To sum it up, the SPM is an additive increasing technique that increases the definition of 3D resolution additively as the dimensionality is increased. Table 5.9 shows the variation of the SPM in summary. The lens array was a very coarse "Large" and there were 22 pixels per lens. Table 5.9 is self-explanatory as rows are well labelled and columns are different variations of SPM dimensionality. It illustrates scalability of the proposed algorithm and surely using a correct lens array type and LCD size, an optimum design of HD-3D display can be achieved. In other words, this pixel mapping method can offer the designing of HD autostereoscopic 3D displays with available LCD technologies regardless of lens array technologies (Parallax barriers and lenticular technology).

Table 5.9 - Summary of SPM techniques and illustration of its dimensionality

Descriptions	Without pixel mapping	3Dimensional	4Dimensional	5Dimensional	6Dimensional	7Dimensional
pixels per lens	22 pixels	$66\ pixels$	$88\ pixels$	$110\ pixels$	$132\ pixels$	$154\ pixels$
(H) 3D pixels	$\dfrac{2048}{22}$ $= 93\ pixels$	$\dfrac{2048}{22} \times 3$ $= 279\ pixels$	$\dfrac{2048}{22} \times 4$ $= 372\ pixels$	$\dfrac{2048}{22} \times 5$ $= 465\ pixels$	$\dfrac{2048}{22} \times 6$ $= 558\ pixels$	$\dfrac{2048}{22} \times 7$ $= 651\ pixels$
(V) 3D pixels	$\dfrac{1536}{1}$ $= 1536\ pixels$	$\dfrac{1536}{3}$ $= 512\ Px$	$\dfrac{1536}{4}$ $= 384\ Px$	$\dfrac{1536}{5}$ $= 307Px$	$\dfrac{1536}{6}$ $= 256\ Px$	$\dfrac{1536}{7}$ $= 219\ Px$
3D pixel distance	$\dfrac{0.096\ mm}{1}$ $= 0.096\ mm$	$\dfrac{0.096\ mm}{3}$ $= 0.032\ mm$	$\dfrac{0.096\ mm}{4}$ $= 0.024\ mm$	$\dfrac{0.096\ mm}{5}$ $= 0.019\ mm$	$\dfrac{0.096\ mm}{6}$ $= 0.016\ mm$	$\dfrac{0.096\ mm}{7}$ $= 0.013\ mm$
3D Resolution	$93\ \times 1536\ Px$	$279\ \times 512\ Px$	372 $\times 384\ Px$	465 $\times 307\ Px$	558 $\times 256\ Px$	651 $\times 219\ Px$
(H) 3D-PPI	$12\ pixels$	$36\ pixels$	$48\ pixels$	$60\ pixels$	$72\ pixels$	$84\ pixels$
(V) 3D-PPI	$264\ pixels$	$88\ pixels$	$66\ pixels$	$52\ pixels$	$44\ pixels$	$37\ pixels$

Row terms descriptions:

- **Pixels per lens**: number of pixels under each microlens also known as viewpoint
- (**H) 3D Pixels**: number of 3D pixels in the space horizontally
- **(V) 3D Pixels**: number of 3D pixels in the space vertically
- **3D Pixel Distance:** this is the distance between two 3D pixels in the space – this term also used to define how shallow and rich 3D resolution
- **3D resolution:** this is in pixels that illustrates number of pixels
- **(H) 3D-PPI:** number of 3D pixels per inch in the space horizontally
- **(V) 3D-PPI:** number of 3D pixels per inch in the space vertically

5.2.5 Novel Distributed Smart Pixel Mapping

In this section, a novel Distributed Smart Pixel Mapping (DSPM) technique is proposed. This particular pixel mapping combines SPM and DPM techniques to offer the best pixel mapping solution to date. It spreads viewpoint pixels in both horizontal and vertical directions to gain high definition 3D resolution with the best 3D experience.

The SPM technique has been proposed to boost the definition of 3D resolution, which achieves almost 2D pixel aspect ratio standards e.g. square / wide screen pixel aspect ratio. More importantly in parallax barrier, it enhances 3D lighting from 1 to 1*N where N is the dimensionality of SPM as it reduces dark areas between two pinholes. Viewpoint pixels are mapped in vertical direction; therefore, it allows fitting N times more pixels under the same lens array. It is discussed in details in section 5.2.4.

The DPM maps viewpoint sub-pixels in horizontal direction. This distributes a micro-image into 3 smaller lenses by creating R sub-pixels micro-image, G sub-pixels micro-image, and B sub-pixels micro-image, which are replayed from 3 different lenses. In particular, it reduces the lens size thus dark areas are reduced in parallax barriers. Its detailed information can be found in section 5.2.3.

The proposed DSPM is a hybrid pixel mapping method that takes best of both vertical and horizontal pixel mapping methods to give the optimal 3D experience. Experiments confirm that it outperforms all state of the art pixel mapping methods due to its omnidirectional pixel mapping strategy. Therefore, it is a good candidate for designing any type of HD 3D display based on either parallax barriers or MLA. It is the first pixel mapping technique that allows users to choose or adjust the pixel aspect ratio where the state of the art [1][2][26] pixel mapping techniques fails to do so.

The proposed DSPM method provides the flexibility of 3D pixel distance in space and it achieves 3D pixel distance of $\frac{1}{2}$, $\frac{1}{3}$ and $\frac{1}{4}$ by mapping viewpoint pixels in vertical direction and its RGB sub-pixels in horizontal direction.

5.2.5.1 Pixel Preparation

Figure 5.25 shows how unidirectional H3D image is remapped in different dimensional. Figure 5.25(i) shows a 2Dimensional DSPM method which reduces the distance of 3D pixels to half by adding a pixel vertically between two successive viewpoint pixels in horizontal direction. This particular one doubles the definition of 3D resolution with smoother viewing zone transition, compared to the traditional approach. The viewpoint pixels and sub-pixels

distributions of 3Dimensional DSPM method are presented in Figure 5.25 (ii). It reduces the 3D pixel distance from 1 to $\frac{1}{3}$ by inserting two viewpoint pixels vertically between the successive neighbouring pixels. The viewpoint pixels are mapped in 3 rows where row one and two contain odd/even pixels and row three contain even/odd viewpoint pixels. The sub-pixels of a viewpoint pixel are replayed from 3 lenses shown by the dotted lines. This method triples the definition of 3D resolution with even smoother viewing zone transition compared to the 2D-SPM. Similarly the 4Dimensional and 5Dimensional DSPM methods make the 3D pixel distance even closer to offer a better spatial visual quality as shown in Figure 5.25 (iii)(iv).
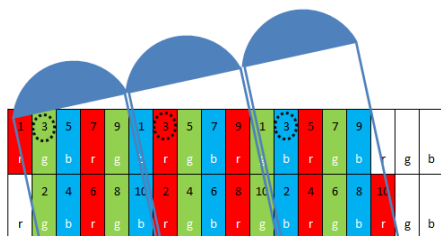
(i) 2D-DSPM, 3D pixel distance: $\frac{1}{2}$
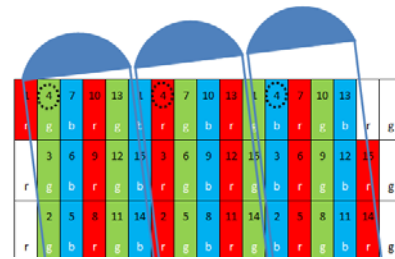
(ii) 3D-DSPM , 3D pixel distance: $\frac{1}{3}$
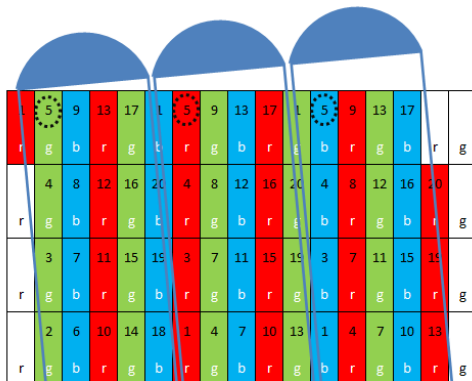
Iii: 4D-DSPM, 3D pixel distance: $\frac{1}{4}$
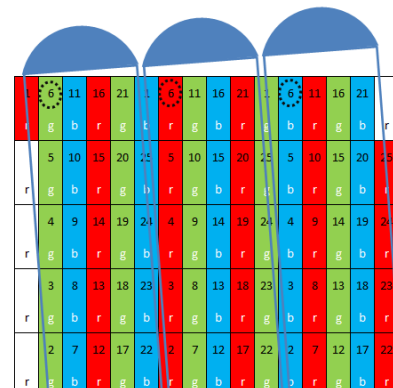
Iv: 5D-DSPM, 3D pixel distance: $\frac{1}{5}$

Figure 5.25 – DSPM method of 2D, 3D, 4D and 5D pixel structure

Figure 5.26 shows omnidirectional H3D image pixel mapping using 2Dimenionsal DSPM method, which doubles 3D resolutions and its 3D definition horizontally. It offers a great flexibility in choosing a pixel aspect ratio as well as 3D resolution. Figure 5.26 shows 2Dimentional one however the other dimensionality i.e. 3Dimenstioanl/4Dimenstional can be applied the same way to achieve the desired 3D resolution and pixel aspect ratio.

This particular pixel mapping improves lighting of parallax barrier technology [10]. Indeed it can be easily developed in parallax based 3D display.
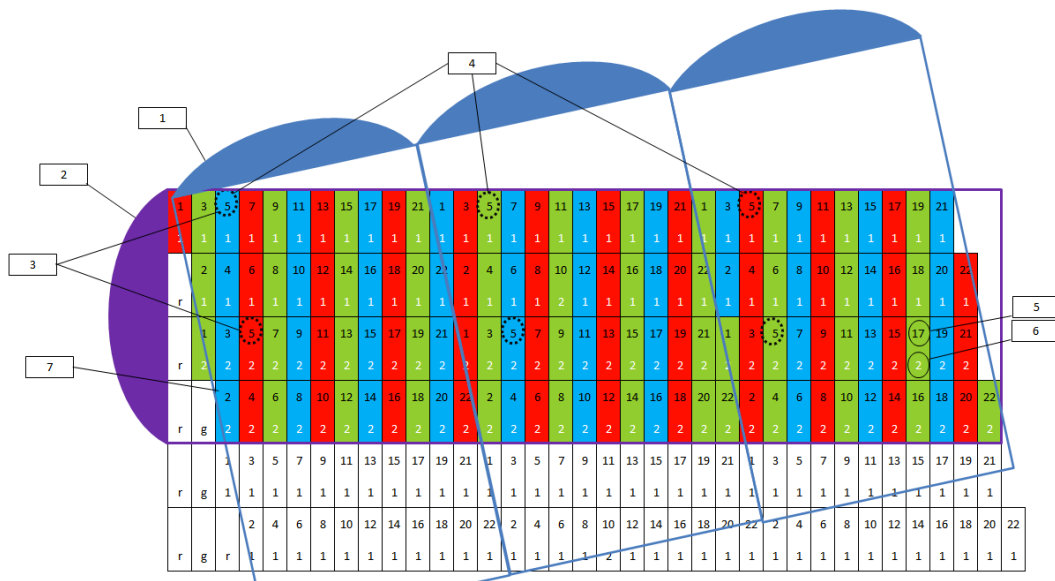
Figure 5.26 - DSPM method for mapping omnidirectional 3D image: (1) horizontal lenticular sheet, (2) vertical lenticular sheet, (3) horizontal viewpoint pixel, (4) construction of a RGB pixel, (5) horizontal viewpoint pixel index, (6) vertical viewpoint pixel index

Table 5.10 illustrates the proposed DSPM method, applied on a 3rd generation iPad. It also shows detailed 3D information at its different dimensionality flavors. In this scenario, the lens array covers 5 sub-pixels (Lens pitch: 480 microns) and the DSPM is applied to fit 10, 15, 20 and 25 pixels per lens. It has managed to gain almost square pixel aspect ratio (1: 0.94), wide screen pixel ratio (2: 0.83) and 3D resolutions of 819 × 768, 1228 × 512, 1638 × 384 and 2048 × 240.

In unidirectional 3D display, the focused is on horizontal resolution where the 3D scene exists and provides movement, and depth parallax. In this experiment, we have managed to achieve 264 3D PPI, which is the display's original 2D PPI. This clearly shows the scalability of the DSPM technique. By choosing the right lens array and the right number of pixels per lens could achieve optimum 3D resolution for any type of 3D displays e.g. for professional and/or home users.

Table 5.10 - The proposed DSMP method with different dimensionality

Descriptions	2D-DSPM	3D-DSPM	4D-DSPM	5D-DSPM
2D Resolution	2048 × RGB × 1536, at 264 PPI			
Microlens pitch	5 physical subpixels			
Pixels per Lens	10	15	20	25
(H) 3D pixels	$\frac{2048 \times 3}{5 \times 3} \times 2$ $= 819$	$\frac{2048 \times 3}{5 \times 3} \times 3$ $= 1228$	$\frac{2048 \times 3}{5 \times 3} \times 4$ $= 1638$	$\frac{2048 \times 3}{5 \times 3} \times 5$ $= 2048$
(H) dots in space	$\frac{2048 \times 3}{5 \times 3} \times 2$ $\times 3 = 2457$	$\frac{2048 \times 3}{5 \times 3} \times 3$ $\times 3 = 3684$	$\frac{2048 \times 3}{5 \times 3} \times 4 \times 3$ $= 4914$	$\frac{2048 \times 3}{5 \times 3} \times 5 \times 3$ $= 6144$
(V) 3D pixels	$\frac{1536}{2} = 768$	$\frac{1536}{3} = 512$	$\frac{1536}{4} = 384$	$\frac{1536}{5} = 240$
(V) dots in space	$\frac{1536}{2} \times 1$ $= 768$	$\frac{1536}{3} \times 1 = 512$	$\frac{1536}{4} \times 1 = 384$	$\frac{1536}{5} \times 1 = 240$
3D pixel distance	$\frac{1}{2}$	$\frac{1}{3}$	$\frac{1}{4}$	$\frac{1}{5}$
(H) 3D-PPI	106 *pixels*	159 *pixels*	212 *pixels*	264 *pixels*
(V) 3D-PPI	132 *pixels*	88 *pixels*	66 *pixels*	52 *pixels*

It is a method which allows achieving various 3D resolutions as well as enhancing the definition of 3D resolution by reducing the distance between two 3D dots in space. Using the same technology (lens array and 2D pixel sheet), the distance between two 3D dots are reduced from 1 to $\frac{1}{2}, \frac{1}{3}, \frac{1}{4}$ *and* $\frac{1}{5}$. This is achieved by fitting 10, 15, 20, and 25 pixels per lens.

5.2.5.2 Playback Results

To prove the theory mentioned above, we have developed a Distributed Smart Pixel Mapping (DSPM) software tool, which applies DSPM technique on H3D images. The experiment of the proposed pixel mapping strategy is conducted on H3D iPad with retina LCD. As shown in Table 5.11, the display has 341 unidirectional lenses. It creates a 3D resolution 341 × 1536 which has unbalanced pixel aspect ratio because there are fewer pixels in the horizontal direction compared to the vertical direction. This issue is resolved by the

proposed method as it reduces the vertical resolution and adds to the horizontal resolution.

Table 5.11 – H3D iPad display technical specification

Title	Description
Display type	*Retina display*
2D Resolution	$2048 \times 1536\ pixels, PPI: 264\ (Pixel\ Pitch\ 0.096\ mm)$
3D Resolution	$341 \times 1536\ pixels$
Horizontal 3D pixel per inch	$44\ pixels$
Vertical 3D pixel per inch (3D-	$264\ pixels$
Lens array	$341\ lenses$
Pixels per lens (PPL)	$6\ pixels$
Microlens pitch	$0.6\ mm$
Microlens focal length	$1.25\ mm$

Traditionally, the H3D iPad supports 6 pixels per lens (PPL). Using DSPM techniques, 25 pixels are fitted under each microlens. The experimental results show HD3D resolution with excellent motion, depth and stereo parallax. In the particular experiment, the 4D-DSPM is applied that fits 25 pixels per lens which enhances definition of horizontal 3D resolutions by 4 times as well as 3D resolution by 3 times. It achieves a 3D resolution of 1365×384 at 176 3D pixels per inch. In addition, it offers a 3D depth and motion parallax. Indeed, the method improves the 3D depth information. The 3D pixel distance is reduced to ¼. More 3D resolution comparison is shown in the able. The experiment playback images are presented in Figure 5.27. The images are captured from various angle of the 3D display to illustrate 3D experience.

In addition, 2Dimenstional DSPM method is implemented on parallax barriers based H3D display to illustrate and prove the point it resolves the lighting issue of parallax barriers. Figure 5.28 shows the playback results of 2Dimenstional DSPM which successfully illustrates that 3D scene quality and lighting are improved tremendously.

Table 5.12 – Comparison of traditional H3D resolutions with the 4D-DSPM 3D resolutions

Descriptions	Without pixel mapping	4D-DSPM Approach
Pixels per lens	6 pixels	$25\ pixels$
Horizontal 3D pixels	$\dfrac{2048}{6} = 341\ pixels$	$\dfrac{2048 \times 3}{6 \times 3} \times 4$ $= 1365\ pixels$
Vertical 3D pixels	$\dfrac{1536}{1} = 1536\ pixels$	$\dfrac{1536}{4} = 384\ pixels$
3D pixel distance	$\dfrac{0.096\ mm}{1} = 0.096\ mm$	$\dfrac{0.096\ mm}{4}$ $= 0.024\ mm$
3D Resolution	$341 \times 1536\ pixels$	$1365 \times 384\ pixels$
Horizontal 3D pixel per inch	$44\ pixels$	$176\ pixels$
Vertical 3D pixel per inch	$264\ pixels$	$66\ pixels$

3D Resolution: 1365 × 384 3D-Pixels
Top-right view

3D Resolution: 1365 × 384 3D-Pixels
Top-left view

Figure 5.27 – Playback resulting images of DSPM method @25PPL

3D Resolution: 1228 × 768 3D Pixels
Top-left view
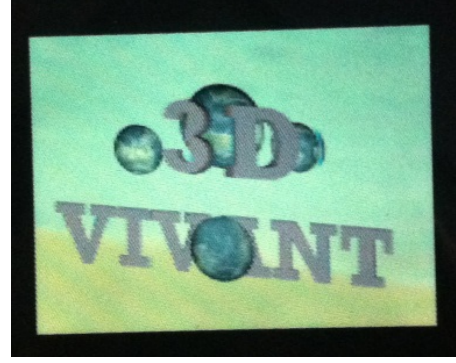
3D Resolution: 1228 × 768 3D Pixels
Top-center view

Figure 5.28 – Playback result of 2D DSPM on Parallax Barriers H3D display @10PPL

2Dimensional smart pixel mapping is implemented in omnidirectional H3D displays using two pieces of off-the-shelf lenticular sheets.

Table 5.13 shows the technical specifications of the display including H3D pixel counts in both horizontal and vertical directions. The experimental result shows promising results shown in Figure 5.30. There is a small cross-talk effect in the playback which is due to mis-alignment of the cross-lenticular lens array and it is manually aligned with accuracy of 30+/-.
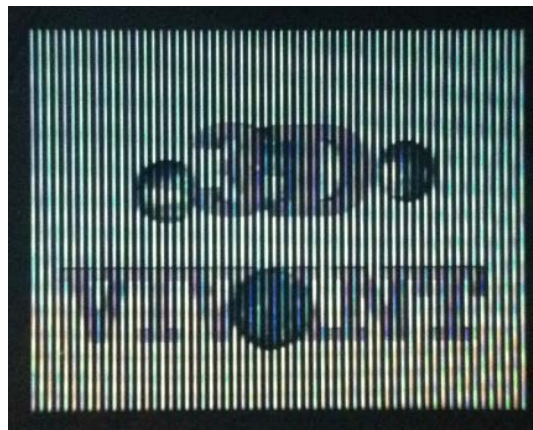
3D Resolution: 204 × 1536 3D Pixels
Without pixel mapping

3D Resolution: 1228 × 768 3D Pixels
With proposed DSPM method

Figure 5.29 - Comparison of distributed smart pixel mapping

Figure 5.29 shows the comparison of the proposed DSPM with the traditional holoscopic pixel mapping technique. There are 10 pixels behind a microlens in both H3D displays and the proposed DSPM fits 10 pixels in the size of 1.66 physical pixel sizes therefore it achieves remarkable spatial resolution by tripling 3D resolution and doubling its visual definition in space.

Table 5.13 - Technical specifications of omnidirectional H3D display

Description	Specification
Liquid Crystal display	*Retina iPad 3*
Pixel pitch	*0.0965(H) × 0.0965 (V) mm*
2D Resolution	*2048 × 1536 pixels*
Pixels per lens	*44 × 11 pixels*
Microlens pitch	*2.12 mm*
Focal length	*2.0 mm*
Horizontal holoscopic resolution	*186 3D-Pixels*
Vertical holoscopic resolution	*70 3D-Pixels*
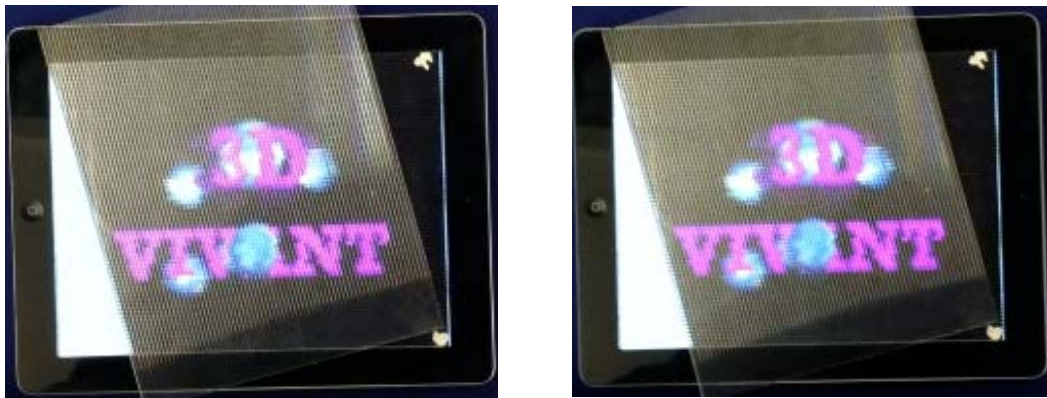
Figure 5.30 - Playback result of omnidirectional 3D display developed using 2Dimensinoal smart pixel mapping

To sum up, the DSPM is an additive increasing technique that increases the definition of 3D resolution additively when the dimensionality is increased. Table 5.10 shows the variation of the DSPM with detailed 3D resolution parameters to prove the concept. The dimensionality must be chosen and defined carefully for application types such as mobile, desktop or wall screens.

5.2.6   Comparison of Pixel Mapping Techniques

Numbers of pixel mapping techniques are proposed that improves and refines holoscopic spatial resolution in space and Table 5.14 shows the comparison of the proposed pixel mapping techniques based on their core features and the optimum pixel mapping is distributed smart pixel mapping which enhances both 3D resolution and visual definition of H3D scene in space.

Table 5.14 - Comparison of pixel mapping techniques

Pixel Mapping	Key feature	Complexity	Applicable
Multiview pixel mapping	Triples the horizontal spatial resolution by trading off vertical and horizontal	Requires de-slanting pre-processing of viewpoint images prior to the pixel mapping: O(d(n))	Applicable to both parallax barriers and lenticular technology
Triangular pixel mapping	Triples the horizontal spatial resolution by trading off vertical and horizontal	O(n) - Does not require any pre-processing	Applicable only to parallax barriers
Distributed pixel mapping	Refines MLA three times smaller by creating R,G,B elemental images and improve quality of H3D scene in space	Does not require any pre-processing: O(n)	Applicable to both parallax barriers and lenticular technology
Smart pixel mapping	Improves (doubles and triples) visual definition of spatial resolution in scalable manor	Requires de-slanting pre-processing of viewpoint images prior to the pixel mapping: O(d(n))	Applicable to both parallax barriers and lenticular technology
Distributed smart pixel mapping	*Improves and refines (doubles and triples) 3Dvisual definition and resolution of spatial resolution in scalable manor in space*	*Requires de-slanting pre-processing of viewpoint images prior to the pixel mapping: O(d(n))*	*Applicable to both parallax barriers and lenticular technology*

5.3   Moiré Free Omnidirectional H3D Display

A 4K omnidirectional H3D display is developed using cross-lenticular technology that offers good 3D depth and movement parallax [Appendix A]. In addition, some work such as crosstalk reduction method [11] has been done to

improve the technology. However the issue with the cross-lenticular is that it generates moiré effect due to pattern matched with the pixel sheet.

This section presents a moiré-free omnidirectional 3D display based on crosstalk-lenticular technology and it has been published in IEEE 3DTV 2013 conference [5]. The moiré effect is furthered studied and the cause is identified. It is proposed slanting one of the lenticular sheets for removing the moiré effect in cross-lenticular approach.

The traditional structure of the cross-lenticular sheet is shown in Figure 5.31 that shows two lenticular sheets are packed together face-to-fact then only the bottom one's focal length (thickness) is used by both lenticular sheets [11]. The setup is the overlapped section of two lenticular sheets form a square aperture microlens which corresponds to elemental images.
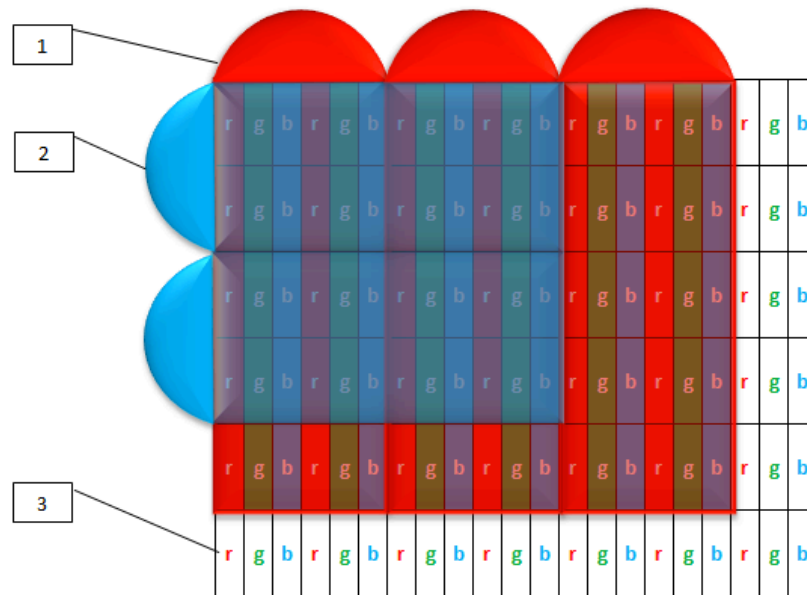
Figure 5.31 - The structure of cross-lenticular sheet: Label description: (1) Horizontal lenticular sheet, (2) vertical lenticular sheet, (3) liquid crystal display pixel sheet [11]

The cross-lenticular approach is investigated using white background image because in white background, the moiré effect is easily noticeable and it is identified that the horizontal lenticular sheet generates the moiré effect as its pattern matches with the liquid crystal display (LCD) pixel sheet shown in Figure 5.32 (a). Also, it is experimented by replayed an omnidirectional H3D image and the moiré effect is persistent as shown in Figure 5.32 (b).
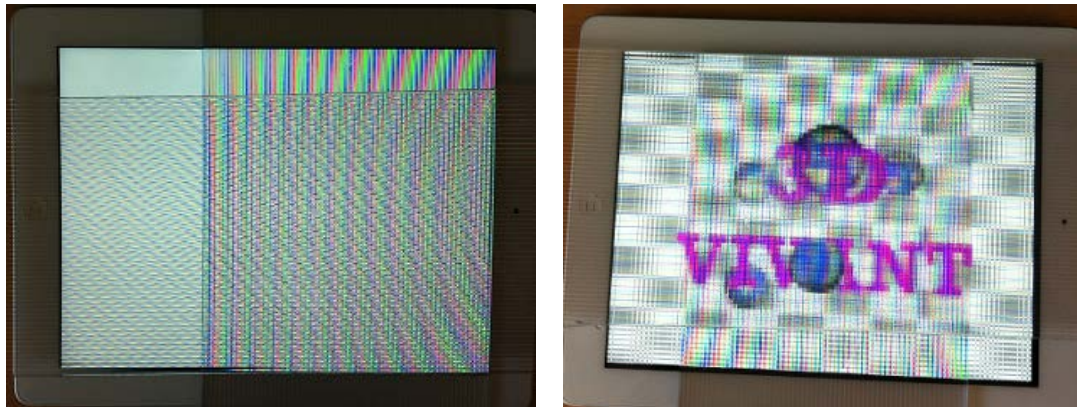
(a) white background   *(b) H3D image playback*

Figure 5.32 - The analysis of moiré effect in cross-lenticular approach without slanting

It is further investigated by slanting cross-lenticular sheet by 18.43° degrees, which removes the moiré effect in the horizontal lenticular sheet but the moiré gets introduced by the vertical lenticular sheet as the LCD pixel sheet's pattern starts matching with the vertical lenticular sheet and the moiré direction is changed too.
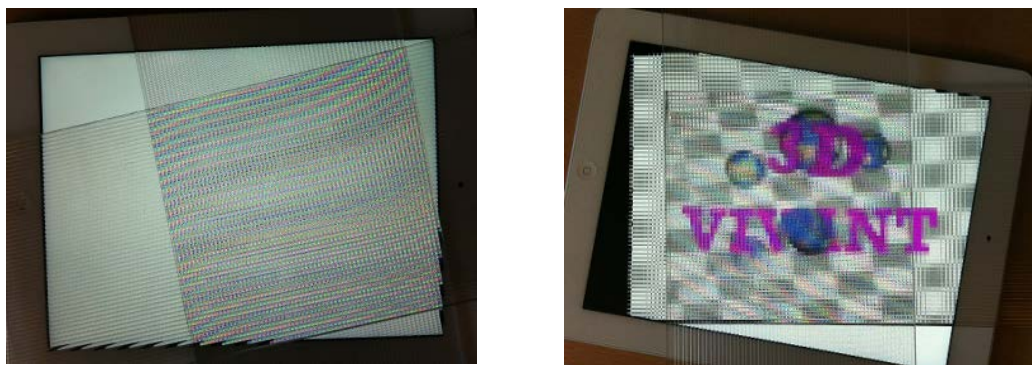
(a) slanted white background   *(b) slanted H3D image playback*

Figure 5.33 - The resulting image of rotated cross-lenticular sheet

A lesson is learnt from the experiment shown in Figure 5.33 and after carrying out many experiments and analysis, we conclude this by proposing not to touch the vertical lenticular sheet, which does not have a moiré effect, instead target the one that generates the moiré effect. Therefore, in the proposed method, which shows in Figure 5.34, rotating the horizontal lenticular sheet by 6.34° degrees removes the moiré effect. The results of the experiment are presented in Figure 5.35.
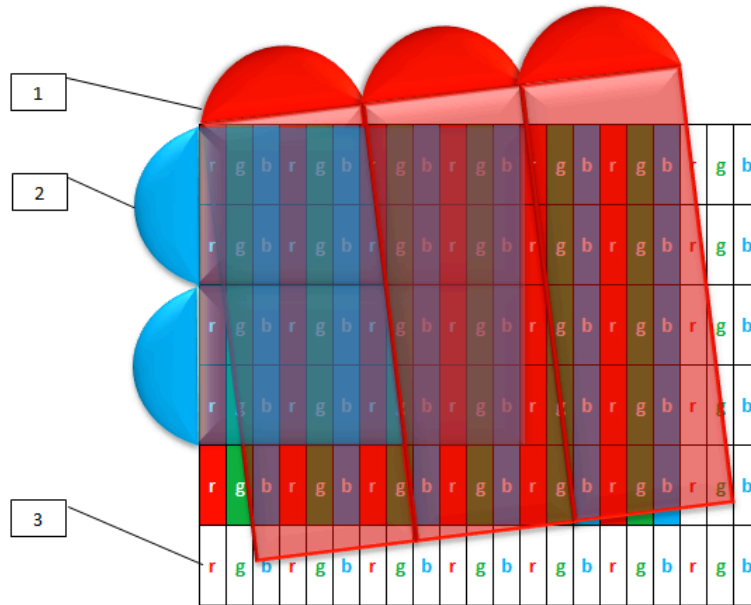
Figure 5.34 - The proposed method of slanting the horizontal lenticular sheet: (1) slanted horizontal lenticular sheet, (2) vertical lenticular sheet, (3) liquid crystal display pixel sheet

(a) white background   *(b) H3D image playback*

Figure 5.35 - The experimental result of proposed approach of slanting only horizontal lenticular sheet

After analysing many experimental results, we propose slanting the horizontal lenticular sheet for removing moiré effect in cross-lenticular approach shown in Figure 5.35 and elemental images of the H3D image requires pre-processing for aligning them with the proposed method.

The display is put together in the lab to test the proposed method and carry out a comparison test with the traditional approach. It is built using an iPad 3 with

two pieces of lenticular sheets and the technical details including pixel pitch size, microlens pitch, and focal length are shown in Table 5.15.

Table 5.15 - The H3D display specification

Description	Specification
Liquid Crystal display	*Retina iPad 3*
Pixel pitch	*0.0965(H) × 0.0965 (V) mm*
2D Resolution	*2048 × 1536 pixels*
Pixels per lens	*22 × 22 pixels*
Microlens pitch	*2.12 mm*
Focal length	*2.0 mm*

5.4   The System Evaluation

The research developments are part of 3DVIVANT project and they have been considered during the validation of user acceptance of 3D VIVANT's project, which focused on all components and prototypes developed in the course of the project [12]. While some components shall be more in the focus of the user acceptance tests, all of them are involved and played an important role for the results of the assessment activities during the process.

The assessment includes pre-view, transport issues, storing, depth of field, playback and many other aspects of TV and video production. The user acceptance validation plan deliverable discusses about the assessment process and outcomes in more details [12].

5.5   Conclusion

This chapter presented novel pixel mapping techniques for unidirectional and omnidirectional H3D displays.   The pixel mapping techniques enhance 3D resolutions and 3D visual definitions (3D pixels per inch) in space.

Multiview pixel mapping methods have been successfully adopted and implemented in both unidirectional and omnidirectional H3D displays that improved spatial resolution and it also improved H3D pixel aspect ratio by trading off horizontal and vertical resolution.

Triangular pixel mapping was proposed that offers distortion-free pixel mapping, which improved spatial resolution and achieved a balanced pixel aspect ratio. It is applicable to both unidirectional and omnidirectional H3D display.

A novel DPM method was proposed that projects R, G and B elemental images from 3 separate microlenses by creating R, G and B colour MLA. It is a new principle for enhancing spatial resolution in space by refining microlens size. In fact, it is compatible with all pixel representation approaches. It was successfully integrated with existing multiview 3D displays.

To date, all the pixel mapping methods improve horizontal 3D resolution by trading horizontal and vertical resolution in fixed manner but they do not enhance the visual definition of 3D resolution in space.   A novel SPM method was proposed to improve 3D definition of the spatial resolution by bringing 3D pixels closer in space. In fact, it is a multi-dimensional pixel mapping method, which offers a scalable 3D pixel mapping solution for advancing the 3D definition with adjustable 3D-PPI.   Most importantly, it is applicable to unidirectional and omnidirectional H3D displays and it is also applicable to enhance lighting issue of parallax barrier technology.

A DSMP method was proposed that incorporates the best features of SPM and DPM to provide the optimum pixel mapping strategy and it obtains square and wide screen pixel aspect ratio in H3D displays by creating multichannel-colour micro-images and spreading viewpoint pixels in multi-directions.   It was

implemented and demonstrated in both unidirectional and omnidirectional H3D displays. The key benefits are as follows:

- Offers adjustable horizontal and vertical 3D resolution
- Offers flexible pixel aspect ratio
- Offers variable 3D pixels per inch
- It is a candidate for enhancing lighting of parallax barrier technology
- Refines coarse lens arrays o lenticular technology
- Applicable to both unidirectional and omnidirectional H3D displays

Manufacturing a large size of spherical/hexagonal lens array is not cost effective and for mass market, we developed a prototype of 4K omnidirectional H3D display using cross-lenticular technology however the main problem with this approach was that stripe cylindrical lenses introduce moiré effect, which was resolved by slanting the horizontal lenticular sheet. The concept was proved by building a moiré free omnidirectional H3D display using cross-lenticular technology. Both real and computer generated H3D images were successfully replayed on the display.

5.6   References

[1] V. Berkel and D. W. Parker, "Autostereoscopic Display Apparatus," U.S. Patent number: 6118584, 2000.

[2] V. Berkel and J. A. Clarke, "Autostereoscopic Display Apparatus," U.S. Patent number: 6064424, 2000.

[3] Alioscopy, "Alioscopy 3D Display Pixel Mapping Principles," Alioscopy, 2013. [Online]. Available: http://www.alioscopy.com/en/principles.php. [Accessed: 01-May-2013].

[4] D. U. Kean, D. J. Montgomery, J. Mather, G. Bourhill, and G. R. Jones, "Parallax barrier and multiple view display," U.S. Patent number: 10/803,2922006.

[5] M.R Swash, A. Aggoun, O. Abdulfatah, B. Li, J. C. Fernández, E. Alazawi and E. Tsekleves, "Moiré-Free Full Parallax Holoscopic 3D Display based on Cross-Lenticular", 3DTV-CON: Vision beyond Depth AECC, Scotland, October 2013

[6] G. Lippmann, 'Epreuves reversibles', Comptes rendus hebdom-adaires des Seances de l'Academie des Sciences 146, 446-451, 1908

[7] G. A. Thomas and R. F. Stevens, "Processing of Images for 3D Display," U.S. Patent number: US6798409B22004, 2004.

[8] Persistence of Vision Pty. Ltd. Persistence of vision raytracer (version 3.6). http://www.povray.org/, 2004.

[9] Y. Zhang, Q. Ji, and W. Zhang, "Multi-View Autostereoscopic 3D Display," International Conference on Optics, Photonics and Energy Engineering, pp. 58–61, 2010.

[10]   W. Mphepo, Y.-P. Huang, and H.-P. D. Shieh, "Enhancing the Brightness of Parallax Barrier Based 3D Flat Panel Mobile Displays Without Compromising Power Consumption," Journal of Display Technology, vol. 6, no. 2, pp. 60–64, Feb. 2010.

[11]   H. Xie, X. Zhao, Y. Yang, J. Bu, Z. Fang, and X. Yuan, "Cross-lenticular lens array for full parallax 3-D display with crosstalk reduction," Science China Technological Sciences, vol. 55, no. 3, pp. 735–742, Dec. 2011.

[12]   N. Pereira, A. Duffy, O. Pidancet, I. Biperis, A. Aggoun, E. Tsekleves, J. Cosmas, J. Steurer, M. Muratori, M. Meier, R. Neudel, Y. Thomas, M. Weitnauer "Deliverable: User Acceptance Validation Plan - Update" 3DVIVANT, 2013

6   **Chapter Six – Conclusions and Future Work**

This chapter presents the conclusions of the PhD research including the potential future work.

6.1 Conclusions

This thesis has three core chapters, which are holoscopic 3D camera technology, holoscopic 3D image processing and holoscopic 3D display technology.

The research aims to investigate holoscopic 3D imaging and display technology. Holoscopic 3D (H3D) imaging technology is the candidate for future 3D digital imaging technology due to its ability e.g. it offers a complete solution for immersive 3D user experience in both capturing and display level.

S3D technology is as simple as viewing right and left images in a specific way where the observer sees the left-eye image with the left eye and sees right-eye image with the right eye by wearing special glasses. It can only offer stereo parallax and it also has other limitations such as unnatural image colour, eye fatigue, and motion sickness. On the other hand, autostereoscopic 3D technology pursues natural 3D user experience by enabling observers to perceive 3D effects with naked eyes. It has numerous concepts such as holographic, volumetric, compressive, multiview and holoscopic.

Holographic and volumetric 3D technologies offer true 3D imaging as 3D objects constructed in space in a supervised environment. However, they have been costly to manufacture for mass market.

Compressive display was first proposed by MIT in 2010. It simulates tomographic technique to construct 3D scene with layers of LCDs. It is targeting to resolve data size and processing challenges of autostereoscopic 3D imaging technology. Multiple different compressive displays have been prototyped. However, the results were not impressive. It is not a true 3D imaging technique as it uses flat 2D images to form a 3D scene "tomographic technique" and more layers of LCDs are required to construct a 3D scene with acceptable resolution; it however, is computationally complex.

Multiview 3D technology mimics human eye technique so, it requires observer to stand in particular place to perceive 3D effects and it suffers from eye fatigue, motion sickness and viewing distance range. The only promising perspective of

this technology is there has been an easy transition for parsing 2D content to multiview 3D with very limited 3D effects.

H3D imaging technology "Integral imaging" is a true 3D imaging technique that mimics fly's eye technique for constructing 3D in space. It offers side-effect free 3D experience such as 3D depth and motion parallax in either continuous unidirectional or omnidirectional parallax depending on the choice of MLA. Due to its natural 3D effects, it has high potential for one of the future 3D imaging technology. In addition, it changes the way images are captured and re-processed i.e. it offers digital refocusing for better post production work and H3D images can be reformatted for stereoscopic and multiview 3D image format.

H3D computer graphics rendering remains a challenge due to its MLA complexity, which consists of perspective microlenses. BBC has proposed a new holoscopic rendering technique based on orthographic projections, which simplified and improved the rendering performance. However, the rendering still remains multi-steps and a great challenge for real-time interactive application.

The distinctive advantage is that H3D imaging offers scalable and flexible solution. It can be used to build unidirectional and omnidirectional H3D display / camera. Presently, there have been some limitations due to existing 2D technology i.e. lens array and LCD to build a HD equivalent H3D display and also the omnidirectional lens array offers the equal ratio 1:1 depth so the movement parallax in both horizontal and vertical directions. Realistically, more 3D parallax effects are required horizontally than vertically as observers tends to move horizontally.

In holoscopic 3D camera chapter, omnidirectional H3D computer graphics rendering techniques were proposed that enables virtual content creators to render H3D images from a 3D model in a rather simpler approach. In addition, we proposed novel smart microlens architecture for H3D camera with smart pixel mapping for doubling spatial resolution of H3D camera.

Omnidirectional H3D image rendering method has been simplified from hundreds to tens rendering steps using 2-dimensional array of orthographic cameras. For instance in the proposed method, number of views e.g. 8 or 8 × 8 views are rendered with orthographic projection cameras instead of rendering hundreds of micro images with perspective pinhole cameras. The playback result illustrated a remarkable depth and motion parallax.

In addition, we proposed a new method for rendering a H3D image in a single step by constructing a virtual lens array in virtual world and rendering it with orthographic camera which acts like a CCD. A microlens is virtually engraved using CSG and index of refraction feature of the tracing software. The single stage rendering method simplifies the process of 3D computer graphics generation as well as improving the performance impressively. This particular approach truly simulates the single aperture 3D camera technique.

Smart microlens architecture was proposed for doubling spatial resolution of H3D image resolution of H3D camera. In this approach, 3D images are recorded through a slanted MLA as the slanted MLA creates hexagonal oriented pixel structure. A smart pixel mapping method is then applied to remap and to create viewpoint pixels. It doubles the spatial resolutions and visual definitions by trading-off horizontal and vertical image in elemental level. In fact, it enhances 3D pixels per inch in space. It also resolves unbalanced pixel ratio of cylindrical lens array. The concept has been demonstrated by replaying the images on the H3D display and processing by refocusing algorithm.

The holoscopic 3D image processing chapter presented pre-processing of H3D images including H3D image stitching and H3D image conversion algorithms.

The camera's lens array introduces dark borders in H3D images. If such noise is not corrected, it adds black moiré in constructed H3D scene. As a result, microlens array dark borders correction algorithm was proposed that uses the MLA as a reference point for detecting and removing dark borders from the H3D image. It is a self-calibrated and effortless solution to correct dark borders of H3D images. The experimental results were promising as the dark borders were corrected without effecting visual data of the H3D image. The algorithm is

computationally very efficient so it makes a good candidate to be implemented on-camera for real time border correction in video recording.

A Barrel correction algorithm was presented that offers effortless calibration and mountable solution to any 3D camera because it takes advantages of MLA for generating calibration grid that is later used for correcting barrel distortions in H3D images. It was successfully demonstrated using the H3D camera developed at Brunel University.

H3D images stitching algorithm was presented that widens overall viewing angle of the H3D camera because the current generation of H3D cameras trade-off a great deal of sensor and 3D image resolution in order to obtain information on the angular directions of the incoming light rays with limited aperture. It was successfully demonstrated in the H3D camera developed by 3DVIVANT team at Brunel University and the resulting 3D image proved H3D images were stitched together at micro-image level using MLA information and grid.

A 3D image conversion algorithm was proposed that reformats a H3D image for autostereoscopic multiview 3D displays. The experiment has been conducted on two state of the art multiview 3D displays namely Alioscopy and Philips. The algorithm converts a H3D image to a 3D image supported by multiview 3D displays. It has been done by developing virtual H3D cameras to render a holoscopic image with correct pixels per lens and lens pitch for the displays. Also the display pixel mapping methods have been implemented that remaps holoscopic pixels into multiview pixel presentation supported by the displays.

A medical image visualisation system based on H3D imaging is assembled that enables to visualise CT scan "tomographic data" on H3D display. The experiment was conducted on real CT scan data provided by King's College Hospital and a promising playback result was achieved.

Development of dynamic hyperlinker is present that facilitates interactive holoscopic video content search and retrieval. The proposed approach offers metadata engineering and synchronisation for creating hypervideos. The system has off-line 3D operators such as centric-view extractor, depth map

extractor, object segmentation, content based search and metadata engineering & synchronisation. The system advances user interaction. Furthermore, it enhances 3D data visualisation and retrieval for content providers such as broadcasters as it allows advanced bookmarking facilities.

The holoscopic 3D display technology chapter presented pixel mapping techniques for enhancing spatial resolutions and visual definition of both unidirectional and omnidirectional H3D displays.

Multiview pixel mapping methods have been successfully adopted and implemented in H3D displays that improved the 3D resolutions. It also improved pixel aspect ratio by trading-off horizontal and vertical resolutions.

Triangular pixel mapping was proposed that improves 3D resolutions of H3D display without any distortions and it can be implemented using traditional LCDs. It is designated for parallax barrier technology, which does not need to be slanted.

Distributed pixel mapping was proposed that improves quality of constructed 3D scene in space by creating sub-elemental images and projecting them from separate lenses. It is a novel approach for enhancing quality of H3D scene. In addition, it is compatible with all other pixel mapping techniques as it has been successfully integrated with Alioscopy autostereoscopic 3D display.

Smart pixel mapping was proposed for improving the visual definition of spatial resolutions i.e. it improves 3D-PPI in space. It is a multi-dimensional pixel mapping method which offers scalable and flexible solution for advancing 3D depth and motion parallax with adjustable 3D-PPI. It is a candidate for increasing lighting of parallax barrier technology.

Distributed smart pixel mapping is hybrid of DSP and SPM that incorporates the best features of both methods to provide optimum pixel mapping strategy. Also, it is flexible enough to obtain square and wide screen pixel aspect ratio in 3D displays.

Last but not least, a slanting approach was proposed for eliminating moiré distortions of cross-lenticular technology.

6.2   Future work

- Built a H3D display with custom engraved/cut microlens array using 4K LCD with distributed smart pixel mapping.

- Build a new camera with flexibility slanting ring which can be adjusted according output result requirement i.e. shooting for refocusing, 3D content generation, and 3D depth measurement.

- Implement the H3D image stitching algorithm on the camera that facilitates real-time stitching.

- Improve the functionality of dynamic hyperlinker i.e. allow users to create semi-automatically bounding-box creation, and including interfacing of all post-processing components.

- Extend the 3D content descriptive protocol for 3D low-level features and integrate the protocol with MPEG7.

- Apply omnidirectional pixel mapping on omnidirectional parallax barriers 3D display with smart pixel mapping as the pixel mapping improves back lighting.

- Perform like-to-like comparison of pixel mapping methods in terms of 3D effects, cross-talk errors, and viewing zone to identify optimum pixel mapping methods for different applications.

- Develop a H3D camera SDK which enables users to visualise the camera in holoscopic, multiview or multiview 3D displays in real-time.

- Develop a H3D camera plugin for 3Ds MAX based on the single stage rendering technique to facilitate omnidirectional 3D content generation.

- Enhance pre-processing of H3D image to recreate lost viewpoint pixels caused by barrel distortion.

- Assemble an omnidirectional H3D display based on parallax barriers and lenticular technology to achieve the best possible 3D effects.

- Explore compression algorithms for H3D content.

Appendix A.

Holoscopic 3D Displays

This appendix presents development works during the completion of the PhD research that includes holoscopic 3D display designs with its pixel mapping technique. The layout of the appendix is as follows: Retina Holoscopic 3D iPad, Flicker-free holoscopic 3D Display, Switchable Content Adaptive Holoscopic 3D Display, Portable Full Parallax Holoscopic 3D Field Display, Cross-Lenticular Full Parallax 4K Holoscopic 3D Display, Flicker-free Full Parallax Holoscopic 3D Display, Augmented Reality Holoscopic 3D Display and Pixel Mapping Techniques.

A.I   Retina Holoscopic 3D iPad

The 9.7 inch retina holoscopic 3D iPad is built based on lenticular technology that offers unidirectional motion parallax with good 3D depth at acceptable 3D resolutions. The experiment is carried out using two different microlens arrays (MLA) e.g. coarse MLA with large lens pitch and refine MLA with very small lens pitch. The MLAs produces two different resolution and 3D effect results. For instance, a smaller microlens array produces rich 3D resolutions compare to a larger microlens array using the same liquid crystal display (LCD). Such experiment is important to identify the user domains and user experiences.

A.I.a   Pixel Mapping

Pixel mapping is a way of structuring viewpoint pixels to enhance 3D resolutions as well as achieving standard 2D like pixel aspect ratio which means to balance the horizontal and vertical 3D resolutions. In this prototype, two variation of smart pixel mapping are implemented that are using coarse and fine microlens array because it is important to identify and validate the right size lens array and acceptable 3D resolution for different applications.

The implemented 3Dimentiaonal and 4Dimensional smart pixel mapping (SPM) are discussed in chapter 4. They are applied to enhance the horizontal resolution by trailing the vertical resolution which is an acceptable 3D pixel aspect ratio.

The 4Dimentional SPM achieves 25-digital number of pixels per lens "25PPL", whereas in traditional approach it shields 6.25 pixels per lens. In particular, this pixel mapping is applied to achieve a good depth parallax because it's a single user portal device; therefore the applicability of motion parallax is less important compare to depth parallax. Indeed, it achieves a stunning sharp 3D resolution even in close-by distance because, normally when one looks at a digital image from close-by distance there is high chance of noticing pixel dots; but in this case, there are enough 3D pixels in the space to construct a HD quality 3D scene.

In addition, a coarse lens array is experimented with that has 66 pixels per lens. This is achieved by using 3Dimentaionl SPM whereas the traditional approach

supports 22 pixels per lens. A rich motion and depth parallax are accomplished, however, the lens array is rather coarse for such personal tablet applications because for mobile and singlet device, depth parallax is important than motion parallax due to viewer's immobility. As a result, a finer lens array is recommended with good depth parallax which also enhances visual richness as fewer pixels per lens, therefore, the 3D scene gets constructed with 3D pixels in the space.

A.I.b   Holoscopic 3D Image Preparation and Rendering

Holoscopic 3D imaging also known as integral imaging is discovered by Lippmann's approach [6]. A H3D camera model is developed using orthographic projection cameras [7]. Detailed discussions on 3D computer graphics generation is reported in [21][7]. The concept of building a holoscopic 3D camera based on orthographic projections in computer graphics is patented by BBC [7]. In this setup, the holoscopic 3D camera is built using multiple orthographic projection type cameras which renders orthographic viewpoint images in POV-Ray [8] and then the viewpoint images are interlaced to form a single holoscopic 3D image.

The MLA presented in Table A.1 is used in the first experiment, 25 orthographic viewpoint images are rendered with resolution of 327 × 384 pixels shown in Equation A.1. They are interlaced to form a H3D image to which the pixel mapping algorithm is applied to create a single pixel mapped H3D image with resolution of 2048 × 1536 as shown in Equation A.2.

Equation A.1 - Rendering viewpoint resolutions for retina Holoscopic iPad 3D @25PPL

(a) **viewpoint Horizental Resolutions** $= \frac{2048 \; LCD \; Resolution}{25 \; PPL} \times 4 \; (\textbf{pixel mapping}) =$ **327 pixels**

(b) **viewpoint Vertical Resolutions** $= \frac{1536 \; LCD \; Resolution}{4 \; (pixel \; mapping)} =$ **384 pixels**

Equation A.2 - calculating 4D SPM H3D image resolution for retina Holoscopic iPad 3D @25PPL

(a) **Horizontal Resolutions** $= \frac{327 \; Viewpoint \; (H) \; Resolution \times 25 PPL}{4 \; (4D \; pixel \; mapping)} =$ **2048 pixels**

(b) **Vertical Resolutions** $=$
   $384 \; Viewpoint \; (H) \; Resolution \; \times 4 \; (4D \; pixel \; mapping) =$ **1536 pixels**

The MLA shown in Table A.2 is considered during rending H3D image for the second experiment, 3D SPM is implemented therefore the viewpoint resolution (H)/ (V) is multiplied / divided by 3. As there are 66 pixels per lens, 66 orthographic viewpoint images are rendered with resolution of 93 × 512 pixels which is calculate using the same formula illustrated in Equation A.1. They are interlaced to form a H3D image on which the pixel mapping algorithm is applied to create a pixel mapped H3D image with resolution of 2048 × 1536.

Table A.1. Holoscopic iPad 3D with 4Dimentional smart pixel mapping with Rich 3D Resolution

Title	Description
Display type	*Retina Liquid crystal display*
2D Resolution	2048
Viewpoint pixels per lens	25 *pixels*
Microlens pitch	0.6 *mm*
Microlens focal length	2 *mm*
Pixel Mapping	*4Dimentional Smart Pixel Mapping*

Table A.2. Holoscopic iPad 3D with 3Dimmentional smart pixel mapping

Title	Description
Display type	Retina Liquid crystal display
2D Resolution	2048
Viewpoint pixels per lens	66 pixels
Microlens pitch	2.12 mm
Microlens focal length	3 mm
Pixel Mapping	3Dimentaional Smart Pixel Mapping

A.I.c   Playback Result

The prototype of retina holoscopic iPad 3D is developed using two different microlens arrays of 44PPL and 25PPL. Figure A.1 shows the playback result of the lens array @25PPL, as seen in the figure, it has a rich depth parallax with HD 3D resolutions of 1310(H) × 382(V) which is achieved using 4D SPM. This is more appealing to tablet users than the other one which has 44PPL as shown in Figure A.2, even though this coarse lens array gives better motion parallax. But the main problem is the lens coarseness reduces the slickness of the device and

today mobile/tablet devices have become more of gadgets. In summary, a fine lens array shall be used for tablet and mobile devices because the finer lens array gives rich HD 3D resolution with good depth parallax which are the expected by users as motion parallax is not really demanded due to viewers stationary position.

(i)	(ii)	
		(iii)
(iv)	(v)	
		(vi)
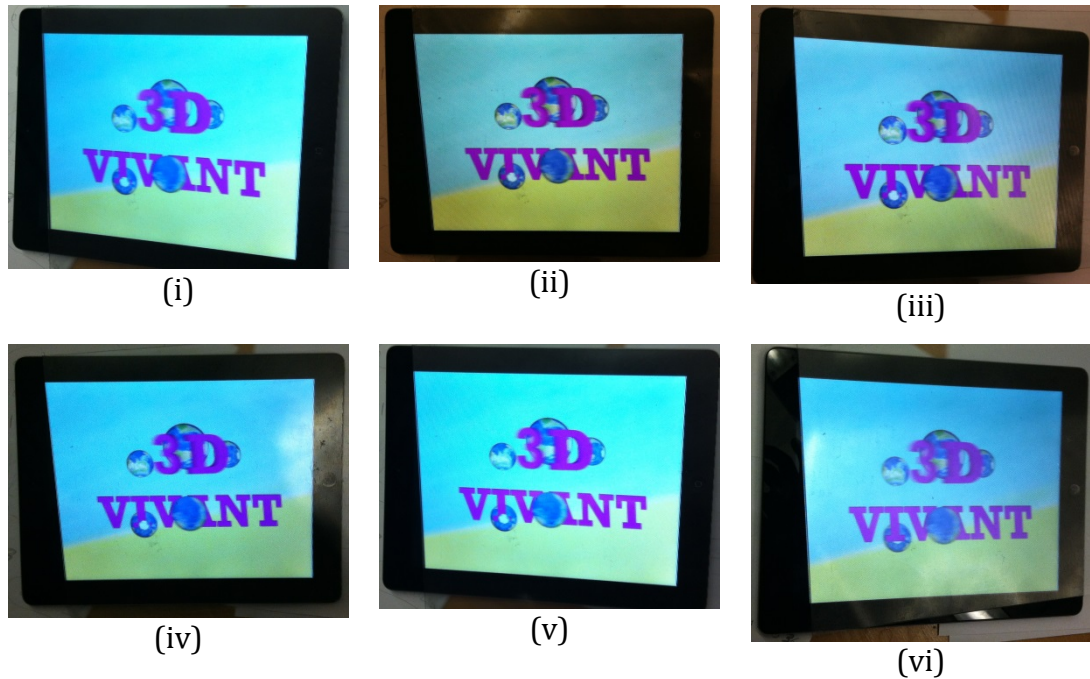
Figure A.1 – Retina holoscopic iPad 3D playback result @25PPL

(i)	(ii)	(iii)	(iv)
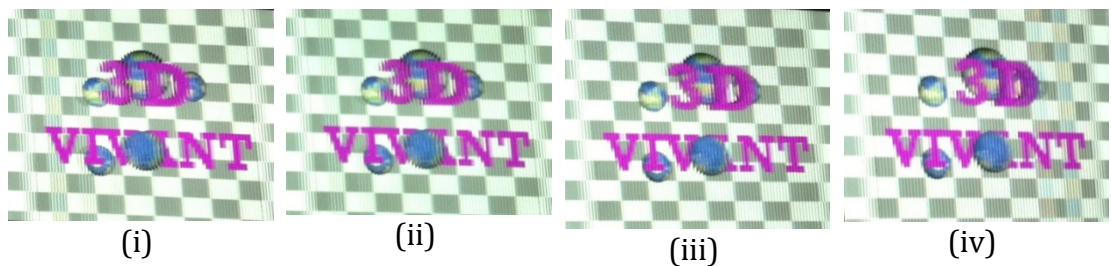
Figure A.2 - Retina holoscopic iPad 3D playback result @66PPL

A.II   Flicker-free Holoscopic 3D Display

One of the main challenges in 3D display technology is viewing angel which is the angle α, the user can move back and forward before changing the viewing zone which causes flickering. All state of art 3D displays have 30 – 40∼ degrees viewing zone in which case there are multiple of the same scene repeated "viewing zones" which is unrealistic compare to the real world. In this section, a pinhole based Holoscopic 3D display is proposed that offers a single viewing

zone as shown in Figure A.3 that viewers perceive a different 3D scene from different angles in horizontal direction.
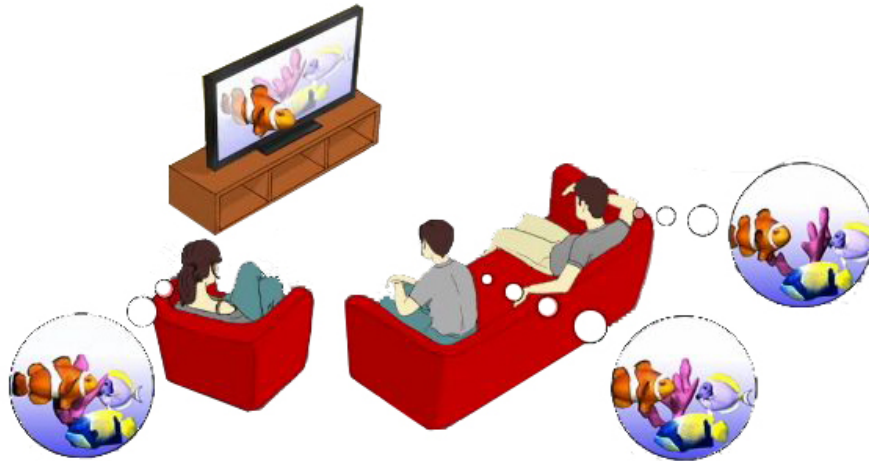
Figure A.3 – Flicker-free holoscopic 3D display offers a single viewing zone [35]

A unidirectional pinhole mask is introduced to holoscopic imaging that enables us to propagate viewpoint rays/pixels efficiently resulting in reduced crosstalk errors. Thus it optically enhances a 3D scene construction because pinhole masks simply works like a micro-projector with a LCD pixel sheet. Figure A.4 illustrates the structure of the display where (a) shows the layers top-to-bottom; (b) is the side-view of the (a).

Backlight Unit (BLU)

Pinhole Mask (PM)

Spacer Sheet (SS)

LCD Pixel Sheet

(a)

B L U   P M   S S   L C D

(b)
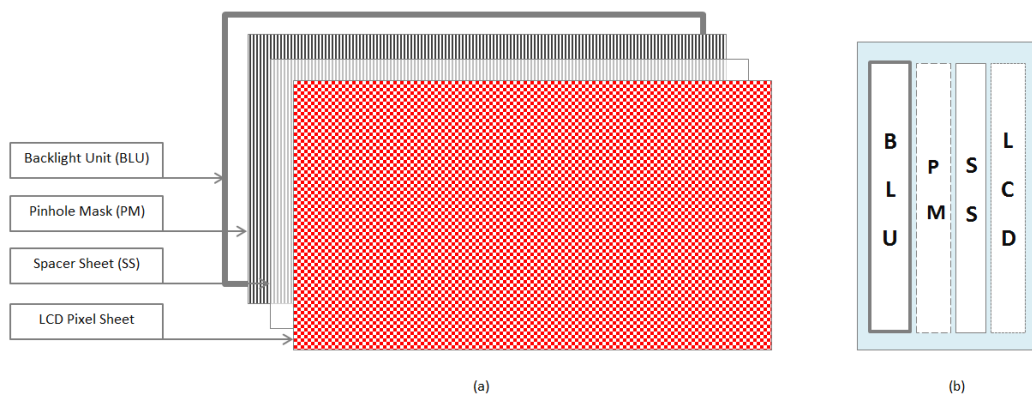
Figure A.4 - Structure of the proposed pinhole based Holoscopic 3D Display

The proposed display has 4 components: backlight unit (BLU), pinhole mask (PM), spacer sheet (SS) and Liquid crystal display (LCD) pixel sheet.

Traditionally the lens array / pinhole mask are placed in the front of the LCD pixel sheet however in this configure, the pinhole mask is placed behind the LCD pixel sheet because it enhances the lighting.   There is a spacer between the pinhole mask and the LCD pixel sheet which enables to project orthographic viewpoint pixels to different angles to construct a true 3D scene in the space with good depth parallax.

The pinhole mask is printed with a specific size where the pinhole size is 294 microns which is equal to a RGB dot pixel pitch of the LCD pixel sheet at resolution 1280 × 1027 pixels.   The display has 3D resolutions of 116 × 1024 pixels as there are 11 pixels per pinhole where there are 1280 ÷ 11 = 116 pinholes. The technical specification is presented in

Table A.3 . The 3D resolution pixel aspect ratio is not one of the standards e.g. square or wide screen which is resolved later by applying pixel mapping techniques in this chapter and the focus is achieving reasonable view angle.

Table A.3- The pinhole based Holoscopic 3D display technical specification

Title	Description
Display type	*Liquid crystal display*
2D Resolution	1280
3D Resolution	$116 \times 1024\ pixels$
Lens array size	$116\ microlenses$
Viewpoint pixels per lens	$11\ pixels$
Microlens pitch	$3.234\ mm$
Microlens focal length	$1.5\ mm$

A.II.a   Hardware and Assembling the Display

The pinhole based holoscopic 3D display prototype is constructed using an off the shift 1208 × 1024 MultiSync LCD1970 60 Hz LCD panel as shown in Figure A.5 (a-l). The LCD panel has a pixel pitch of 294 µm and it is put together back-to-back with a pinhole mask by adding a spacer sheet of 1.5 mm in between them.   The pinhole mask is manual-aligned with the LCD to project 11 orthographic viewpoint images to construct unidirectional 3D scene in the

space. The prototype 3D display supports a single field of view; a view sees correct imagery when moving within ~70° angle.
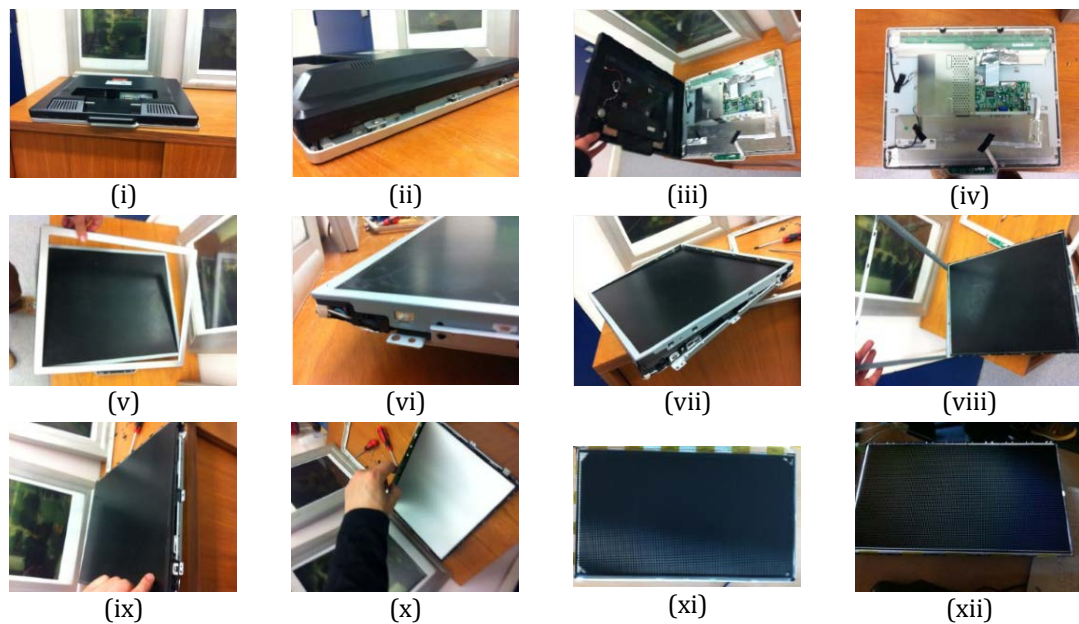
Figure A.5 - Assembling the display for building a Holoscopic 3D Display.

The rear Backlight unit layer is unmodified. It typically has 250 cd/m² white luminance with 550:1 contrast ratio. Its brightness intensity is not strong enough as the parallax barriers introduces darkness as a result, the backlight is further enhance to produce ~1100 cd/m² by adding two LED strips.

As shown in Figure A.5 (i-xii), the steps are: open the monitor and remove the cover with care to avoid damaging the hardware cables; after stripping off the front and back cover, remove the LCD holder metal cover; now unfold the LCD from backlight and add the pinhole mask with spacer sheet and align the pinhole mask with the LCD if these are not aligned correctly, the 3D scene will contain ghost and crosstalk errors. Furthermore make sure the pixel sheet is not touched because finger print damages the liquid crystal display and the LCD has to be handle with care as the data-bus gets broken very easily.

A.II.b   Backlight Brightness Enhancement

The display has a built-in backlight unit which has the brightness intensity of 250 cd/m². This is not sufficient enough for projecting a light field image data (3D image) thus the backlight unit is further enhanced by adding two LED

stripes, which are simply attached to the top and bottom of the backlight box as shown in Figure A.6.

(i) (ii) (iii)

(iv) (v) (vi)
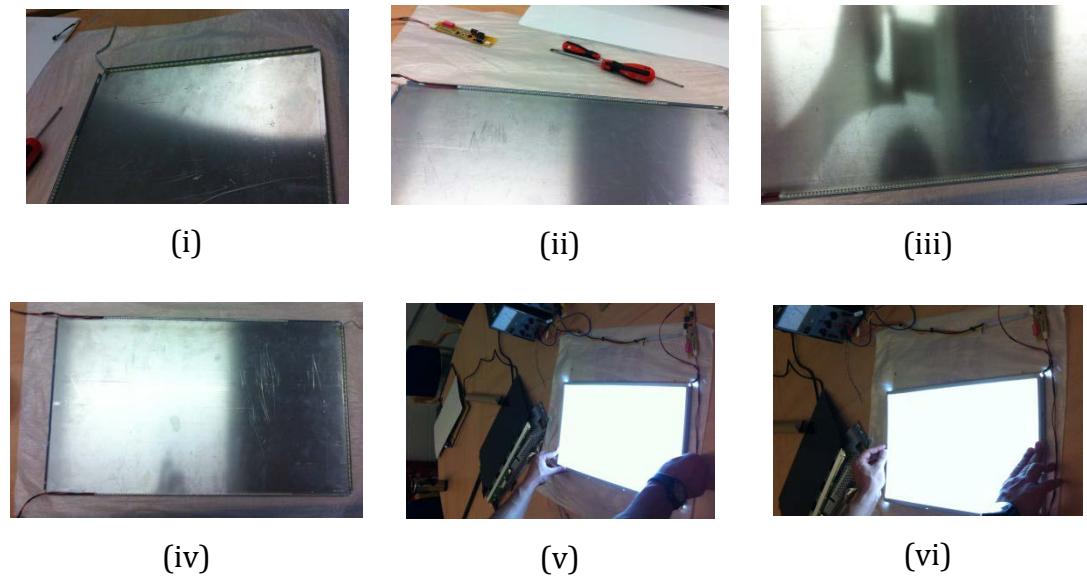
Figure A.6 – Steps of adding two strings of LEDs to a PC Monitor to increase the monitor backlight

The backlight unit is removed from the display and its brightness intensity is measured before measuring the improved backlight brightness. As shown in Figure A.7, the backlight brightness is improved and it reaches 1150 cd/m² (fc). A digital luminance meter is used to carry out the experiment.

(i) Original backlight unit: 256 fc   (ii) Improved:1156 fc
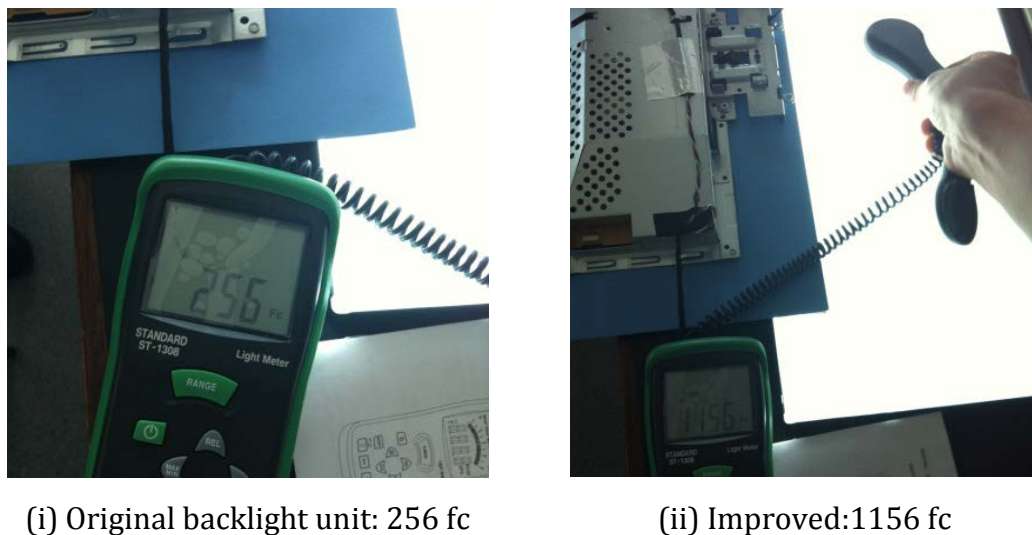
Figure A.7 - comparison of the original backlight brightness with the improved backlight brightness

A.II.c   Mask Alignment Technique

One of the challenges while designing a prototype 3D display is aligning the pinhole mask with the LCD pixel sheet. It needs to be ensured that these are aligned in parallel to keep noises to minimum. Almost 50% of the whole assembling time is spent on the alignment, therefore, in here a single pixel alignment technique is proposed to speed up the alignment process while achieve acceptable alignment.
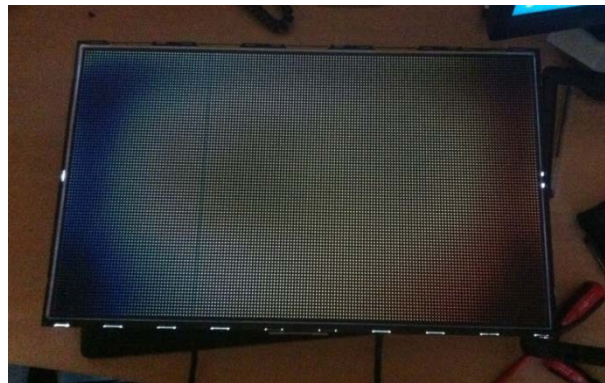
Figure A.8 - Manual mask alignment technique with most accurate alignment indication

The proposed process is as simple as creating a digital image of the pinhole mask: create an image with black background and adding 1 while pixel per pinhole which must be the centric pixel of the pinhole. Reply the 1-white-dot image on the display; align the pinhole mask until it turns into a white screen when it's perceived in straight parallel line at $90^°$ degrees. If it does not go white when it is viewed in the centre, it will create unbalance angle e.g. either left or right side will have more view angle.   As seen in Figure A.8, the display shows white which means the pinhole is fairly aligned at this stage.

A.II.d   H3D Image Preparation and Rendering

A H3D image is rendered off-line using POV-Ray [8]. A customised camera module is developed based on orthographic projection that allows objects to appear floating in front of, behind the rear display panel or right on display panel. Display, spacer sheet, and pinhole mask parameters including pixel pitch, pinhole pitch, screen aspect ratio and spacer thickness are used to generate 11 orthographic 2D viewpoint images which are later interlaced to form a holoscopic 3D image in C#.NET as shown in Figure A.9. The interlacing

program implemented in C#.NET simply creates a new image with a resolution of 1280 × 1024, loops 11 viewpoint images and copies one pixel from each viewpoint image to the new image at one time. It keeps looping the viewpoint images until it finishes. Just to summarise that the width of the holoscopic 3D image is equal to 11 × viewpoint image width and the height is equal to height of the viewpoint image.

(a)　　　　　　　　　　　　　　　　(b)
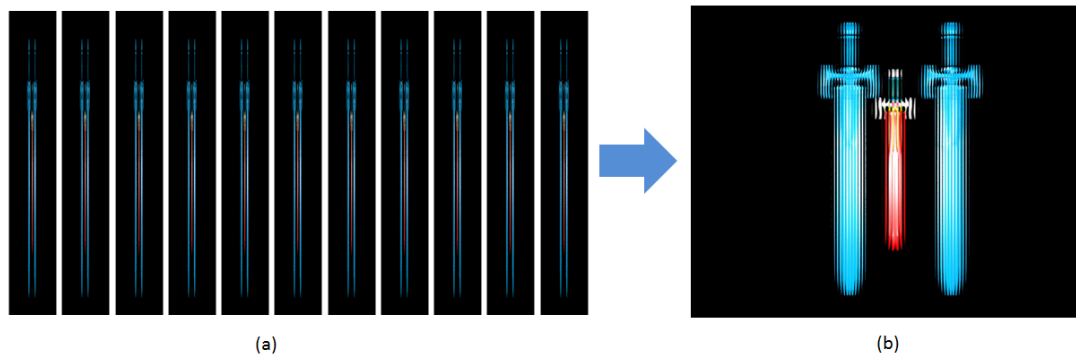
Figure A.9 – Rendering H3D image in POV-Ray: (a) Orthographic 2D viewpoint images; (b) interlaced viewpoint images to form a H3d image

A.II.e   Playback Result

The prototype Holoscopic 3D display has a single viewing zone that is a flicker-free 3D viewing zone. Indeed the display facilitates wide angular light field information therefore the viewers can move around without losing 3D effect. There is no confusion zone in which the viewer would be puzzled to pick up correct images. The minimum and maximum range for perceiving 3D is not applicable for holoscopic imaging. Shown in Figure A.10 (i-vi), a rich motion and depth parallax are gained in this prototype while the pinhole mask alignment with the LCD is manually done therefore there is a small risk of it not being 100% aligned which will create small errors

(i)

(ii)

(iii)

(iv)

(v)

(vi)
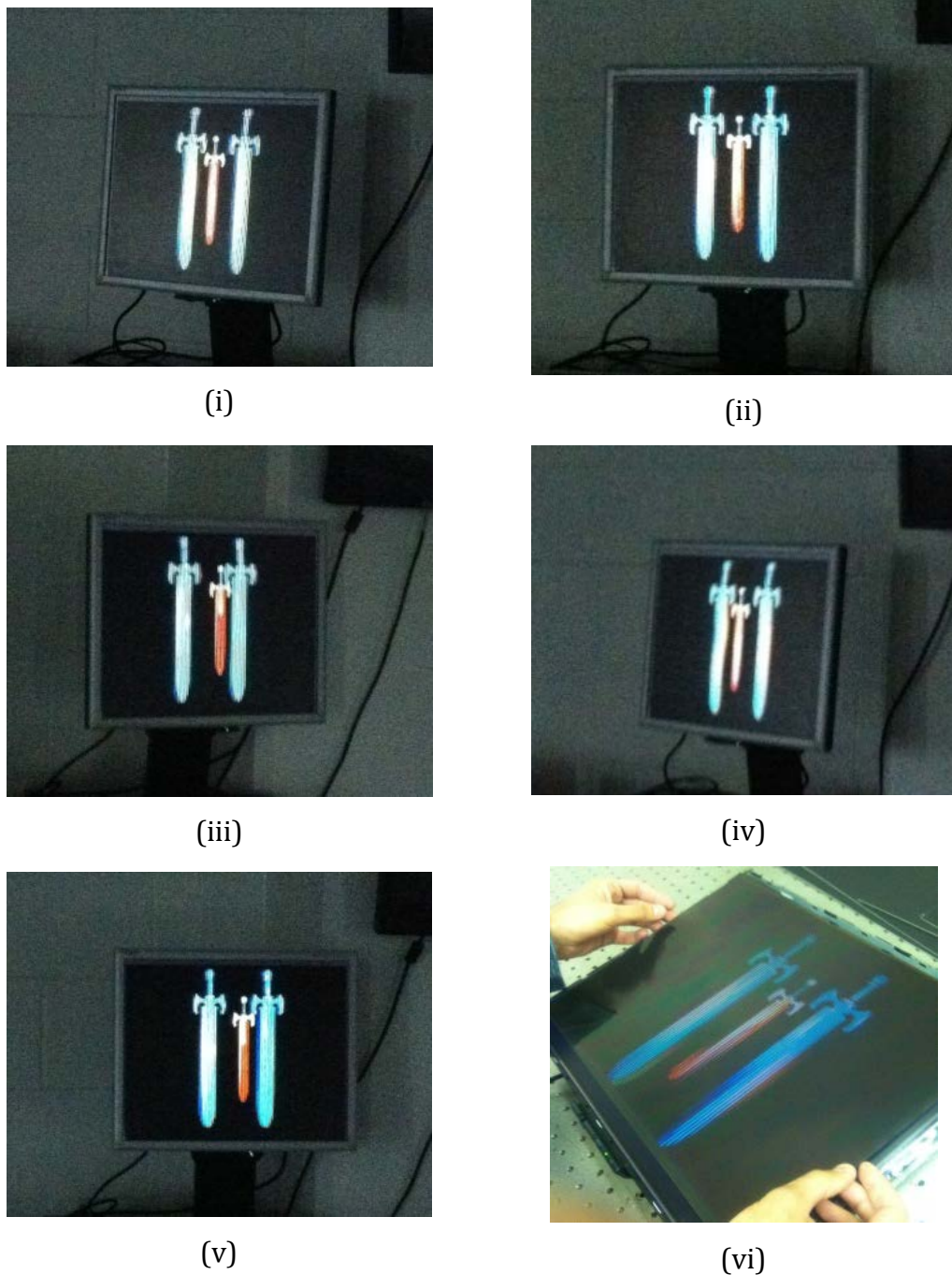
Figure A.10 - Replay result of pinhole based holoscopic 3D display: (i-iii) shows the motion parallax when the viewer moves from right to left including (iv) and (vi) where (v) shows the final manual alignment.

A.III Switchable Content Adaptive Holoscopic 3D Display

Traditional autostereoscopic 3D displays [26] have a non-switchable lens array or printed pinhole mask which adds distortions to 2D content. One of such display is proposed and developed in the previous section. Researchers have proposed a 2D/3D switchable solutions [23][24][25] that allows users to switch between 2D and 3D mode as necessary. Recently MIT researchers proposed a

compressive 3D content adaptive display which creates 3D illusions forming stack of layered LCDs using tomographic oriented technique. This is not a true 3D imaging as it uses stack of 2D flat images giving space in between and forces human brain to created 3D depth parallax. In this section, a new switchable content adaptive holoscopic 3D display is proposed and built using a pair of transparent LED liquid crystal display [27].

The proposed display uses a transparent LED liquid crystal [27] pinhole mask (LCPM) which is dynamic and reconfigurable in runtime. It offers 2D/3D switch-ability with 3D content adaptability. It replays 3D contents which are recorded / generated at different pixels per lens configuration in other words, a 3D content with different number of viewpoints. In addition, it supports multiview 3D content because the pinhole size is configurable so it can be configured to adapt to the multiview 3D content.

The main benefits of liquid crystal pinhole mask (LCPM) are (1) it offers 2D/3D switch-ability, (2) the pinhole is reconfigurable at user end in runtime, and therefore, it can support multiple type of 3D content. If necessary it can be further extended to supported stereoscopic system e.g. having only two perspective views under each LCPM to project left/right images similar to Nintendo 3DS [13] .

A.III.a   Hardware and Assembling the Display

The prototype of Switchable Content Adaptive H3D display is built using two a pair of Samsung's transparent LED LCDs [27], which have a 2D resolution of 1680 × 1050 pixels at RGB dot pixel pitch 0.282 mm. One is used as a LCPM and the other one is used as an image source. Before anything, these two LCDs are dissembled from their original frame, as shown in Figure A.11, because they are assembled back by putting them in back-to-back style.

Figure A.12 shows the block diagram of the front and side view; there is a focal length sheet "a see-through acrylic sheet" in between the LCDs. In this setup, the LCPM is placed behind the imaging LCD because when the LCPM is turned off, it can act like a backlight, without adding any noise to the image source even though it is minimal. If it is placed in front then when it is turned off, it becomes

transparent glass sheet. However it does add small noise to the scene as viewers can notice seeing things behind a glass sheet. It is important to note that the RGB dot pixel pitch and pixels per pinhole shall be taken under consideration while choosing the focal length size because its important RGB dot pixels are propagated into space correctly.

| (i) | (ii) | (iii) | (iv) |

| (v) | (vi) | (vii) | (viii) |
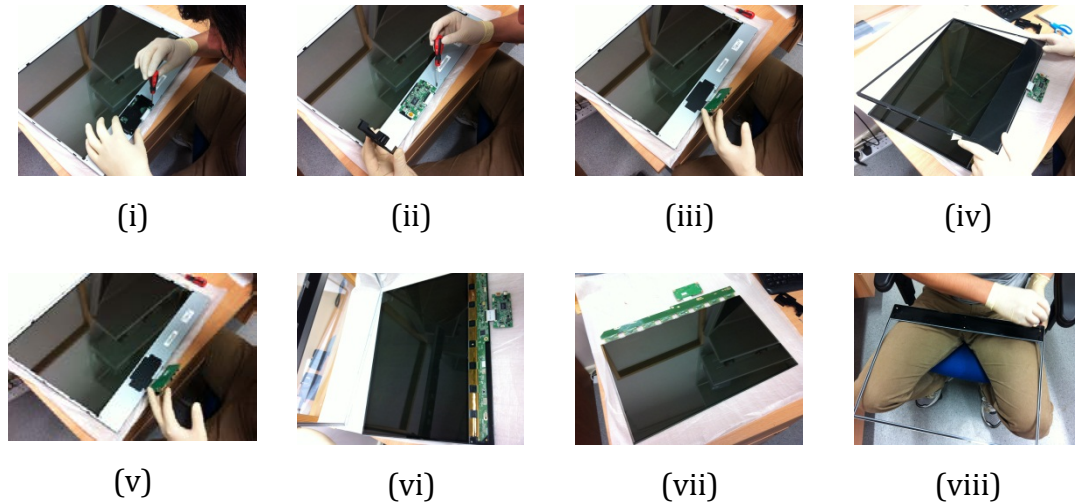
Figure A.11 - Assembling steps for converting two transparent LCDs to a switchable 3D Display

(a)   (b)

Figure A.12 – Block diagram of 2D/3D Switchable Content Adaptive H3D Display: (a) front view, (b) side view

The NL22B 22" LCD Transparent Display [27] is LED LCD that has a linear polarization so its output signal is a linear signal and it requires a circular lighting signal. If two of the LCDs are packed back-to-back, the 2nd LCD does not support the linear signal produced by the 1st LCD. As a result, a half-wave plate [28][29] is used to convert linear signal to circular signal as shown in Figure A.12. Due to human alignment, there is a small noise in the display but it does

the job. The alternative approach would be removing the linear polarization sheet from one of the LCD.

A.III.b   Holoscopic 3D Image Preparation and Rendering

Multiple H3D images are rendered off-line using virtual H3D camera developed in POV-Ray [8]. The virtual H3D camera module is developed based on orthographic projection that allows objects to appear floating in front of, behind the rear display panel or right on display panel. The display and parallax barriers parameters shown in Table A.4 are considered during rendering a 3D content with 10 PPL and also more 3D contents are rendered with 7 PPL / 8 PPL / 9 PPL as shown in Figure A.13.

| 7PPL | 8PPL | 9PPL | 10PPL |
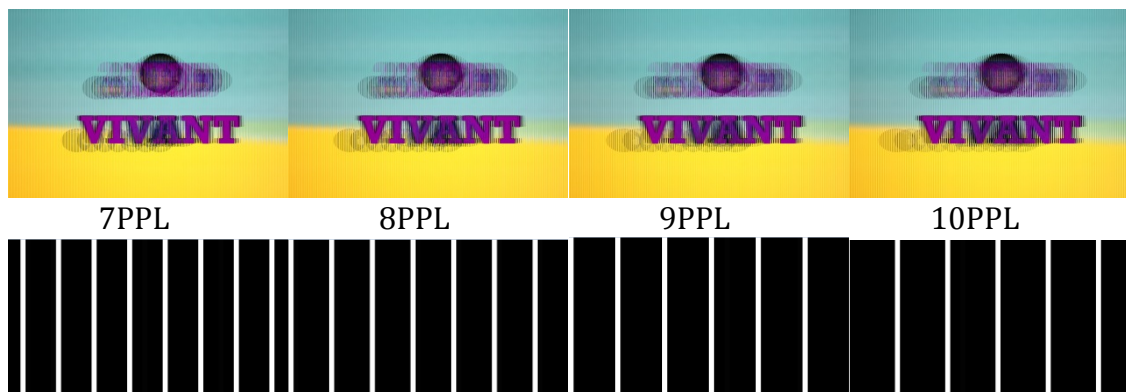
Figure A.13 - Multiple H3D images rendered with different PPL

Table A.4 – The content adaptive H3D display parameters

Items	Specification
Active display area	473.76(H) × 296.1(V) mm
Pixel pitch	0.282(H) × 0.282 (V) mm
2D Resolution	1680 × 1050 pixels
Backlight source	250 cd/m2
Pixels per pinhole	10 pixels
Pinhole pitch	*10 × 0.282 mm = 2.82 mm*
Pinhole sheet	*168 pinholes*

The rendering process is a simple two-steps process: 1 – render viewpoint images with orthographic projection cameras in POV-Ray, 2 – interweave the viewpoint images to form a H3D image in custom built interweaving application .NET and in both steps, the display and parallax barriers parameters are considered.

A.III.c   Playback Result

Multiple H3D images are rendered at different PPL that are replayed on the H3D display by opening in full screen mode. Figure A.14 shows the playback results which have a small difference in visual richness.   Also, 7PPL has smaller viewing angle than the others in other hand, 10PPL gives widest viewing angle of all. In this case, 10 PPL gives optimal of both viewing angle and 3D resolution of 168 × 1050 because increasing PPL increases darkness of the display and also reduces 3D resolution. The playback result is very promising even though the LCDs are cheap off the shelf devices with 2D resolution of 1680 × 1050 pixels. A better 3D resolution will be achieved with better LCDs e.g. Full HD or 4K LCD.

Figure A.14 – Playback result of Switchable Content Adaptive Holoscopic 3D Display

A.III.d   Pixel Mapping for improving Quality of the Constructed 3D scene

In this section, we propose to use pixel mapping methods for improving H3D image quality of the constructed H3D scene in space because pixel mapping refines 3D resolutions and achieves better 3D pixel aspect ratio. In addition, it offers a smoother motion parallax because it reduces lens array size. In other words, it fits more pixels under the same size microlens size. As a result, pixel mapping is the right candidate for improving quality of constructed 3D scene.

Particularly, pixel mapping techniques have been applied for multiview 3D displays and our recent paper [18] discusses parsing a holoscopic 3D image format to multiview 3D displays compatible format, in which case, the Philips pixel mapping is implemented 5.6. In this section, the focus is on applying pixel mapping technique [26] for improving quality of constructed H3D image scene as well as H3D resolution in Parallax barriers based holoscopic 3D displays. As it fits a pixel into a subpixel, it triples the horizontal 3D resolution where the vertical resolution is reduced to 1/3 and the 3D-DPI remains unchanged. Chapter 3 presents more detailed information on this particular pixel mapping.

After the H3D images were rendered and prepared, we replayed the 3D images on the custom built holoscopic 3D displays and as seen the resulting image playback in Figure A.15, the result is very promising and the dark spacing barriers between two pinholes is not visible with the naked eye. Also it does improve quality of the constructed H3D scene (see the visual richness quality of earth in both images).
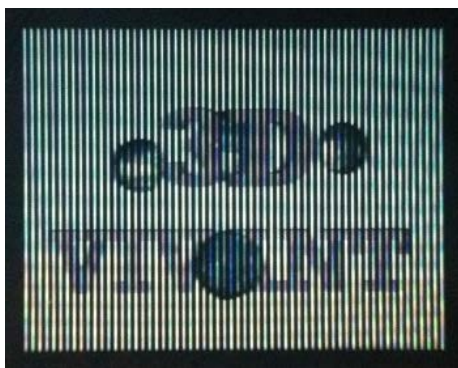
(a) Without pixel mapping   (b) with proposed pixel mapping

Figure A.15 - Playback result of proposed method (b) vs. tradition method (a)

The experimental result proves that pixel mapping improves quality of the constructed 3D scene. The experiment is conducted on custom built H3D displays (Parallax barriers) and the result is promising as dark areas between two pinholes are reduced (3 times smaller) and the overall H3D scene quality is improved significantly. Also like-to-like comparison is performed as shown in Figure A.15.

A.III.e Dual Pinhole Projection Technique for 3D Lighting Enhancement

Parallax barrier technology [30] uses multiplexing oriented technique to project pixels into space or human eyes. It has a pinhole with a size of a RGB dot pixel size for x number of pixels (x is pixels per lens). Only one pixel is perceived from a particular angle while the rest of the pixels are blocked. For instance, 10 pixels per lens require a dark space of 10 pixels between two pinholes therefore more pixels under each lens reduce the lighting and make it more deem.

Recently researchers proposed a time-multiplexed technique [31] and solutions [10] for mobile device which can be applied for improving lighting in parallax barrier technology. Also alternative solutions e.g. directional backlight [33][34] and compressive layered stack LCDs [36] to overcome the limitation but still there is a small advancement made.

The parallax barrier technology performs well with less numbers of pixels per lens. However one of the main requirements of autostereoscopic 3D display is motion parallax which is achieved by having more pixels under each microlens. Thus researchers are in seeking a solution to overcome the lighting issue in parallax barriers technology.

Multiview pixel mapping 5.6[26] is proposed to overcome 3D pixel aspect ratio issue and enhance 3D resolution in lenticular technology. The adaptation of multiview pixel mapping in parallax barrier technology is proposed and discussed in section A.III.d for improving the quality of the constructed H3D scene. In this section, we propose a dual pinhole projection technique (DPPT) for doubling lighting throughput in parallax barriers technology.

The proposed DPPT projects two neighbouring pixels simultaneously by having dual pinhole. It has two pinholes per elemental image unlike the tradition one shown in Figure 5.2(a). The idea is to project 1 to N-1 pixels (N is pixels per lens) from one pinhole and to project 2 to N pixels from the other pinhole thus dual 3D pixel construct a 3D scene. It gives a smoother transition between views because the 3D scene gets constructed with dual pixels which facilitate smooth transitions. It also increases the overall viewing angle at a particular

focal length as shown in Figure A.16 because viewpoint images are viewed from wider angle due to pinhole size being doubled.
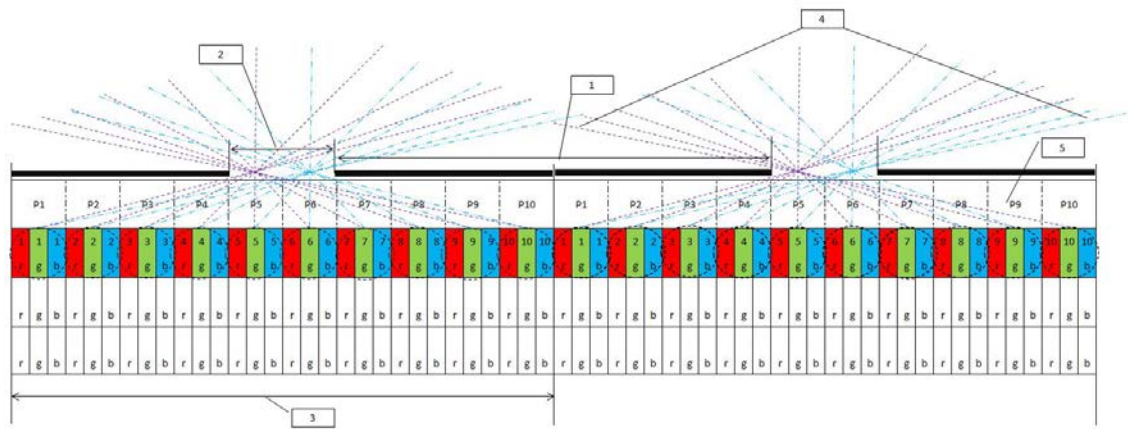
Figure A.16 - Dual pinhole projection method schematic drawings (1: dark area distance between two microlenses, 2: dual pinhole pitch size, 3: pixels per lens, 4: Overall view angle of microlens, 5: pixels per lens

A.III.e.i   Holoscopic 3D Image Preparation and Rendering

A H3D image is rendered off-line using virtual H3D camera which is developed based on 11 orthographic projection type cameras [7] in POV-Ray [8]. The LCD, pinhole mask and focal length parameters e.g. pixel pitch, pinhole pitch, screen aspect ratio and spacer thickness (focal length) are taken under consideration while rendering 11 orthographic viewpoint images which are later interlaced to form a H3D image in C#.NET as shown in Figure A.17.

It's important to note that a H3D image should be rendering with lens pitch size of N – 1, where N is pixel per lens. For instance, in this particular case, there are 11 pixels per lens where RGB dot pixel pitch is 0.282 mm and then the lens pitch is calculated as (11 – 1) × 0.282 mm = 2.82 mm. This is because we target to project 1 to N – 1 pixels from one pinhole and to project 2 to N pixels from the other pinhole.
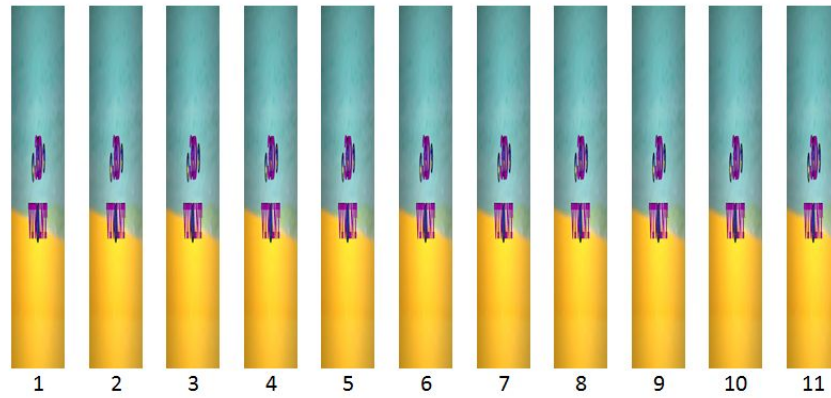
(a)
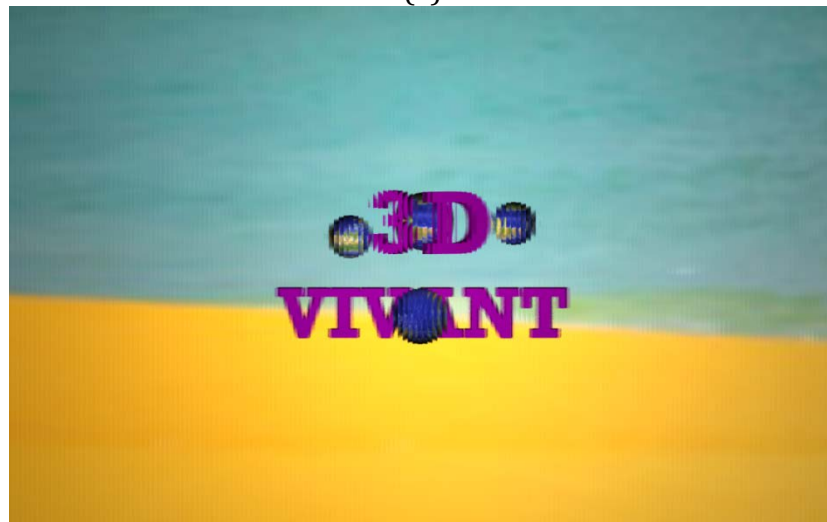
(b)

Figure A.17 - Rendering H3D image in POV-Ray: (a) Orthographic viewpoint images; (b) interlaced image

A.III.e.ii Playback Result

The prepared H3D image is replayed on custom built H3D display described in section 0.   The playback result shows that the lighting intensity is well improved. Indeed, the lighting is calculated using a digital light meter and it enhance the brightness significantly as shown in Figure A.18.

Figure A.18 shows the comparison of the proposed DPPT (b) with the traditional approach (b) and it clearly shows the proposed method has a better lighting intensity. However it introduces a very small cross-talk noises which could be due to manual alignment of pinhole array. If the pinhole mask is aligned with 100% accuracy then this small cross talk error will be reduced further and the error will be unnoticeable.

(a) traditional approach   (b) proposed dual pinhole projection

Figure A.18- brightness measurement of the traditional approach (a) and the proposed approach (b) @11PPL
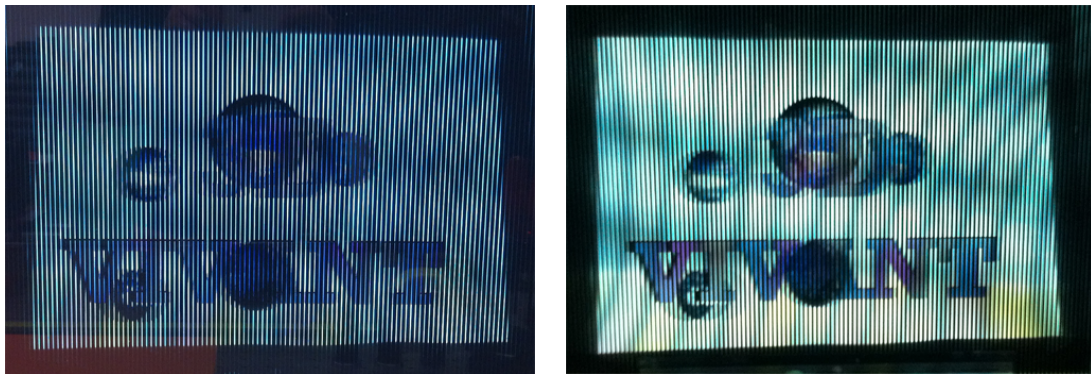
(a) tradition approach   (b) proposed dual pinhole projection

Figure A.19 - Playback result of the traditional approach (a) and the proposed approach (b)

A.III.f   4K Holoscopic 3D Display

The current generation of holoscopic 3D Displays trade off a great deal of LCD and 3D resolution in order to obtain an acceptable resolution on low resolution HD and FULL HD LCDs.   The state of the art 3D displays have been built with slanted lenticular sheets to trade off horizontal and vertical resolution. However it is very tempting to study 3D depth and motion parallax of the technology as proposed by the inventor Lipmann [6] in 1908.   It is a great advantage having 4K LCD available to prototype a traditional H3D display with 4K LCD which has finest pixel pitch of 124.5 micron to give the richest possible resolution with existing LCDs.

As a result, a 4K H3D display is built on lenticular sheet that has a classical 3D resolution of 226 × 2400 pixels as there are 17 pixels per lens. The microlens has a pitch of 2.12 mm with focal length of 3 mm. The complete technical specification is presented in Table A.5. The LCD has the 2D resolution 3840 × 2400 pixels employing 226 microlenses.

Table A.5 - 4K H3D Display technical specifications

Title	Description
Display type	*IBM 4K Liquid crystal display*
2D Resolution	3840
Viewpoint pixels per lens	17 *pixels*
Microlens pitch	2.12 *mm*
Microlens focal length	3 *mm*
3D Pixels	$226 \times 2400 \ Pixels$
Pixel Mapping	*Traditional Pixel arangement without slanting*

A.III.f.i Playback Result

H3D Display is a true 3D imaging system that offers stunning 3D depth and motion parallax. The prototype has 3D pixels of (H) 226 × (W) 2400 pixels which produced an amazing visual result as shown in Figure A.20. It is worth to mention that H3D pixels in horizontal and vertical does not directly defines 2D like resolution because H3D scene is created by multiple of 226-pixels images horizontally. As seen the playback result, a good result is achieved even it has unbalance pixel aspect ratio.

Figure A.20 - Playback result of 4K Holoscopic 3D Display

A.IV Portable Full Parallax Holoscopic 3D Field Display

Omnidirectional autostereoscopic holoscopic 3D displays enable users to experience the illusion of depth and motion parallax in all directions without using any head gear device that has become a target of future 3D display market. In such systems, binocular depth cues are achieved by constructing a 3D scene in space. The viewer's eyes see the virtual object in the real world space in both horizontal and vertical direction. This technique does not require human brain to do 3D processing; it therefore, is side-effect free such as eye fatigue, motion sadness and headache.

As portable devices are being widely used for different proposes for instant from taking note to data visualisation and modelling. In this section a portal omnidirectional holoscopic 3D display is proposed that offers 3D motion and depth parallax in complete directions that viewers perceive a 3D effect vertically as well as horizontally.

(a) front-view   (b) side-view
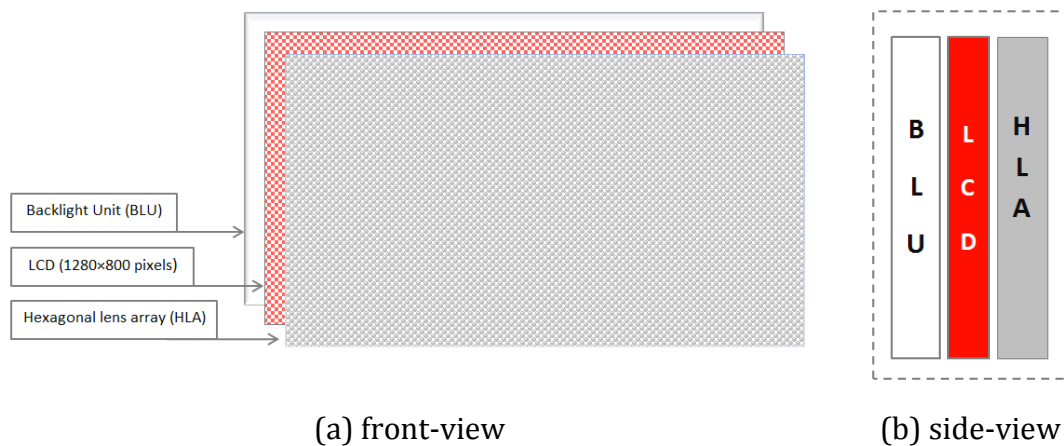
Figure A.21 - Block diagram of portable omnidirectional holoscopic 3D field display

A hexagonal lens array shown in Figure A.22 is shielded onto the portal LCD of 1280 × 800 pixels which replays omnidirectional holoscopic 3D image(s). It is manually aligned to elemental images of 10 × 10 pixels with accuracy of 20+/- microns. The microlenses project elemental images collectively construct a true 3D scene in space.

Figure A.21 illustrates the structure of the developed 3D display where (a) shows the layers top-to-bottom view; (b) is the side-view of the display which has 3 components: backlight unit (BLU), liquid crystal display (LCD) and

hexagonal lens array (HLA). The holoscopic 3D image is rendering with 10 × 10 pixel per lens however the lens array does not cover the digital number of 10 × 10 pixels therefore a slight error is expected on the playback result.

(1) microlens pitch, (2) number of microlens in vertical direction of lens array, (3) number of microlens in horizontal direction of lens array
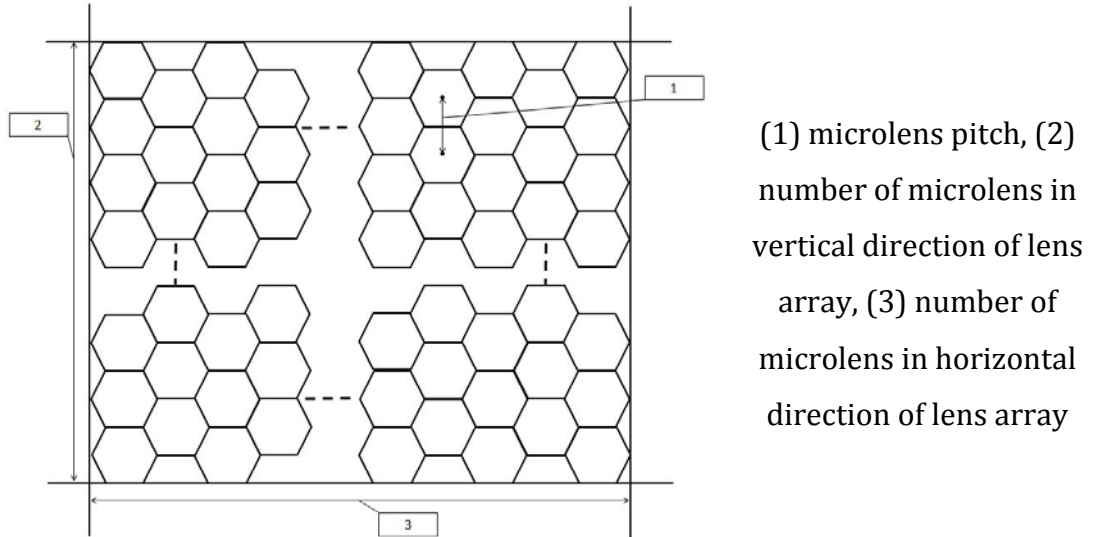
Figure A.22 - hexagonal lens array structure

Table A.6- Technical specification of the portable omnidirectional holoscopic 3d display

Description	Specification
Liquid Crystal display	*1280 × 800 pixels*
Active display dimension	*120.96 × 75.6 mm*
Pixel pitch	*0.0945(H) × 0.0945 (V) mm*
Lens array size	*142~ × 89~ lenses*
Pixels per lens	*9.5~ × 9.5~ pixels*
Microlens pitch	*0.850 mm*
Focal length	*1.0 mm*

The display has holoscopic 3D resolutions of 120 × 75 3D-pixels. A holoscopic 3D pixel is the intersection of two viewpoint pixels in space that is unlike 2D pixel/resolution. The lens array does not cover integer number of pixels of LCD because we use of-the-shelf lens array and display to reduce the cost as low as possible; the complete technical specifications of the display including its lens array are presented in Table A.6.

A.IV.a Playback Results

The holoscopic 3D image is rendered from a 3D model using a virtual holoscopic 3D camera developed using hexagonal style virtual lens array, which has 10 × 10 pixels per lens in POV Ray [8]

5.6" omnidirectional holoscopic 3D field display is developed based on fly's eye technique. In this particular case, a hexagonal type microlens sheet is used to reduce black unutilised areas. The display has 12638 microlenses which contribute for 3D scene construction in the space with resolution of 142*89 3D dots (3D resolution). Figure A.23 shows the display's component infrastructure and playback results are shown in Figure A.24. As seen, a good immersive 3D efficient in both directions is achieved even though the numbers of pixel per lens are not in integer. It proves the concept of having a 3D field display connected to light field 3D cameras for real time 3D depth and motion parallax visualisation on the camera.
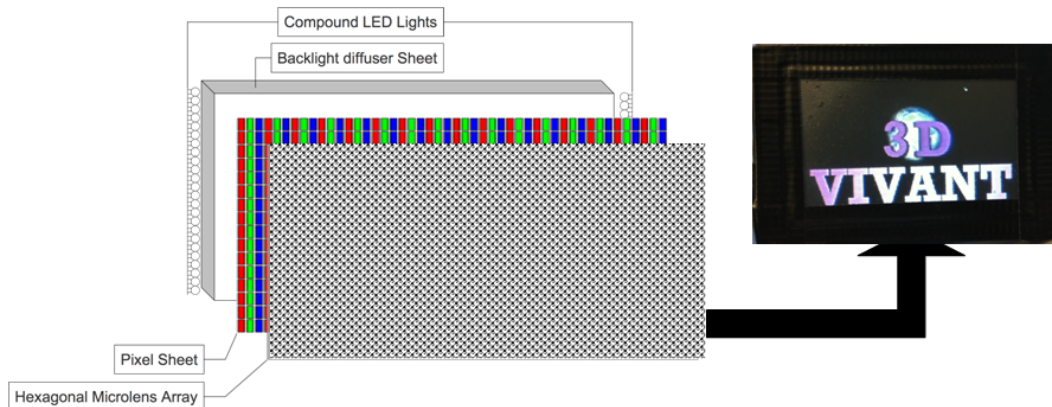
Figure A.23 – Components and infrastructure of holoscopic 3D field display

Figure A.24 - Playback Results of portable holoscopic 3D field display

A.V   Cross-Lenticular Full Parallax 4K Holoscopic 3D Display

Recently, the full parallax autostereoscopic 3D display attracted great attentions from both researchers and consumers that offers complete 3D depth

and motion parallax with standard pixel aspect ratio. However, the main problem is that manufacturing a large size of spherical microlens lens array is rather expensive or almost impossible due to its cost. An alternative solution was first proposed in 1998 using a cross-lenticular sheet [37], which is putting two lenticular sheets back-to-back as shown in Figure A.25(b) whereas Figure A.25 (a) illustrates structure of the lenticular sheet structure in which *P* represents the microlens pitch covers *N* number of pixels and *D* represent focal length (thickness) of the lenticular sheet.

D = focal length (thickness)
P = microlens pitch

(a)   (b)
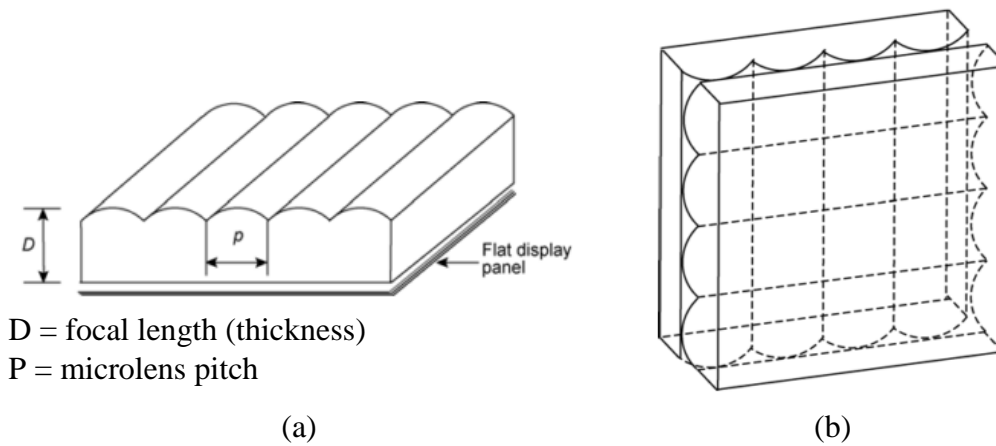
Figure A.25 - Block diagram of cross-lenticular sheet [37]

Table A.7- Technical specification of the cross-lenticular holoscopic 3d display

Description	Specification
Liquid Crystal display	*3840 × 2400 pixels*
Active display dimension	*478.08 × 298.8 mm*
Pixel pitch	*0.1245(H) × 01245 (V) mm*
Lens array size	*225 ×141 lenses*
Pixels per lens	*17 × 17 pixels*
Microlens pitch	*2.12 mm*
Focal length	*3.0 mm*

A.V.a Playback Results

The holoscopic 3D image is rendered from a 3D model using a virtual holoscopic 3D camera developed using 2Dimensional array of orthographic cameras [38] in POV Ray [8].   As shown in Table A.7, there are 225 x 141 = 31725 elemental images of 17 × 17 pixels which contribute in construction of true 3D scene in space. 4K omnidirectional holoscopic 3D display is designed

based on fly's eye technique using cross-lenticular technology which creates square aperture type microlens array. The display has 31725 microlenses which contribute to the 3D scene construction in space. The playback results are shown in Figure A.26. As seen, good immersive 3D effects in both directions are achieved.

In addition, we captured a real scene using holoscopic 3D camera developed at Brunel University. The 3D camera lens array has the microlens pitch of 90 microns which generate elemental images of 29 × 29 pixels. The captured real image is pre-processed "resampled" in order to replay it on the 3D display which supports 17 × 17 pixels per lens. The playback result is shown in Figure A.27 that gives a good motion parallax and depth parallax. Having said that, there are small distortions and noises which are due to different microlens focal length is used for recording and replying. The image is captured with the focal length of ~1 mm and replayed with the focal length of 3mm.

Figure A.26 - Playback result of omnidirectional holoscopic 3D image on full parallax holoscopic 3D display
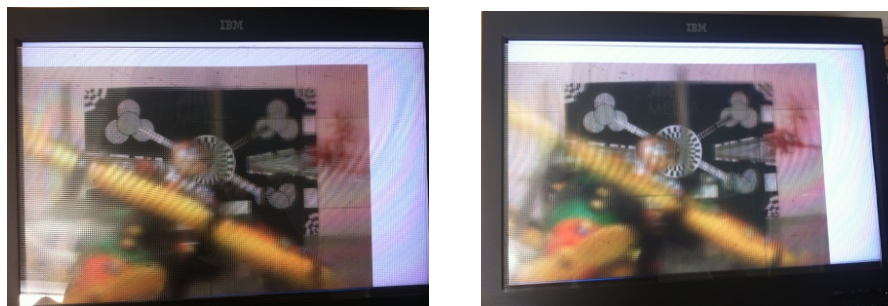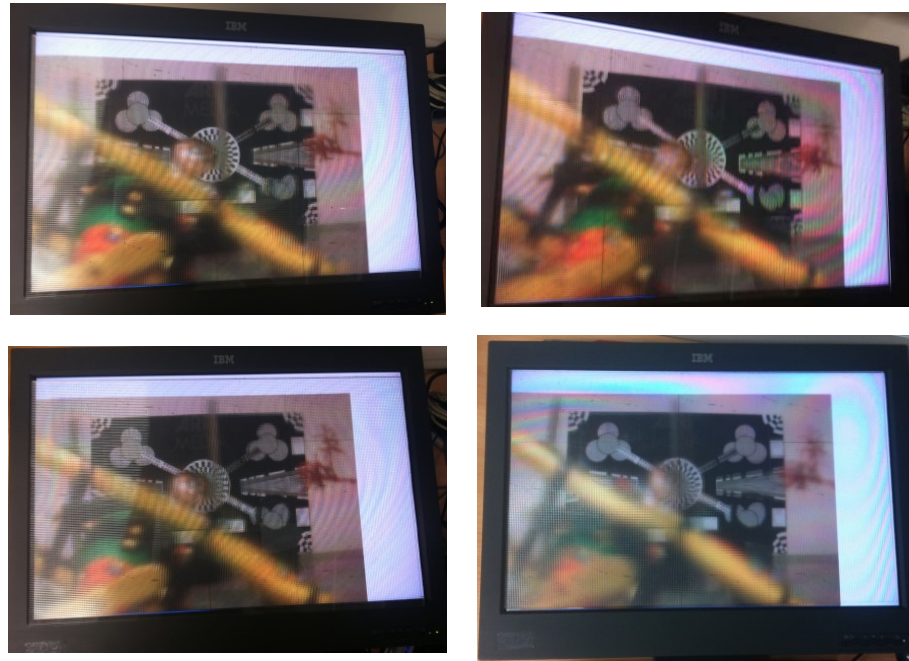
Figure A.27- Playback of real holoscopic 3D image on cross-lenticular based holoscopic 3D display

A.VI Flicker-free Full Parallax Holoscopic 3D Display

In the previews section, a cross-lenticular 3D display was proposed that offers reasonable viewing zone. However, it suffers from repeating the same scene; in other words, changing viewing-zones which makes it very unnatural and unrealistic compared to the real world.   Therefore, there is a great demand for a single viewing zone 3D display.

The empirical studies prove the parallax barrier technology offer better quality of 3D experience. Indeed a unidirectional flicker-free holoscopic 3D display was developed in section 3.3 of chapter 3. In this section, we propose and develop a full parallax holoscopic 3D display using parallax barrier technology. The proposed display offers a wide viewing angle and viewers can move left/right and up/down and the viewing zone remains unchanged.

The proposed 3D display is assembled using an off the shelf 2D LCD of 1600 × 900 pixels with printed static pinhole array sheet. It uses the traditional pixel mapping method and has 10 pixels per lens as shown in Figure A.28 that gives holoscopic 3D resolution of 160 × 90 3D-Pixels in the space.   The technical specification of the display including the pinhole array is presented in Table A.8.
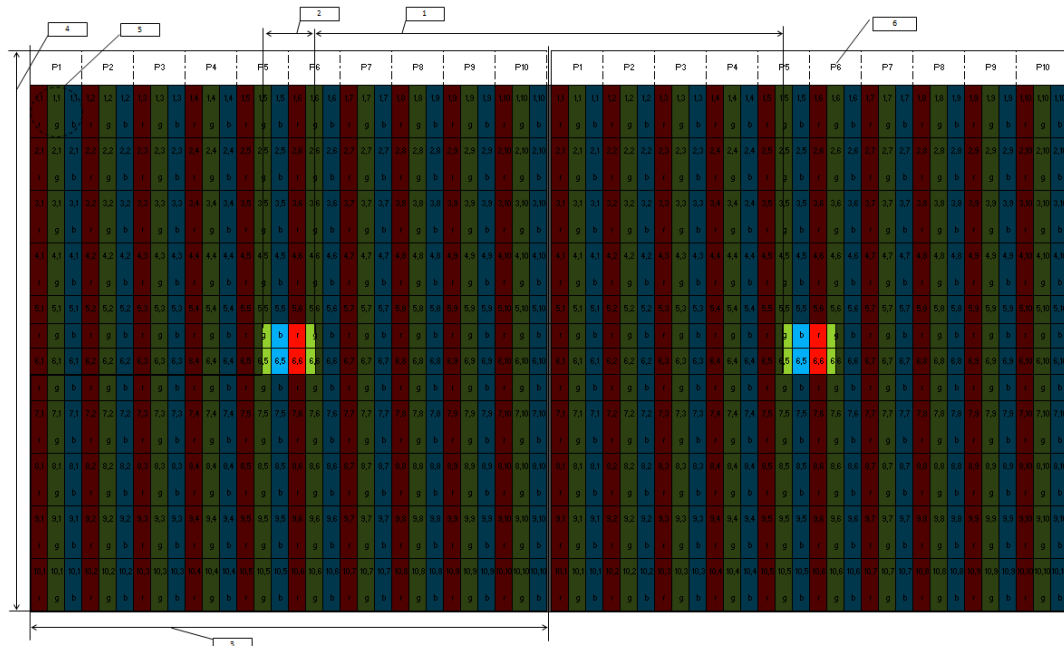
Figure A.28 – Pinhole array structure with its pixel mapping method: (1) distance between pinholes | 9 pixels, (2) pinhole pitch size | 1 RGB dot pixel size, (3,4) lens pitch | 10 pixels, (5) construction of a single RGB pixel, (6) pixel number under the microlens

The instruction of assembling the LCD with the pinhole array is presented in Figure A.29 (a) – (b). The most challenging and important step is aligning the pinhole array with the LCD pixel sheet. In this setup, we use a single pixel per lens technique which is done by having the centric pixel as white pixel and then align the pinhole sheet until the screen goes white as shown in Figure A.29 (c). As seen, the screen appears white which means the pinhole array is aligned with the accuracy of 30+/- microns.
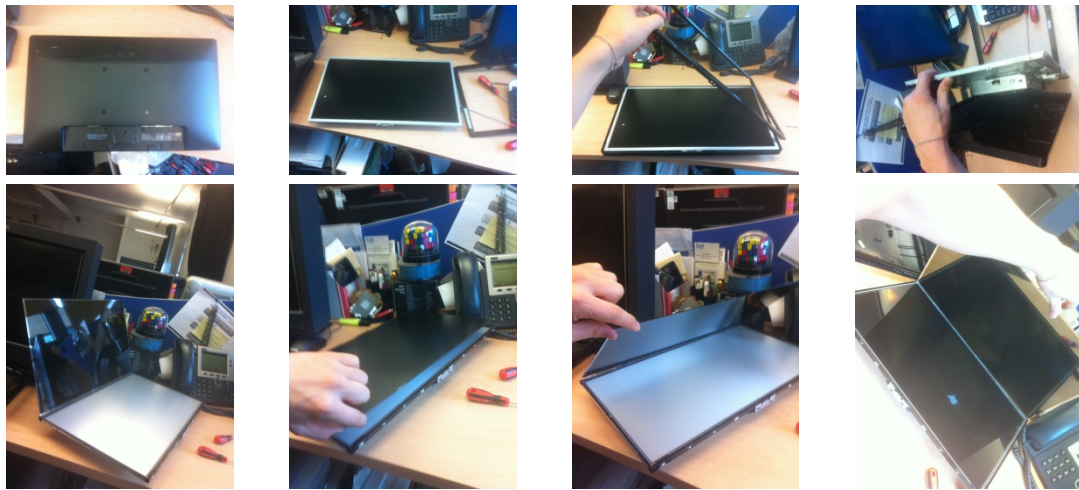
(a)
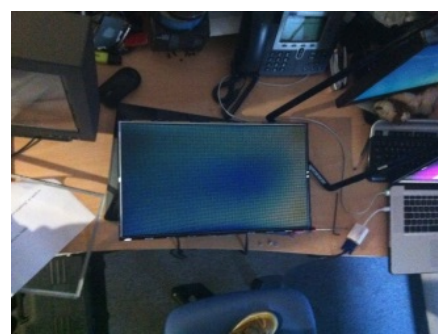
(b)   (c)

Figure A.29 – Steps: Converting 2D Display into 3D Display by adding a static pinhole sheet

Table A.8 – Technical specifications of the proposed flicker-free 3D display

Description	Specification
Liquid Crystal display	*1600 × 900 pixels*
Pixel pitch	*0.270(H) × 0.270 (V) mm*
Pixels per lens	*10 × 10 pixels*
Microlens pitch	*2.70 (H) × 2.70 (V) mm*
Focal length	*2.0 mm*
Parallax barrier size	*160 × 90 lenses*

A.VI.a Playback Results

The holoscopic 3D image is rendered using a virtual holoscopic 3D camera developed using 10 × 10 orthographic cameras [38] in POV Ray [8].   As shown in Table A.8, there are 160 x 90 = 14400 elemental images of 10 × 10 pixels which contribute in construction of true 3D scene in space. Playback results of the developed 3D display are shown in Figure A.30.   As seen, a wide angle

viewing zone is achieved as well as immersive 3D effects in both directions, however, it does not have a good backlight unit as it is using the original backlight designated for 2D LCD.

Figure A.30 – Playback result of full parallax holoscopic 3D display: Images captured from various angle
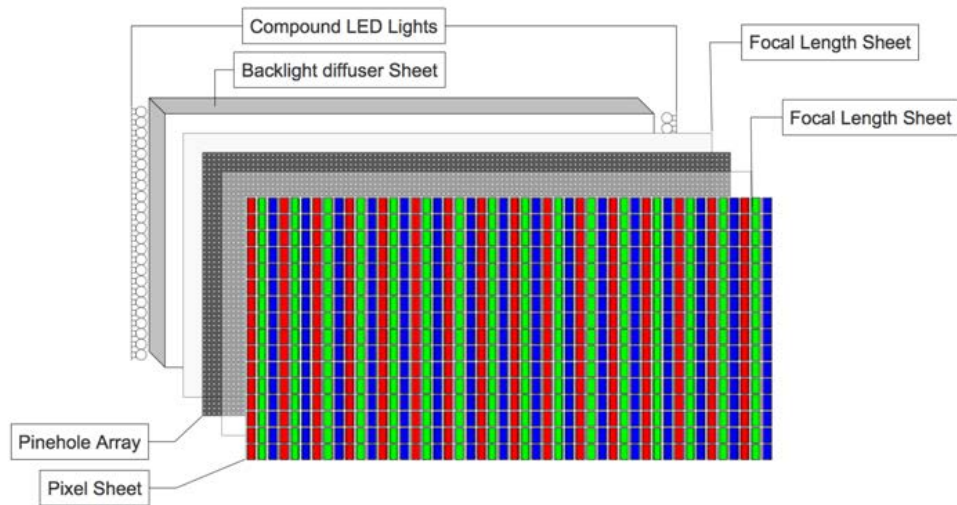
Figure A.31 – Block diagram of backlighting enhancement

In order to improve the lighting of the proposed 3D display, we add 20 high brightness intensity LED lights by placing 10 LED lights in each side of the display as shown in Figure A.31. The playback images were captured in darker room in the original display without improving backlight. Figure A.32 shows the playback results of the display with improved backlight in day light. As seen the display lighting is improved tremendously.

Figure A.32 – Omnidirectional holoscopic 3D display width improved backlight

A.VII Augmented Reality Holoscopic 3D Display

Augmented reality (AR) is defined as mixing real-world environment whose elements are augmented (or supplemented) by computer-generated sensory input such as sound, video, graphics. In AR, a view of reality is modified such as enhanced, diminished, and mixed by a computer. As a result, the technology is used to enhance one's current perception of reality. It is unlike virtual reality which replaces the real world with a simulated one. Augmentation is conventionally in real-time and a very good example is Google Glasses, which allows users to view computer generated data such as map and at the same time real world roads.

Augmented Reality is intensively used in 2D imaging system such as in medical imaging. Recently, SAMSUNG manufactured transparent LCDs which are used to augment real world object with 2D computer content. The LCD does not have white pixels because white pixels define the transparency thus by setting a pixel as white, will be see-through. AR technology attracts a great attention from researchers, manufactures, and consumers because it does truly enhance the real world but not replaces the real world.

Recently, a 50-inch transparent 3D display has been prototyped by Hisense that makes it possible to have objects behind the screen completely visible. It is a stereoscopic display shown in Figure A.33 which requires viewers to wear special glasses to perceive 3D depth parallax and augmentation. Therefore, it is

not a true 3D imaging system as left/right images are projected to human eyes and viewers focus on a pair of images. As a result, it suffers from limitations of stereoscopy and it is, also not suitable for unsupervised environments.

Figure A.33 – Hisense 50-inc Transparent Stereoscopic 3D display Error! Reference source not found.

The first attempt was proposed to develop a true augmented 3D projector by De Montfort University that rather has a complex setup as shown in Figure A.34. It uses a large lens array as the image is project through the lens array and 3D pixels are bounced back by Retro reflector and then an immersive 3D scene gets constructed in space via half-mirror "Beam splitter". The important fact is that it constructs a true 3D scene in real world environment but it has a bulky setup which makes it limited to supervised environments.
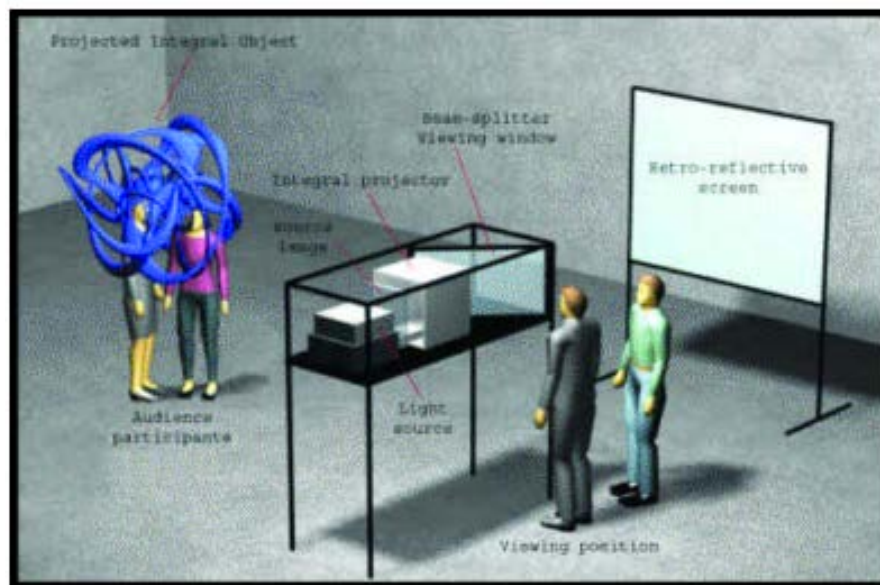
Figure A.34 – Augmented 3D projector setup Error! Reference source not found.

In this section, an Augmented Reality Holoscopic 3D display is proposed that has a smart setup which makes it a candidate for mobile and desktop displays. The proposed augmented reality 3D imaging system is developed based on holoscopic 3D imaging system which constructs a true 3D scene in space for the real world. It uses a see-through beam splitter optical component to replicate and bind 3D pixels onto real world environment. This enables viewers to view the computer content in real world scene shown in Figure A.35.

Beam Splitter is an optical component used to split input light into two separate parts. It is a common component in laser or illumination systems. It is also ideal for optical interferometry and stereoscopic imaging systems. Light can be split by percentage of overall intensity, wavelength, or polarization state.
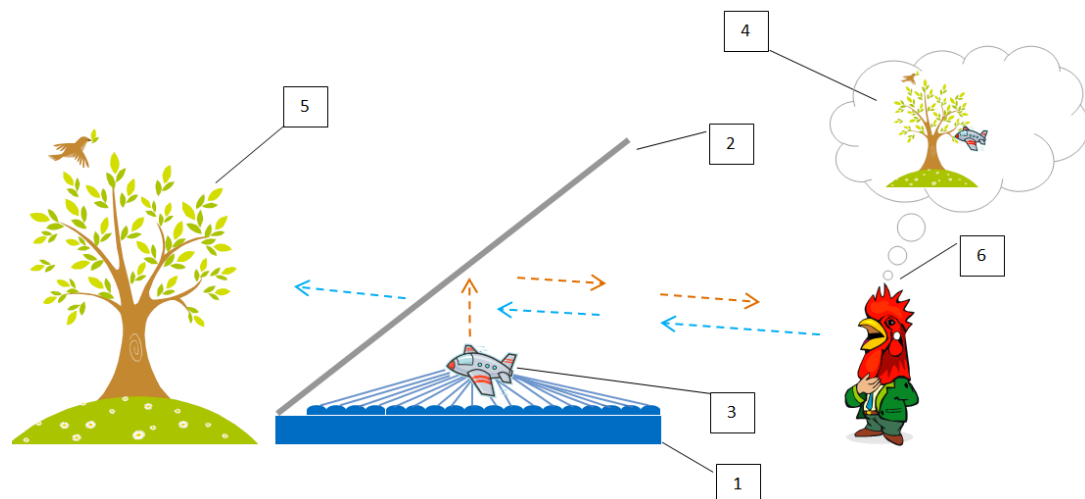
Figure A.35 - Proposed Augmented Reality Holoscopic 3D Display: (1) Holoscopic 3D Display, (2) Beam Splitter also known as half mirror, (3) constructed 3D scene in the space, (4) augmented 3D scene is perceived by the user, (5) real world scene, (6) viewers in real world environment

The proposed AR 3D display offers side-effect free 3D visualisation that facility holoscopic 3D imaging system for constructing a true 3D scene in space and then a beam splitter is used to augment the constructed 3D scene with real world scene as shown in Figure A.36. It allows viewers to perceive 3D motion parallax as well as true 3D depth in augmented 3D scene.
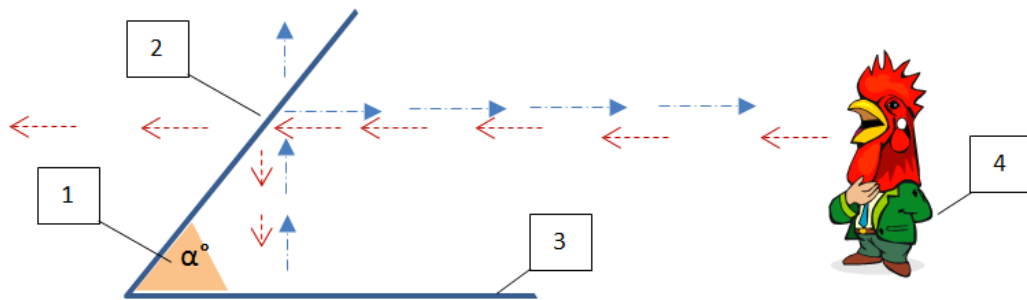
Figure A.36 - AR 3D display augmentation block diagram: (1) slanting angle of beam splitter | α = 45 °, (2) beam splitter also known as half mirror, (3) Holoscopic 3D display, see appendix for more details (4) viewer in the real world environment

Figure A.36 illustrates augmentation of real world and computer content. The beam splitter "half mirror" has a transmission rate of 50/50 which means it goes 50% of ray in both directions. By slanting the beam splitter by 45° degrees, full transparency is achieved and at that particular angle, viewers see computer content and real world.

Most importantly, a transparency pixel is defined which is a black pixel. Any pixel is set to full transparency is achieved and at that particular angle, viewers perceives augmented scene (computer content and real world scene). A transparency pixel is defined which is a black pixel. Any pixel set to [00,00,00] (Hexadecimal representation of RGB for black pixel) becomes see-through. Black pixels introduce a dark shadow onto the scene but that is resolved by adding a defused light. On the other hand, colour pixels are unlike black pixels as they block the light and are not see-through.

A.VII.a Playback Results

The proposed AR H3D display is developed using a unidirectional H3D display and a beam splitter. The H3D Display has 8 pixels per lens that uses lenticular technology to construct a unidirectional 3D scene in space. An amazing result is achieved using 8 pixels per lens as shown in Figure A.37. The 3D resolution is not HD resolution but the quality of augmented 3D scene is very promising because the constructed virtual 3D object is solid and both real and virtual objects are comparable. If/As necessary, improving 3D resolution of the display will further enhance the augmented scene.

Figure A.37 - Playback resulting images of Augmented Reality H3D display

A.VIII Pixel Mapping Techniques

Pixel mapping is a pixel arrangement in digital LCDs which have rectangular subpixels / square RGB pixels in array style shown in Figure 5.1 (a).   This particular pixel structure is proposed and implemented in existing 2D display technology in different resolutions and pixel aspect ratio standards, such as the widely known Full-HD 1920 × 1080 pixels @16:9. Some of widely used pixel aspect ratios and standards in 2D imaging systems are presented shown in Figure 5.1 (b).

Recently, Autostereoscopic 3D displays with flat panel LCD and lenticular sheets (or parallax barriers) are receiving much attention as the main moiré effect issue was resolved by slanting the lenticular sheet. In addition, Pixel mapping techniques [2] were proposed for unidirectional 3D displays that enabled viewers to achieve 2D like pixel aspect ratios by trading off horizontal and vertical 3D resolutions.

As Holoscopic 3D display [14] is truly an autostereoscopic 3D system as a true 3D scene is constructed in space, and multiple users perceive 3D depth and motion parallax independent of their position whereas multiview 3D displays have a sweet spot and require viewers to be in fixed position(s) to experience stereo and motion parallax.

(a) Traditional Pixel Structure

(b) State of the art pixel aspect ratio standards

	5:4	4:3	3:2	16:10	16:9
CGA				320 x 200	
QVGA		320 x 240			
VGA		640 x 480			
NTSC			720 x 480		
PAL		768 x 576			
SVGA		800 x 600			
WVGA					854 x 480
XGA		1024 x 768			
-			1152 x 768		
-		1280 x 960			
HD 720					1280 x 720
SXGA	1280 x 1024				
-			1280 x 854		
SXGA+		1400 x 1050			
-			1440 x 960		
UXGA		1600 x 1200			
WSXGA+				1680 x 1050	
HD 1080					1920 x 1080
WUXGA				1920 x 1200	
QXGA		2048 x 1536			
WQXGA				2560 x 1600	
QSXGA	2560 x 2048				

Figure A.38 - Traditional Pixel structure of liquid crystal display and SAO pixel aspect ratio standards

Presently, the main target is making the viewing experience as natural as possible with natural enough 3D effects and 3D resolution are of prime importance. The challenges are to design FULL HD equivalent autostereoscopic 3D displays using available LCDs technology for mass digital market. In this section, multiple pixel mapping techniques and smart pixel distributions are presented to overcome some of the limitations and challenges in designing HD H3D displays.

A.VIII.a   Traditional Pixel Mapping Of Holoscopic 3D Display

Holoscopic 3D Display utilises MLA to construct a true 3D scene and MLA represent perspective micro-images whereas viewpoint pixels are projected

successively into space as shown in Figure 5.2. Therefore in traditional approach, increasing number of 3D pixels growths horizontal size of the 3D display and also number of 3D pixels per inch depends on physical 2D LCD pixel pitch.
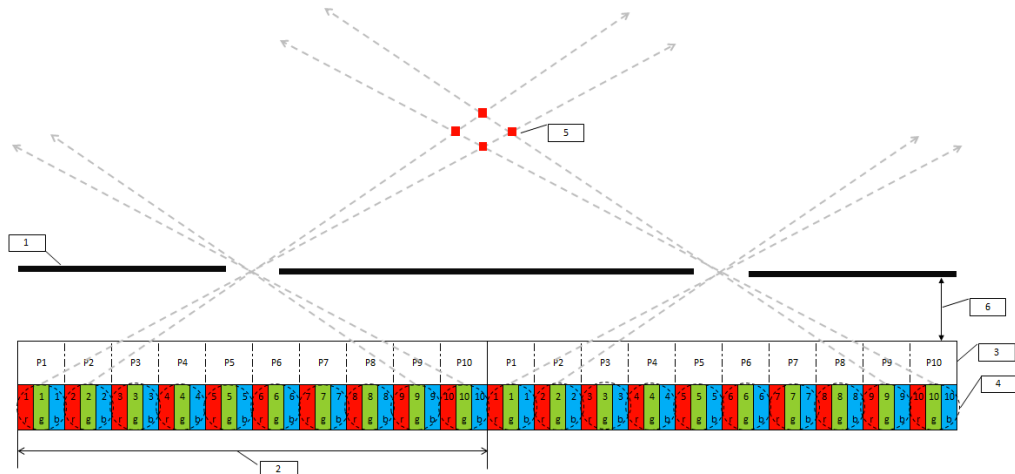
(a) Parallax Barriers: Viewpoint pixels representation (1: Pinhole array, 2: Pinhole pitch size, 3: Pixels per pinhole, 4: Viewpoint RGB dot pixel structure, 5: 3D pixel 'viewpoint pixels Intersections', 6: Focal length)
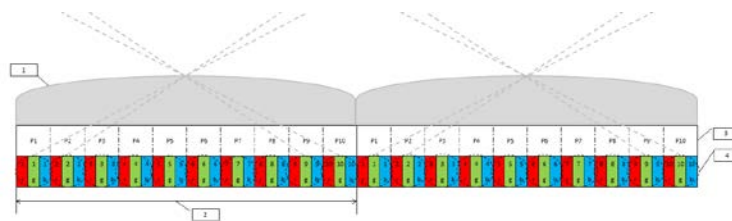
(B) Lenticular Sheet: Viewpoint pixels representation (1: Microlens array, 2: Microlens-pitch size, 3: Pixels per lens, 4: Viewpoint pixel structure)

Figure A.39 – Traditional Holoscopic 3D Display pixel mapping in (a) parallax barriers and (b) lenticular sheet

A.VIII.b   Vertical Pixel Mapping

The state of the art pixel mapping techniques improves the 3D resolution and achieves acceptable pixel aspect ratio by shifting sub-pixels in both horizontal and vertical directions. These pixel mapping create slanting angles of 9.46° and 18.43° as shown in 5.6[2][26] The slanting removes moiré effect which is the prime aim. The pixel mapping in lenticular technology is aimed at the slanted

style. However slanting the lenticular sheet increases cross-talk noises as small portions of neighbouring pixels appear.

The parallax barrier technology has an advantage over lenticular sheet because it does not produce moiré effect therefore there is no need to slant the pinhole array. In this section, a vertical pixel mapping is proposed as an alternative pixel mapping for parallax barriers based 3D displays. It trades off horizontal and vertical resolution to improve the quality of constructed 3D scene without a distortion.

The proposed pixel mapping does not distort or slant the 3D scene because sub-pixels are mapped and shifted in vertical direction. It also improves the computation of 3D content processing because there is no need to perform the de-slanting viewpoint images whereas the SOA pixel mapping methods require viewpoint images to be de-slanted before the process to achieve a correct shape in 3D image. It improves 3D resolutions as well as 3D pixel aspect ratio by enhancing horizontal 3D resolutions three times better at the same pixels per lens. It also reduces dark spaces between pinholes which improves overall 3D scene quality as the scene gets constructed with finer pinhole array as shown in Figure A.40 compare to the traditional approach Figure 5.2(a).

(1) distance between two pinholes | 9 sub-pixel; (2) pinhole pitch | 1 subpixel; (3) Lens pitch | 10 subpixels; (4) RGB dot pixel; (5) sub/pixels numbers under microlens
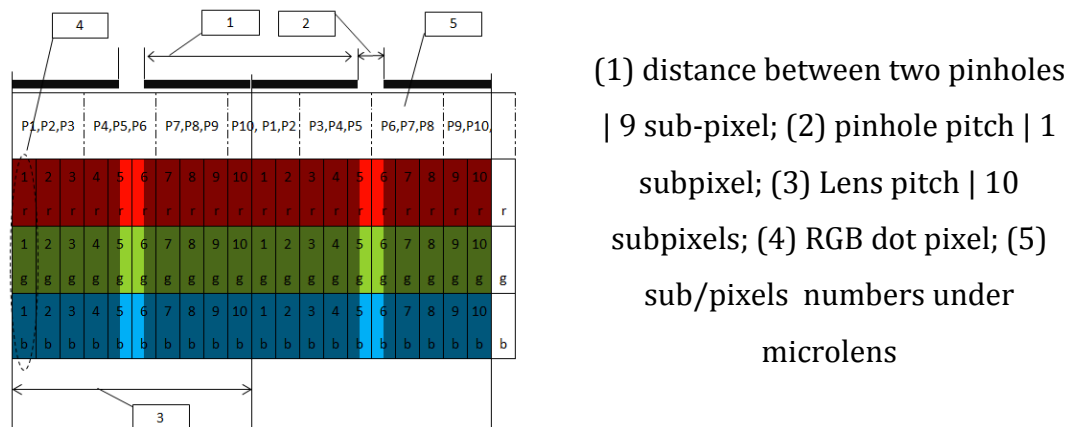
Figure A.40 – The proposed vertical pixel mapping pixel representation in Parallax barrier technology

A.VIII.b.iPlayback Result

In particular, the proposed pixel mapping technique is designed for pinhole based H3D display but also implemented and replayed on lenticular based 3D display to illustrate the concept constructs a clear H3D scene as shown in

Figure A.41 (a). Indeed, it has a very smooth transition between views which creates a natural motion parallax. In this particular setup, there are 51 pixels per lens of 226 microlenses therefore it is 51-view H3D display which is built using a 4K LCD whereas the parallax barriers 3D display is built using two LCDs of 1680 × 1050 pixels and still a clear and crisp H3D scene is constructed.

(a)   (b)
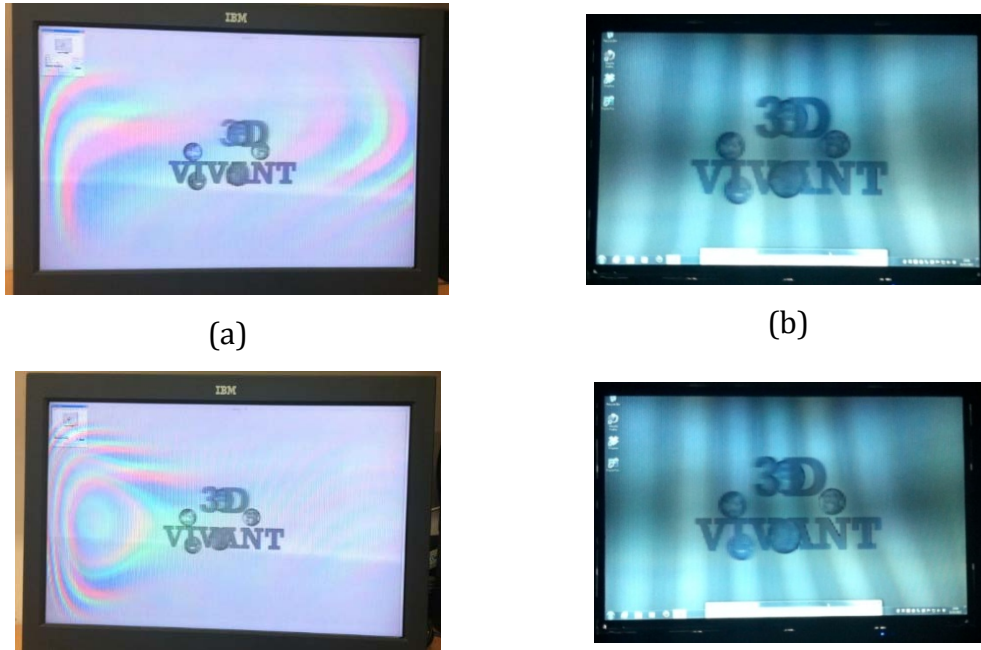
Figure A.41 - Playback result of vertical pixel mapping technique: (a) Lenticular based H3D display, (b) Parallax barriers based H3D Display

The resulting image for replay on the 3D display is in grayscale to avoid colour distortions because this pixel mapping techniques requires a special type RGB pixel structure LCD which is implementable. There is a moiré effect in lenticular technology which should be ignored as this particular pixel mapping proposed for parallax barriers 3D display whose playback result is shown in Figure A.41 (b).

A.VIII.cIntegrated Triangular Pixel Mapping

Triangular pixel mapping was presented in chapter 3 that reduced 3D pixel distance to 1 subpixel size and improved 3D resolutions by trading off horizontal and vertical resolution. This section proposes an integrated triangular pixel mapping to further improve the pixel mapping. It is a hybrid approach of Dual projection and triangular pixel mapping. It projects a pair of 3D pixels which enhances the constructed 3D scene in terms of visual intensity.

This is achieved by the re-structure of the pixel mapping in such way that two neighbouring pixels are projected at the same angle.

(1) Pinhole pitch | 1 × subpixel size, (2) lens pitch | 5 × subpixels size, (3) dark spacing between pinholes | 4 × subpixels, (4) viewpoint pair pixels, (5) LCD pixel sheet
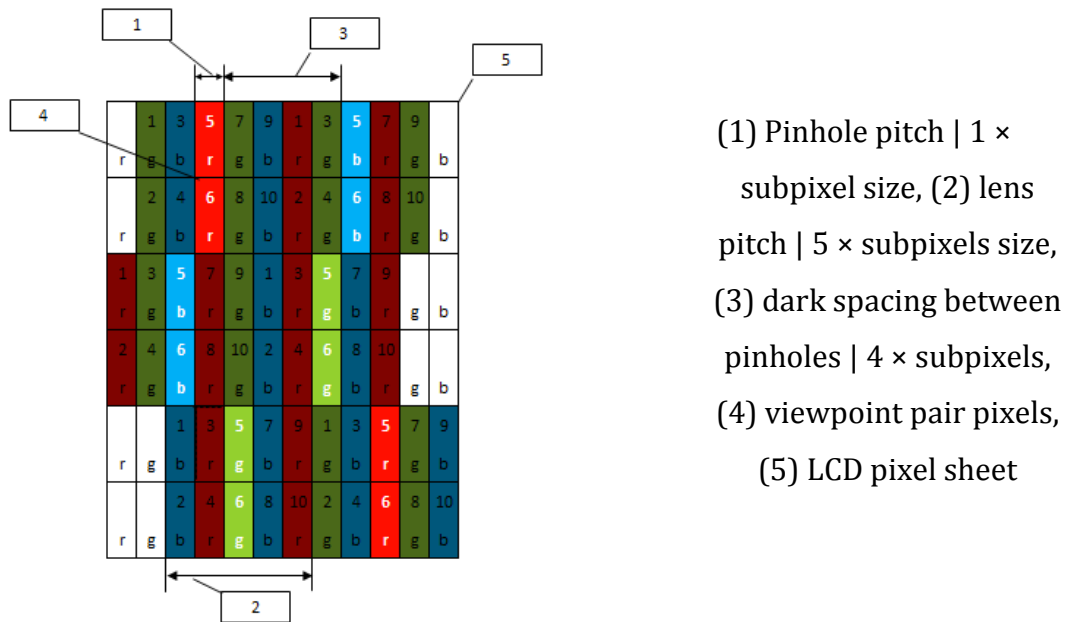
Figure A.42 – The proposed integrated triangular pixel mapping systematic

As a result, the proposed integrated pixel mapping offers smoother motion parallax because both viewpoint 1 and 2 are projected at the same time. 3D-PPI in space is doubled which also improves 3D depth definition. It trades off horizontal and vertical 3D resolution e.g. It reduces vertical 3D resolution to 6 times lower resolutions and improves horizontal 3D resolution by 6 times therefore it can offer wide screen pixel aspect ratio.

In other words, it is dual projection pixel mapping without slanting errors and distortions. Also it is computationally efficient compare to SOA pixel mapping [2][26] because the pixel mapping process does not re-shape the image therefore there is no need for de-slanting process.

Figure A.42 shows the pixel mapping systematic that illustrates structure of subpixels as well as construction of a RGB-dot-pixel and in this particular case, there are 10 pixels per lens shown Figure 5.2 that is remapped in Figure A.42. Viewpoint pixels are remapped in integrated triangular style which is also compatible with existing LCDs pixel structure. The traditional triangular pixel mapping projects a single viewpoint pixel at one angle whereas the proposed method projects a pair of viewpoint pixels and viewers perceive pair pixels of

small difference. The process method's visual quality improves if more pixels are added in smaller pixel pitch.

A.VIII.c.i Playback Results

The experiment is performed on a custom built H3D display which is specifically designed for the proposed pixel mapping. Also the pixel mapping module is implemented in .NET that applies the pixel mapping on a H3D image and then the prepared H3D images are directly replayed on the H3D display. This particular pixel mapping gives a smoother transition as there are two images of a very slight different perspective which viewers perceive at the same time. It sixfolds horizontal 3D resolution and it doubles lighting throughput as it uses dual pinhole projection technique (Figure A.43). It is a candidate for designing a wide screen pixel aspect ratio.
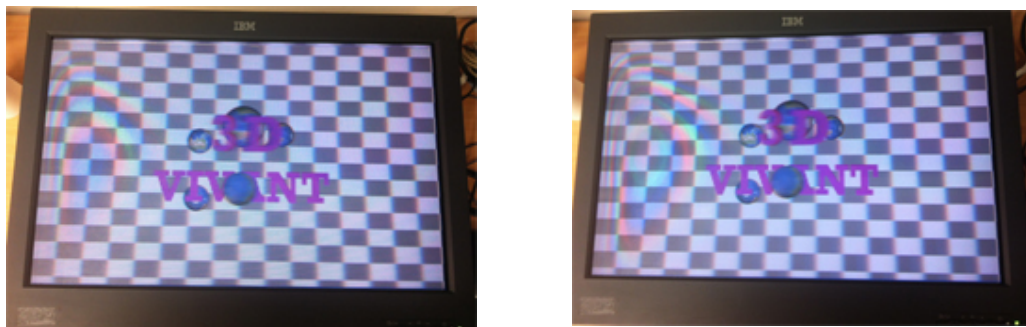

Figure A.43 - Playback results of Integrated Triangular pixel mapping

References

[13]   Nintendo, "Nintendo 3DS Game Console," Nintendo. [Online]. Available: http://www.nintendo.com/3ds. [Accessed: 30-Jun-2013].

[14]   A. Aggoun, E. Tsekleves, M. R. Swash, D. Zarpalas, A. Dimou, P. Daras, P. Nunes, and L. D. Soares, "Immersive 3D Holoscopic Video System," MultiMedia, IEEE, vol. 20, no. 1, pp. 28–37, 2013.

[15]   V. Berkel and D. W. Parker, "Autostereoscopic Display Apparatus," U.S. Patent 6118584, 2002.

[16]   V. Berkel and J. A. Clarke, "Autostereoscropic Display Apparatus," U.S. Patent 6064424, 2000.

[17]   Persistence of Vision Pty. Ltd. Persistence of vision raytracer (version 3.6). http://www.povray.org/, 2004.

[18]   M.R. Swash, A. Aggoun, O. Abdulfatah, B. Li, J. C. Fernández, and E. Tsekleves, "Holoscopic 3D image rendering for Autostereoscopic Multiview 3D display," IEEE international Symposium on Broadband Multimedia Systems and Broadcasting, 2013.

[19]   Alioscopy, "Alioscopy 3D Display Pixel Mapping Principles," Alioscopy, 2013. [Online]. Available: http://www.alioscopy.com/en/principles.php. [Accessed: 01-May-2013].

[20]   G. Lippmann, 'Epreuves reversibles', Comptes rendus hebdom-adaires des Seances de l'Academie des Sciences 146, 446-451, March 1908

[21]   G. Milnthorpe, M. McCormick, A. Aggoun, and N. Davies, "Computer generated content for 3D TV displays," International Broadcasting Convention, 2002.

[22]   G. A. Thomas and R. F. Stevens, "Processing of Images for 3D Display," U.S. Patent US6798409B22004

[23]   D. Liang, J.Y. Luo, W.X. Zhao, D.-H. Li, and Q.-H. Wang, "2D/3D Switchable Autostereoscopic Display Based on Polymer-Stabilized Blue-Phase Liquid Crystal Lens," Display Technology, Journal of, vol. 8, no. 10, pp. 609–612, 2012.

[24]   T. Dekker, S. T. de Zwart, O. H. Willemsen, M. G. H. Hiddink, and W. L. IJzerman, "2D/3D switchable displays," p. 61350K–61350K–11, 2006.

[25]   J. Harrold, D. Wilkes, and G. Woodgate, "Switchable 2D/3D Display–Solid Phase Liquid Crystal Microlens Array," Proc. IDW, pp. 2–3.

[26]   N. a. Dodgson, "Autostereoscopic 3D displays," Computer, vol. 38, no. 8, pp. 31–36, Aug. 2005.

[27]   SAMSUNG, "SAMSUNG NL22B 22" LED LCD Transparent Display," Samsung.   [Online].   Available: http://www.samsung.com/us/business/commercial-display-solutions/LH22NLBVLVC/ZA-features. [Accessed: 01-Jul-2013].

[28]   E. Shapiro, "POLARIZATION ROTATORS." Google Patents, 1967.

[29]   C. Ye, "Construction of an optical rotator using quarter-wave plates and an optical retarder," Optical Engineering, vol. 34, no. 10, pp. 3031–3035, 1995.

[30]   D. U. Kean, D. J. Montgomery, J. Mather, G. Bourhill, and G. R. Jones, "Parallax barrier and multiple view display," U.S. Patent 10/803,2922006.

[31]   J. Cui, Y. Li, J. Yan, H. Cheng, and Q. Wang, "Time-Multiplexed Dual-View Display Using a Blue Phase Liquid Crystal," Journal of Display technology, vol. 9, no. 2, pp. 87–90, 2013.

[32]   W. Mphepo, Y.-P. Huang, and H.-P. D. Shieh, "Enhancing the Brightness of Parallax Barrier Based 3D Flat Panel Mobile Displays Without Compromising Power Consumption," Journal of Display Technology, vol. 6, no. 2, pp. 60–64, Feb. 2010.

[33]   T. Sasagawa, A. Yuuki, S. Tahata, O. Murakami, and K. Oda, "P-51: Dual Directional Backlight for Stereoscopic LCD," SID Symposium Digest of Technical Papers, vol. 34, no. 1, pp. 399–401, 2003.

[34]   R. Brott and J. Schultz, "16.3: Directional Backlight Lightguide Considerations for Full Resolution Autostereoscopic 3D Displays," SID Symposium Digest of Technical Papers, pp. 218–221, 2010.

[35]   G. Wetzstein, D. Lanman, M. Hirsch, and R. Raskar, "Tensor displays: compressive light field synthesis using multilayer displays with directional backlighting," ACM Transactions, 2012.

[36]   D. Lanman, M. Hirsch, Y. Kim, and R. Raskar, "Content-adaptive parallax barriers: optimizing dual-layer 3D displays using low-rank light field factorization," ACM Transactions on Graphics , 2010.

[37]   H. Xie, X. Zhao, Y. Yang, J. Bu, Z. Fang, and X. Yuan, "Cross-lenticular lens array for full parallax 3-D display with crosstalk reduction," Science China Technological Sciences, vol. 55, no. 3, pp. 735–742, Dec. 2011.

[38]   M. R. Swash, A. Aggoun, O. Abdulfatah, B. Li, J. C. Jacome, and E. Tsekleves, "Omnidirectional Holsocopic 3D Content Generation Using Dual Orthographic Projection," IEEE Int. Symp. Broadband Multimed. Syst. Broadcast., 2013.

Appendix B.

Holoscopic 3D Computer Graphics

This appendix presents plugins or add-ons, which were developed during the completion of the PhD research.

B.I Unidirectional Holoscopic 3D Computer Graphics Rendering

We implemented the orthographic method [7], which was patented by BBC. It renders viewpoint images using orthographic projection type cameras as shown in Figure B.1.
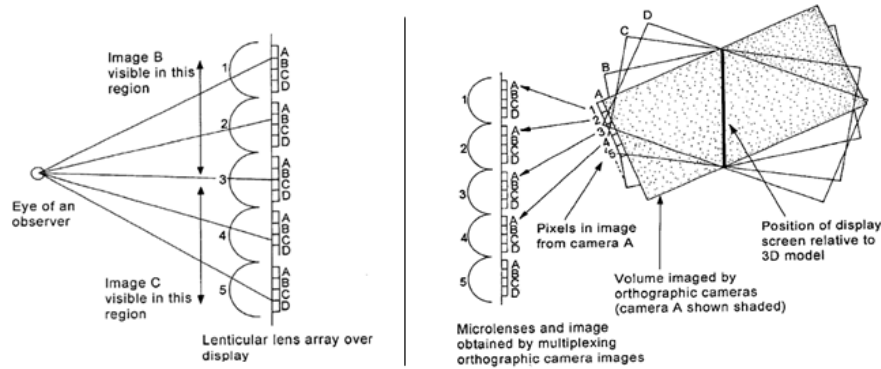

Figure B.1 – Relationship of microlens perspective images with viewpoint orthographic images [7]

As seen in the figure, it does a reverse engineering because traditionally a viewpoint image is formed by collecting a pixel from a particular location of every microlens image in the lens array. It renders one particular pixel of all microlens images at once. For instance, if there are 6 microlenses and each microlens covers 4 pixels then it renders 4 orthographic viewpoint images with resolution of 5 pixels as it is clearly illustrated in Figure B.1. Empirical studies of state of art 3D displays shows a normal 3D display has between 700 – 1000 microlenses and each microlens covers up to 28 pixels.

As a result, the proposed method is rather fast and simplified technique for rendering holoscopic 3D computer graphics because traditionally these hundreds of microlens images are rendered using a perspective pinhole hundreds of time to form a H3D image [14] which is computationally heavy, time consuming and complex for end users.

It simulates the single aperture holoscopic 3D camera which allows tracing objects in front or behind the screen. Figure B.2 shows 3D objects in the virtual scene in *X,Y,Z* space. The grid is the imaging panel which is used as the reference point to trace 3D objects in front or behind the screen. The

orthographic camera is in negative **Z** and the objects placed in negative **Z** appear in front of screen after depth transformation, required for computer graphics.
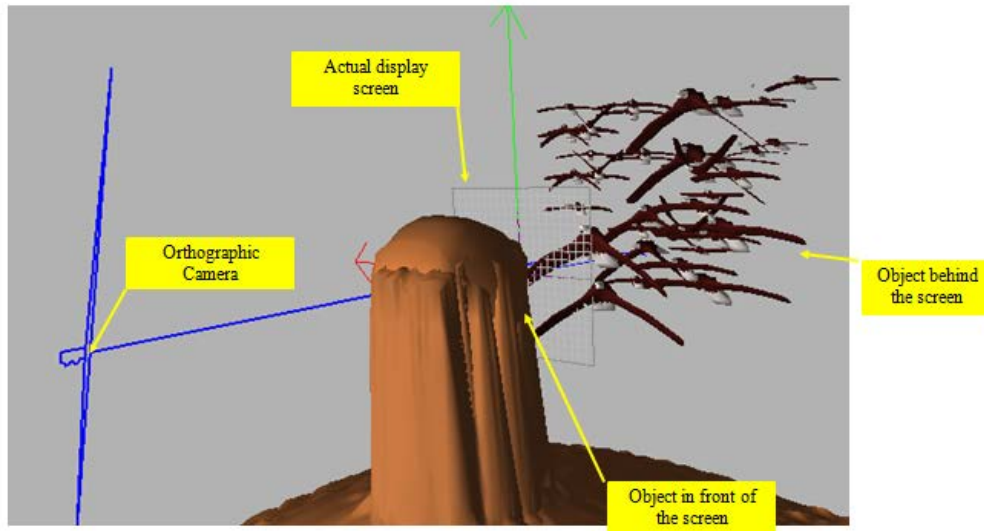

Figure B.2 – Imaging reference point for tracing objects in front/behind the screen

3D Camera Plug-in for Non-Photo-Realistic Rendering

Three dimensional computer generated content [21] is one of the important and challenging stages in holoscopic 3D imaging technologies [14]. As the technology is in its initial research phase, there is not yet a plugin available for rendering non-photo realistic [45] holoscopic 3D images in commercially available CAD tools.

In this section, a holoscopic 3D Camera plugin is developed for rendering non-photo realistic [45] H3D images from 3D models in "3Ds MAX". The proposed plugin is built using multiple orthographic cameras which is implemented in MAX Scripting based on the principle [7] patented by BBC. The orthographic cameras are created based on the lens array parameters such as pixels per lens, focal length and size. At this stage, the lens array parameters are hard coded in the scripted. However it will be user re-configurable using settings screen in the next release.

Table B.1 – The virtual holoscopic 3D camera's lens array parameters

Description	Specification
Microlens Array Size	*720 lenses*
Microlens Pitch	*1.292 mm*
Lens Focal length	*~2.0*
Pixels per lens (views)	*8 pixels*
physical subpixels per lens	*8 subpixels*
Number of horizontal 3D pixels	*720 pixels*
Number of vertical 3D pixels	*350 pixels*
2D Resolution	*1920 × 1080 Pixels*

The plugin eases H3D image rendering process and 3D animators/modellers can render holoscopic 3D images from 3D models for autostereoscopic 3D displays. It is seamlessly integrated to 3Ds MAX software and the installation process is the same way as standard plugins installation which is as simple as copying the camera plugin files (H3DC.ms and H3DC.bmp) into the startup folder (%3DsMAXRootFolder% \ Scripts \ Startup) as shown in Figure B.3. The installation shall be carried out when all instances of 3Ds MAX application are closed.
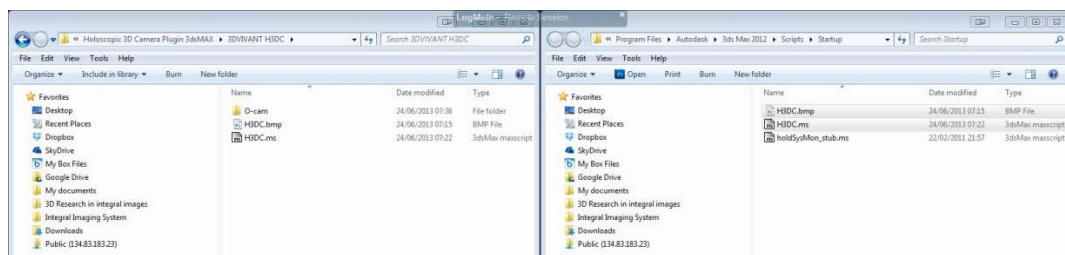
Figure B.3 – Installation of holoscopic 3D Camera plugin by copping the plugin files into the startup folder

Once the holoscopic 3D camera plugin is installed successfully, a virtual display panel needs to be created that defines the reference point. The virtual display frame is used to float objects in front and behind the screen. Creating a virtual display frame is performed in two steps:

(1) Create a display panel via Create Toolbox -> select H3D Frame from objects category combo box shown in Figure B.4 (a)

(2) Select the Frame object and drag it onto the scene to create the display screen reference point illustrated in Figure B.4 (b)
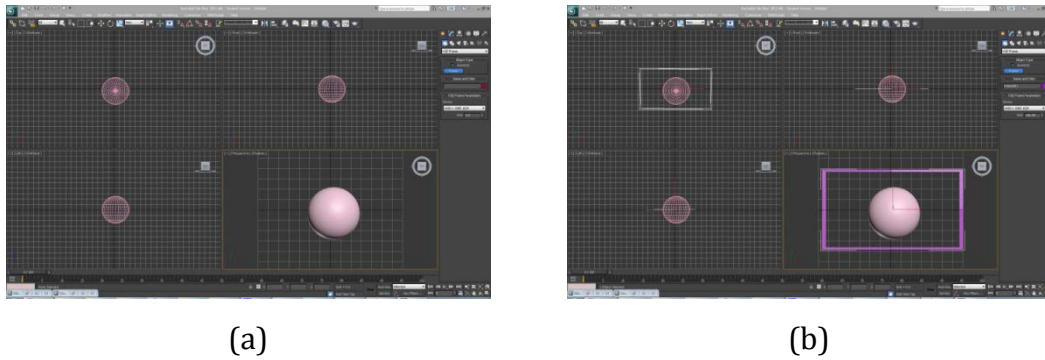

(a)   (b)

Figure B.4 - Creating a Display panel which is a referencing Z depth point used by H3D camera plugin
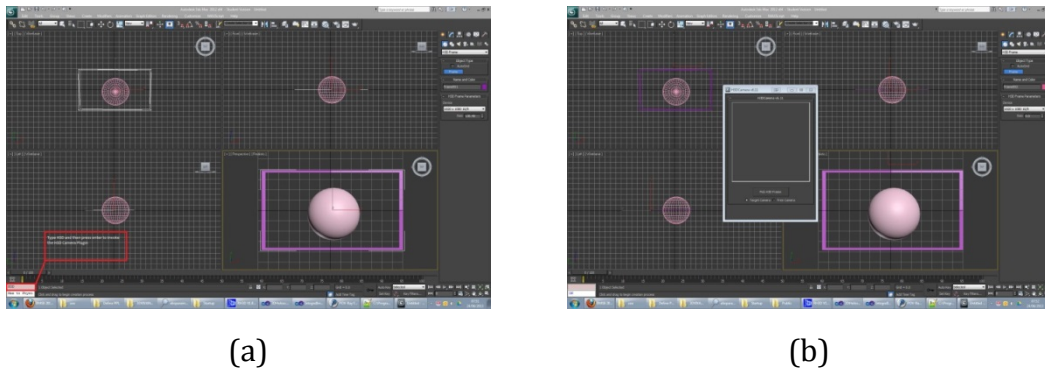

(a)   (b)

Figure B.5 - Executing the camera script for completing holoscopic 3D camera setup

The appropriate settings according users preferences are configured in the settings panel for targeted display resolution for example, in this particular example the LCD is full HD 1920 × 1080.   As the H3D frame represents the display panel, any object in front of the frame will appear in front of the display and anything behind the frame will appear behind the display and so forth. Once the H3D frame is created and aligned according to the display and 3D content preferences, The H3D camera script is invoked by typing the script code **H3D()** as shown in Figure B.5 (a), which pops out a screen from where the user can select the camera type e.g. Target/Free as shown in Figure B.5 (b). On the H3D frame pickup event, 8 Orthographic projection cameras are created and placed in correct positions that are ready for rendering H3D content.

At this stage, the H3D camera plugin is fixed to 8 pixels per lens therefore it creates 8 orthographic cameras in default and it has H3D rendering button provided in the settings panel which renders 8 cameras images and saves the

images in 8 different folders e.g. cam01, … cam08. Having said that, the user can use the 3D MAX render button in which case, one has to take care of naming if not then the user must take care of naming individual camera image. The user has full control of 3D depth and motional parallax because the MLA parameters are configurable via the H3D camera control panel as shown in Figure B.6; this includes the screen "H3D frame" settings e.g. depth, 3D environment, and MLA settings. Due to propagating three-dimensional information to all 8 cameras, the setting panel must be used to bring any changes if not the scene will be invalided.
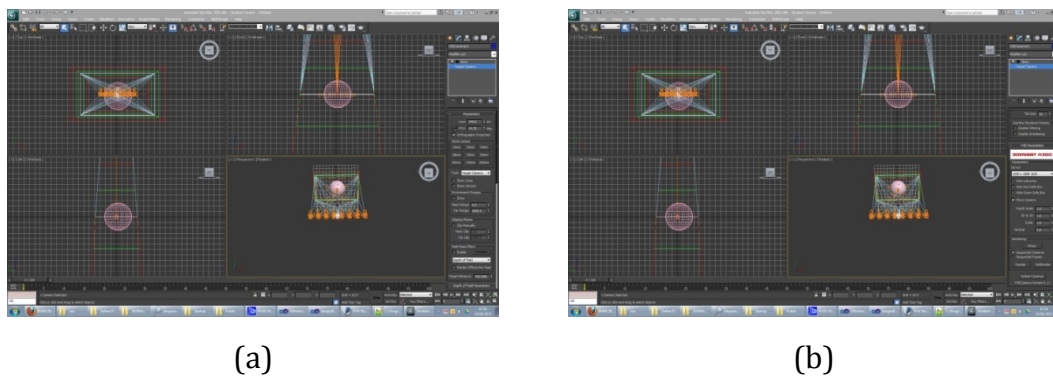

(a)   (b)

Figure B.6 - The H3D Camera settings (a) first section, (b) second section of the configuration panel

Playback Result

At this stage, the plugin is built to generate holoscopic 3D images for Alioscopy autostereoscopic display. The rendered images are feed into the 3D display and the playback result is shown in Figure B.7. As seen, the object is truly constructed in space without any noise and motion and depth parallax is considerably rich.

The developed method constructs rather a natural 3D scene in space. Multiple holoscopic 3D videos and images are rendered and replayed. The playback results are promising as it offers wider view zone angles compared to the traditional multiview 3D content. In fact, it does not limit viewers with minimum and maximum distance to perceive 3D effect whereas the traditional multiview 3D image shall be viewed within a particular distances. Last but not least, there is no sweet spot to perceive 3D effect in the proposed approach as it simply converts the display into a light field 3D display.
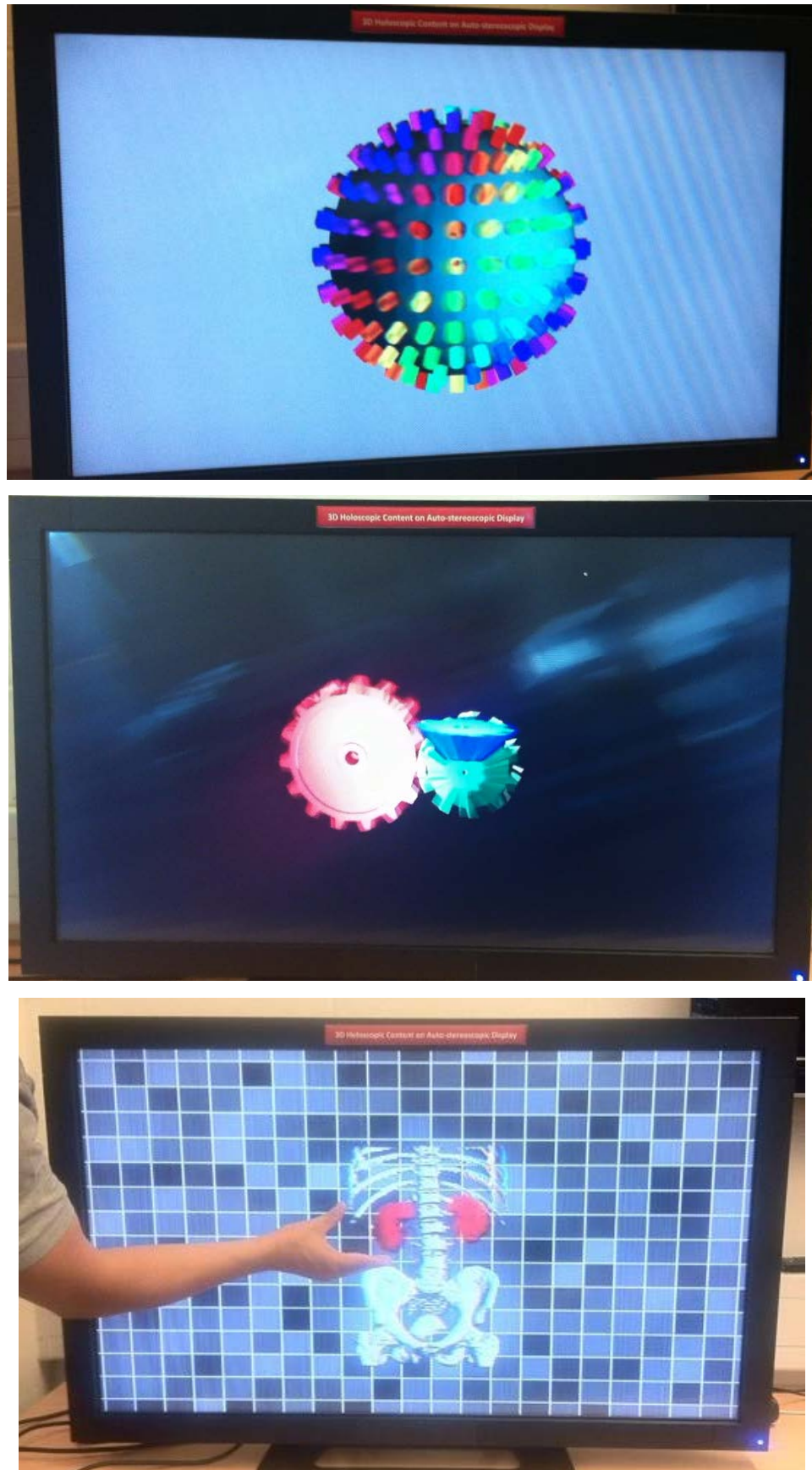
Figure B.7 - The playback result of the rendered images by the holoscopic 3D camera plugin in 3Ds MAX

3D Model Re-formatting Add-on for Holoscopic 3D Camera Plugin

A holoscopic 3D camera plugin was developed for 3Ds MAX in section 0 and it renders a H3D image from 3D models in 3Ds MAX. To further expand the camera plugin to support various other 3D models e.g. Maya, the camera script must be re-built and deployed on to the CAD tool using the native scripting language which requires a huge development effort and time instead, a 3D model re-formatting add-on is proposed to resolve the issue in this section. The proposed approach enables the camera plugin to support 3D models of different formats.

The proposed 3D modelling re-formatting add-on is built on 3DWin convertor library [44]. In particular it utilises 3Win library to reformat 3D model to speed up the development. Because, the research focus is not investigating and developing 3D model re-formatting framework. As a result, available frameworks/libraries are considered to build the proposed add on.

It is a rather simple process for parsing 3D models as shown in Figure B.8, a user inputs a 3D model file with the file format and specify the desire output 3d model file then the system parse the 3d model via 3DWin parsing framework and output the resulting 3D model. Also the user has options of choosing parsing all or specific type 3D objects e.g. include or exclude camera and/or lighting.
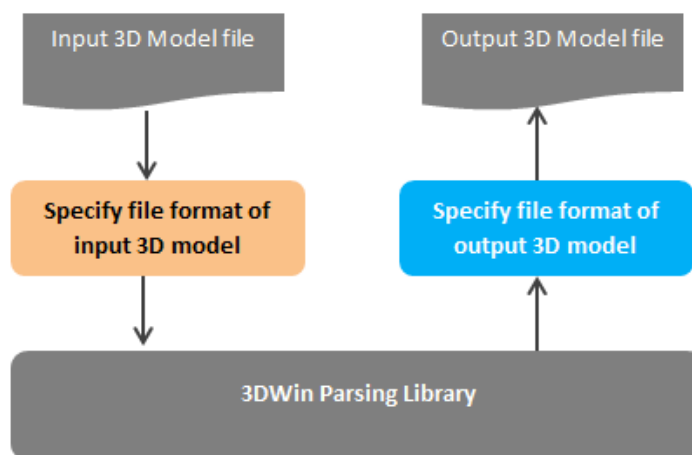

Figure B.8 - Block diagram of 3D model re-formatting framework

Table B.2 - Supported 3D model formats

Application	Extension	Imp.	Exp.	Mat	UV	L&C	Comment/Info**
-	raw	√	√				Generic ASCII format
3D Studio Max	ase	√		√	√	√	Discreet
3DStudio	3ds, prj, asc, shp	√	√	√	√	√	Discreet
Imagine	iob, obj	√		√			Impulse
Lightwave	lwo, lws	√	√	√	√		Newtek
Autodesk	dxf	√	√	√			Autodesk
Maya	ma		√	√	√		Alias Wavefront
Alias/Wavefront	obj	√	√	√	√		Alias Wavefront
Inventor 2.0	iv		√	√	√		Autodesk
VRML 1.0/2.0	wrl	√	√	√	√		Web 3D
Direct X 3D	x	√	√	√	√		Direct X
OpenGL	cpp		√	√	√		OpenGL Org
POV-Ray/Moray	pov, inc, udo	√	√	√	√		Moray and POV-Ray
Lightflow	py		√	√	√	√	Lightflow
Protein Data Bank	pdb	√					The Protein Data Bank
Quake Models	mdl, md2	√	√	√	√		Quake
RenderMan	rib		√	√	√	√	PRenderMan and BMRT
Digistar	vla		√				Astronomy
Rhino	3dm	√					Rhino3D (up to V3.x, mesh only)
CAD-3D 2	3d2	√					
NFF	nff	√					
OFF	off	√					
Truespace	cob, scn	√		√	√	√	Caligari
MS Fontfile	ttf	√					TrueType
LDraw (Lego)	dat ,ldr	√	√	√			Ldraw
IGES	igs		√				Initial Graphics Exchange Specification
STL	stl	√	√				STereoLithography
Nendo	ndo	√					Izware

Column descriptions: / Application: Main 3d Application / Extension: file format extension / Imp.: File format supported as import format / Exp.: File format supported as export format / Mat: Import/Export of material/image maps supported / UV: Import/export of UV mapping supported / L&C: Import/Export of Lights/Cameras

The 3DWin framework is well developed and covers majority 3D model formats. However, in some occasions it fails to parse a 3D model due to the scene complexity e.g. hundreds of thousands objects in the scene because some of these 3D model formats is limited in size e.g. number of objects a scene can have and also it could produce small glitches for example converting a rich complex scene from 3Ds MAX into a POV-Ray model. This is due to lack of features in POV-Ray such as different lighting effect. In fact, POV-Ray rendering engine is a photo realistic rendering engine so it works well on real oriented content rather than non-photo realistic content.

Holoscopic 3D Content Rendering Tool

In this section, a photo-realistic [45] holoscopic 3D image rendering tool is developed based on orthographic projection approach [7]. In fact, photo-realistic rendering was reported in 2007 [43] using different approach. It enables users to render a photo-realistic [46] holoscopic 3D images from their 3D models. Having both photo-realistic and non-realistic H3D cameras opens a gate for rendering augmented reality holoscopic 3D images and game 3D graphics.

The proposed H3D image rendering tool is developed based on open source ray tracing engine called "POV-Ray" [8] which is redistributed without licensing issue. . It is a deployable H3D rendering tool which allows users to render H3D images from 3D models of any formats. It is packaged with the 3D model re-formatting add-on to offer independent 3D rendering tool which can render POV-Ray 3D model directly by including the H3D camera script.

Figure B.9 shows the block diagram of the proposed rendering tool. As seen in Figure B.9, a 3D model is reformatted to POV-Ray supported 3D model before it is rendered using the H3D camera script in POV-Ray [8]. Most importantly, the H3D camera is scalable and fully customisable to render H3D images for different lens arrays because the parameters such as focal length, lens array size, lens pitch, pixels per lens and screen ratio are reconfigurable. A single click renders all orthographic viewpoint images to form a H3D image.
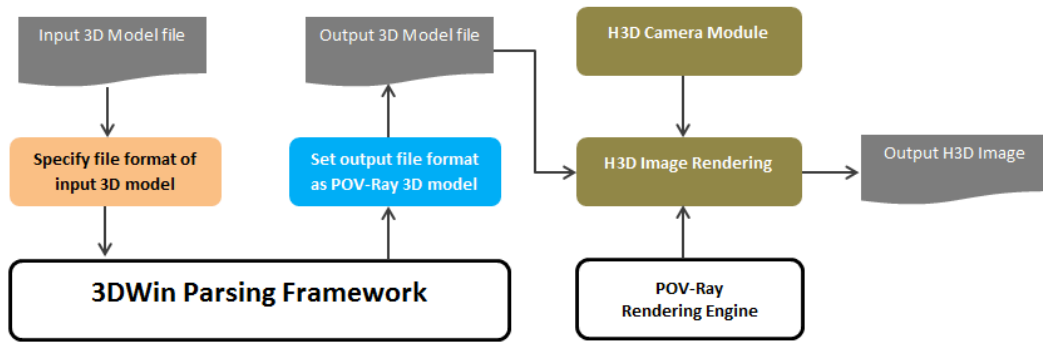
Figure B.9 - Block diagram of proposed holoscopic 3D image rendering tool
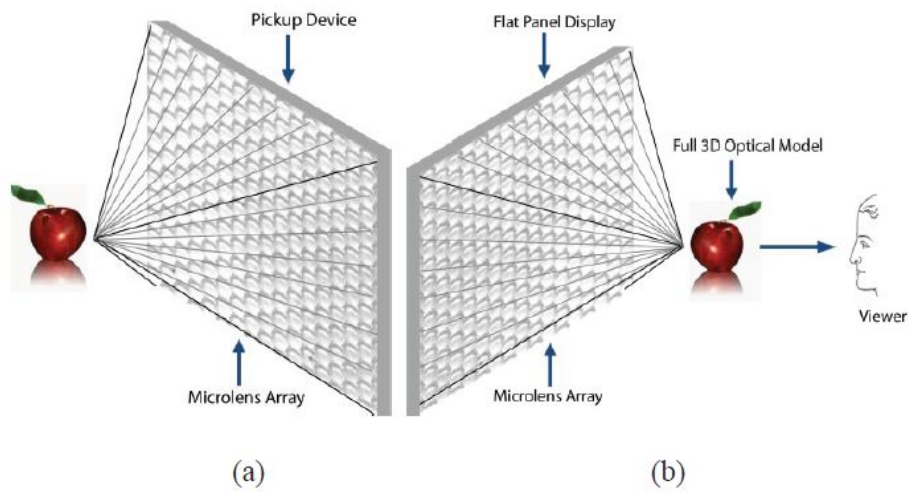

Figure B.10 - Holoscopic 3D imaging system - (a) Recording and (b) replaying [14]

References

[39]   A. Aggoun, E. Tsekleves, M. R. Swash, D. Zarpalas, A. Dimou, P. Daras, P. Nunes, and L. D. Soares, "Immersive 3D Holoscopic Video System," MultiMedia, IEEE, vol. 20, no. 1, pp. 28–37, 2013.

[40]   Persistence of Vision Pty. Ltd. Persistence of vision raytracer (version 3.6). http://www.povray.org/, 2004.

[41]   G. Milnthorpe, M. McCormick, A. Aggoun, and N. Davies, "Computer generated content for 3D TV displays," International Broadcasting Convention, 2002.

[42]   G. A. Thomas and R. F. Stevens, "Processing of Images for 3D Display," U.S. Patent US6798409B22004

[43]   M. Eljdid, A. Aggoun, and H. Youssef, "Computer Generated Content for 3D TV," 3DTV Conf. 2007, pp. 1–4, 2007.

[44]   TB-Software, "Framework, 3DWin Parsing library." [Online]. Available: http://www.tb-software.com/solutions.html. [Accessed: 05-Jul-2013].

[45]   B. Gooch and A. Gooch, Non-photorealistic rendering, vol. 201. AK Peters Wellesley, 2001.

[46]   K. Agusanto, "Photorealistic rendering for augmented reality using environment illumination," The Second IEEE and ACM International Symposium on Mixed and Augmented Reality, 2003. Proceedings. pp. 208–216.

Appendix C.

Holoscopic 3D Image Resampling

This appendix presents fundamental resampling of holoscopic 3D images.

C.I   Holoscopic 3D Imaging Resampling

A digital image consists of square RGB dot pixels or a rectangular grid of subpixels, which are evenly spaced. A pixel can be thought of as a measuring unit for a digital image in simple terms. There are other terms e.g. pixels per inch (DPI) which is used to refer to visual richness of a digital image. Resampling is the mathematical technique used to generate a new image with different size (height / width) and resolutions of the same image. Upsampling / downsampling terms are used to refer to increasing / decreasing the size of a digital image. It is used exhaustively in 2D digital images in the situation of adjusting images for printing, emailing, etc. Indeed there are number of variations of resampling methods such as Nearest-neighbour, Bilinear, and Bicubic.

2D image resampling methods are not applicable to digital H3D images as a H3D image consists of a low resolution square, rectangular micro-images "elemental images" because a H3D image is recorded using a regularly spaced array of microlens arrays (MLA) which view the scene at a slightly different angle to its neighbour and produce elemental images. Pixels in elemental images should be synchronised to construct a H3D scene in space--otherwise the H3D scene will be distorted. As a result, 2D resampling methods are proposed and applied on H3D images at micro-image level as shown in Figure C.1. Individual micro-image is resampled with a 2D resampling method unconnectedly. Any 2D resampling method can be used that is up to the user preferences. Once all micro-images are resampled recursively, a new H3D image is created from the resampled micro-images.

As stated above, resampling method is profoundly important in 2D images and it is equally important for 3D images because it is not always possible to playback at the same pixels per lens as an image is captured due to many reasons e.g. LCDs are lower resolution compare to CCDs, thus it is more likely that H3D images are replayed in lower resolution. For instance, a real scenario, the H3D camera has a MLA of 90 micron which shields 30 pixels per lens while the H3D display supports 10 pixels per lens. In such case, a new H3D

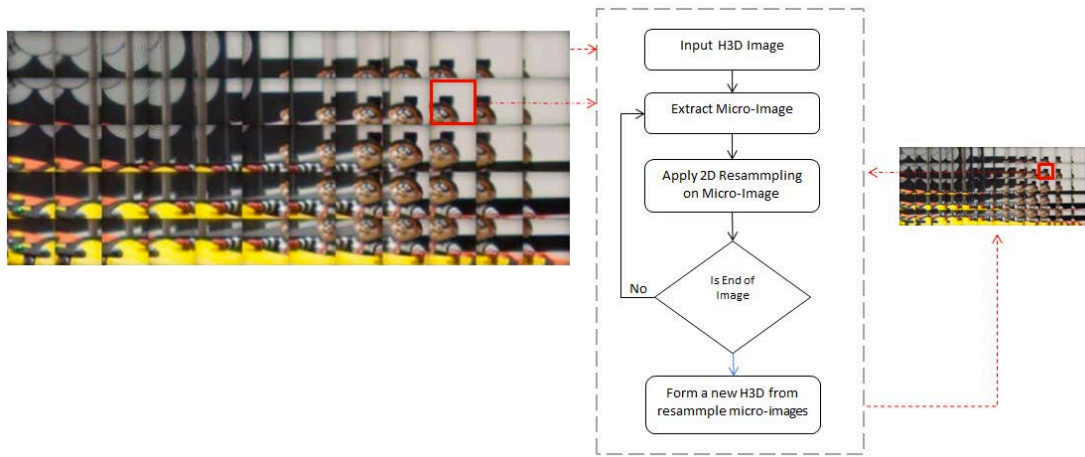resampling method is proposed that downsamples micro-images and Upsamples the H3D image.

Figure C.1 – Block diagram of Resampling of H3D image with 2D resampling methods at micro-image level

Figure C.2 shows the proposed method for upsampling 3D resolutions from downsampling micro-images, which means it losses viewpoints or user views to improve the 3D resolution. Indeed angular information is used to generate more depth information. As seen in the figure, there are 6 pixels per lens in the original image from which 3 microlens images of 2 pixels per lens are created. The newly created H3D image should be replayed with the focal length that supports the newly created image.
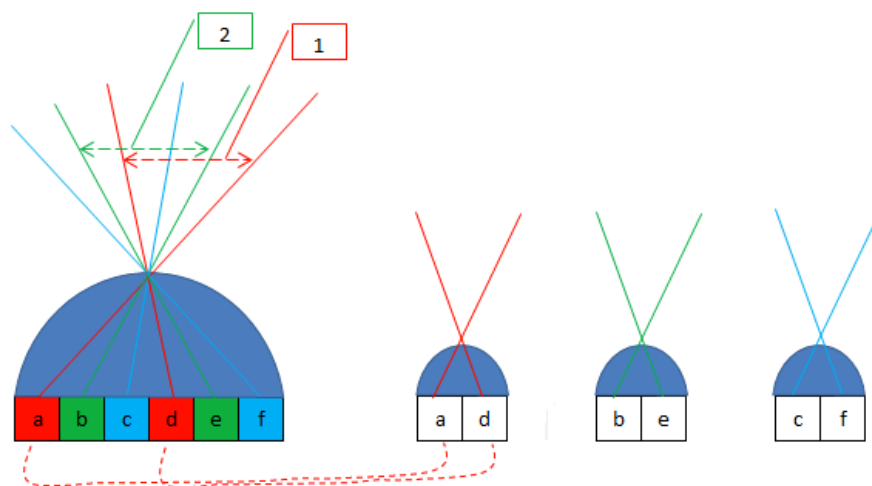

Figure C.2 – Systematic of H3D resampling for downsampling micro-images to Upsampling 3D resolution: (1) viewing angle of virtual lens a & b, (2) viewing angle of virtual lens b & c

The process simply creates virtual microlens images from a real large microlens and the newly created virtual microlens viewing angle remains the same for all newly created virtual micro-images. As shown in Figure C.2, viewing angle of a & b is equal to the viewing angle of b & d. This resampling method is an ideal candidate for improving 3D depth with 3D angular information. It can also be used to resample a H3D image to a H3D display which has lower angular information or fewer viewpoints (pixels per lens).